ISOBEL ROMERO-SHAW

ECCENTRICITY IN GRAVITATIONAL-WAVE TRANSIENTS

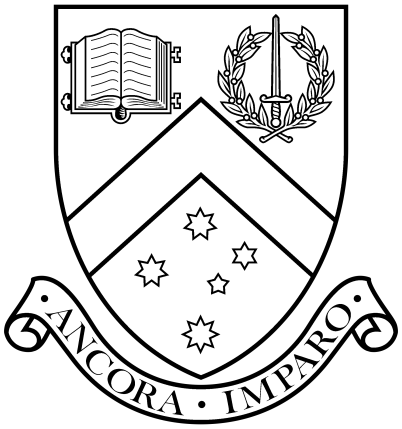

MONASH UNIVERSITY

DOCTORAL THESIS

ECCENTRICITY IN GRAVITATIONAL-WAVE TRANSIENTS

MEASUREMENTS AND IMPLICATIONS

Author
Isobel ROMERO-SHAW

Supervisors
Assoc. Prof. Paul D. LASKY
& Prof. Eric THRANE

A thesis submitted in fulfillment of the requirements for the degree of Doctor of Philosophy

in the

School of Physics and Astronomy

NOVEMBER 2021

Copyright Notice

eccentricity
ec •cen •tri •city

Etymology [314]

eccentric, English
⟶ *excentrique* , French
⟶ *excentricus*, Medieval Latin
⟶ *ékkentros*, Greek

From Greek *ek*, meaning "out", and *kéntron*, meaning "center".
⟶ *ek*, from Proto-Indo-European *égs*, meaning "out"
⟶ *kéntron*, from Proto-Indo-European *ḱent-r-om*, meaning "pointed tool", from *ḱent-*, "to pierce or point"

ABSTRACT

The era of gravitational-wave astrophysics is upon us, with advanced gravitational-wave observatories making multiple detections per observing week. These signals come from the inspiral, merger, and ringdown of binaries containing black holes and neutron stars. The LIGO-Virgo-KAGRA collaboration has so far observed 90 such signals over three observing runs. As the population grows, so does the scale of a persistent question in gravitational-wave astrophysics: *how do merging compact binaries form?* There are two overarching theories: they may form in *isolation*, if a pair of bound stars evolve to become a pair of closely-bound stellar remnants, or *dynamically*, if two compact objects become bound due to interactions with other objects in a populous environment. While the masses and spins of its components can indicate a binary's formation channel, non-negligible orbital eccentricity at detection is considered a "smoking gun" of dynamical formation. In this thesis, I present the first measurements of the orbital eccentricities of binaries detected by Advanced LIGO and Virgo. These measurements include the first observational evidence for non-zero eccentricity in the orbit of a system detected with gravitational waves: intermediate-mass binary black hole GW190521. Its high component masses, hint of in-plane component spin, and signature of orbital eccentricity suggest that GW190521 may have been dynamically formed. I also report a second event with evidence for significant eccentricity at detection: GW190620. Since the fraction of mergers with measurable eccentricity at detection is a robust prediction of globular-cluster simulations, the detection of two eccentric events suggests that more than 27% of merging compact binaries are assembled in globular clusters, at 95% confidence. However, it is not yet possible to measure eccentricity and spin-induced precession simultaneously, and—as I demonstrate using simulations of signals from GW190521-like systems—these quantities can be mistaken for each other in gravitational-wave signals. Finally, I envision a future in which mergers from different formation channels can be distinguished. I demonstrate how future gravitational-wave detectors may pinpoint the formation epochs of globular clusters by tracing the redshift evolution of the mergers in their cores. I conclude with some thoughts about the near- and far-future science that can be built upon the work presented here.

PUBLICATIONS

- **Searching for Eccentricity: Signatures of Dynamical Formation in the First Gravitational-Wave Transient Catalogue of LIGO and Virgo**, I. M. Romero-Shaw, P. D. Lasky, E. Thrane. Published October 2019, *Monthly Notices of the Royal Astronomical Society*.
DOI:10.1093/mnras/stz2996.

- **On the Origin of GW190425**, I. M. Romero-Shaw, N. Farrow, S. Stevenson, E. Thrane, X-J. Zhu. Published May 2020, *Monthly Notices of the Royal Astronomical Society Letters*.
DOI:10.1093/mnrasl/slaa084.

- **Bayesian inference for compact binary coalescences with BILBY: Validation and application to the first LIGO-Virgo gravitational-wave transient catalogue**, I. M. Romero-Shaw, C. Talbot, S. Biscoveanu, V. D'Emilio *et al.*. Published September 2020, *Monthly Notices of the Royal Astronomical Society*.
DOI:10.1093/mnras/staa2850.

- **GW190521: Orbital Eccentricity and Signatures of Dynamical Formation in a Binary Black Hole Merger Signal**, I. M. Romero-Shaw, P. D. Lasky, E. Thrane, J. Calderón Bustillo. Published October 2020, *Astrophysical Journal Letters*.
DOI:10.3847/2041-8213/abbe26.

- **Neutron Star Extreme Matter Observatory: A Kilohertz-Band Gravitational-Wave Detector in the Global Network**, The OzGrav Collaboration: K. Ackley et al. incl. I. M. Romero-Shaw. Published November 2020, *Publications of the Astronomical Society of Australia*.
DOI:10.1017/pasa.2020.39

- **GWTC-2: Compact Binary Coalescences Observed by LIGO and Virgo During the First Half of the Third Observing Run**, The LIGO-Virgo-KAGRA Collaboration incl. I. M. Romero-Shaw. Published April 2021, *Physical Review X*.
DOI:10.1103/PhysRevX.11.021053

- **Population Properties of Compact Objects from the Second LIGO-Virgo Gravitational-Wave Transient Catalog**, The LIGO-Virgo-KAGRA Collaboration incl. I. M. Romero-Shaw. Published May 2021, *Astrophysical Journal Letters.*
DOI:10.3847/2041-8213/abe949

- **Gravitational waves as a probe of globular cluster formation and evolution**, I. M. Romero-Shaw, K. Kremer, P. D. Lasky, E. Thrane, J. Samsing. Published July 2021, *Monthly Notices of the Royal Astronomical Society*.

DOI:10.1093/mnras/stab1815.

- **An Interactive Gravitational-Wave Detector Model for Museums and Fairs**, S. Cooper et al. (incl. I. M. Romero-Shaw). Published July 2021, *American Journal of Physics*. DOI:10.1119/10.0003534

- **Implications of Eccentric Observations on Binary Black Hole Formation Channels**, M. Zevin, I. M. Romero-Shaw, K. Kremer, P. D. Lasky, E. Thrane. Published November 2021, *Astrophysical Journal Letters*. DOI:10.3847/2041-8213/ac32dc.

- **Signs of eccentricity in two gravitational-wave signals may indicate a sub-population of dynamically assembled binary black holes**, I. M. Romero-Shaw, P. D. Lasky, E. Thrane. Published November 2021, *Astrophysical Journal Letters*. DOI:10.3847/2041-8213/ac3138.

- **GWTC-3: Compact Binary Coalescences Observed by LIGO and Virgo During the Second Part of the Third Observing Run**, The LIGO-Virgo-KAGRA Collaboration incl. I. M. Romero-Shaw. Submitted for publication in *Physical Review X*, November 2021. arXiv:2111.03606

- **The Population of Merging Compact Binaries Inferred using Gravitational Waves through GWTC-3**, The LIGO-Virgo-KAGRA Collaboration incl. I. M. Romero-Shaw. Submitted for publication in *Astrophysical Journal Letters*, November 2021. arXiv:2111.03634

I am also a co-author on many LIGO Scientific Collaboration papers which are not listed here and for which my contributions vary.

DECLARATION

I, Isobel Romero-Shaw, declare that this thesis titled *Eccentricity in Gravitational-Wave Transients* and the work presented in it are my own. I, Isobel Romero-Shaw, confirm that this thesis contains no material which has been accepted for the award of any other degree or diploma at any university or equivalent institution and that, to the best of my knowledge and belief, this thesis contains no material previously published or written by another person, except where due reference is made in the text of the thesis.
In this thesis, I include six original published papers published in peer-reviewed journals of which I am the lead author. These papers are provided in Chapters 2–7. Although I was responsible for the management, the primary results, and some of the writing of the paper that constitutes Chapter 2, I do not claim to be the principal contributor to this work; this article was written as a collaboration between more than 50 authors and the five leading co-authors contributed in relatively equal parts to the paper itself. Due to the collaborative nature of this project, it is not examinable under the university rules, however, it is included to preserve the narrative of the thesis. I, the student, working within the School of Physics and Astronomy under the supervision of Associate Professor Paul Lasky and Professor Eric Thrane, played a majority role in contributing to the papers constituting Chapters 3–7. My contributions to the papers presented in Chapters 2–7 are the following:

- Chapter 2
  Title: Bayesian inference for compact binary coalescences with BILBY: Validation and application to the first LIGO-Virgo gravitational-wave transient catalogue
  Status: Published September 2020, *Monthly Notices of the Royal Astronomical Society*
  Contribution: Management, analysis, writing, development (25%)
  Co-author contributions: Colm Talbot (20%-writing, analysis, development), Sylvia Biscoveanu (20%-management, analysis, writing, development), Virginia d'Emilio (15%-management, analysis, writing, development), Greg Ashton (5% - analysis, writing, development), Christopher Berry (5%-writing), Paul Lasky (5%-concept, writing, development), other authors (5%-writing, appendix studies)

- Chapter 3
  Title: Searching for Eccentricity: Signatures of Dynamical Formation in the First Gravitational-Wave Transient Catalogue of LIGO and Virgo
  Status: Published October 2019, *Monthly Notices of the Royal Astronomical Society*

Contribution: Development, analysis, writing (70%)
Co-author contributions: P. Lasky (15%-concept, writing, development); E. Thrane (15%-concept, writing, development)

- Chapter 4
  Title: On the Origin of GW190425
  Status: Published May 2020, *Monthly Notices of the Royal Astronomical Society Letters*
  Contribution: Analysis, writing, development (55%)
  Co-author contributions: N. Farrow (25%-analysis, writing, development); S. Stevenson (5% - development, writing); E. Thrane (5%-concept, writing, development); X. Zhu (10%-concept, writing, development)

- Chapter 5
  Title: GW190521: Orbital Eccentricity and Signatures of Dynamical Formation in a Binary Black Hole Merger Signal
  Status: Published October 2020, *Astrophysical Journal Letters*
  Contribution: Concept, development, analysis, writing (85%)
  Co-author contributions: P. Lasky (5%-concept, writing, development); E. Thrane (5%-concept, writing, development), J. Calderón-Bustillo (5%-concept, writing)

- Chapter 6
  Title: Signs of eccentricity in two gravitational-wave signals may indicate a sub-population of dynamically assembled binary black holes
  Status: Accepted for publication October 2021, *Astrophysical Journal Letters*
  Contribution: Concept, development, analysis, writing (90%)
  Co-author contributions: P. Lasky (5%-concept, writing, development); E. Thrane (5%-concept, writing, development)

- Chapter 7
  Title: Gravitational waves as a probe of globular cluster formation and evolution
  Status: Published July 2021, *Monthly Notices of the Royal Astronomical Society*
  Contribution: Concept, development, analysis, writing (65%)
  Co-author contributions: K. Kremer (10%-writing, development); P. Lasky (10%-writing, development); E. Thrane (10%-writing, development); J. Samsing (5%-development)

Clayton, November 8, 2021

Isobel Romero-Shaw

I, Paul Lasky, hereby certify that the above declaration correctly reflects the nature and extent of the student's and co-authors' contributions to this work. In instances where I am not the

responsible author I have consulted with the responsible author to agree on the respective contributions of the authors.
Clayton, November 8, 2021

_____

Paul D. Lasky

ACKNOWLEDGMENTS

Firstly, I would like to thank Paul and Eric, who took a gamble on a random email from an excited potential PhD student on the other side of the world and proceeded to put in a lot of effort to make her an independent researcher; I truly appreciate your confidence and kindness. Thank you both for enticing me to Australia with promises of great coffee and exotic creatures, for digging through the CDF trenches with me, and for being so generous with your time, especially during the pandemic. Paul – Thank you for your enthusiasm and energy, which have been a buoyant force over the last three years.[1] Eric – Thank you for your patience and for meticulously combing through my various drafts with a gold-depositing fine-toothed comb.[2] You've both taught me countless lessons about things that happened before I was born, including binary compact object mergers. I am also grateful for the productive collaborations and interesting discussions made possible by the many researchers who have contributed to the papers presented in this thesis.

To everyone in PhD office 125 (real and virtual) – thank you for always being funny, understanding, and sometimes even willing to share your snacks. You have all become valued friends as well as colleagues, and have made my time here much richer both socially and academically. Also Kym, honorary Astro group member, whose friendship has been a true gift since we met.

Thank you to my parents, without whom this thesis would (obviously) not exist. Mum, thank you for teaching me that no problem is unsolvable if you are determined enough. Dad, thank you for teaching me to wonder about the Universe during our deep chats and long runs. Thank you both for having a house full of books, for working so hard, and for forging a reasonable adult out of a most contrary child. Thank you also to objectively the funniest and most excellent people on the planet: Emily and Dylan, the best siblings I could have wished for. Here's hoping we'll be reunited soon.

Finally, Adrian – who dropped everything to move across the world, who has shared this tiny flat with me through six lockdowns, who has listened to my incoherent ramblings on every 5pm walk and delivered his own Neerim Road Rants, who has weathered all of the storms with me, and who has been my home-away-from-home – I cannot thank you enough.

No thanks are given to powdered custard, which will always be my nemesis.

1 Thank you also, Paul, for teaching me how to use compound-modifying hyphens – I look forward to passing on this critical, vital, and urgent message to everyone I work with in the future.

2 Thank you also, Eric, for all of the plant cuttings – while the first may have died after I foolishly fed it ground coffee, the final two are alive and happily sprawling over my kitchen.

Contents

Part I

ECCENTRICITY IN GRAVITATIONAL-WAVE TRANSIENTS

1 INTRODUCTION

1.1 COMPACT OBJECT ORBITS, OR: DOES NATURE ABHOR A CIRCLE?

To open his 1841 essay *Circles*, Ralph Waldo Emerson writes: "The eye is the first circle; the horizon which it forms is the second; and throughout nature this primary figure is repeated without end". The idea of the simple circle as a repeated motif throughout the Universe is charming, but inaccurate. Ellipses are everywhere, from the shape of the human eye to the shape of the Earth.

In the case of orbits, nature does *tend towards* a circle. After enough time, eccentric orbits decay to circular under the influence of gravity if they are isolated from external influence [343]. Energy and angular momentum are lost from an elliptical orbit via gravitational radiation, which reduces the eccentricity of the orbit. If this gravitational radiation is powerful enough, we can detect it on Earth with kilometer-scale interferometers such as Advanced LIGO, Virgo, and KAGRA [29].

To produce detectable gravitational waves, the orbiting bodies must be extremely massive (to reach the strain sensitivity of current ground-based detectors, the strain amplitude must be around $h \sim 10^{-21}$) and rapidly accelerating (to reach the sensitive frequency range of current ground-based detectors, $10 \lesssim f_{GW} \lesssim 2000$ Hz, the orbital frequency of a binary must be at least $f_{orb} = 5$ Hz) [219]. The first detection of gravitational waves was made in 2015, and came from the coalescence of two black holes with masses roughly 30 times that of the Sun [27]. Since that first signal, the LIGO-Virgo-KAGRA collaboration has accumulated almost 100 binary merger observations [30, 37, 443]. These binaries all contain compact objects: mostly black holes, some neutron star-black hole pairs, and some neutron star binaries.

The question of how these binaries were able to form and merge within the age of the Universe is unsolved. Gravitational radiation reduces the orbital energy of a binary, decreasing its separation. This happens on timescales [343]

$$t = \frac{5}{256}\frac{c^5}{G^3}\frac{r^4}{m_1 m_2 (m_1 + m_2)} \tag{1.1}$$

$$\approx 10^5 \text{ Gyr} \left(\frac{r}{\text{au}}\right)^4 \left(\frac{10\ \text{M}_\odot}{m}\right)^3, \tag{1.2}$$

where r is the binary separation, m_1 and m_2 are the masses of the primary and secondary components of the binary, and the second equation assumes equal component masses ($m_1 = m_2 = m$).

Slowly-rotating massive stars typically reach radii of 100 au before the end of their lives. Compact binaries formed under normal

circumstances will therefore be much further apart than 1 au, and will not merge within the age of the Universe. So how can our observed abundance of compact binary mergers be explained?
There are two broad channels that proposed compact binary merger formation scenarios fall into, each with several sub-channels. An *isolated* stellar binary that is bound from birth may evolve into a close compact binary if its development proceeds via a certain path. Most commonly discussed are *common envelope evolution*, in which unstable mass transfer leads to one star overflowing its Roche lobe and engulfing the other in gas, the drag from which reduces the separation between the donor and companion [239]; and *chemically homogeneous evolution*, in which rapidly-rotating stars fail to develop a steep chemical gradient and hence are prevented from expanding as they approach the end of their lives [313]. This thesis is predominantly concerned with binaries arising from the alternative channel: *dynamical assembly*. In this case, the two objects become bound only once they have already evolved into stellar remnants. This occurs in populous environments, such as globular star clusters, where the frequency of interactions between objects is high. Compact binaries that assemble dynamically can be distinguished from those that form in isolation by a number of their characteristics, which can be decoded from their gravitational-wave signals. One such characteristic is their orbital eccentricity.
Since compact object binaries lose orbital energy and momentum efficiently via gravitational radiation, their orbits tend to circularise if unperturbed by outside influences and left to their own devices for sufficiently long [343]. However, if the binary is somehow driven to merge very quickly after it becomes bound, it can retain some eccentricity close to merger. Since more gravitational energy is lost from the orbit when the binary is at periapsis than when it is at apoapsis, eccentric compact binary mergers have a distinctive modulation to their gravitational-wave signatures. If the eccentricity is large enough, this modulation can be distinguished within its gravitational-wave signal, which is detected by the current generation of gravitational-wave observatories after it reaches a frequency of ~ 10 Hz [29, 39]. Isolated binary evolution should lead to negligible eccentricity at detection, so detectable orbital eccentricity in the gravitational-wave signal can imply that a merging binary was formed dynamically.

1.1.1 *Orbital Eccentricity of Compact Object Binaries in Different Environments*

Compact objects can become bound to one another in regions of high population density. There are many different environments in which this can happen, and the attributes of those environments influence the lives of the binaries that merge within them. This changes the distribution of eccentricities expected from mergers within each environment. In the papers presented in this thesis, I focus on the

eccentricities expected from merging binary black holes that formed in *globular clusters*. The fraction of compact-object binaries that retain measurable eccentricity at detection is a relatively robust prediction from globular cluster simulations that assume a variety of cluster properties. This makes them convenient to compare to the detected population: we can use this known fraction to constrain the contribution from globular clusters to observations. Other dynamical formation environments can also produce measurably eccentric mergers, albeit with distributions and merger rates that are less confidently constrained. The ranges of eccentricities at a gravitational-wave frequency of 10 Hz, e_{10}, that can be expected from these environments are as follows:

- *Globular clusters.*—Compact binaries that form in globular clusters may have eccentricities $10^{-8} \lesssim e_{10} \lesssim 10^{-3}$ if they merge after being ejected from the cluster, $10^{-7} \lesssim e_{10} \lesssim 10^{-2}$ if they merge inside the cluster between strong dynamical interactions, and $10^{-3} \lesssim e_{10} \lesssim 1$ if they merge during strong gravitational encounters that leads to a capture event [e.g., 491].

- *Nuclear star clusters.*—Galactic nuclei have a much steeper density profile than globular clusters, enabling more frequent encounters. Binaries can become bound and merge in the same ways and with the same eccentricities as in globular clusters. There are also extra possibilities. Eccentric mergers regularly form in these extremely dense environments through single-single encounters, which have an eccentricity distribution peaking close to $e_{10} \sim 1$, especially for high-mass black holes that merge close to the central supermassive black hole [200]. Binaries that are driven to high eccentricities by the perturbing presence of the supermassive black hole have eccentricities $10^{-5} \lesssim e_{10} \lesssim 10^{-1}$ [50].

- *Active galactic nuclei.*—A small fraction of observed supermassive black holes in galactic nuclei appear to be actively accreting gas, and have a dense accretion disk inside which smaller black holes can reside. Binaries in active galactic nuclei can merge via similar mechanisms as in quiescent galactic nuclei, but with rates and properties that are influenced by the accretion disk. Capture events during binary-single and single-single encounters in these environments can have eccentricities $10^{-1} \lesssim e_{10} \lesssim 1$ [430].

It is also possible to produce field binaries that merge with detectable orbital eccentricity if the system originates as a triple, with the inner binary driven to high eccentricity through Kozai-Lidov resonance [263, 282]. These may have eccentricites $10^{-5} \lesssim e_{10} \lesssim 1$ if black hole natal kicks are zero, with the distribution narrowing to $10^{-4} \lesssim e_{10} \lesssim 10^{-1}$ with even small natal kicks [51]. The rate of detectably-eccentric mergers expected from Kozai-Lidov field triples in the absence of natal kicks is only $\sim 0.1\ \mathrm{Gyr}^{-3}\ \mathrm{yr}^{-1}$, and decreases

by up to two orders of magnitude if modest natal kicks are assumed [365, 409].

1.2 PARAMETER ESTIMATION WITH BAYESIAN INFERENCE

In this Section, I briefly outline the difficulties that have prevented eccentricity measurements, and how we overcome these in the papers presented in this thesis. A more detailed technical description of the method can be found in the Appendix.
Usually, the parameters of compact binaries observed with gravitational waves are estimated using Bayesian inference. Chapter 2 provides an overview of the computational Bayesian methods employed within the analyses presented in this paper. We take an efficient shortcut to measure eccentricity, which I motivate and delineate here.
In the context of gravitational-wave astrophysics, Bayes' Theorem [67] is often written as [444]

$$p(\theta|d) = \frac{\mathcal{L}(d|\theta)\pi(\theta)}{\mathcal{Z}(d)}. \tag{1.3}$$

Using this equation, we aim to calculate $p(\theta|d)$, the *posterior* probability distribution for the parameters represented by θ, given the data, d. The *prior*, $\pi(\theta)$, describes our knowledge (or expectations) of θ. The *likelihood*, $\mathcal{L}(d|\theta)$, describes the probability that we obtain the observed data, given a set of parameters θ. In gravitational-wave astrophysics for compact binary coalescences, the likelihood contains a model for both the gravitational waveform and the detector noise profile, and takes the form of a Whittle likelihood [475]

$$\mathcal{L}(d_k|\theta) = \frac{1}{2\pi\sigma_k^2}\exp\left(-\frac{\Delta f}{2}\frac{|d_k - \mu_k(\theta)|^2}{\sigma_k^2}\right), \tag{1.4}$$

where μ is our waveform model and σ is the noise amplitude spectral density at the gravitational-wave detector. Here, π represents the mathematical constant rather than the prior. Equation 1.4 is the likelihood for a single frequency bin, k, out of M frequency bins of width Δf. Because the likelihood in each frequency bin is considered to be statistically independent, the full likelihood is the product of Equation 1.4 evaluated over many frequency bins,

$$\mathcal{L}(d|\theta) = \prod_{k=1}^{M}\frac{1}{2\pi\sigma_k^2}\exp\left(-\frac{\Delta f}{2}\frac{|d_k - \mu_k(\theta)|^2}{\sigma_k^2}\right) \tag{1.5}$$

$$\propto \exp\left(-\frac{\Delta f}{2}\sum_{k=1}^{M}\frac{|d_k - \mu_k(\theta)|^2}{\sigma_k^2}\right). \tag{1.6}$$

Finally, the *evidence*, $\mathcal{Z}(d)$, is a normalisation term comprising the integral of the product of the prior and likelihood over all possible θ,

$$\mathcal{Z} = \int \mathcal{L}(d|\theta)\pi(\theta)d\theta. \tag{1.7}$$

The details of how we obtain posterior probability distributions in practice are described in Chapter 2. We end up with a set of *posterior samples* distributed throughout the parameter space with a density profile that represents the posterior probability distribution.
For gravitational waveform models, the parameter space has a large number of dimensions. The intrinsic nature of a binary compact object is described by ten parameters: the masses of the two components (2), a three-dimensional spin vector for each component (6), and the orbital eccentricity of the system and its associated argument of periapsis (2). Binary neutron star systems, containing objects that can be disrupted under each other's gravitational influence, have two (2) extra parameters that describe the tidal deformation of each component. Additionally, the observed gravitational signal from a compact binary changes depending on seven extrinsic parameters: the distance of the system from the detector (1), its two-dimensional sky location (2), its phase at detection (1), the signal polarisation (1), the angle of the binary's orbital plane to the line of sight (1), and the time of detection (1). For binary black holes, the complete description of the waveform is therefore 17-dimensional; however, the most complex existing waveform models are 15-dimensional, neglecting the two parameters that describe the eccentricity of the system.
Waveforms containing the influence of orbital eccentricity do exist. These models are 12-dimensional, neglecting the four parameters describing the spin-tilt of both components, adding one extra dimension—eccentricity—and with an argument of periapsis that is fixed by the starting frequency. Eccentric waveform models are more complicated than those that represent signals from systems in quasi-circular orbits, and they are not as well-developed. Therefore, eccentric waveform models are typically slow to generate: the eccentric model used in this work, SEOBNRE [103], takes $\mathcal{O}(1)$ s to generate templates for short-duration [GW190521-like; 34] signals, and $\mathcal{O}(300)$ s for long-duration signals like those of binary neutron star mergers. In contrast, non-eccentric waveform models that are commonly employed for Bayesian inference studies can generate even long-duration signals in < 0.1 s. Slower waveforms cannot be used for direct parameter estimation with Bayesian inference, which requires many hundreds of thousands of waveforms to be generated in the process of thoroughly sampling the parameter space.
The first key contribution of this thesis is to enable the measurement of orbital eccentricity without directly performing Bayesian inference with inefficient eccentric waveform models. The second is to obtain the first evidence for orbital eccentricity in merging binary black hole systems detected with gravitational waves.

1.2.1 *Constructing an eccentricity measurement*

I wish to obtain a 12-dimensional posterior distribution containing the measured orbital eccentricity at a gravitational-wave frequency of 10 Hz, $p(\theta, e_{10}|d)$ (neglecting misaligned spins and a variable initial

argument of periapsis by necessity), where the eccentricity is written separately from the other parameters θ for clarity. However, I cannot compute this directly with an inefficient waveform model.[1] Instead, I first importance-sample the parameter space using an 11-dimensional *proposal* with waveform approximant $\mu_{\varnothing}(\theta)$ that does not contain eccentricity, giving us a set of posterior samples that represent $p_{\varnothing}(\theta|d)$. Each of these samples i is defined by its parameters, θ_i. For every θ_i, I compute the *target* likelihood over a grid of eccentricities using eccentric waveform model $\mu(\theta, e_{10})$, and use this to *reweight* the proposal posterior samples to the *target* distribution, $p(\theta, e_{10}|d)$. The results of this procedure are presented in Chapters 3–6, and a detailed mathematical description of the method can be found in the Appendix.

1.3 THESIS LAYOUT

Chapters 2—7 consist of published papers. Chapter 2 serves as a description of the Bayesian inference software library (and associated analysis tools) that underpin our analyses. Chapter 3 contains the first measurements of eccentricity for binary compact objects detected with gravitational waves: eccentricity upper limits for the ten binary black holes in the first gravitational-wave transient catalogue of Advanced LIGO and Virgo, which all have eccentricities $e_{10} \leq 0.05$ at 90% credibility. In Chapter 4, I deviate from binary black hole analyses to discuss how eccentricity may be used to identify the formation channel of a particularly unusual binary neutron star system, GW190425, and constrain its eccentricity to $e_{10} \leq 0.007$ at 90% credibility. Chapter 5 contains the first event with the tantalising suggestion of measurable eccentricity: GW190521. However, given that we cannot distinguish eccentricity from spin-induced precession for this event, this result remains suggestive rather than conclusive. Chapter 6 contains 25 new eccentricity measurements for binary black hole systems in the second gravitational-wave transient catalogue, including GW190620, another event with strong support in its posterior probability distribution for high eccentricity close to merger. The final paper in this thesis looks past our current difficulties with measuring all binary black hole parameters simultaneously. In Chapter 7, I picture the future of gravitational-wave astrophysics: an era when third-generation detectors will be able to detect compact binary mergers from before and during reionization. In this era, gravitational waves may be detected from compact binary mergers within newborn globular clusters, and binaries from competing formation channels may be cleanly distinguished by confidently measuring all of their parameters. I demonstrate that in such a future,

1 Supercomputers can be used to perform direct, highly-parallel inference with an inefficient eccentric model on short-duration signals like GW190521 (for which it is relatively quick to generate templates). This is demonstrated in Chapter 5, where a year of CPU hours was compressed into about one day. However, this required the simultaneous use of 800 cores, a demand that is neither sustainable nor practical for catalogues of events.

gravitational-wave detectors may allow us to pinpoint the formation epochs of globular clusters. Finally, I summarise and recap the work presented in this thesis in Chapter 8, and propose some ideas for working towards that ideal scenario.

Part II

PARAMETER ESTIMATION WITH BAYESIAN INFERENCE

2

BAYESIAN INFERENCE FOR COMPACT BINARY COALESCENCES WITH BILBY: VALIDATION AND APPLICATION TO THE FIRST LIGO-VIRGO GRAVITATIONAL-WAVE TRANSIENT CATALOGUE

This chapter is, in majority, a copy of the original publication [378]. Some tables have been edited for improved readability, and some figure captions have been adjusted to reflect new figure layouts. The Appendices appear as Sections in the same order and location as in the original text. Appendix E contains a table that provides a useful reference table for symbols and units used in tables, figures and text throughout the remainder of this thesis. The original first column of this table, containing the Bilby *code name for the parameter, has been deleted for formatting reasons; for the full table, see the original text. The final paragraph of that final Appendix is particularly poignant for this thesis, and motivates the work presented in Chapters 3–6.*

ABSTRACT

Gravitational waves provide a unique tool for observational astronomy. While the first LIGO–Virgo catalogue of gravitational-wave transients (GWTC-1) contains eleven signals from black hole and neutron star binaries, the number of observations is increasing rapidly as detector sensitivity improves. To extract information from the observed signals, it is imperative to have fast, flexible, and scalable inference techniques. In a previous paper, we introduced Bilby: a modular and user-friendly Bayesian inference library adapted to address the needs of gravitational-wave inference. In this work, we demonstrate that Bilby produces reliable results for simulated gravitational-wave signals from compact binary mergers, and verify that it accurately reproduces results reported for the eleven GWTC-1 signals. Additionally, we provide configuration and output files for all analyses to allow for easy reproduction, modification, and future use. This work establishes that Bilby is primed and ready to analyse the rapidly growing population of compact binary coalescence gravitational-wave signals.

2.1 INTRODUCTION

Gravitational-wave astronomy presents a revolutionary opportunity to probe fundamental physics and astrophysics, ranging from the neutron star equation of state and stellar evolution to the expansion of the Universe. The first direct observations of gravitational-wave signals have been made by Advanced LIGO [29] and Advanced Virgo [39]; their first gravitational-wave catalogue of transients [GWTC-1; 30] contains ten binary black hole coalescences

and one binary neutron star coalescence. The third observing run may yield $\mathcal{O}(10^2)$ additional observations [29], with signals from a second binary neutron star merger [33], one merger of a black hole with a $2.6\,M_\odot$ compact object, and an additional two binary black hole mergers [24, 34] already confirmed.

Gravitational-wave signals encode information about their sources which can be difficult, if not impossible, to otherwise obtain. To extract information from the observed signals requires careful statistical inference. The inferred source parameters can inform our understanding of binary stellar evolution [5, 15, 64, 65, 70, 424, 490], the equation of state of neutron-star matter [17, 25, 146, 317], and the nature of gravity [7, 23, 236, 484, 485]. Multimessenger observations of gravitational and electromagnetic radiation [14] can give an even richer understanding, enabling measurements of cosmological parameters [8, 20, 102, 108, 134, 229], insights into the structures of gamma-ray bursts [13, 82, 170, 302, 315], and identifying the origins of heavy elements [10, 111, 244, 440, 472]. However, electromagnetic emission can fade rapidly, necessitating rapid localization of the gravitational-wave source [29]. To maximize the scientific return of gravitational-wave observations, it is therefore of paramount importance to make use of and continue to develop efficient, reliable, and accurate computational inference.

The namesake of Bilby *is the* bilby*, a smallish Australian mammal that is like a cross between a mouse and a rabbit.*

Bilby is a user-friendly Bayesian inference library that can be used to analyse gravitational-wave signals to infer their source properties [54]. Bilby is modular and can be easily adapted to handle a range of inference problems in gravitational-wave astronomy and beyond [e.g., 148, 199, 352, 400]. In the context of gravitational-wave astrophysics and compact binary mergers, it has been used to extract information about short gamma-ray burst properties [82], neutron star parameters [83, 123, 220, 221], the formation history of binary compact objects [291, 356, 374, 376, 488], population properties using hierarchical inference [38, 190, 254, 435], and test general relativity [53, 231, 247, 341, 471, 494]. This paper concentrates on using Bilby to infer the properties of individual signals from compact binary coalescences—the inspiral, merger and ringdown of binaries composed of neutron stars and black holes.

Here I refer to two chapters in this thesis: Chapters 3 and 4.

We outline the developments included in the Bilby software to accurately and efficiently infer the properties of compact binary coalescence (CBC) signals, and demonstrate their validity both through tests using simulated signals and via comparisons to existing observational results. In Section 2.2, we describe the applications of Bayesian inference to compact binary coalescence events detected in gravitational waves. In Section 2.3, we focus on the Bilby package, with particular emphasis on improvements made since the publication of Ashton et al. [54] in Section 2.3.1. We outline our code validation tests in Section 2.3.2, and describe the automation of Bilby—allowing for efficient and immediate analysis of gravitational-wave event candidates—in Section 2.3.3. In Section 2.4, we reanalyse the eleven signals from GWTC-1, ensuring that we use both identical data and identical data processing techniques as used

to produce the public GWTC-1 results obtained using the Bayesian parameter estimation package LALInference [456]. We cross-validate our results for GWTC-1 against these previous results. We defer analysis of detections from the third observing run in anticipation of a future Bilby catalogue. Results of the analyses presented here, in a format matching recent releases of LIGO–Virgo posterior samples, are provided as accompaniments to this paper. Our investigations confirm the effectiveness of Bilby as it begins to be used for LIGO–Virgo parameter estimation [24, 33]. Throughout this paper, we use notations for CBC source parameters that are defined in Appendix 2.10.

2.2 Bayesian inference for compact binaries

In this section, we outline the fundamental procedures carried out by Bilby and provide a summary of new features implemented since the first Bilby paper [54]. For a thorough and up-to-date description of Bilby, the reader is directed to the Bilby documentation.[1]

2.2.1 *Applications of Bayesian Inference to Compact Binary Coalescences*

The primary objective of gravitational-wave inference for compact binary merger signals is to recover posterior probability densities for the source parameters $\boldsymbol{\theta}$ (defined in Appendix 2.10), like the masses and spins of the binary components, given the data and a model hypothesis. The posterior can be computed using Bayes' theorem [67],

$$p(\boldsymbol{\theta}|d,\mathcal{H}) = \frac{\mathcal{L}(d|\boldsymbol{\theta},\mathcal{H})\pi(\boldsymbol{\theta}|\mathcal{H})}{\mathcal{Z}(d|\mathcal{H})}, \tag{2.1}$$

where $\mathcal{L}(d|\boldsymbol{\theta},\mathcal{H})$ is the likelihood, $\pi(\boldsymbol{\theta}|\mathcal{H})$ is the prior, $\mathcal{Z}(d|\mathcal{H})$ is the evidence, and $\mathcal{H}$ is the model. The prior is chosen to incorporate any *a priori* knowledge about the parameters. The likelihood represents the probability of the detectors measuring data d, assuming a signal (described by the model hypothesis $\mathcal{H}$) with source properties $\boldsymbol{\theta}$. The evidence, or marginalized likelihood,

$$\mathcal{Z}(d|\mathcal{H}) = \int p(d|\boldsymbol{\theta},\mathcal{H})\pi(\boldsymbol{\theta}|\mathcal{H})\,\mathrm{d}\boldsymbol{\theta}, \tag{2.2}$$

serves as a measure of how well the data is modeled by the hypothesis; it acts as a normalization constant in parameter estimation, but is important in model selection.
The standard likelihood function used to analyse gravitational-wave transients is defined in, e.g., Finn [163] and Romano and Cornish [371], where both the data and the model are expressed in the frequency domain. This likelihood has stationary Gaussian noise, which is a good approximation in most cases [e.g., 9, 21, 77] unless one of the instruments is affected by a glitch [337, 351]. We assume

1 lscsoft.docs.ligo.org/bilby/

the noise power spectral density (PSD) is independent of the model parameters and therefore ignore the normalization term, yielding

$$\ln \mathcal{L}(d|\boldsymbol{\theta}) \propto -\sum_k \frac{2|d_k - h_k(\boldsymbol{\theta})|^2}{TS_k}, \tag{2.3}$$

where k is the frequency bin index, S is the PSD of the noise, T is the duration of the analysis segment. The data d and waveform model $h(\boldsymbol{\theta})$ are the Fourier transforms of their time-domain counterparts. Given the likelihood and the prior, we can calculate the posterior probability distribution for the source parameters.
There are multiple approaches to calculating the posterior probability distribution. For example,
RapidPE [336] and its iterative spin-off RIFT [275] use highly-parallelized grid-based methods to compute the posterior probability distribution, while BAYESTAR [410, 411] rapidly localizes gravitational-wave sources, calculating probabilities on a multiresolution grid of the sky. Bayesian inference schemes using various machine-learning algorithms are also being developed [188, 193]. However, the majority of Bayesian inference analysis is done by stochastically sampling the posterior probability distribution.
Over many years, Markov-chain Monte Carlo [MCMC; 112, 113, 383, 384, 500, 501] and nested sampling [454, 455] algorithms for gravitational-wave inference have been developed. This work culminated in the development of LALInference, a Bayesian inference library using custom-built Markov-chain Monte Carlo and nested sampling algorithms [456].[2] LALInference has been the workhorse of gravitational-wave inference since the initial LIGO–Virgo era [1], through the first observation [6] to the production of GWTC-1 [30]. Other stochastic sampling packages used for gravitational-wave inference include PyCBCInference [84] and Zackay, Dai, and Venumadhav [486], which uses relative-binning [117, 120] to reduce the computational cost of the likelihood. In addition to these sampling packages which fit CBC waveform templates to the data, BayesWave [118] uses a trans-dimensional MCMC to fit an *a priori* unknown number of sine-Gaussian wavelets to the data. BayesWave also implements the BayesLine algorithm [285] to generate a parameterised fit for the interferometer noise PSD. Power spectral densities produced by BayesLine are widely used in gravitational-wave parameter estimation and are used in this work.
Bilby has been designed to adapt to the changing needs of the gravitational-wave inference community, emphasizing modularity and ease of accessibility.
While LALInference implements customized stochastic samplers, Bilby employs external, off-the-shelf samplers, with some adaption. This allows the user to easily switch between samplers with minimal disruption: a useful feature for cross validating results using different

2 In this work, we focus on Bayesian inference for ground-based gravitational-wave detection. Similar techniques have been developed for studying the gravitational-wave observations of other instruments, such as pulsar timing arrays [279, 461] and future space-based detectors [56, 58, 303].

samplers. Typically, external samplers need to be tuned and adapted for use in gravitational-wave inference. In some cases, this is a simple case of choosing sensible settings; we provide details of the settings that have been verified for gravitational-wave analysis in Section 2.4 and Appendix 2.7. However, we also find cases where the off-the-shelf samplers themselves need to be adjusted. Where possible, we propagate those proposed changes to the original sampling packages. Alternatively (e.g., when the change is perhaps gravitational-wave specific), we adjust the sampler from within Bilby.

2.2.2 *Stochastic Sampling*

Various Monte Carlo sampling schemes have been developed to solve the Bayesian inference problem and estimate the posterior distribution described by Eq. (2.1). For low-dimensional problems, a solution might be to estimate the best-fit parameters by computing the posterior probability for every point on a grid over the parameter space. However, as the number of dimensions increases, this becomes exponentially inefficient.[3] The common alternative to solve this problem has been to use stochastic samplers, which fall broadly into two (not mutually exclusive) categories: MCMC [216, 310] and nested sampling [414]. In general terms, independent samples are drawn *stochastically* from the posterior, such that the number of samples in the range $(\boldsymbol{\theta}, \boldsymbol{\theta} + \boldsymbol{\Delta\theta})$ is proportional to $p(\boldsymbol{\theta}|d, \mathcal{H})\Delta\theta$.
MCMC methods generate posterior samples by noting the positions of particles undergoing a biased random walk through the parameter space, with the probability of moving to a new point in the space given by the transition probability of the Markov chain. Sampling is completed once some user-specified termination condition is reached, usually a threshold for the number of posterior samples that should be accumulated to provide an accurate representation of the posterior.
Nested sampling methods generate posterior samples as a byproduct of calculating the evidence integral $\mathcal{Z}(d|\mathcal{H})$. A set of live points is drawn from the prior distribution, and at each iteration, the live point with the lowest likelihood is replaced by a new nested sample that lies in a part of the parameter space with a higher likelihood. The evidence is approximated by summing the products of the likelihood at the discarded point and the difference in the prior volume between successive iterations. The nested samples are converted to posterior samples by weighting by the posterior probability at that point in the parameter space. The nested sampling algorithm stops once a predefined termination condition has been reached. The most commonly used termination condition is when the fraction of the

3 Quasi-circular binary black hole coalescence waveform models typically have $n_{\text{dim}} = 15$, depending on the number of spin orientations included in the waveform model. Binary neutron star coalescence models include an additional two parameters that describe their tides. We provide definitions of all parameters describing binary compact objects in Appendix 2.10. There are a further ≈ 20 parameters per interferometer that describe uncertainties in detector calibration.

evidence in the remaining prior volume is smaller than a predefined amount.
For more details on both MCMC and nested sampling methods, we refer the reader to [226] and [420], respectively.

2.3 THE BILBY PACKAGE

Bilby has a modular structure, allowing users to extend and develop it to suit their needs; examples include online Bilby (Section 2.3.3.3), bilby_pipe (Section 2.3.3) and parallel Bilby [pBilby; Section 2.3.3.2; 417], amongst others [e.g., 435]. Bilby comprises three main subpackages. The core subpackage contains the basic implementation of likelihoods, priors, sampler interfaces, the result container class and a host of utilities. The gw subpackage builds on core and contains gravitational-wave specific implementations of priors and likelihoods. These implementations include a detailed detector and calibration model, an interface to waveform models, and a number of utilities. Finally, the hyper subpackage implements hyper-parameter estimation in Bilby, which in the gravitational-wave context is used for population inference.

2.3.1 *Changes within* Bilby

Since the original Bilby paper [54], there have been a number of significant changes and added features to the code package. We describe these in the following subsections. We discuss prior constraints in Section 2.3.1.1, conditional priors in Section 2.3.1.2, and the implementation of cosmological priors in Section 2.3.1.3. We detail the custom jump proposals implemented for the cpnest [457] and ptmcmc [143] samplers in Section 2.3.1.5, and the various available prior boundary conditions in Section 2.3.1.6. Sampling processes can be accelerated using likelihood marginalizations and reduced-order quadratures; we explore how these methods can be applied to Bilby analyses in Sections 2.3.1.8 and 2.3.1.9, respectively. In Section 2.3.1.10, we explain how uncertainties in detector calibration are folded into Bilby parameter estimation. Finally, in Section 2.3.1.11 we present some of the gravitational-wave transient-specific plots that Bilby can create. In addition to the changes described below, Bilby now also supports the kombine [152], ptmcmc [143], PolyChord [212, 213], and UltraNest [95, 96] samplers. A full and up-to-date list of changes can be found in the Bilby changelog.[4]

2.3.1.1 *Constrained priors*

Each time the sampler chooses a new point to test from the multi-dimensional parameter space, it selects this point from within the region specified by the multi-dimensional prior. It is often advantageous to be able to cut out parts of the prior space by placing

4 git.ligo.org/lscsoft/bilby/blob/master/CHANGELOG.md

restrictions on relationships between parameters. For example, in gravitational-wave inference we frequently wish to specify a prior on the binary component masses, m_1 and m_2, while enforcing that $m_1 \geq m_2$, which is equivalent to the constraint that the mass ratio $q = m_2/m_1 \leq 1$.
In Bilby, the collection of priors on all parameters is stored as a PriorDict object. In order to enforce a constraint, a Bilby user can add a Constraint prior object to the PriorDict. It is necessary to tell the PriorDict how to convert between its sampled parameters and its constrained parameters; this is done by passing a conversion_function at instantiation of the PriorDict. The Bilby default binary black hole and binary neutron star prior set classes (BBHPriorDict and BNSPriorDict, respectively) can impose constraints on any of the known binary parameters. This ensures that users can sample in the set of parameters that best suits their problem, while ensuring that the relevant indirectly-sampled quantities are constrained. Without applying any prior constraints, all Bilby prior distributions are correctly normalised. When constraints are imposed on the prior distribution, the updated normalisation is approximated using a Monte Carlo integral.

2.3.1.2 *Conditional priors*

One may choose to make the prior for one parameter conditional on the value of another. This can increase efficiency, particularly if large parts of the prior space would be forbidden by an equivalent constraint prior. A commonly used parameterisation of the population distribution of binary black hole masses is

$$\begin{aligned} p(m_1|m_{\rm min}, m_{\rm max}, \alpha) &= (1-\alpha)\frac{m_1^{-\alpha}}{m_{\rm max}^{1-\alpha} - m_{\rm min}^{1-\alpha}}, \\ p(q|m_1, m_{\rm min}, \beta) &= (1+\beta)\frac{m_1^{1+\beta} q^{\beta}}{m_1^{1+\beta} - m_{\rm min}^{1+\beta}}, \end{aligned} \tag{2.4}$$

where $m_{\rm min}$ and $m_{\rm max}$ are the maximum and minimum allowed masses for the primary component, and α and β are power-law indices [38, 165]. If we wish to use a similar prior to analyse individual binary black hole coalescences, we require a prior for mass ratio which is conditioned on the primary mass. We provide a ConditionalPriorDict and conditional versions of all implemented priors within Bilby to facilitate analyses of this kind. Further, Bilby is able to handle nested and multiple dependencies, and automatically resolves the order in which conditional priors need to be called. The conditional relationship between different priors can have any functional form specified by the user.

2.3.1.3 *Cosmological priors*

Most previous parameter estimation analyses of CBCs have assumed a prior on luminosity distance $d_{\rm L}$ which is $\pi(d_{\rm L}) \propto d_{\rm L}^2$ [e.g., 6, 30]. A $\pi(d_{\rm L}) \propto d_{\rm L}^2$ prior would distribute mergers uniformly throughout a

Euclidean universe. This is an adequate approximation at small redshifts, as illustrated in Figure 2.1; however, beyond a redshift of ~ 1, the difference between a prior which is uniform in the comoving (source) frame volume and uniform in luminosity volume is large. We therefore implement a range of cosmologically-informed prior classes. The Cosmological base class allows the user to specify a prior in either luminosity distance, comoving distance, or redshift using any cosmology supported in Astropy [353, 362].[5] Additionally, users can specify the prior in terms of redshift and then convert to an equivalent prior on luminosity distance if desired. We implement two new source distance priors: a UniformComovingVolume prior, defined as

$$\pi(z) \propto \frac{\mathrm{d}V_\mathrm{c}}{\mathrm{d}z}, \tag{2.5}$$

where V_c is the comoving volume, and a UniformSourceFrame prior, defined as

$$\pi(z) \propto \frac{1}{1+z}\frac{\mathrm{d}V_c}{\mathrm{d}z}. \tag{2.6}$$

The additional factor of $(1+z)^{-1}$ accounts for time dilation. Additional Cosmological prior classes of the form

$$\pi(z) \propto \frac{\mathrm{d}V_c}{\mathrm{d}z} f(z) \tag{2.7}$$

can be defined by providing $f(z)$.

2.3.1.4 *Joint priors*

In cases where one requires more complex priors that depend on multiple parameters we implemented the JointPrior class in which the user can define a distribution that describes the prior on multiple parameters. This is implemented in Bilby in the MultivariateGaussian prior that lets the user define multi-modal and multivariate Gaussian priors. It is also used in the HEALPixMap prior in which a user can implement a prior on the sky position and optionally distance according to a given HEALPix [204, 205] map.

2.3.1.5 *Custom jump proposals*

Users of Bilby can define custom jump proposals through its interface to the cpnest and ptmcmc samplers. Jump proposals describe how the sampler finds new points in the parameter space. cpnest has a defined cycle of proposals that can be changed by the user. These proposals can be useful when there are known degeneracies in the parameter space, e.g., phase ϕ and polarization angle ψ under a shift by $\pi/2$ in either parameter [456]. Sampling in right ascension α and declination δ can also be improved using custom jump proposals; degeneracy typically leads to a ring-shaped two-dimensional

5 By default, Bilby uses the Planck Collaboration et al. [345] cosmology.

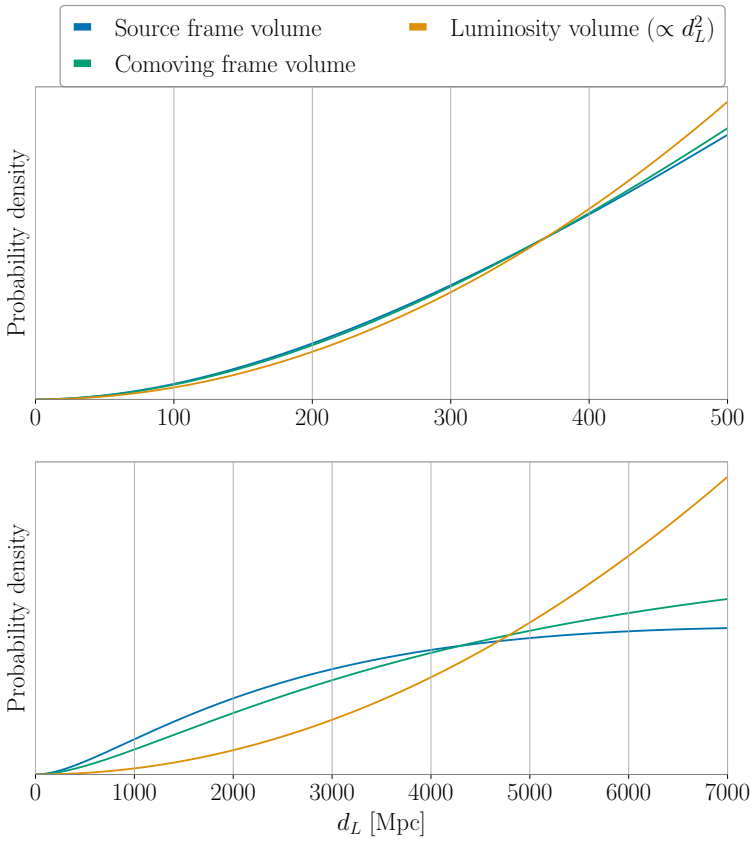

Figure 2.1: Comparison of distance priors out to redshift $z = 0.10$ (top panel) and $z = 1.02$ (bottom panel), respectively corresponding to $d_{\mathrm{L}} = 500$ Mpc and $d_{\mathrm{L}} = 7000$ Mpc, according to Planck Collaboration et al. [345] cosmology. The upper and lower panels show the range of the luminosity distance priors for the default 128 s and high-mass prior sets, respectively. We display priors that are uniform in luminosity volume, comoving volume, and the (comoving) source frame. The probability density of each curve is normalized with respect to the upper limit cut-off displayed in that panel.

posterior in these parameters for signals detected by two detectors [77, 413]. We provide proposals for the above two cases in the Bilby implementation of cpnest, while additional proposals can be defined by the user to suit their needs.

2.3.1.6 *Boundary conditions*

For many parameters, such as the mass ratio q and spin magnitudes a_1, a_2, posterior distributions have significant support close to the prior boundaries. This is expected behaviour and a direct result of the choice of prior (e.g., the choice to fix $m_1 \geq m_2$ ensures $q \leq 1$). In Bilby, Prior objects have boundaries that can be specified by the user as None, reflective, or periodic. For samplers which support these settings, these options specify the behaviour of the sampler when it proposes a point that is outside of the prior volume. For a None boundary, such a point is rejected. Priors that have reflective boundaries are reflected about the boundary (a proposed mass ratio of $1 + \epsilon$ is reflected to $1 - \epsilon$) while periodic boundaries wrap around (a proposed phase of $\pi + \epsilon$ is wrapped to ϵ).
The dynesty sampler [420] supports all available parameters boundary settings. The pymultinest sampler [94, 160–162] can implement periodic boundary conditions, but not reflective, which are treated as None. All other samplers implemented in Bilby treat all prior boundaries as None.
While reflective boundaries are implemented, their usage is not recommended due to concerns that they break detailed balance [e.g., 427]. When using the dynesty sampler, we recommend using periodic boundaries for relevant parameters (e.g., the right ascension and phase). These recommendations are mirrored in our choices of default priors, discussed in Section 2.4.1.

2.3.1.7 *Alternative sky and time parameterisations*

The most common way to describe the location of the source on the sky and its time of arrival is with the equatorial coordinates right ascension α and declination δ, and the coalescence time at the center of the Earth t_c. However, particularly when the signal is only observed in two detectors, the likelihood is determined primarily by the time delay between the arrival of the signal at each detector. The posterior distribution on these parameters often assumes a broken ring shape misaligned with the equatorial coordinate system [77, 413], making sampling difficult. A more natural parameterisation of the problem is given by sampling in the time of arrival at one of the detectors (ideally the one with the largest SNR), and rotating the sky coordinates such that the ring structure is uncorrelated in the sampling parameters. We allow the user to specify a reference_frame and time_reference. The argument reference_frame can either be an InterferometerList, a string with the names of two known detectors, e.g., H1L1, or sky to sample in α and δ. Cases where sampling in α and δ is preferred include when the astrophysical location of the source is exactly

known, e.g., by using the location of the host galaxy of a binary neutron star merger, the user can sample in α and δ by specifying `reference_frame=sky`. In this parameterisation the zenith angle κ is related to the time delay of the merger between the two detectors and is therefore well measured. The azimuthal angle ϵ is only weakly constrained for a two-detector network. The argument `time_reference` can be the name of any known interferometer, e.g., `H1`, or `geocent` to sample in the time at the geocenter.
The detector-based sampling frame is defined in terms of the zenith κ and azimuthal ϵ angles relative to the vector connecting the vertices of the two interferometers specified δr. We perform the transformation from (κ, ϵ) to (δ, α) by constructing the rotation matrix R which maps $\hat{z}$ to the unit vector $\delta\hat{r}$. The rotation matrix R can be described by three Euler angles (α, β, γ)

$$R = R_3(\gamma)R_2(\beta)R_3(\alpha), \tag{2.8}$$

$$\tan\alpha = \frac{-\delta r_y \delta r_z}{\delta r_x}, \quad \cos\beta = \delta r_y, \quad \tan\gamma = \frac{\delta r_y}{\delta r_x}.$$

Here $\delta r_{\{x,y,z\}}$ are the Cartesian components of δr and $R_{2,3}$ are rotation matrices about the y- and z-axes respectively.

2.3.1.8 *Analytic likelihood marginalizations*

The likelihood in Eq. (2.3) can be costly to evaluate for some signal models, and the size of the coalescence-time posterior relative to its much wider prior can make sampling the entire space difficult. Therefore, we reduce the dimensionality of the CBC problem by analytically marginalizing over certain parameters, speeding up computation and improving the sampler convergence. The parameters we commonly marginalise over are the coalescence time, binary orbital phase, and luminosity distance. In the frequency domain, a waveform of total duration T can be written in terms of a reference time t_0, phase ϕ_0, and luminosity distance d_0 as

$$h_k(\boldsymbol{\lambda}, t, \phi, d_\mathrm{L}) = h(\boldsymbol{\lambda}, t_0, \phi_0 = 0, d_0) \times \exp\left[-2\pi i k \frac{(t - t_0)}{T}\right] \exp\left(2i\phi\right) \frac{d_0}{d_\mathrm{L}}, \tag{2.9}$$

where k indicates the frequency bin and $\boldsymbol{\lambda}$ represents the set of the other binary parameters, including the masses and spins, whose contributions to the waveform cannot be separated and thus cannot be analytically marginalized. The phase dependence can only be factored out for waveforms that include just the dominant $\ell = 2,\ m = |2|$ mode; however, this factorization has been shown to be a reasonable approximation in some cases when precession is not measurable [11]. The marginalized likelihood is obtained by integrating the likelihood in Eq. (2.3) over phase, distance, and coalescence time after using the factorisation in Eq. (2.9). The phase integral simplifies to a modified Bessel function of the first kind, evaluated at the magnitude of the complex inner product of the waveform and the data [453, 456].

The distance marginalization is performed numerically, using a Riemann sum in matched filter and optimal signal-to-noise ratio (SNR) over the range $\rho \in [10^{-5}, 10^{10}]$, spaced uniformly in log-space [410, 411, 444]. To improve efficiency at run-time, we build a lookup table which is interpolated and then evaluated. The lookup table is computed before the sampling phase begins, and can be cached and reloaded from previous analyses that used the same distance prior.
The marginalization over time involves performing a quadrature integral over an evenly spaced array of times separated by the sampling frequency. This marginalization is enabled by the fact that the inner product of the time-domain waveform and data can be rewritten as a fast Fourier transform [153]. The sky location inferred when sampling in the sky frame and using the time-marginalised likelihood is not generally correct and we do not recommend combining these two features.
If the signal is loud and the sampling frequency is too low, the reconstructed coalescence-time posterior appears discrete, since each of the generated parameters lies on one of the nodes of the array. One solution to this is to increase the resolution of the array times by increasing the sampling frequency. However, this increases the computational cost of the marginalized likelihood evaluation. Additionally, gravitational-wave detector data is natively sampled at 16 kHz [36], so increasing the time resolution beyond this level would require a different technique, e.g., zero-padding. In order to avoid increasing the sampling frequency, we maintain a continuous coalescence-time posterior by introducing a TIME_JITTER δt. This parameter varies the position of the time array over which the numerical integral is performed. We apply a uniform prior with bounds such that

$$\frac{-T}{2} \leq \delta t < \frac{T}{2}, \tag{2.10}$$

thus reducing the prior space to be searched.
When using the analytically-marginalized likelihood, the sampler does not produce posterior samples for the marginalized parameters. However, BILBY is able to generate samples for these parameters in post-processing. Using BILBY, we recalculate the likelihood by recomputing the optimal matched filter signal-to-noise ratio and the inner product of the waveform and data. We then obtain a posterior array for the marginalized parameter in question, evaluated at discrete points in the parameter's prior space. We generate posterior samples by sampling from this interpolated posterior array. By drawing a single sample for each of the marginalized parameters for each posterior sample we maintain the degeneracies between, e.g., distance and binary orbital inclination. For detailed derivations of the analytically marginalized likelihood and the posterior sample reconstruction process, see Thrane and Talbot [444].

2.3.1.9 *Reduced-order quadrature*

In order to reduce the number of frequencies at which the likelihood in Eq. (2.3) must be evaluated, we implement the reduced-order quadrature (ROQ) likelihood [418]. This method works by identifying a reduced basis that can describe the signal model well over a certain range of the parameter space. Application of reduced-order methods have been crucial for expediting inference for long duration signals, such as the binary neutron star merger GW170817 [30]. Evaluating the ROQ likelihood requires access to the appropriate basis. A set of bases for the most commonly used waveform, IMRPhenomPv2, are publicly available online.[6]
The ROQGravitationalWaveTransient likelihood class in Bilby is able to analyse arbitrary reduced-order bases. This likelihood can also be marginalized over phase and/or distance. A time-marginalized ROQ likelihood has not yet been implemented.

2.3.1.10 *Calibration*

The imperfect nature of the detector calibration introduces a systematic error in the measured astrophysical strain [5].
Following Farr, Farr, and Littenberg [154], we split this error into frequency-dependent amplitude and phase offsets, $\delta A(f)$ and $\delta\phi(f)$ respectively. The observed strain can then be related to the true strain as

$$h_{\rm obs}(f) = h(f)\left[1+\delta A(f)\right]\exp\left[i\delta\phi(f)\right]. \tag{2.11}$$

Since the calibration error is small, we perform a small angle expansion in the phase correction,

$$\exp\left[i\delta\phi(f)\right] = \frac{2+i\delta\phi(f)}{2-i\delta\phi(f)} + \mathcal{O}\left(\delta\phi^3\right). \tag{2.12}$$

Substituting this, we obtain

$$h_{\rm obs}(f) = h(f)\left[1+\delta A(f)\right]\frac{2+i\delta\phi(f)}{2-i\delta\phi(f)}. \tag{2.13}$$

The amplitude and phase uncertainty are modeled as cubic splines in Bilby,

$$\delta A(f) = s(f;\{f_j,\delta A_j\}), \tag{2.14}$$
$$\delta\phi(f) = s(f;\{f_j,\delta\phi_j\}), \tag{2.15}$$

Here, s denotes a cubic spline function, the form of which varies over frequency f and depends on the spline nodes in curly brackets.

where the spline nodes f_j are fixed and distributed uniformly in log-space between the minimum and maximum frequencies included in the likelihood, and the values of the splines at the nodes, δA_j and $\delta\phi_j$, are sampled parameters [463].
The priors on the spline values are taken to be normal distributions, with means and widths that can either be constant or loaded from a frequency-dependent calibration envelope file [98, 460]. The

6 git.ligo.org/lscsoft/ROQ_data

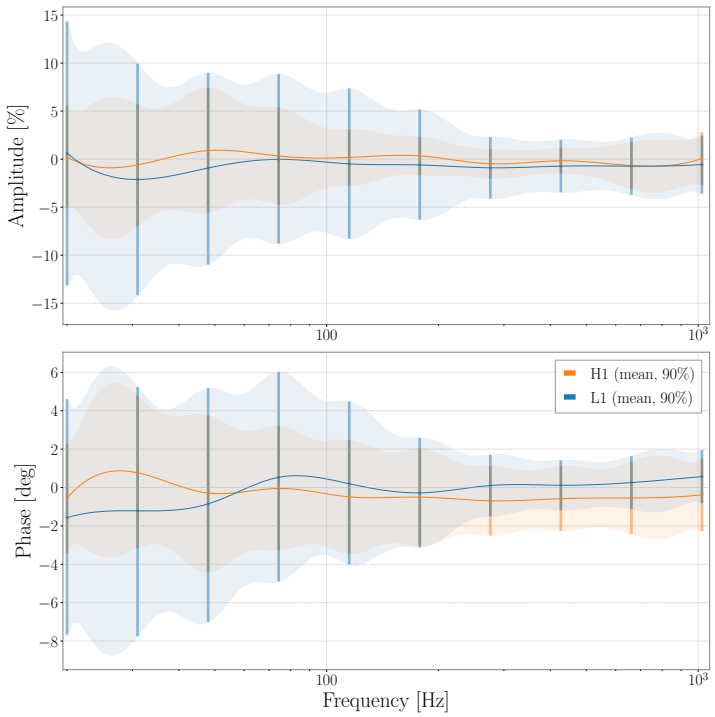

Figure 2.2: Calibration posteriors for the amplitude (top) and the phase uncertainty (bottom) for both LIGO Hanford (orange) and Livingston (blue) detectors for GW150914. The solid curves shows the mean, while the shaded region represents the 90% credible intervals. The vertical lines show the locations of the spline points.

calibration factor defined in Eq. (2.14) and Eq. (2.15) are applied to the waveform calculated for each prior sample before the likelihood is computed. Figure 2.2 shows an example plot of the calibration spline posterior for both the amplitude and phase uncertainties.

2.3.1.11 *Gravitational-wave transient-specific plots*

Bilby users can produce sets of posterior plots specific to gravitational-wave transient analysis. We use the skymap [410, 411] package to produce sky maps in both the fits format commonly used for electromagnetic observation and standard image formats. We are also able to produce plots showing our inferred posterior on the detector calibration and waveform models, in addition to the parameters describing these models. We present examples of these plots for GW150914 in Figures 2.2 and 2.3 respectively. In such plots, we show the mean reconstructed model and symmetric 90% credible intervals.

2.3.2 *Validation of* Bilby

A common consistency test of the performance of sampling algorithms is to check that the correct proportion of true parameter values are found within a given probability interval for simulated systems [116, 437]—i.e. that 10% of events are found within the 0.1

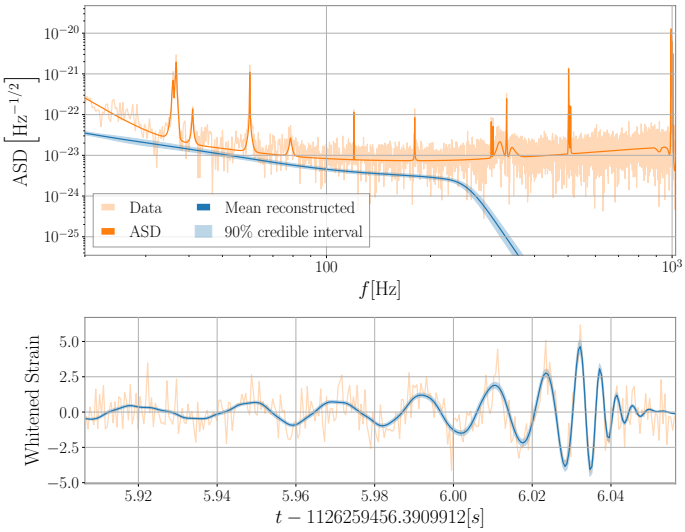

Figure 2.3: Reconstructed waveform for GW150914 for LIGO Hanford. The top panel shows the amplitude spectral density of the signal (blue), data (light orange), and estimated noise amplitude spectral density (dark orange). The bottom panel shows the time domain data (light orange) and waveform estimate (blue). The dark blue curves show the mean recovered waveform and the light blue shaded region the 90% credible interval.

probability credible interval, 50% are found within the 0.5 probability credible interval, etc. We generate a set of CBC signals with true parameter values drawn from our prior probability distributions and inject these into simulated noise. Parameter estimation is then performed on each signal to determine the credible level at which the true value of each parameter is found. This test is traditionally used in validating gravitational-wave inference codes [77, 84, 130, 336, 406, 410, 456].

To test Bilby's parameter estimation, we simulate 100 synthetic CBC signals for a two-detector Hanford–Livingston network and add the signals to Gaussian noise colored to the anticipated Advanced LIGO design sensitivity [29]. The parameters of the simulated events are drawn from the default 4 s prior set, detailed in Section 2.4.1. Parameter estimation is performed using the dynesty sampler with the distance, time, and phase-marginalized likelihood. Analysis of the performance of other samplers is left to future work. Results of the test are shown in Figure 2.4, where the fraction of events for which the true parameter is found at a particular confidence level is plotted against that particular confidence interval.[7] We also show the individual parameter p-values representing the probability that the fraction of events in a particular confidence interval is drawn from a uniform distribution, as expected for a Gaussian likelihood, and the combined p-value quantifying the probability that the individual p-values are drawn from a uniform distribution. The combined

7 These plots are referred to as P–P plots, where P could stand for probability, percent or proportion. Instructions for generating P–P plots are provided in the Bilby documentation at git.ligo.org/lscsoft/bilby_pipe/wikis/pp/howto.

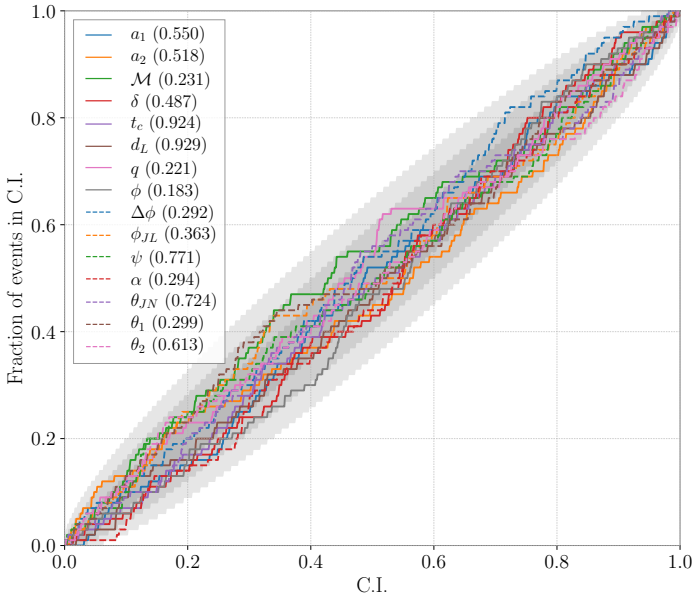

Figure 2.4: Results of 100 injections drawn from the four-second prior defined in Section 2.4.1. The gray regions cover the cumulative 1-, 2- and 3-σ confidence intervals in order of decreasing opacity. Each colored line tracks the cumulative fraction of events within this confidence interval for a different parameter. The combined p-value for all parameters, over all tests, is 0.7206, consistent with the individual p-values being drawn from a uniform distribution. Individual parameter p-values are displayed in parentheses in the plot legend. The marginalised parameters—geocenter time t_c, luminosity distance d_L and phase ϕ–are reconstructed in post-processing. Other parameters provided in the plot legend are defined in Appendix 2.10.

p-value obtained with the latest version of Bilby is 0.7206 and the minimum is 0.183 for ϕ, which is entirely consistent with chance for the set of 15 parameters, indicating that the posterior probability distributions produced by Bilby are well-calibrated. The grey regions show the 1, 2, and 3σ confidence intervals so we expect the lines to deviate from this region approximately 0.3% of the time, which is consistent with what we see.
In addition to the procedure described above, we verify the suitability of the sampler settings for the problem of sampling the CBC parameter space using a series of review tests. These are described in detail in Appendix 2.6. The settings used for each of the tests described here are provided in Appendix 2.7. In addition to these review tests, Bilby has an extensive set of unit tests, which scrutinize the behaviour of the software in high detail every time a change is made to the code; these unit tests can be found within the Bilby package.[8]

2.3.3 *Automation of* Bilby *for gravitational-wave inference*

With the improvement in sensitivity and expansion of the gravitational-wave observatory network comes an increasing rate of detections. Streamlining the deployment of Bilby analysis is therefore vital. We introduce bilby_pipe, a Python package providing a set of command-line tools designed to allow performance of parameter estimation on gravitational-wave data with all settings either passed in a configuration file or via the command line.[9] This tool was used to perform the analyses of the GWTC-1 catalogue events presented in Section 2.4, and is integral to the automatic online parameter estimation that is triggered by potential gravitational-wave events. The bilby_pipe workflow consists of two key stages: data generation, and data analysis. These steps are outlined in Section 2.3.3.1. The pipelines provided by Bilbypipe can be utilized to distribute analysis of a single event over multiple CPUs using pBilby [417], which is described in Section 2.3.3.2. The workflow for the automated running of Bilby on gravitational-wave candidates is detailed in Section 2.3.3.3.

2.3.3.1 *Data generation and analysis*

Gravitational-wave detectors record and store time-domain strain data and information about the behavior internal to the detectors, as well as data from a suite of environmental sensors. To obtain gravitational-wave strain data, we recommend using the GWpy library [294]. GWpy can retrieve both public data from the Gravitational Wave Open Science Center [36], and proprietary data using the Network Data Server protocol (NDS2) to acquire data from LIGO servers. Given a GPS trigger time and a required data duration,

8 git.ligo.org/lscsoft/bilby/tree/master/test
9 The source-code is available on the git repository git.ligo.org/lscsoft/bilby_pipe. Specifics about the installation, functionality and user examples are also provided lscsoft.docs.ligo.org/bilby_pipe.

BILBY_PIPE uses GWPY to extract an analysis segment of strain data around the trigger, as well as a segment of strain data used to estimate the noise PSD. The default duration for the analysis segment is $T = 4\,\mathrm{s}$, which is considered adequate for sources with detector-frame chirp masses $\mathcal{M} \gtrsim 15\,\mathrm{M}_\odot$. Sources with lower $\mathcal{M}$ have longer signals, so longer analysis segments should be used. A portion of data following the trigger time is required to encompass the remaining merger and post-coalescence ringdown signal; this is 2 s by default. A BILBY_PIPE user can provide pre-generated PSDs, and a range of design-sensitivity noise spectra for current and future detectors are available as part of the BILBY package. For the analyses we present in Section 2.4, we use event-specific PSDs produced using BAYESWAVE [118]. When a PSD is not provided, BILBY_PIPE uses the median-average power spectrum method described by Allen et al. [42], and implemented in GWPY, to calculate the PSD; this method has the advantage of downweighting outliers in the off-source data [42, 456]. In order to avoid including any signal in the PSD calculation, BILBY_PIPE uses a stretch of data preceding the analysis segment. Following Veitch et al. [456] and Chatziioannou et al. [107], we use data stretches of length $\min(32T, 1024\,\mathrm{s})$ by default, although both of these values can be altered by the user. The upper limit of 1024 s is required because the PSD of gravitational-wave detectors is non-stationary over long time-periods [107]. To further mitigate this issue, the data is divided into segments of length T, with each segment overlapping 50% of the previous segment; this allows a shorter total stretch of data to be used to calculate the PSD. Following Allen et al. [42], segments are Tukey windowed with a 0.4 s roll-off to suppress spectral leakage [21], before computing their one-sided power spectra.

See Section VI of Allen et al. [42] for this calculation.

The priors for the analysis can be specified by the user, either by providing a path to a file containing the priors in BILBY syntax, or by giving the name of one of the default BILBY_PIPE priors described in Section 2.4.1. By default, the BILBY GRAVITATIONALWAVETRANSIENT likelihood is used with the waveform template generated by LALSIMULATION [272]. However, users can specify their own source models and modified likelihoods in the configuration file. After saving the necessary data, BILBY_PIPE launches parameter estimation on the analysis segment in accordance with the procedure outlined in Section 2.2.1.

2.3.3.2 *Parallel* BILBY

Parallel BILBY [417] is a parallel implementation of BILBY which uses Message Passing Interface [MPI; 148] to distribute the DYNESTY nested sampling package over a pool of CPUs. Nested sampling requires drawing successive samples satisfying a likelihood constraint from the prior. Faithfully drawing samples from this constrained prior requires many likelihood evaluations. We use a CPU pool to draw prior samples in parallel at each iteration of the algorithm to reduce the wall-time needed to complete an analysis.

Qualitatively, pBilby works by using a pool of n_{cores} CPUs to draw $n_{\text{cores}} - 1$ samples from the prior in parallel at each iteration of the sampling algorithm. The $n_{\text{cores}} - 1$ proposed samples are ranked by likelihood and the lowest-likelihood live point is replaced. The prior volume is then updated on all n_{cores} processes and the sampling step is repeated until the algorithm is converged to the highest-likelihood region of the parameter space. The speedup S of the parallel implementation is a function of the number of live points n_{live} and the number of parallel processes [417]:

$$S = n_{\text{live}} \ln\left(1 + \frac{n_{\text{cores}}}{n_{\text{live}}}\right). \tag{2.16}$$

Currently, pBilby only supports the dynesty and ptemcee sampling packages. All of the functionality of Bilby, as described in Section 2.3.1, is supported by pBilby.
pBilby is highly scalable, and is thus well suited to accelerating applications in which the gravitational-wave signal or noise models are computationally expensive to evaluate, e.g., time-domain signal models such as spin-precessing effective-one-body models with higher-order modes [88, 331], numerical-relativity surrogate models [85] and models including tidal effects [273, 320]. Other well-suited applications include those where sampling convergence can be slow due to high dimensionality of the parameter space, e.g., when calibration [154] or beyond-general-relativity parameters are used [7, 23], or when a large number of live points is required to effectively estimate the evidence.
In order to facilitate efficient inter-CPU communication with MPI, pBilby is a stand-alone package, though it still uses the underlying Bilby modules.
In addition to the hugely parallel pBilby, many of the implemented sampling packages support parallelization through a user specified pool of processes. For these samplers Bilby natively supports local parallelization using the Python multiprocessing package. When available, the number of parallel computational threads to use is specified using the nthreads argument.

2.3.3.3 *Online* Bilby

The gravitational-wave candidate event database GraceDB[10] provides a centralized location for collecting and distributing gravitational-wave triggers uploaded in real time from search pipelines. Once uploaded, each trigger is assigned a unique identifier, and LIGO–Virgo users are notified via an lvalert (LIGO–Virgo Alert Network). GWCelery [412], a Python-based package designed to facilitate interactions with GraceDB, responds to an alert by first creating a Superevent, which groups triggers from multiple search pipelines and then chooses a preferred event based on the signal-to-noise ratio of the triggers. If the preferred candidate has a false-alarm-rate (FAR) below a given threshold, GWCelery

10 gracedb.ligo.org

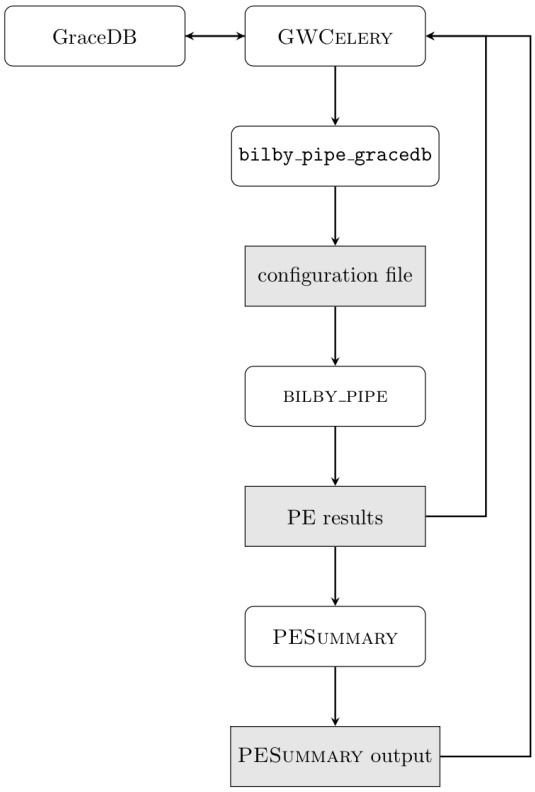

Figure 2.5: Workflow for online Bilby parameter estimation.

automatically launches multiple parameter estimation jobs. For the case of Bilby, this involves making a call to the bilby_pipe_gdb executable.
The bilby_pipe_gdb executable takes the GraceDB event ID as input and generates a configuration file based on the trigger time of the candidate. A prior file is selected from the set of default priors using the chirp mass of the gravitational-wave signal template that triggered the lvalert. Further details about the default priors can be found in Section 2.4.1. These files are then passed to the bilby_pipe executable, which runs parameter estimation on the event. PESummary [230], a Python-based package designed to post-process inference package output in a number of formats, then generates updated source classification probabilities and webpages displaying diagnostic plots. Once this step is complete, GWCelery uploads the posterior samples, post-processing pages and updated source classification probabilities to GraceDB. Figure 2.5 illustrates the process of automated parameter estimation from the trigger of a gravitational-wave event to the upload of Bilby parameter estimation results to GraceDB.

2.3.3.4 *Run times*

The overall run time of a Bilby parameter estimation job depends on the specific input data and can vary considerably based on the chosen sampler settings and signal-to-noise ratio. The overall wall time can be reduced by allowing for marginalization over certain parameters, as described in Section 2.3.1.8, or by using the parallelization methods

described in Section 2.3.3.2. For a GW150914-like binary black hole merger, the expected run time for a time, distance and phase marginalized BILBY analysis using the default waveform model IMRPHENOMPV2 [402] is $\mathcal{O}(10)$ hours. The waveform models needed to analyse binary neutron star merger events are much longer than those required for binary black holes, and therefore are more computationally expensive. Hence, for a GW170817-like binary neutron star merger event, we use PBILBY to distribute the analysis over a pool of CPUs, as described in Section 2.3.3.2; the expected run time in this case is $\mathcal{O}(10)$ hours.

2.4 GRAVITATIONAL-WAVE TRANSIENT CATALOGUE

This section contains our run settings for performing parameter estimation on GWTC-1 events using BILBY, in addition to the results we obtain from this analysis. We describe our default priors and sampler settings in Sections 2.4.1–2.4.4. Further details about these settings are given in Appendix 2.7. We provide our results in Section 2.4.6, where we assess their statistical similarity to those published in GWTC-1 [30].[11] All BILBY_PIPE configuration files, posterior samples and BILBY results files are made available online [372].

2.4.1 *Default priors*

The default prior distributions contained in BILBY_PIPE are predominantly tailored to specific signal durations, with the exception of a high-mass prior tailored to particularly heavy sources with detector-frame chirp mass $\mathcal{M}$ up to $175M_{\odot}$. For each event in GWTC-1, we choose the default prior that best covers the prior volume studied using LALINFERENCE for the original samples release. This means that two events (GW150914 and GW151012) are analysed using priors suited to signals of duration $T = 4\,\mathrm{s}$, even though we match the data duration to that used in the original LALINFERENCE analysis ($T = 8\,\mathrm{s}$). The prior on $\mathcal{M}$ is uniform in the detector frame, while the prior on d_{L} is uniform in comoving volume and source frame time, as implemented in the UNIFORMSOURCEFRAME prior class described in Section 2.3.1.3. The $\mathcal{M}$, d_{L} and spin magnitude prior limits vary between prior sets, while the other source parameters are assigned priors that are consistent between sets. The shapes and limits of all priors are defined in Appendix 2.7.2. The prior files can be found in the BILBY_PIPE git repository.[9]

11 The LALINFERENCE posterior samples that we show in this section are taken from the Parameter Estimation Sample Release for GWTC-1 [16]. The posterior samples from LALINFERENCE are obtained using a mixture of the nested sampling algorithm of LALINFERENCENEST and the Markov-chain Monte Carlo algorithm of LALINFERENCEMCMC [456].

Table 2.1: Summary statistics for each event in GWTC-1, as recovered by Bilby. We quote median values along with the symmetric 90% credible interval range around the median. For mass ratio q, we quote the 90% lower limit (10% quantile), with all events being consistent with equal mass ($q = 1$). We use a fixed-sky prior on source location for GW170817, the binary neutron star merger, fixing the source at the right ascension and declination of its electromagnetic counterpart [14]. The 90% credible areas for sky location are computed using 3000 samples from each posterior. The final column lists the maximum Jensen–Shannon (JS) divergence statistic (a measure of the similarity between two distributions) between the Bilby GTWC1 samples, and the LALInference GWTC-1 posterior samples across the model parameters. We consider JS divergence values greater than 0.002 nat to be statistically significant.

Event	Prior	$\mathcal{M}/M_\odot$	$\mathcal{M}^{\text{source}}/M_\odot$	q lower limit	d_L/Mpc	χ_eff	$\Delta\Omega/\text{deg}^2$	Max-JS/nat
GW150914	4 s	31^{+1}_{-1}	28^{+2}_{-1}	0.72	420^{+160}_{-165}	$-0.0^{+0.1}_{-0.1}$	169	$\text{JS}_{\theta_{JN}} = 0.0019$
GW151012	4 s	18^{+2}_{-1}	15^{+2}_{-1}	0.41	1015^{+498}_{-472}	$0.0^{+0.2}_{-0.2}$	1457	$\text{JS}_{\mathcal{M}} = 0.0014$
GW151226	8 s	$9.7^{+0.1}_{-0.1}$	$8.9^{+0.3}_{-0.3}$	0.38	428^{+196}_{-189}	$0.2^{+0.1}_{-0.1}$	1022	$\text{JS}_{q} = 0.0017$
GW170104	4 s	26^{+2}_{-2}	22^{+2}_{-2}	0.48	935^{+441}_{-411}	$-0.0^{+0.2}_{-0.2}$	900	$\text{JS}_{\mathcal{M}} = 0.0007$
GW170608	16 s	$8.5^{+0.0}_{-0.0}$	$7.9^{+0.2}_{-0.2}$	0.49	317^{+122}_{-115}	$0.0^{+0.1}_{-0.0}$	1462	$\text{JS}_{q} = 0.0011$
GW170729	High-mass	51^{+8}_{-9}	35^{+6}_{-5}	0.43	2548^{+1369}_{-1235}	$0.3^{+0.2}_{-0.3}$	1050	$\text{JS}_{\alpha} = 0.0026$
GW170809	4 s	30^{+2}_{-2}	25^{+2}_{-2}	0.51	995^{+311}_{-411}	$0.1^{+0.2}_{-0.2}$	300	$\text{JS}_{\mathcal{M}} = 0.0010$
GW170814	4 s	27^{+1}_{-1}	24^{+1}_{-1}	0.69	572^{+154}_{-212}	$0.1^{+0.1}_{-0.1}$	77	$\text{JS}_{\theta_1} = 0.0009$
GW170817	Custom	$1.1975^{+0.0001}_{-0.0001}$	$1.187^{+0.004}_{-0.002}$	0.74	40^{+8}_{-16}	$0.00^{+0.02}_{-0.01}$	N/A	$\text{JS}_{\tilde{\Lambda}} = 0.0019$
GW170818	4 s	32^{+2}_{-2}	27^{+2}_{-2}	0.58	1017^{+407}_{-348}	$-0.1^{+0.2}_{-0.2}$	29	$\text{JS}_{\alpha} = 0.0064$
GW170823	High-mass	39^{+5}_{-4}	29^{+4}_{-3}	0.54	1771^{+857}_{-831}	$0.0^{+0.2}_{-0.2}$	1570	$\text{JS}_{\theta_N} = 0.0009$

2.4.2 *Likelihood*

Our likelihood is marginalized over reference phase and source luminosity distance, as described in Section 2.3.1.8. For binary black hole merger analyses, we use the waveform model IMRPhenomPv2 [87, 214, 249, 402] as our signal template. For the binary neutron star GW170817, we use the IMRPhenomPv2_NRTidalv2 waveform model with tidal effects [137].

2.4.3 *Sampling*

We use dynesty [420] as our sampler; see Appedix 2.7.1 for the detailed sampler settings. We use the static version of dynesty, as is default for bilby_pipe. For each event, we run five analyses in parallel, merging the resultant posterior samples in post-processing. When combining results, care must be taken to weight each set of samples appropriately by its relative evidence. The weight applied to the ith component of N sets of posterior samples is given by

$$w_i = \frac{\mathcal{Z}_i}{\sum_{j=i}^{N} \mathcal{Z}_j}, \tag{2.17}$$

where $\mathcal{Z}_i$ is the evidence of the ith set of samples.

2.4.4 *Data used*

We use detector noise PSDs and calibration envelopes data from the data releases accompanying GWTC-1 [18, 19, 30]. The data for each event are obtained through bilby_pipe using methods from the GWpy [294] package as outlined in Section 2.3.3.1. Appendix 2.7 contains details of the trigger times and data segment durations specified for each event, which we choose to match those used in the original LALInference analysis.

2.4.5 *Analysis of binary neutron star merger GW170817*

The first observation of a binary neutron star coalescence, GW170817, by LIGO–Virgo [12] presented a new challenge for gravitational-wave transient inference. The longer signal durations increase the typical computing requirements, and for systems containing a neutron star, tidal effects become important in the waveform models. The original discovery [12] and subsequent follow-up studies [22] analysed the data with a variety of waveform models and under differing assumptions.

We employ pBilby for this analysis, with bilby_pipe default sampler settings. We use priors chosen to match those of the LVC analysis [22], but sample in chirp mass and mass ratio rather than component masses. Our likelihood is computed using the tidal waveform model IMRPhenomPv2_NRTidalv2 [137]. This pBilby analysis took approximately 11 hours on 560 cores.

2.4.6 *Results*

We make posterior samples and BILBY_PIPE configuration settings files available online [372, 373]. To directly compare BILBY posterior samples to those obtained using LALINFERENCE, we reweight the LALINFERENCE posterior distributions by BILBY_PIPE default priors. Appendix 2.8 contains the details of this reweighting procedure.
To quantitatively assess the similarity between BILBY and LALINFERENCE posterior samples, we measure their Jensen–Shannon [JS; 284] divergence. This is a symmetrized extension of the Kullback–Leibler divergence [270] that is used to quantify the information gain going between two distributions. The JS divergence is defined to be between 0 nat and 1 nat, where 0 nat represents no additional information going from one distribution to the other (the two distributions are identical) and $ln(2)$ nat $= 0.69$ nat represents maximal divergence.[12] For different sets of samples drawn from the same Gaussian distribution, we find JS divergence values of $\lesssim 0.0010$ nat while the number of samples $N \gtrsim 2000$, and JS divergence values of $\lesssim 0.0004$ nat when $N \gtrsim 5000$. To compare BILBY and LALINFERENCE results, we use $N = \min(N_{LI}, 10000)$, where N_{LI} is the number of samples left in the LALINFERENCE posterior after the reweighting procedure.
Our goal is to use the JS divergence as a quantitative indicator that the BILBY GWTC-1 samples are in agreement with those produced by LALINFERENCE. To investigate the typical distributions of JS divergence values due to sampling error, we calculated JS values for posteriors from two distinct LALINFERENCE runs on GW150914 with identical configurations. Bootstrapping was used to generate 100 posterior realizations from each run, which were used to obtain a distribution of JS divergences for each of the binary parameters included in the public LALINFERENCE GWTC-1 posterior sample release. Across different parameters, we typically found mean values of 0.0007 nat, with a maximum of 0.0015 nat. As such, we determined the following naive criteria for evaluating the JS divergence values when comparing the BILBY and LALINFERENCE GWTC-1 posteriors. For a JS divergence value less than 0.0015 nat, we conclude the samples are, to within statistical uncertainties, drawn from the same distribution, and values larger than 0.0015 nat require manual inspection.
In Table 2.1, we list the maximum JS divergence for the model parameters for each event. Of these, six pass our naive criterion described above. For the remaining events, we manually inspect the posterior distributions to look for discrepancies. The parameter with the largest JS divergence value across all BBH events is the right ascension, α. Events with large sky areas, such as GW170729, suffer from large deviations between the BILBY and LALINFERENCE posteriors in the sky position parameters. The sky position was fixed to the location of the EM counterpart for GW170817. We show the

12 In v1 of this paper, we stated JS divergence values with incorrect units (bits). These units have now been corrected.

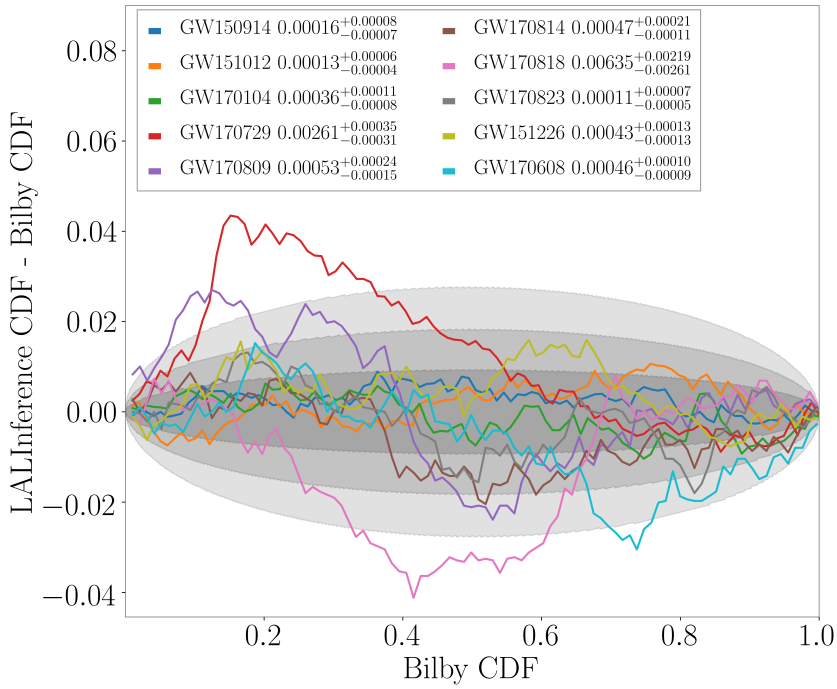

Figure 2.6: Difference between the right-ascension (α) samples recovered by Bilby and LALInference for all BBH events. This is the worst recovered parameter according to the JS-divergence. Labels show the mean JS-divergence between α samples, evaluated by random re-sampling over 100 iterations.

difference between the Bilby and LALInference posterior cumulative density functions (CDFs) for α in Figure 2.6 and for the luminosity distance d_L, which passes the naive criterion on the JS divergence for all events, in Figure 2.7. For GW170818, α has the largest JS divergence value (0.006 nat) despite the fact that the Bilby and LALInference CDFs match at the 2σ level. This is because the distribution is approximated using a kernel density estimate (KDE) in order to compute the JS divergence, and the posterior for this particular event has a sharp drop-off, which is difficult to model faithfully using the KDE.

Upon manual inspection, we find that the posteriors with JS divergence values up to ~ 0.002 nat are consistent between the LALInference and Bilby samples. The remaining parameters with significant deviations between the two samplers are the sky position parameters for GW170729. Investigations into the source of these discrepancies are ongoing. The differences between the Bilby and LALInference CDFs for all events and all parameters are shown in Appendix 2.9. A similar comparison was made in [30] analyzing the posterior distributions obtained using two different waveform approximants for each event. The maximum difference between the posteriors assuming the two different waveform models in that work is typically ~ 0.02 nat, an order of magnitude larger than the differences here.

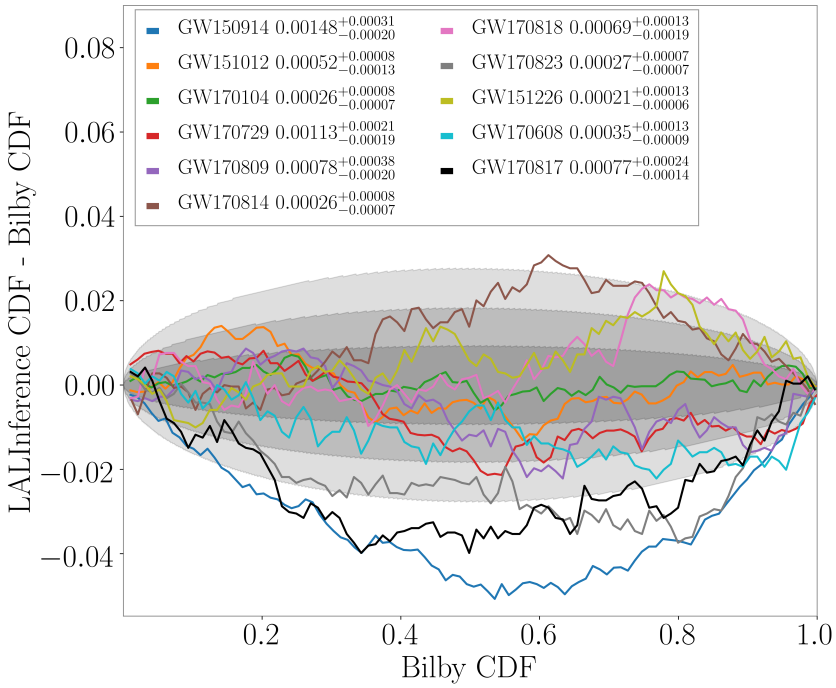

Figure 2.7: Difference between the luminosity distance (d_L) samples recovered by Bilby and LALInference for all events. Labels show the mean JS-divergence between d_L samples, evaluated by random re-sampling over 100 iterations.

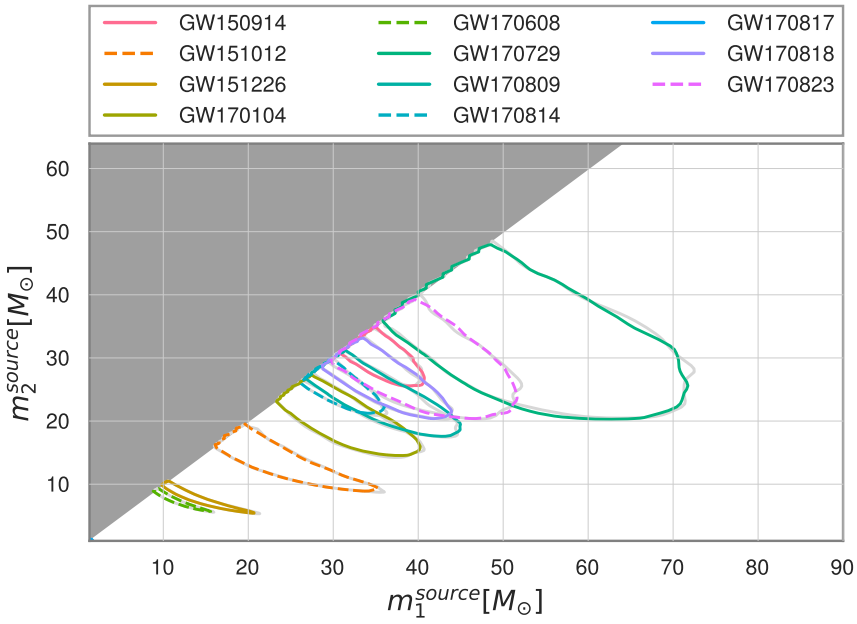

Figure 2.8: Comparison of the posterior distributions between the LALInference (gray) and Bilby (colored) packages over the source primary mass m_1^{source} and source secondary mass m_2^{source} parameter space. Each contour shows the 90% credible area, with the LALInference posterior samples reweighted to the Bilby priors.

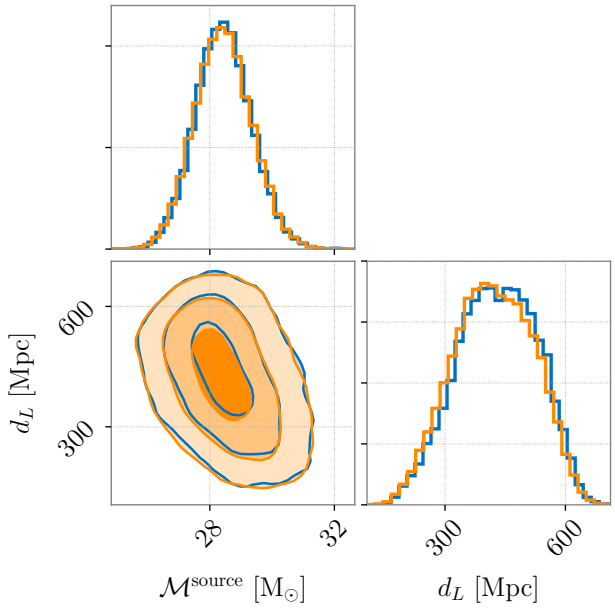

Figure 2.9: Posterior probability distributions for source-frame chirp mass $\mathcal{M}^{\rm source}$ and luminosity distance $d_{\rm L}$ for GW150914. We display posteriors obtained using Bilby in orange, and LALInference posteriors in blue. We reweight the LALInference posteriors to the Bilby default priors using the procedure outlined in Appendix 2.8. The one-dimensional JS divergence on chirp mass $\mathcal{M}$ and luminosity distance $d_{\rm L}$ for this event are $\mathrm{JS}_{\mathcal{M}} = 0.0017\,\mathrm{nat}$ and $\mathrm{JS}_{d_{\rm L}} = 0.0015\,\mathrm{nat}$.

As another way to visualize the differences between the Bilby and LALInference samples, in Figure 2.8, we compare the 90% credible areas of the two posteriors on the source-frame primary mass $m_1^{\rm source}$ and secondary mass $m_2^{\rm source}$ for all GWTC-1 events. As indicated by the low JS divergence values for the mass parameters, the two samplers produce posteriors on these parameters that agree within expected statistical fluctuations.

We compare Bilby posteriors on source-frame chirp mass $\mathcal{M}^{\rm source}$ and luminosity distance $d_{\rm L}$ for the first observed gravitational-wave event, GW150914 [27], in Figure 2.9. The LALInference distance posterior here matches the Bilby posterior more closely than was demonstrated in Figure 2 of Ashton et al. [54]. This is due to an issue in the application of the time-domain window being fixed in LALInference, which had affected the distance posterior [434].

For the first observed binary neutron-star merger event, GW170817, we compare the Bilby posterior distributions on tidal parameters $\tilde{\Lambda}$ and $\delta\tilde{\Lambda}$, as well as θ_{JN} and $d_{\rm L}$, to those obtained using LALInference in Figure 2.10. The maximum JS divergence for this event is $\mathrm{JS}_q = 0.0017\,\mathrm{nat}$. Additional posterior probability plots for all parameters of all eleven CBC events can be found within the online resources that accompany this paper [372].

Based on these results, we conclude that Bilby and LALInference produce statistically indistinguishable results for all parameters and

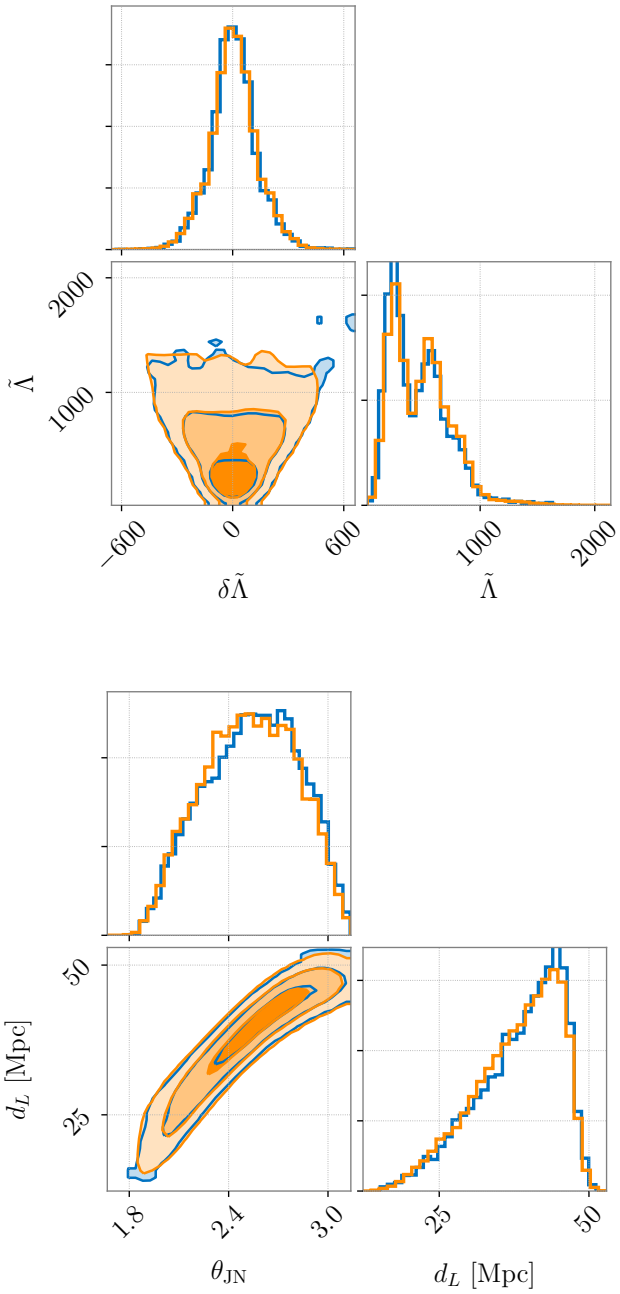

Figure 2.10: Joint posterior distributions for parameters of GW170817, comparing pBilby posteriors in orange and LALInference posteriors in blue. Top: Posterior probability distributions for tidal parameters $\tilde{\Lambda}$ ($\mathrm{JS}_{\tilde{\Lambda}} = 0.0019\,\mathrm{nat}$) and $\delta\tilde{\Lambda}$ ($\mathrm{JS}_{\delta\tilde{\Lambda}} = 0.0008\,\mathrm{nat}$). Bottom: Posterior probability distributions for inclination angle $\theta_{\rm JN}$ ($\mathrm{JS}_{\theta_{\rm JN}} = 0.0009\,\mathrm{nat}$) and luminosity distance $d_{\rm L}$ ($\mathrm{JS}_{d_{\rm L}} = 0.0008\,\mathrm{nat}$).

all events reported in GWTC-1 with the exception of the sky area for GW170729 and GW151226. We emphasize that the differences in the CDFs for these parameters are still small compared to other sources of error such as waveform systematics [30] and uncertainty in the power spectral density [81]. We provide PESummary comparison pages between Bilby and reweighted LALInference posteriors for all GWTC-1 events online.[13]

2.5 Summary

Bilby is a modern and versatile Bayesian inference library, and has been primed for analysis of gravitational-wave observations. Bilby performs reliably, producing accurate and unbiased parameter estimation results when analysing simulated signals. We validate Bilby results for GWTC-1 using the JS divergence statistic between posterior distributions obtained using Bilby and the previously published LALInference results, finding a maximum JS value of $\mathrm{JS}_\alpha = 0.0026$ nat for GW170729. The similarity between the two results indicate that both the Bilby samples obtained with dynesty and the LALInference samples are well-converged, and efforts to further validate these results using alternative samplers within Bilby are ongoing. Posterior probability distributions generated by Bilby and LALInference, when run on the same GWTC-1 data and using identical analysis settings, are consistent to the level of sampling noise. The Bilby posterior samples for events in GWTC-1 are available online [373]. We conclude that Bilby is well-suited to meet the challenges of gravitational-wave parameter estimation in the era of frequent detections.

2.6 Appendix A: Additional Bilby validation tests

In addition to the tests described in the main body of the paper, we performed several additional validation tests which are standard benchmarks for stochastic sampling codes.

2.6.1 *Prior sampling*

The initial distribution of samples drawn from the prior must faithfully represent the shape of the prior function. In addition to being used for review, the prior sampling test also forms part of Bilby's unit test suite. Prior samples can be obtained using Bilby via two different methods. The first is to use the sample method of each Prior object, which generates samples by rescaling from a unit cube. The second is to run the sampler with a null likelihood using the ZeroLikelihood object so that the returned posterior samples actually reflect the prior. To test the consistency of the two methods, we generate prior samples via both methods for a standard 15-dimensional binary black hole signal injected into simulated

13 bilby-gwtc1.github.io

Gaussian noise. We perform a Kolmogorov–Smirnov test [260, 416] to evaluate the similarity of the two sets of samples, calculating a p-value for each parameter, which quantifies the probability that the two sets of samples are drawn from identical distributions. A combined p-value is then computed, representing the probability that the ensemble of individual-parameter p-values is drawn from a unit uniform distribution. We consider the test to pass if this combined p-value is greater than 0.01. For a representative run with the latest version of Bilby, we obtain a combined p-value of 0.017.

2.6.2 *15-dimensional Gaussian*

Sampling an analytically-known likelihood distribution is an important test to verify that we can recover the correct posterior. For this test, we choose the scipy implementation of a multivariate normal distribution (scipy.stats.multivariate_normal) as our likelihood. We choose the distribution to be 15-dimensional since this reflects the typical number of dimensions we encounter in binary black hole problems. We set the means of all parameters to be zero, and choose a covariance matrix COV_{ij} with standard deviations for each of the parameters ranging between 0.15 and 0.25 to match past tests done with LALInference. Using the Bilby default sampler settings for a 15-dimensional problem, we test if we correctly recover the posterior distribution by drawing samples from this 15-dimensional likelihood and comparing the obtained means and standard deviations to the true values. Additionally, we verify that we recover the expected evidence within the estimated error. Since the likelihood distribution is normalized and we use uniform priors for each parameter in the range $[-5, 5]$, the evidence can be approximated by the prior volume, since the standard deviations are small enough that the value of the likelihood evaluated at the edges of the prior is negligible:

$$\ln \mathcal{Z} \approx -\ln X\,, \tag{2.18}$$

where X is the prior volume. In Figure 2.11 on the left hand side we find the measured standard deviations and the evidence to be in broad agreement with analytical expectations. While the evidence errors quoted by dynesty are not truly Gaussian, the one-sigma credible interval is consistent with covering the true evidence 68% of the time if one uses more than 1000 live points. Additionally, the overshoot at high values of the credible interval indicates that there are fewer outliers than we would for a Gaussian distribution. The top panel of Figure 2.11 demonstrates that the width of the posterior distribution is correctly recovered. We have thus shown that the dynesty implementation in Bilby has no significant issues in recovering the shape of posterior distributions and the correct evidence for this fundamental problem.
We performed the same test using a bimodal Gaussian distribution, with means separated by 8 standard deviations in each dimension. While it is more difficult to correctly sample a degenerate likelihood

surface, we still find 1000 live points sufficient to reasonably recover the evidence. Individual runs of the bimodal likelihood may produce a biased set posterior samples in favour of one of the modes over the other, which is why multiple runs should be combined. We verified that none of the modes is preferred if we use all 100 runs. Thus, there are also no substantial issues that arise in sampling multimodal distributions with Bilby.

2.6.3 *Fiducial event simulations*

We analyse two fiducial simulated signals; one binary black hole merger, and one binary neutron star merger with tides. We use a LIGO Hanford–Livingston detector network and add the simulated signals into design sensitivity Gaussian noise. For the binary black hole, we use the IMRPhenomPv2 waveform and the default 4 s prior described in Table 2.3. For the binary neutron star, we use the ROQ implementation of the IMRPhenomPv2_NRTidalv2 waveform [68] with the 128 s tidal low-spin prior. The binary black hole and neutron star systems have network optimal SNRs of 8.8 and 27.9, respectively.[14] In Table 2.2, we show the true values along with the recovered median and 90% credible interval values for each parameter. Nearly all the true parameter values for both systems are recovered within the 90% credible interval, and those that are not are consistent with deviations due to the Gaussian noise realization. Full corner plots for both simulated signals are available online [372].

2.7 Appendix B: run setting details

2.7.1 *Sampler settings*

The default sampler used by Bilby is dynesty [420], an off-the-shelf nested sampling [414] package. The first step in nested sampling is to draw N random live points from the prior. At each iteration, the lowest-likelihood sample from the initial N points is discarded in favour of a higher-likelihood point, again randomly chosen from the prior. After every step, the actively-sampled region of the prior shrinks to the volume contained by the hyperplane of constant minimum likelihood for the current population of live points. When the live domain has reduced sufficiently, it becomes inefficient to select higher-likelihood points uniformly from the restricted prior space.
After the uniform sampling becomes sufficiently inefficient, new points are selected by randomly walking using a custom Markov-chain Monte Carlo algorithm starting from the sample being replaced. The transition probability is determined by the distribution

14 The binary black hole analysis was performed using Bilby version 0.6.3, while the neutron star analysis used Bilby 1.0.0. The default Advanced LIGO design PSD changed between these two versions of Bilby to reflect the updated detector sensitivity predictions [29]. Parameter estimation is performed using dynesty with the default settings.

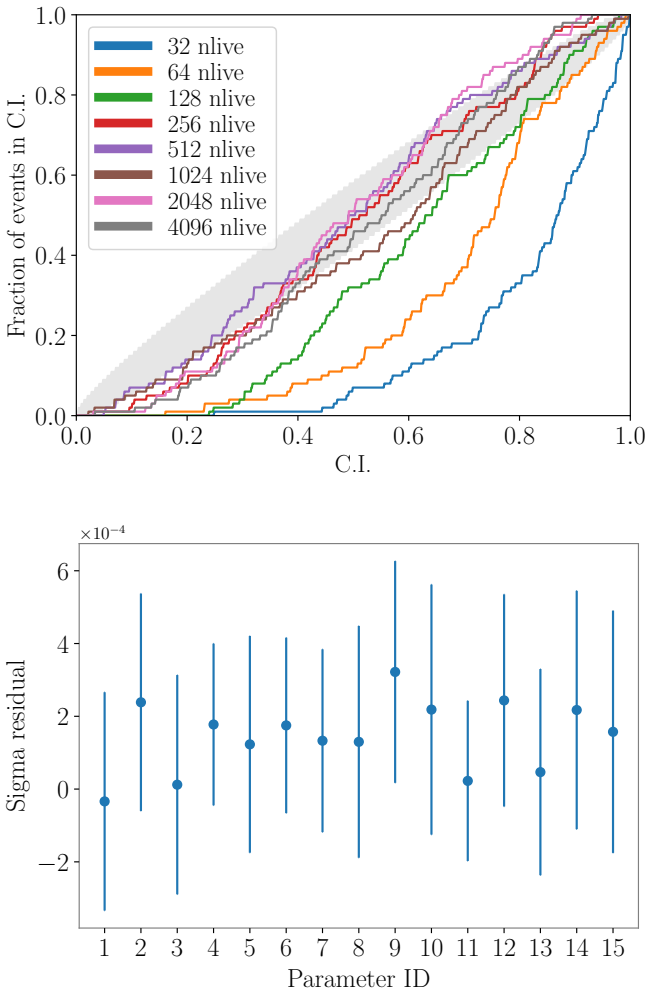

Figure 2.11: Top: Illustration of the frequency with which the true evidence is within a given credible interval for the unimodal Gaussian-shaped likelihood. The legend shows how many live points are used to produce the individual curves. For lower number of live points, systematic errors in the evidence estimation cause significant underestimates of the error. Starting at 1024 live points, the evidence error reasonably reflects the true uncertainty. The grey band shows the 90% confidence interval. Bottom: Residuals of the true width of the analytical likelihood minus the average recovered one for 1024 live points in each dimension based on 100 independent runs. The error bars show the 90% confidence interval of the average mean of the distribution. There is a small $\mathcal{O}(0.1\%)$ systematic bias to underestimate the width, i.e. the parameter is on average slighty overconstrained. However, this bias is negligibly small compared to stochastic sampling uncertainties for individual runs.

Table 2.2: Our injected and recovered values for the two fiducial event analyses. Recovered median values are quoted with the symmetric 90% credible interval around the median.

	BBH		BNS	
Parameter	Inject	Recover	Inject	Recover
$\mathcal{M}/\mathrm{M}_\odot$	15.53	$15.4^{+0.3}_{-0.4}$	1.486	$1.486^{+0.0001}_{-0.0001}$
q	0.52	$0.7^{+0.3}_{-0.4}$	0.9	$0.9^{+0.1}_{-0.2}$
a_1	0.65	$0.6^{+0.3}_{-0.5}$	0.04	$0.02^{+0.02}_{-0.02}$
a_2	0.65	$0.5^{+0.4}_{-0.4}$	0.01	$0.02^{+0.02}_{-0.02}$
θ_1	1.24	$1.1^{+0.8}_{-0.6}$	1.03	$1.5^{+1.0}_{-0.9}$
θ_2	0.80	$1.3^{+1.1}_{-0.9}$	2.17	$1.6^{+1.0}_{-1.0}$
ϕ_{12}	1.5	$3.1^{+2.9}_{-2.8}$	5.10	$3.2^{+2.8}_{-2.9}$
ϕ_{JL}	3.01	$3.2^{+2.8}_{-2.9}$	2.52	$3.1^{+2.9}_{-2.8}$
$d_\mathrm{L}/\mathrm{Mpc}$	614	1018^{+1147}_{-623}	100	86^{+17}_{-26}
δ	1.00	$0.7^{+0.4}_{-1.6}$	0.2	$0.3^{+0.1}_{-0.1}$
α	2.00	$4.6^{+1.0}_{-2.7}$	3.95	$3.9^{+0.1}_{-0.1}$
θ_{JN}	1.65	$1.8^{+1.0}_{-0.8}$	0.25	$0.6^{+0.7}_{-0.4}$
ψ	1.50	$1.6^{+1.4}_{-1.4}$	2.70	$1.5^{+1.5}_{-1.4}$
ϕ	2.00	$3.1^{+2.8}_{-2.8}$	3.69	$3.1^{+2.8}_{-2.8}$
$t_\mathrm{geo}/\mathrm{s}$	0.04	$0.04^{+0.00}_{-0.02}$	-0.01	$-0.01^{+0.00}_{-0.00}$
Λ_1	–	–	1500	752^{+915}_{-657}
Λ_2	–	–	750	1437^{+1294}_{-1216}

of the set of current live points. The number of steps taken in the chain is determined such that the length of the chain is at least some multiple $n_{\rm act}$ of the auto-correlation length of the chain [419]. For the analysis in this paper, we require $n_{\rm act} = 10$. A Markov-chain Monte Carlo walker algorithm then takes at least n steps to draw a new sample from the restricted prior. In order to reduce bottlenecks while using multiprocessing we impose a maximum length of the chain. If no point with a higher likelihood than the original point is found within this number of steps, we return a random point from the prior distribution. Nested sampling is able to well-resolve multimodal distributions, making it useful for exploring complicated parameter spaces. For all events in GWTC-1, we give the sampler $N = 2000$ live points and $n = 100$ steps.

Table 2.3: Lower and upper limits on chirp mass $\mathcal{M}$, luminosity distance d_L and dimensionless spin magnitude a_1, a_2 priors for each of the default prior sets contained in BILBY_PIPE.

Prior	$\mathcal{M}/M_\odot$	d_L/Mpc	a_1, a_2
High-mass	25–175	100–7000	0–0.99
4 s	12.299703–45	100–5000	0–0.88
8 s	7.932707–14.759644	100–5000	0–0.8
16 s	5.141979–9.519249	100–4000	0–0.8
32 s	3.346569–6.170374	100–3000	0–0.8
64 s	2.184345–4.015883	20–2000	0–0.8
128 s	1.420599–2.602169	1–500	0–0.8
128 s tidal	1.485–1.49	1–300	0–0.89
128 s tidal low-spin	1.485–1.49	1–300	0–0.05

Table 2.4: Default prior settings for 10 of the 17 parameters studied for CBCs observed with gravitational waves. The settings given in this table are consistent between all default prior sets contained in BILBY_PIPE.

Parameter	Shape	Limits	Boundary
q	Uniform	0.125–1	–
θ_1, θ_2	Sinusoidal	0–π	–
ϕ_{12}, ϕ_{JL}	Uniform	0–2π	Periodic
θ_{JN}	Sinusoidal	0–π	–
ψ	Uniform	0–π	Periodic
ϕ	Uniform	0–2π	Periodic
α	Uniform	0–2π	Periodic
δ	Cosinusoidal	$-\pi/2$–$\pi/2$	–

2.7.2 *Priors*

We sample directly in $\mathcal{M}$ and q to avoid issues associated with sampling extremely thin regions of parameter space, which occurs when sampling in component masses (BILBY and BILBY_PIPE can easily be made to sample in other parameters such as component masses; here we only discuss default parameters and priors used for analysis of the eleven events in GWTC-1). Our prior on mass ratio is uniform in the range $0.125 \leq q \leq 1.0$, with the lower limit determined due to limitations of the IMRPHENOMPV2 ROQ.
Prior limits used for $\mathcal{M}$, d_L, a_1 and a_2 are provided in Table 2.3. The chirp mass prior limits are based on those stated in the ROQ git repository.[6] We use a luminosity distance prior that is uniform in the source frame, with limits motivated by the scaling of gravitational-wave amplitude with both chirp mass and distance. The uniform-in-source-frame prior, which indicates a uniform distribution

Table 2.5: GPS trigger time and data segment duration used for each event. By default, the data segment is positioned such that there are 2 s of data after the trigger time.

Event	GPS trigger time t_{trig}/s	Data duration T/s
GW150914	1126259462.391	8
GW151012	1128678900.400	8
GW151226	1135136350.600	8
GW170104	1167559936.600	4
GW170608	1180922494.500	16
GW170729	1185389807.300	4
GW170809	1186302519.700	4
GW170814	1186741861.500	4
GW170817	1187008882.430	128
GW170818	1187058327.100	4
GW170823	1187529256.500	4

of mergers in our Universe [345], differs from the d_{L}^2 power-law prior used in the LALINFERENCE analyses, which indicates a uniform distribution in a Euclidean, non-expanding universe. We use dimensionless component spin priors that are uniform between 0 and an upper limit that is determined by the mass range assumed. For non-tidal waveform models, we use an upper limit that is either 0.8, 0.88 or 0.99. For tidal approximants, both a low-spin and a high-spin prior are available. Our component spin prior upper limits are 0.05 (low-spin) and 0.89 (high-spin) in these cases. The upper limits on spin magnitude are determined by the training range of the ROQ basis [e.g., 418]. For analysis of binary neutron star coalescence signal GW170817, we sample in the dimensionless tidal parameters Λ_1 and Λ_2, which describe the deformability of the primary and secondary masses. If $\Lambda_i = 0$, the neutron star is non-deformable and thus has no tides. We set our priors on Λ_1 and Λ_2 to be uniform between 0 and 5000 to reflect our ignorance of the neutron star equation of state. The remainder of our priors are standard and geometrically motivated.

2.7.3 *Data*

The data segments we use are accessed using the GWPY [294] method TIMESERIES.GET(CHANNEL_NAME, START_TIME, END_TIME). The START_TIME t_{start} and END_TIME t_{end} are defined relative to the TRIGGER_TIME t_{trig} of each event, such that

$$t_{\mathrm{end}} = t_{\mathrm{trig}} + t_{\mathrm{post-trig}}; \quad t_{\mathrm{start}} = t_{\mathrm{end}} - T. \tag{2.19}$$

Here T is the total duration of the data segment and $t_{\mathrm{post-tri}}$ is the post-trigger duration, which is 2 s in BILBY by default. We provide the trigger times and data segment durations for all GWTC-1 events in Table 2.5. The CHANNEL_NAME used to obtain strain data from both

the LIGO Hanford and LIGO Livingston detectors is DCS-CALIB_STRAIN_C02 for all events, with the exception of GW170817, for which we use the CHANNEL_NAME of DCH-CLEAN_STRAIN_C02_T1700406_v3 to obtain glitch-subtracted strain data from LIGO Livingston. We also obtain Virgo data for events that occurred from July until mid-August 2017 (GW170729, GW170809, GW170814, GW170817 and GW170818) using the CHANNEL_NAME of HREC_HOFT_V1O2REPRO2A_16384HZ.
Strain data is available from the Gravitational Wave Open Science Centre [36] sampled at both 16384 Hz (the native sampling frequency of advanced LIGO and advanced Virgo) and down-sampled to 4096 Hz. We download the data sampled at 16384 Hz. The LALINFERENCE [272] analysis of binary black holes in [30] was performed with data down-sampled to 2048 Hz using a LAL down-sampling function and integrated to the Nyquist frequency (1024 Hz).
In BILBY_PIPE the user can choose to either not down-sample, down-sample using the same LAL routine as done in LALINFERENCE and BAYESWAVE [118], or down-sample using the GWPY method. In general, we recommend users do not down-sample the time domain data, but rather apply cuts directly in the frequency domain. However, since the PSDs used in this analysis were made with BAYESWAVE and the LALINFERENCE analysis we compare with use the LAL down-sampling, we also use this method.
The default method implemented in LAL and used by LALINFERENCE and BAYESWAVE is done in the time domain and consists of two stages. First the data are low-passed using a 20th-order zero-phase Butterworth filter. The filter is customised such that the power at the low-pass frequency f_c is reduced by a factor of ten. The frequency response of the filter is given by

$$R(f; f_c, n, a_c) = \left[1 + \left(a_c^{-1/2} - 1\right)\left(\frac{f}{f_c}\right)^{2n}\right]^{-1}. \tag{2.20}$$

The data are then down-sampled by a factor of N by taking every Nth sample, this aliases the data. This aliasing means that any signal close to the new Nyquist frequency will be suppressed and aliased which may introduce a bias in our inference. The final frequency domain strain after downsampling by a factor of N is given by

$$\begin{aligned}\bar{h}(f; f_c, n, a_c) = h(f)R(f; f_c, n, a_c) \\ + \sum_{i=\mathrm{odd}}^{N} h((i+1)f_c - f)R((i+1)f_c - f; f_c, n, a_c) \\ + \sum_{i=\mathrm{even}}^{N} h(if_c + f)R(if_c + f; f_c, n, a_c).\end{aligned} \tag{2.21}$$

Here $h(f)$ is the frequency-domain data without low-pass filtering or downsampling. Of the events analysed in this work, the lowest mass events (GW151226, GW170608, and GW170817) have frequency content close to or above the down-sampled Nyquist frequency. We expect the bias introduced by this to be small.

In Figure 2.12 we show the data containing GW170608 along with the PSD produced by BayesWave with (top) and without (bottom) downsampling the data to a new sampling rate of 2048 Hz for the LIGO Livingston observatory. In the bottom panel we can see the turnover in the data and the PSD close to the new Nyquist frequency 1024 Hz.

2.8 Appendix C: Prior reweighting

In order to compare posterior samples that are unbiased by differing prior choices, we reweight samples obtained using LALInference priors $\pi_{\rm LI}$ by Bilby default priors $\pi_{\rm B}$, with weights expressed as

$$\mathcal{W} = \frac{\pi_{\rm B}}{\pi_{\rm LI}}. \tag{2.22}$$

We must also account for the fact that bilby_pipe uses default priors that are flat in $\mathcal{M}$ and q, whereas LALInference uses priors that are uniform in component masses. We therefore rejection sample from the released posterior samples with weights given by the inverse of the Jacobian given in Eq. (21) of Veitch et al. [456],

$$\mathcal{J} = \frac{\mathcal{M}}{m_1^2}. \tag{2.23}$$

The complete reweighting procedure can be written

$$p_{\pi_{\rm B}} = \mathcal{W}\mathcal{J}p_{\pi_{\rm LI}}, \tag{2.24}$$

where $p_{\pi_{\rm B}}$ and $p_{\pi_{\rm LI}}$ are the posterior probabilities computed using Bilby and LALInference priors, respectively. In practice, we reweight by rejection sampling in order to preserve the independence of samples. We also account for a difference in the definition of the Solar mass $\mathrm{M}_\odot$ between the current version of Bilby and the version of LALInference used to produce the public GWTC-1 samples that we compare against.

2.9 Appendix D: CDF comparisons for GWTC-1 events

In this Appendix we present the comparisons of the CDFs obtained using Bilby and LALInference for all parameters and for all events. The legend shows the JS divergence and uncertainty for each parameter, and the shaded regions represent the 1-, 2-, and 3-σ confidence intervals.

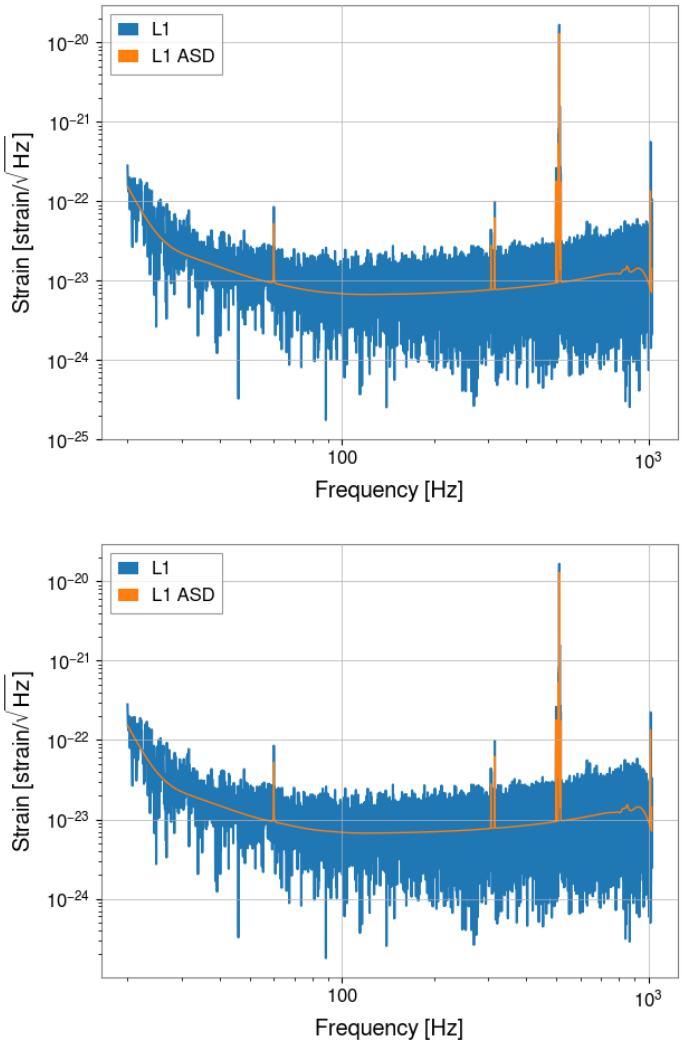

Figure 2.12: The data and PSD in the LIGO Livingston interferometer at the time of GW170608. In the upper/lower panel we show the data with/without being low-pass filtered and down-sampled to 2048 Hz. We can see the effect of the low-pass filter in suppressing the data above $\sim$ 900 Hz. The filtering and down-sampling was applied when computing the PSD and so the data in the top panel better matches the PSD.

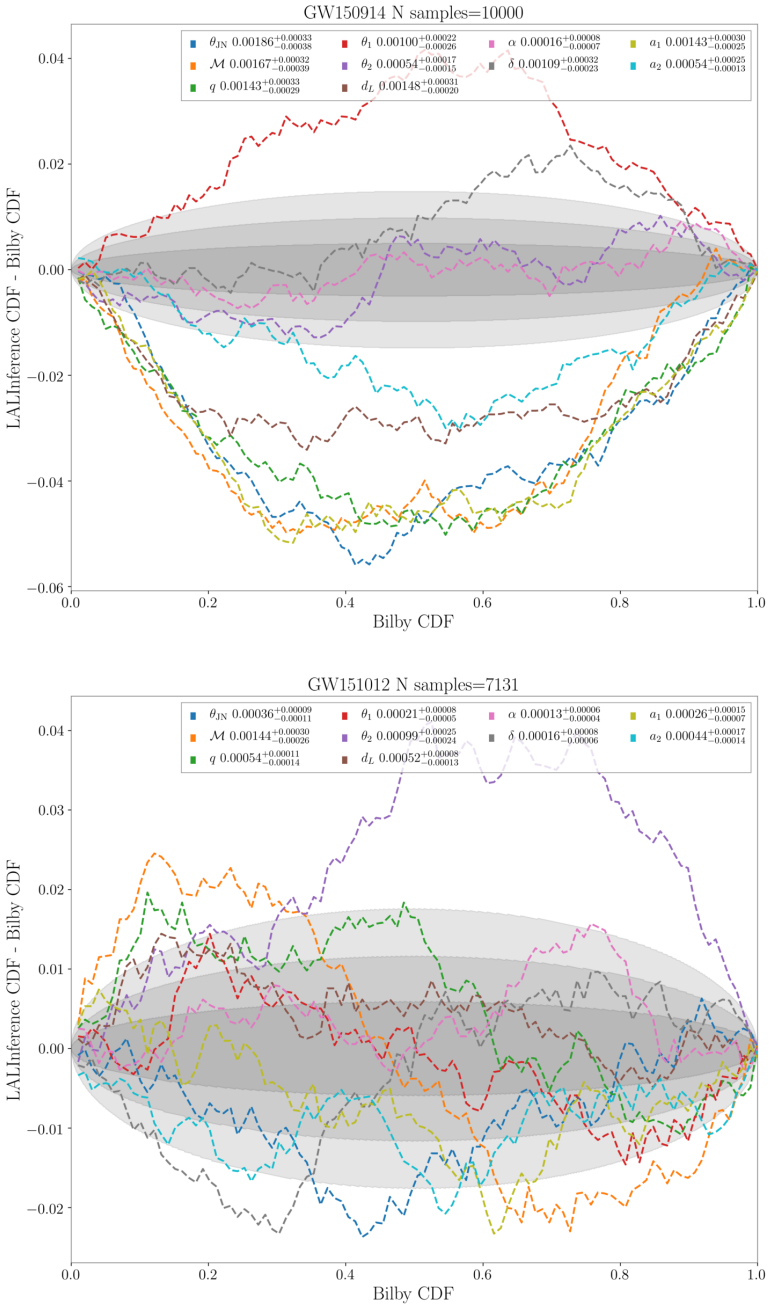

Figure 2.13: CDF comparison between Bilby and LALInference for GW150914 and GW151012.

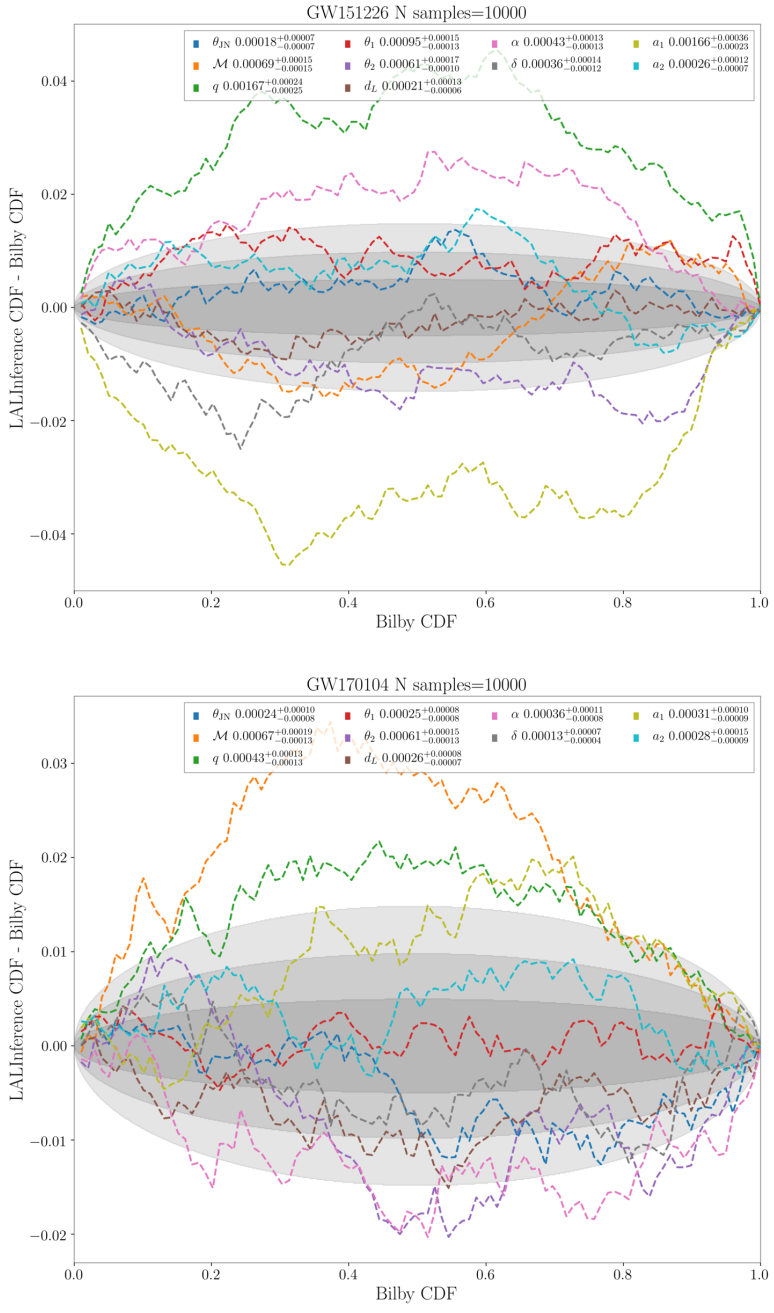

Figure 2.14: CDF comparison between BILBY and LALINFERENCE for GW151226 and GW170104.

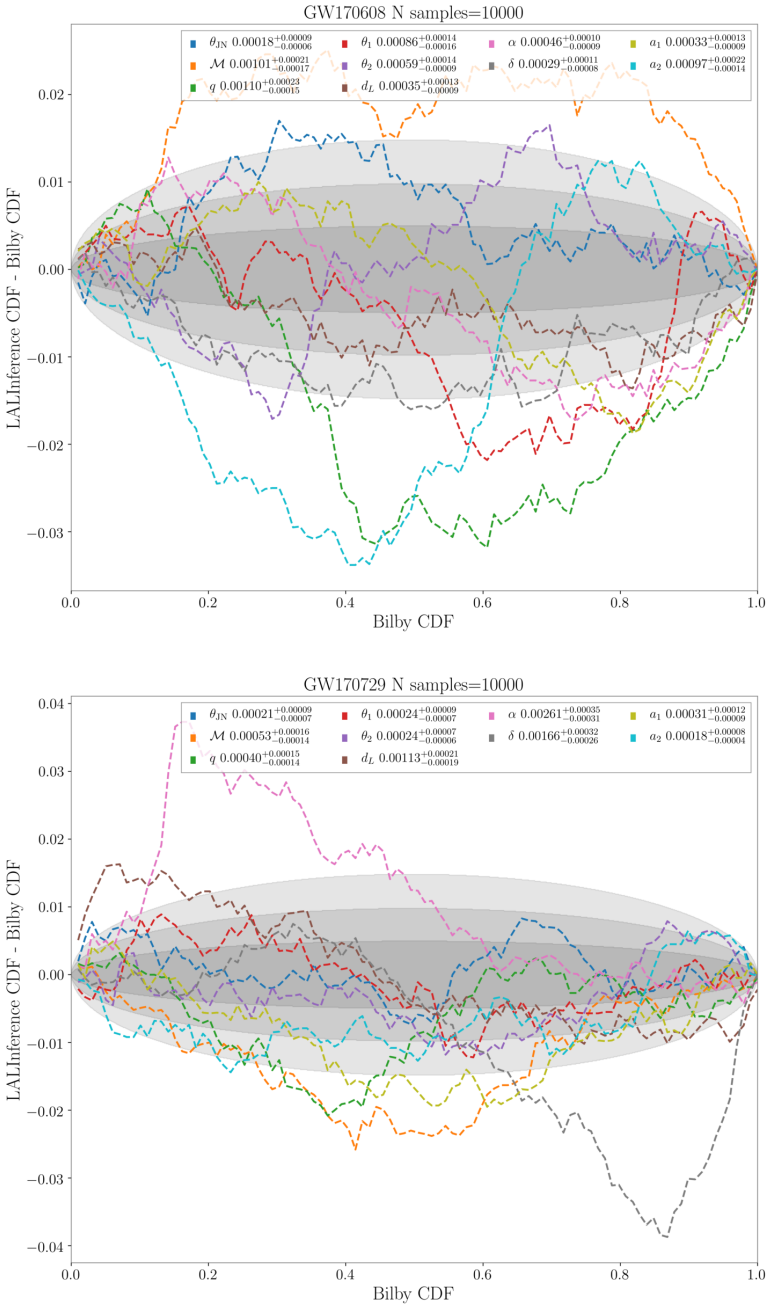

Figure 2.15: CDF comparison between Bilby and LALInference for GW170608 and GW170729.

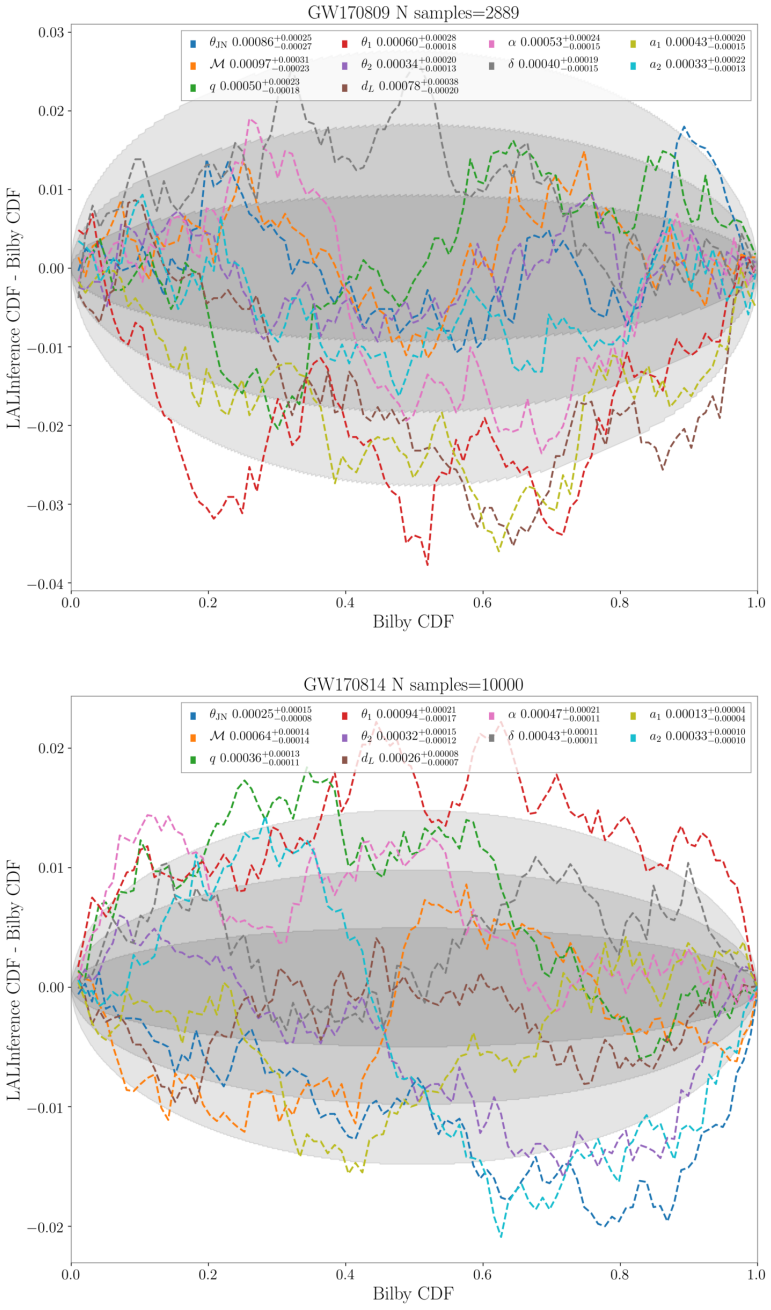

Figure 2.16: CDF comparison between Bilby and LALInference for GW170809 and GW170814.

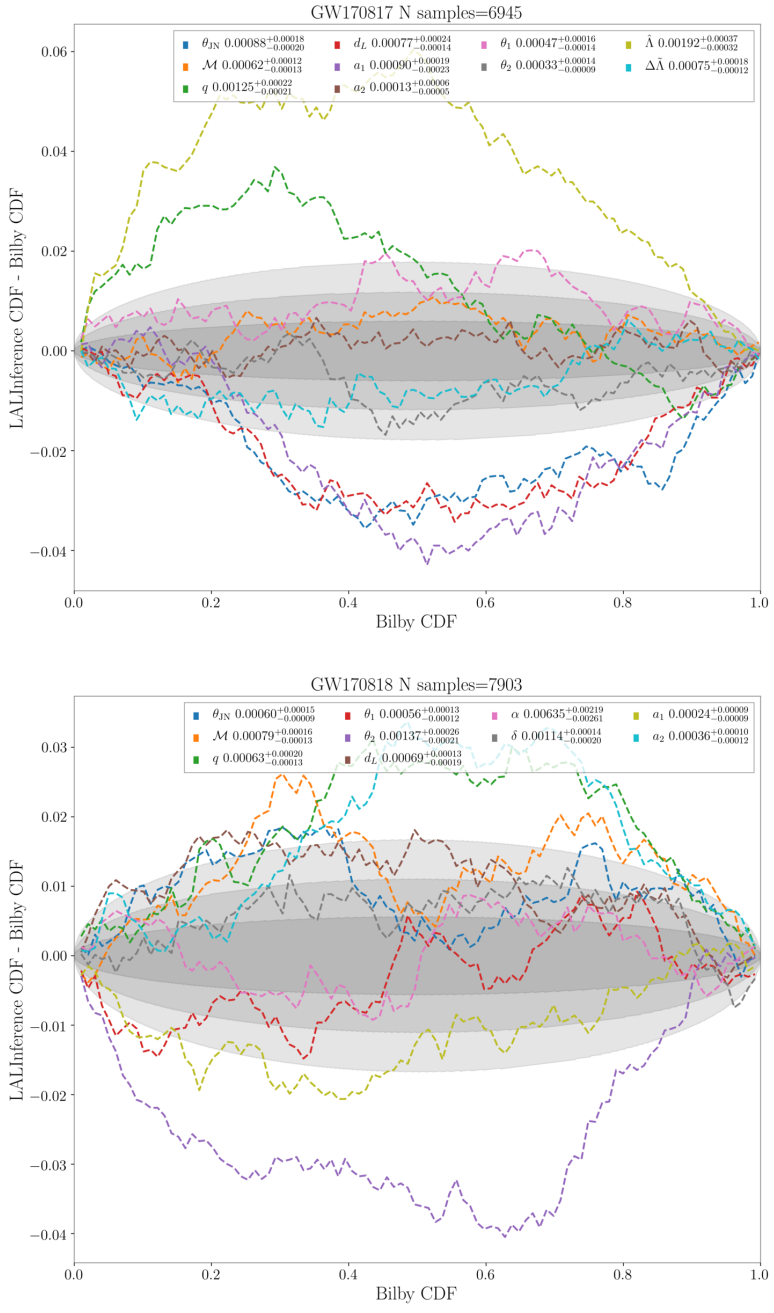

Figure 2.17: CDF comparison between Bilby and LALInference for GW170817 and GW170818.

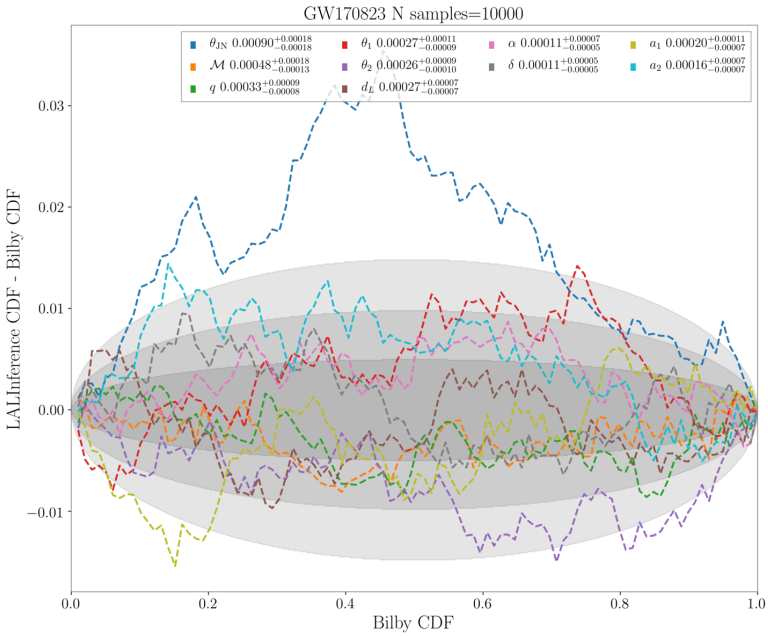

Figure 2.18: CDF comparison between Bilby and LALInference for GW170823.

2.10 APPENDIX E: PARAMETER DEFINITIONS

BILBY is able to sample in a range of different parameterisations of compact binaries. In Table 2.6, we describe the definitions of these parameters as implemented in BILBY. Unless otherwise specified all of these parameters can be sampled in, using the standard waveform model, likelihood, and conversion functions.

This sentence motivates the development of the eccentricity-reweighting technique detailed in Chapter A and utilised in Chapters 3–6.

Currently, there is a relative lack of support for sampling parameters describing eccentric orbits: the eccentricity e and the argument of periapsis ω. This is because the frequency-domain eccentric waveforms available in LALSIMULATION are less complete than their quasi-circular counterparts, containing only the inspiral section of the signal.

Table 2.6: Definition of parameters typically considered for CBC inference. Subscript $i = 1, 2$ indicates whether the parameter pertains to the primary (1) or secondary (2) binary object. Subscript $k = x, y, z$ refers to a quantity measured in the $\hat{x}$, $\hat{y}$ or $\hat{z}$ direction; $\hat{z}$ points along the binary axis of rotation, while the $\hat{x}$, $\hat{y}$ directions are orthogonal to each other and $\hat{z}$, defined at reference phase ϕ, and differ by phase offset ϕ_{12} between the two objects.

Parameter	Label	Units
Detector-frame (redshifted) mass of the ith object	m_i	$\mathrm{M}_\odot$
Detector-frame chirp mass $\mathcal{M} = (m_1 m_2)^{3/5}/(m_1 + m_2)^{1/5}$ [86, 164, 346]	$\mathcal{M}$	$\mathrm{M}_\odot$
Detector-frame combined mass of the primary and secondary masses	M	$\mathrm{M}_\odot$
The ratio of the secondary and primary masses $q = m_2/m_1 \leq 1$	q	–
A definition of mass ratio which is independent of the identity of the primary/secondary $\eta = q/(1+q)^2$	η	–
Source-frame mass of the ith object $m_i^{\mathrm{source}} = m_i/(1+z)$ [266]	m_i^{source}	$\mathrm{M}_\odot$
Source-frame chirp mass $\mathcal{M}^{\mathrm{source}} = \mathcal{M}/(1+z)$	$\mathcal{M}^{\mathrm{source}}$	$\mathrm{M}_\odot$
Source-frame total mass $M^{\mathrm{source}} = M/(1+z)$	M^{source}	$\mathrm{M}_\odot$
Dimensionless spin magnitude of the ith object	a_i	–
Zenith angle between the spin and orbital angular momenta for the ith object	θ_i	rad
Cosine of the zenith angle between the spin and orbital angular momenta for the ith object	$\cos\theta_i$	–
Difference between total and orbital angular momentum azimuthal angles	ϕ_{JL}	rad

Difference between the azimuthal angles of the individual spin vector projections onto the orbital plane	ϕ_{12}	rad
ith object aligned spin: projection of the ith object spin onto the orbital angular momentum $\chi_i = a_i \cos(\theta_i)$	χ_i	–
ith object in-plane spin: magnitude of the projection of the ith object spin onto the orbital plane $\chi_i^\perp = \lvert a_i \sin(\theta_i)\rvert$	$\chi_i^\perp$	–
Effective inspiral spin parameter $\chi_{\rm eff} = (\chi_1 + q\chi_2)/(1+q)$ [40, 398]	$\chi_{\rm eff}$	–
Effective precession spin parameter $\chi_p = \max\{\chi_1^\perp, q(3q+4)/(4q+3)\chi_2^\perp\}$ [214, 403]	χ_p	–
kth component of ith object spin in Euclidean coordinates	$S_{i,k}$	–
Dimensionless tidal deformability of the ith object	Λ_i	–
Combined dimensionless tidal deformability [157, 169]	$\tilde{\Lambda}$	–
Relative difference in the combined tidal deformability [157, 469]	$\delta\tilde{\Lambda}$	–
Orbital eccentricity defined at a reference frequency	e	–
The angle between the secondary mass and the ascending node of the orbit when the secondary mass is at periapsis	ω	rad
Right ascension	α	rad
Declination	δ	rad
Zenith angle in the detector-based sky parameterisation	κ	rad
Azimuthal angle in the detector-based sky parameterisation	ϵ	rad
Luminosity distance to the source	$d_{\rm L}$	Mpc
Comoving distance depending on specified cosmology	$d_{\rm C}$	Mpc
Redshift depending on specified cosmology	z	–
GPS reference time at the geocenter, typically merger time	$t_{\rm c}$	s
GPS reference time at the detector with name IFO, e.g., H1_time, typically merger time	$t_{\rm IFO}$	s
Shift to apply for time array used in time marginalization	δt	s
Polarization angle of the source	ψ	rad
Binary phase at a reference frequency	ϕ	rad

Zenith angle between the total angular momentum and the line of sight	θ_{JN}	rad
Cosine of the zenith angle between the total angular momentum and the line of sight	$\cos\theta_{JN}$	–
Zenith angle between the orbital angular momentum and the line of sight	ι	rad
Cosine of the zenith angle between the orbital angular momentum and the line of sight	$\cos\iota$	–

Part III

MEASURING THE ORBITAL ECCENTRICITY OF MERGING BINARY COMPACT OBJECTS

3

SEARCHING FOR ECCENTRICITY: SIGNATURES OF DYNAMICAL FORMATION IN THE FIRST GRAVITATIONAL-WAVE TRANSIENT CATALOGUE OF LIGO AND VIRGO

This Chapter was originally published as [376].

ABSTRACT

Binary black holes are thought to form primarily via two channels: isolated evolution and dynamical formation. The component masses, spins, and eccentricity of a binary black hole system provide clues to its formation history. We focus on eccentricity, which can be a signature of dynamical formation. Employing the spin-aligned eccentric waveform model SEOBNRE, we perform Bayesian inference to measure the eccentricity of binary black hole merger events in the first Gravitational-Wave Transient Catalogue of LIGO and Virgo. We find that all of these events are consistent with zero eccentricity. We set upper limits on eccentricity ranging from 0.02 to 0.05 with 90% credibility at a reference frequency of 10 Hz. These upper limits do not significantly constrain the fraction of LIGO-Virgo events formed dynamically in globular clusters, because only $\sim 5\%$ are expected to merge with measurable eccentricity. However, with the Gravitational-Wave Transient Catalogue set to expand dramatically over the coming months, it may soon be possible to significantly constrain the fraction of mergers taking place in globular clusters using eccentricity measurements.

3.1 INTRODUCTION

The first Gravitational-Wave Transient Catalogue (GWTC-1) of Advanced LIGO [29] and Virgo [39] records eleven gravitational-wave signals, each of which was produced by the coalescence of compact stellar remnants [30]. The question of how these binaries formed has become paramount. With perhaps $\mathcal{O}(100)$ events expected following the third observing run of Advanced LIGO and Virgo, we are rapidly accumulating the data required to answer this question.
It is challenging to explain how compact binaries form with separations small enough to merge within the age of the Universe. Most viable scenarios fall into two categories: *isolated binary evolution* and *dynamical formation*. The two categories are distinguishable because the formation history of a binary is imprinted on its component masses, component spins, and eccentricity. These binary parameters can be probed using gravitational waves. In this paper, we

make steps towards identifying the formation channels of binary black hole mergers in GWTC-1 using measurements of eccentricity. The isolated evolution scenario begins with a binary star system. In order to merge within the age of the Universe, the stars must be extremely close; two $\sim 10\,M_\odot$ compact objects in a quasi-circular orbit must have a separation less than ~ 0.1 AU to merge within ~ 14 Gyr [105]. Normal stellar evolution prevents binary compact object formation at such small distances since stars expand and consume nearby companions as they age. A number of processes have been proposed to avoid this problem. The common envelope hypothesis allows the binary components to co-evolve within the extended gas structure of one expanded star (see, e.g., Bethe and Brown [78], Ivanova et al. [239], Kruckow et al. [267], and Livio and Soker [290]). The chemically homogeneous pathway bypasses the expansion problem, with both stars remaining relatively compact throughout their entire evolution [313, 498]. Ambient gas-driven fallback has also been suggested to harden initially distant binaries [432].
In the dynamical formation case, the merger progenitors do not encounter each other until they are already compact objects. Binaries assemble through encounters in dense environments, such as young star clusters, globular clusters and galactic nuclei; see, e.g., Sigurdsson and Hernquist [407] and Portegies Zwart and McMillan [349], plus recent works such as Fragione and Kocsis [176], Fragione and Bromberg [178], Gondán et al. [202], Morscher et al. [316], O'Leary et al. [327], Randall and Xianyu [357], Randall and Xianyu [358], Rodriguez et al. [363, 364], Samsing [389], Samsing and D'Orazio [391], Samsing et al. [393], and Samsing, MacLeod, and Ramirez-Ruiz [395] and Bouffanais et al. [89]. Binaries that form in such environments can interact frequently, and one compact object can swap in and out of many binaries before it merges with another compact object. During an interaction between a binary and a single black hole, gravitational binding energy from the incoming binary tends to be converted into the kinetic energy of whichever object leaves the interaction unbound. This leaves the resultant binary with a smaller separation than the binary that entered the interaction.
The component spins of a binary can be used to distinguish between formation channels (see, e.g., Belczynski, Kalogera, and Bulik [74], Bianchi et al. [79], Farr et al. [155], Fishbach, Holz, and Farr [166], Rodriguez et al. [370], Vitale et al. [467], and Wysocki, Lange, and O. 'shaughnessy [477]). An isolated binary is likely to be observed with component spins that align with its orbital angular momentum vector due to the co-evolution of the components [100, 423]. Dynamically-formed binaries have no spin preference, due to their chaotic interactions, so we expect them to be detected with an isotropic distribution of spin orientations (e.g., Rodriguez et al. [370] and Talbot and Thrane [436]).
The mass distribution of a merger population may give some insight into its dominant formation channel (e.g., Stevenson et al. [426], Talbot and Thrane [433], and Zevin et al. [490]). Pulsational pair instability supernovae restrict an isolated merger's total mass to

$\lesssim 80 M_\odot$ [166, 218], whilst mass segregation and runaway mergers in dense environments lead to an extended tail out to high masses for dynamical mergers [89, 194, 369].

Perhaps the most compelling evidence for dynamical binary formation, however, is eccentricity. Due to the efficient loss of energy through gravitational-wave emission, long-lived binaries circularise rapidly, so we expect binaries from this channel to have negligible eccentricities when they enter the LIGO-Virgo band at $\sim 10\,\mathrm{Hz}$ [223, 343].

Dynamically-formed binaries can have a wide range of eccentricities at 10 Hz, with some having eccentricities close to unity [203, 363, 393, 490, 492]. These systems go from formation to merger much faster than their isolated counterparts — fast enough to retain significant orbital eccentricity when the gravitational-wave frequency reaches 10 Hz. By studying the spin, mass, and eccentricity distributions of the mergers we detect with gravitational waves, we can build a concordant picture of compact binary formation. It is possible for Kozai-Lidov resonance [263, 282] to drive up the eccentricity of binaries within hierarchical field triples [51, 166, 182, 288, 365, 409] and quadruples [181, 287], leading them to merge with eccentricity and spin distributions similar to those expected for dynamical mergers. The fraction of mergers from Kozai-Lidov resonance in the field is highly uncertain, although it is expected to be small unless natal kicks and/or environment metallicities are low [51, 182, 288, 365, 409].

Whilst compact binaries with negligible eccentricity near merger can form by either channel, a single event with significant eccentricity ($e \gtrsim 0.1$) would provide a strong argument for dynamical formation. Furthermore, the eccentricity of a binary can indicate which subset of dynamically-formed binaries it belongs to. Dynamically-formed binaries that are ejected from their host cluster are expected to circularise in the field, eventually reaching $e \sim 10^{-6}$ at 10 Hz [364]. Compact objects that remain in the dense cluster core may form triples and quadruples, which can experience chaotic resonant interactions [47, 363, 364, 393, 474]. Binaries that harden during such interactions can merge before their next strong encounter, and have an eccentricity distribution that peaks at $e \sim 10^{-4}$ at 10 Hz [363, 364, 492]. During a close dynamical encounter between two compact objects in a globular cluster, the strong loss of gravitational energy at periapsis can lead to a gravitational-wave capture merger. In the simulations of Samsing [389], Rodriguez et al. [364] and Rodriguez et al. [363], this kind of binary enters the LIGO-Virgo band with $10^{-3} \lesssim e \lesssim 1$. These simulations suggest that we can expect $\sim 5\%$ of dynamically-formed binaries to have $e \geq 0.1$ at 10 Hz, a prediction that is thought to be relatively robust to the assumptions of the globular cluster model. The largest values of eccentricity, $e \sim 1$, are obtained when a binary forms with a gravitational-wave frequency already greater than $\sim 10\,\mathrm{Hz}$. Lower et al. [291] carried out Bayesian inference on simulated gravitational-wave data using an eccentric waveform template, improving upon the Fisher-matrix-type approach demonstrated by

Gondán et al. [201]. The former study found that GW150914-like events with eccentricities $\gtrsim 0.05$ at 10 Hz could be distinguished from quasi-circular events using an Advanced LIGO and Virgo detector network at design sensitivity. However, the EccentricFD [233] waveform used to obtain these results models only the inspiral, leaving out merger physics. This waveform also neglects spin effects. Additionally, this analysis was not applied to real data. Abbott et al. [31] conducted an unmodelled search on real data from Advanced LIGO's first two observing runs. No candidate events were observed (beyond the binaries previously described using quasicircular templates in GWTC-1). Moreover, the search in [31] is unable to provide a measurement of eccentricity.
In this work, we present the first measurements of eccentricity for binary events detected by Advanced LIGO and Virgo. Using spin-aligned waveforms with inspiral, merger, and ringdown, we construct posterior distributions for eccentricity for ten binary black hole merger events. In order to reduce the computational resources required to perform the computationally intensive analysis, we employ a "likelihood reweighting technique" from [341] that enables us to introduce an extra parameter, eccentricity, in post-processing. We find that all of the events in GWTC-1 are consistent with zero eccentricity. We obtain event-specific upper limits at 90% credibility ranging from 0.024 to 0.054 at a reference frequency of 10 Hz.
The remainder of this paper is structured as follows. We outline our analysis methods, including our Bayesian inference approach and post-processing procedure, in Section 3.2. We validate our methodology with an injection study in Section 3.3. We present our results in Section 3.4, and discuss these results in the context of dynamical binary formation in Section 3.5.

3.2 Method

Aligned-spin gravitational waveform models usually depend on eleven parameters: four intrinsic (component masses and spins) and seven extrinsic (e.g., luminosity distance and binary inclination angle). Including eccentricity increases the number of dimensions to twelve. The additional variable is the eccentricity, e, at some reference frequency, which we choose to be 10 Hz. The gravitational energy released by an eccentric binary at periapsis is greater than that released at apoapsis, so non-zero eccentricity modulates the gravitational-wave signal. The effect of a small binary eccentricity of 0.1 is shown in Figure 3.1.
For non-precessing systems, the gravitational waveform depends only trivially on the argument of periapsis because it can be absorbed into the phase of coalescence. The situation is more complicated for precessing binaries, but since none of the events in GWTC-1 exhibit clear signs of precession, the effect of precession is likely to be small for published LIGO-Virgo binaries. At present, there are not publicly available gravitational waveform approximants for eccentric binaries

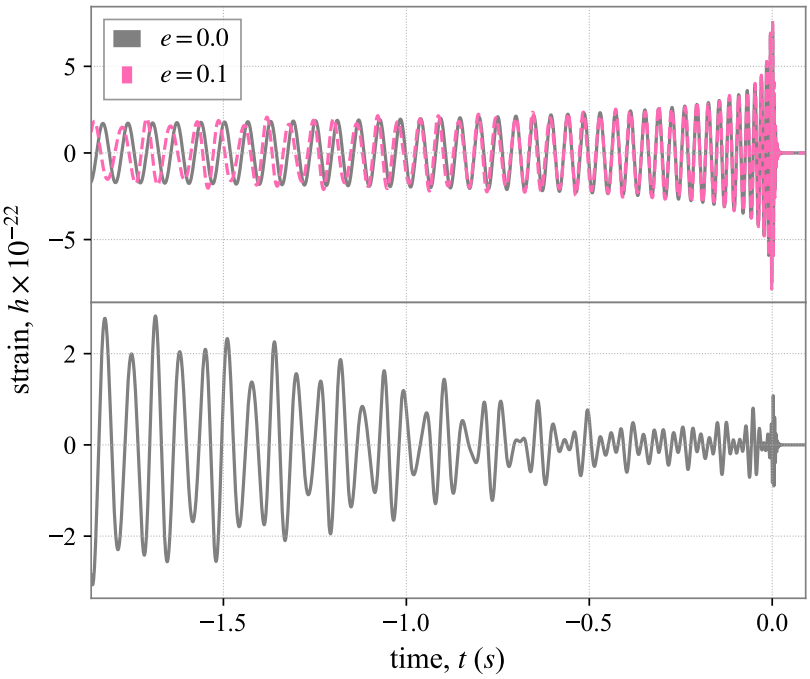

Figure 3.1: TOP: Gravitational waveforms with eccentricities $e = 0.0$ (solid grey) and $e = 0.1$ (dashed pink) at 10 Hz for a GW150914-like signal. The inclusion of a small eccentricity introduces a slight amplitude and phase modulation, which is most prominent in the early inspiral. BOTTOM: The difference between the quasi-circular and eccentric waveforms as a function of time.

that include precession, although new waveforms are under development; see, for example, Tiwari et al. [445].

We use Bayesian inference to measure the parameters describing the binary. The posterior probability, $p(\theta|d)$, describes the probability that the model with source parameters θ is responsible for data d. The posterior is the product of the likelihood of d occurring if the source model is described by θ, $\mathcal{L}(d|\theta)$, and our prior knowledge of the probability of θ occurring at all, $\pi(\theta)$. Normalising by the model evidence, $\mathcal{Z} = \int d\theta \mathcal{L}(d|\theta)\pi(\theta)$, we can write the posterior probability as

$$p(\theta|d) = \frac{\mathcal{L}(d|\theta)\pi(\theta)}{\mathcal{Z}}. \tag{3.1}$$

We use nested sampling, introduced by Skilling [414] and popular for gravitational-wave data analysis due to its handling of high-dimensional spaces [456]. For a thorough review of Bayesian inference in the context of gravitational-wave astrophysics, see Thrane and Talbot [444].

Our gravitational-wave transient likelihood $\mathcal{L}(d|\theta)$ is of the form

$$\mathcal{L}(d|\theta) = \frac{1}{2\pi\sigma^2} \exp\left(-\frac{1}{2}\frac{(d-\mu(\theta))^2}{\sigma^2}\right), \tag{3.2}$$

where μ is our waveform template and σ is the detector noise amplitude spectral density[1]. We assume Gaussian noise, using the noise power spectral densities σ^2 that were used to produce the GWTC-1 results. We neglect calibration uncertainty. We generate μ using SEOBNRE [103], an effective one-body numerical-relativity waveform model which can produce non-circular waveforms with eccentricities in the range $0 \leq e \leq 0.2$ at 10 Hz. The SEOBNRE waveform model incorporates more complex physics than the waveform used in Lower et al. [291]. It includes aligned dimensionless component spin magnitudes between -1 and 0.6, and models the merger and ringdown in addition to the inspiral.

SEOBNRE *stands for "Spin-aligned Effective-One-Body Numerical Relativity with Eccentricity".*

We carry out Bayesian inference with BILBY [54], using DYNESTY [420] as our nested sampler. We use the publicly available strain data associated with the ten binary black hole events in GWTC-1. We implement the same priors as used in GWTC-1 for almost all parameters. The exceptions are eccentricity, which is not included in GWTC-1, and aligned dimensionless component spins, which are only supported in SEOBNRE between -1 and 0.6. Our prior on eccentricity is uniform in $\log_{10}(e)$ in the range $-6 \leq \log_{10}(e) \leq -0.7$. Our aligned dimensionless component spin prior is uniform between -0.6 and 0.6. Our prior boundaries for cyclic parameters (e.g. coalescence phase, right ascension, declination), are periodic, whilst our priors for non-cyclic parameters (e.g. mass, distance) have reflective boundaries.

Generating a posterior probability distribution demands many thousands of likelihood calculations, each requiring waveform template evaluation. Whilst standard quasi-circular waveform models are fast enough to facilitate reasonable computation times, eccentric waveforms including merger and ringdown physics are not. SEOBNRE takes roughly a million times longer to evaluate a GW150914-like signal than aligned-spin quasi-circular waveform model IMRPHENOMD [249]. As such, SEOBNRE is infeasible to use as our waveform template within the nested sampler calculation. Instead, we do our initial analysis with IMRPHENOMD and *reweight* our results by the eccentricity-marginalised Bayesian likelihood for SEOBNRE, following the prescription of [341].

Adopting the terminology from [341], our 'proposal' likelihood $\mathcal{L}_{\text{ø}}(d|\theta)$ is obtained using the quasi-circular IMRPHENOMD waveform model denoted by $\mu_{\text{ø}}$, whilst our 'target' likelihood $\mathcal{L}(d|\theta)$ is the eccentricity-marginalised likelihood calculated using the eccentric SEOBNRE waveform denoted by μ. The ratio $\mathcal{L}/\mathcal{L}_{\text{ø}}$ provides weights, w, that are applied to our proposal posterior samples to obtain an eccentricity-marginalised posterior distribution.

The *efficiency* of reweighting is $(n_{\text{effective}}/n_{\text{samples}})$, where n_{samples} is the number of samples and

$$n_{\text{effective}} = \frac{\left(\sum_{i=1}^{n} w_i\right)^2}{\sum_{i=1}^{n} w_i^2}, \tag{3.3}$$

1 It should be noted that both d and $\mu(\theta)$ are functions of frequency, and that the notation making this explicit has been omitted for brevity. There is an implied product over frequency bins.

Table 3.1: Properties of the injected signal source.

Chirp mass $\mathcal{M}$	28.2 $M_\odot$
Mass ratio q	0.86
Luminosity distance d_L	820 Mpc
Eccentricity e	0.1
Dimensionless spin magnitude χ_1	0.0
Inclination θ_{JN}	0.4
Right ascension	1.02 radians
Declination	-0.55 radians
Phase at coalescence ϕ	3.54
Polarization angle ψ	2.44
Network signal-to-noise ρ	24.9

where w_i is the weight associated with the i^{th} sample, is the effective number of samples after reweighting [257]. The efficiency determines how well-sampled the posteriors are after reweighting, relative to the proposal posteriors. When efficiency is low, we increase the number of proposal posterior samples to ensure a sufficient number of target samples.

In order to obtain one-dimensional eccentricity posterior probability distributions, we construct a grid of 60 eccentricities, log-uniformly distributed between $\log_{10}(e) = -6$ and $\log_{10}(e) = -0.7$ at 10 Hz to match the prior. Following [341], we set the time and phase by maximising the overlap between the target and proposal waveforms. For each value of eccentricity in our grid, we compute the eccentric gravitational-wave transient likelihood using SEOBNRE. We take the average of this grid to find our eccentricity-marginalised likelihood. We then draw an eccentricity at random, weighted by the cumulative likelihood grid, and add this to the unweighted posterior distribution. Finally, we apply our array of weights, w, to this eccentricity distribution to obtain the weighted posterior probability distribution for eccentricity at 10 Hz.

The Bayes factor, $\mathcal{B}$, is a measure of how much one hypothesis is preferred over the other. It is calculated by taking the ratio of the evidences of two differing models. The circular evidence $\mathcal{L}_\circ$ is given by $\mathcal{L}(d|e=0)$. The eccentric evidence is obtained by marginalising over eccentricity,

$$\mathcal{L}_e = \int_{10^{-6}}^{0.2} de \mathcal{L}(d|e). \tag{3.4}$$

As such, the Bayes factor can be written

$$\mathcal{B} = \mathcal{L}_e / \mathcal{L}_\circ. \tag{3.5}$$

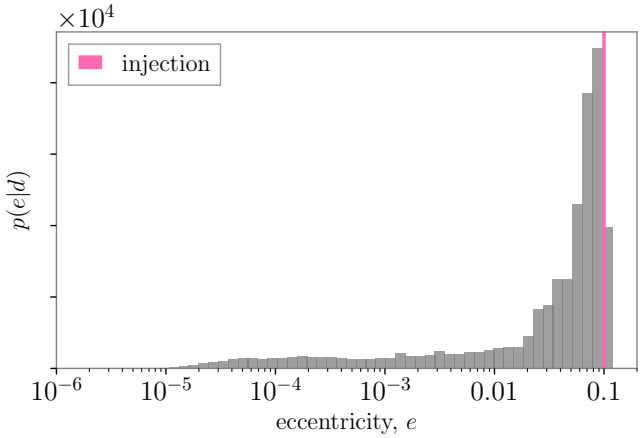

Figure 3.2: Reconstructed posterior probability distribution over eccentricity for our injected eccentric waveform, which has parameters as listed in Table 3.1. For this injection, the Bayes factor for eccentricity is $\ln \mathcal{B} = 6.99$.

3.3 INJECTION STUDY

In order to validate our methodology, we inject a signal with eccentricity $e = 0.1$ into simulated noise and recover posterior probability distributions for all parameters including eccentricity. We assume a two-observatory network consisting of LIGO Hanford and LIGO Livingston operating at design sensitivity, with a minimum frequency of 30 Hz to mimic the low-frequency noise from the first and second observing runs. The parameters of the injected waveform are provided in Table 3.1. The parameters are chosen to be GW150914-like, with an increased luminosity distance of 820 Mpc such that the network signal-to-noise $\rho \approx 25$ to match the loudest signal-to-noise ratio in the catalogue.
With reweighting, we obtain an eccentricity posterior that peaks at the injected value of $e = 0.1$. We present this posterior in Figure 3.2. As shown in Figure 3.3, our initial analysis (turquoise posteriors) successfully recovers our injected signal, whilst reweighting (grey posteriors) pushes the posteriors further towards the injected values (pink lines). A full reweighted corner plot is available online[2]. For this injection, our reweighting has an efficiency of 20% and the Bayes factor for eccentricity is $\ln \mathcal{B} = 6.99$.

3.4 RESULTS

Our analysis yields no strong evidence for non-zero eccentricity in the first Gravitational Wave Transient Catalogue of LIGO and Virgo. We plot our 90% credible upper limits on eccentricity at 10 Hz against the mean of the system's chirp mass posterior in Figure 3.4. These limits range between 0.024 for GW150914 to 0.054 for GW151012. We provide event-specific log Bayes factors $\ln \mathcal{B}$ and 90% upper credible limits on eccentricity at 10 Hz in Table 3.2. Negative values of $\ln \mathcal{B}$

2 github.com/IsobelMarguarethe/eccentric-GWTC-1/injection

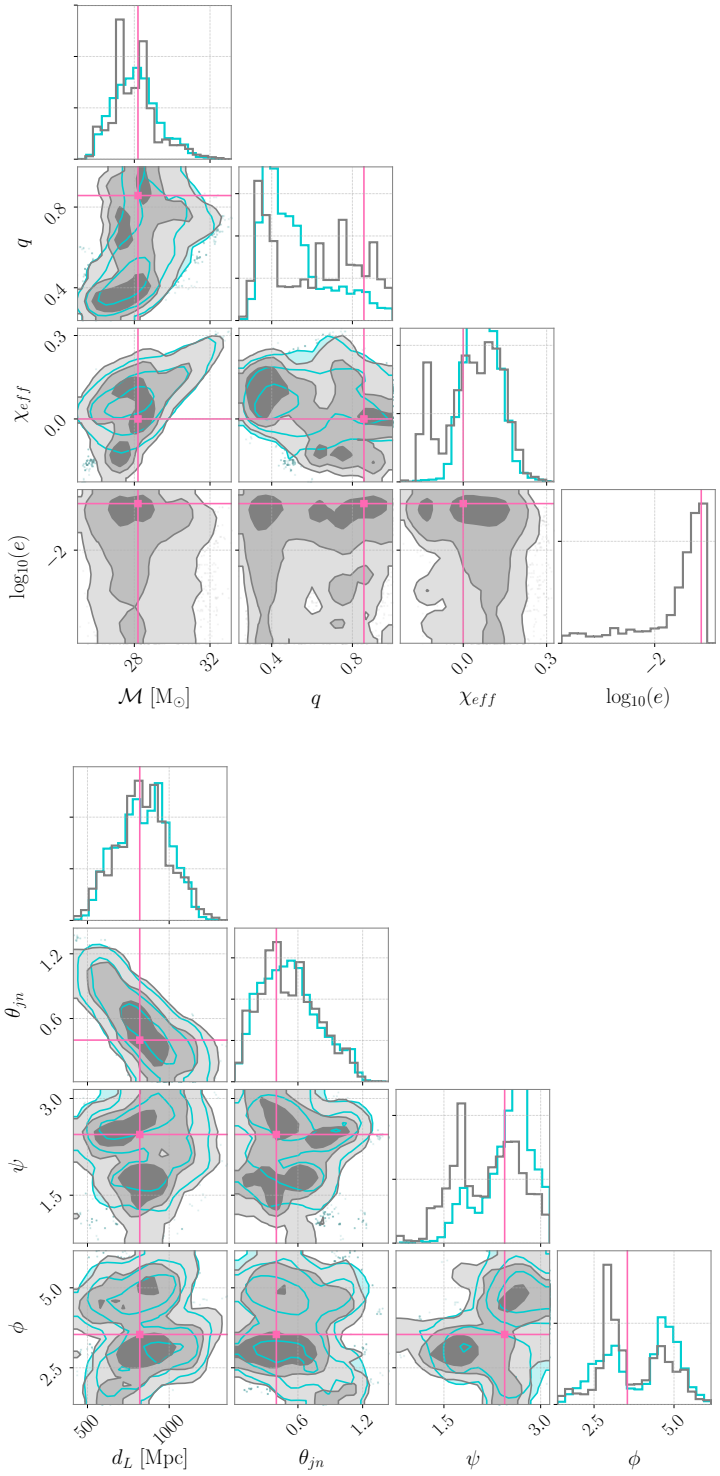

Figure 3.3: Recovered posterior probability distributions for an injected binary black hole merger signal with eccentricity $e = 0.1$ and network signal-to-noise ratio $\rho \approx 25$. The upper plot shows intrinsic parameters: chirp mass $\mathcal{M}$, mass ratio q, effective aligned spin χ_{eff}, and log eccentricity $\log_{10}(e)$. The lower plot contains extrinsic parameters: luminosity distance d_L, binary inclination angle θ_{jn}, polarisation angle ψ, and orbital phase ϕ. The underlying turquoise distributions are the posterior probabilities recovered using quasi-circular waveform model IMRPhenomD [249]. The grey distributions are those obtained through reweighting with eccentric waveform model SEOBNRE [103]. The pink lines indicate the true parameters of the injected SEOBNRE waveform.

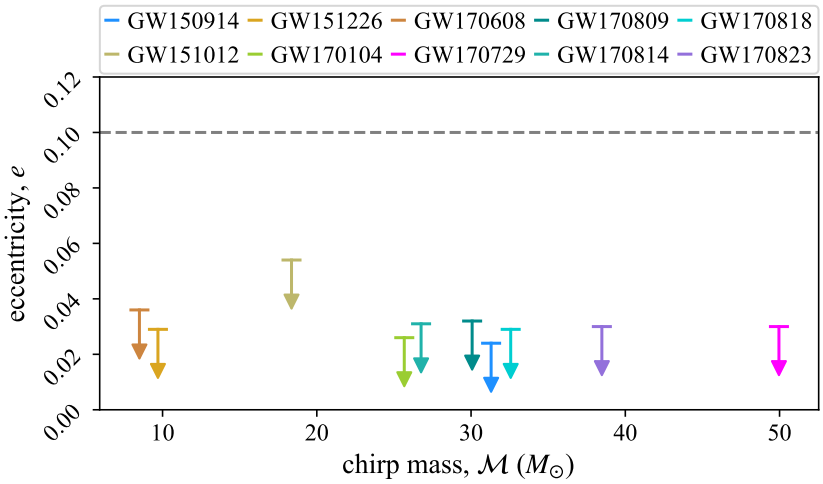

Figure 3.4: The 90% credible interval upper eccentricity limit for each of the ten GWTC-1 binary black hole mergers against the mean chirp mass of the event. A dashed line is plotted at $e = 0.1$, above which we should expect to see $\sim 5\%$ of all mergers from globular clusters [363, 393].

Table 3.2: Upper 90% credible interval limits on eccentricity, e^{90}_{max}, and log Bayes factors, $\ln \mathcal{B}$, for all ten binary black hole merger events published in GWTC-1 [30].

Event	$e^{90}_{10,\text{max}}$	$\ln \mathcal{B}$
GW150914	0.024	−0.07
GW151012	0.054	−0.12
GW151226	0.029	−0.08
GW170104	0.026	−0.05
GW170608	0.036	−0.28
GW170729	0.030	−0.05
GW170809	0.032	−0.28
GW170814	0.031	0.05
GW170818	0.029	−0.05
GW170823	0.030	−0.12

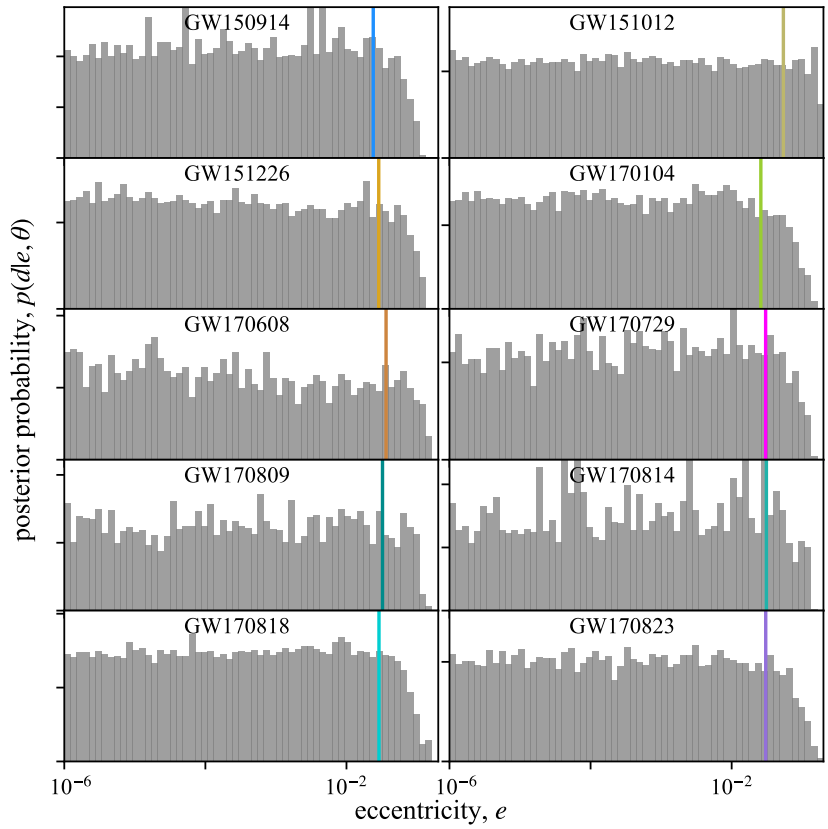

Figure 3.5: Eccentricity posteriors for all ten GWTC-1 events. We indicate the 90% credible upper limit on eccentricity at 10 Hz for each event with a vertical line, coloured to match the event-specific colours of the same limits plotted in Figure 3.4.

indicate that the data prefers the zero-eccentricity hypothesis. Using Equation 3.3, we calculate the efficiency of reweighting to range from $\sim 1\%$ for GW170814 to $\sim 75\%$ for GW151012. We highlight that our result does not rule out the dynamical formation channel for these mergers, since only $\sim 5\%$ of globular cluster mergers are expected to be highly eccentric. If we subsequently observe about 50 (90) events consistent with $e = 0$, we can rule out the dynamical hypothesis as the only source of mergers with 90% (99%) confidence.

We present eccentricity posterior probability histograms for all ten events in Figure 3.5. These are the first measurements of eccentricity in binary black holes detected with gravitational waves. The posteriors exhibit oscillatory behaviour because the overlap between an eccentric and a non-eccentric waveform rises and falls quasi-periodically. Although we maximise over coalescence phase, it is not always possible to match an eccentric waveform's phase evolution to that of a quasi-circular waveform. Thus, although the overlap follows a decreasing trend as the eccentricity increases, the overlap oscillates around this trend, and this is reflected in the likelihood. We highlight that the heaviest event, GW170729, has the second-lowest network signal-to-noise ratio and the second-highest eccentricity upper limit. Gravitational waves from heavy binaries reach 10 Hz only a few cycles before the binary merges, so it is harder

The posteriors shown in Figure 3.4 do not show any oscillation that is clearly inconsistent with sampling noise. However, we know from experience that quasi-circular signals have e_{10} posteriors that follow the shape of the overlap between a quasi-circular and eccentric signal, which has oscillations due to changes in the phase evolution of an eccentric signal.

to distinguish a mildly eccentric signal from a quasi-circular one. The full posteriors for all binary parameters for each event are available online[3]; we recover posterior probability distributions on event parameters that are consistent with those published in GWTC-1 [30].

3.5 DISCUSSION

We present measurements of eccentricity for the ten binary black hole mergers in the first Gravitational Wave Transient Catalogue, finding that all of these events have eccentricities consistent with zero at 10 Hz. This result does not rule out the dynamical formation channel as the primary channel for LIGO-Virgo observations. We expect only $\sim 5\%$ of globular cluster mergers to have $e \geq 0.1$ at 10 Hz. We require ≈ 15 events before it becomes more likely than not to detect eccentricity if all mergers are produced in globular clusters. Of course, more are required if there are multiple formation channels that produce non-eccentric mergers. Additionally, since the signal-to-noise ratio of an eccentric signal is smaller than that of its quasi-circular counterpart, quasi-circular binary signals will preferentially be detected over eccentric signals [93, 304, 359]. This effect will be most pronounced for $e \geq 0.1$, when the overlap between the eccentric signal and the quasi-circular signal begins to decrease rapidly. Although unmodelled searches are able to uncover loud eccentric events (see Abbott et al. [31]), current detection pipelines are likely to be preferentially detecting circular events due to as-yet-unmeasured selection effects. Therefore, GWTC-1 may be biased towards quasi-circular binaries. These selection effects will be investigated in future work.

It is worth clarifying here that this is only true if searches are conducted using quasi-circular waveform templates. The true SNR of an eccentric signal can be higher than for quasi-circular signals, e.g., [326].

If binary neutron stars like GW170817 [12] efficiently form in a dynamical environment, they could retain detectable eccentricity at 10 Hz [46, 334]. However, studies suggest that the dynamical formation of binary neutron stars in globular clusters is highly inefficient, so mergers contributed by this channel are likely to form a small fraction of the overall binary neutron star merger rate (e.g., Bae, Kim, and Lee [59], Grindlay, Portegies Zwart, and McMillan [208], and Zevin et al. [489]). In this work, we have restricted our analysis to binary black hole systems, since modifications will need to be made to our method in order to accommodate neutron star tidal affects. However, we intend to make our analysis applicable to binaries with neutron star components the future.

3 github.com/IsobelMarguarethe/eccentric-GWTC-1/events

4

ON THE ORIGIN OF GW190425

The original publication of this work [374] included two very short Appendices, which I have incorporated into the main body of the text here to aid the natural flow of this chapter. Some figures have been rescaled for formatting reasons.

ABSTRACT

The LIGO/Virgo collaborations recently announced the detection of a binary neutron star merger, GW190425. The mass of GW190425 is significantly larger than the masses of Galactic double neutron stars known through radio astronomy. We hypothesize that GW190425 formed differently than Galactic double neutron stars, via unstable "case BB" mass transfer. According to this hypothesis, the progenitor of GW190425 was a binary consisting of a neutron star and a $\sim$4–5 $M_\odot$ helium star, which underwent common-envelope evolution. Following the supernova of the helium star, an eccentric double neutron star was formed, which merged in $\lesssim$10 Myr. The helium star progenitor may explain the unusually large mass of GW190425, while the short time to merger may explain why similar systems are not observed in radio. To test this hypothesis, we measure the eccentricity of GW190425 using publicly available LIGO/Virgo data. We constrain the eccentricity at 10 Hz to be $e \leq 0.007$ with 90% credibility. This provides no evidence for or against the unstable mass transfer scenario, because the binary is likely to have circularized to $e \lesssim 10^{-4}$ by the time it was detected. Future detectors will help to reveal the formation channel of mergers similar to GW190425 using eccentricity measurements.

4.1 INTRODUCTION

Gravitational waves produced by a binary neutron star (BNS) merger have been detected for the second time [12, 30, 33] by Advanced LIGO [29] and Virgo [39]. The binary GW190425 is remarkable because it is significantly more massive than Galactic BNS [33]. Of the 17 Galactic BNS with reported mass measurements [see 156, and references therein], the most massive has total mass $M = 2.886 \pm 0.001 M_\odot$ [159, 277]. For GW190425, $M = 3.4^{+0.3}_{-0.1} M_\odot$, which is inconsistent with the observed Galactic population [33]. This invites speculation about its formation channel.

BNS may form through isolated binary evolution [76, 101, 196–198, 243, 268, 298, 348, 350, 415, 422, 462] or through dynamical interactions [46, 75, 141, 240, 251, 271, 334, 344, 408]. The dominant formation channel for Galactic BNS is thought to be isolated

evolution: a stellar binary in the field experiences successive supernovae, and the stellar remnant of each component is a neutron star [441, 462]. While many neutron stars *not* in BNS are known to have masses consistent with the components of GW190425 [43, 332], the high mass of this system in not easily explained by standard isolated evolution, since the large supernova kicks associated with massive NS formation are expected to disrupt binaries; see Michaely, Ginzburg, and Perets [311], and references therein.

In the dynamical formation case, BNS form through interactions inside dense stellar environments, such as globular clusters. A NS, which may have a stellar companion, sinks to the cluster core through dynamical friction. This can only occur once the number of black holes in the core has been depleted, either due to merger-induced kicks or because they gain velocity through dynamical interactions [e.g., 91]. In the core, the NS preferentially swaps any existing stellar companion for another NS, forming a BNS with a short merger time [489]. While the dynamical hypothesis provides an explanation for the large mass of GW190425, it is difficult to reconcile the implied merger rate with that predicted by N-body simulations [59, 71, 208, 482]; see also Papenfort, Gold, and Rezzolla [338], and references therein. Current estimates sit at around 0.003—6 $\mathrm{Gpc}^{-3}\mathrm{yr}^{-1}$ [448], which, for advanced LIGO's BNS range of $\sim 100\,\mathrm{Mpc}$ [29], translates to a predicted rate of 1.25×10^{-5}—$2.5 \times 10^{-2}\,\mathrm{yr}^{-1}$. For a different perspective see Andrews and Mandel [46], who highlight that tight and highly-eccentric Galactic-field BNS may form dynamically, provided that their host clusters have sufficiently high central densities.

We argue that massive BNS like GW190425 may evolve in isolation if they undergo a process known as unstable "case BB" mass transfer (MT) [73, 74, 131, 133, 238, 347, 348, 449, 450, 489]. We illustrate this process in Fig. 4.1. The He star companion of a NS (panel A) fills its Roche lobe after the end of its He core burning phase (panel B), initiating common-envelope evolution (panel C). The He envelope is ejected, leaving behind a NS–CO core binary (panel D) that is tight enough to survive the supernova of the He star (panel E). The resulting BNS inspirals due to emission of gravitational waves (panel F) and eventually merges, leaving behind a NS or black hole remnant (panel G). Unstable case BB MT may produce heavy BNS with unequal masses [238, 318]. The supernova kick can also leave the binary with significant eccentricity [90], which can act as an identifier for this formation channel. During standard isolated evolution, gravitational radiation gradually circularizes binaries before they get close to merger [222, 343]. On the other hand, as we show in Sec. 4.2 of this work, binaries formed through unstable case BB MT have eccentricities $10^{-6} \lesssim e \lesssim 10^{-3}$ when they enter the LIGO/Virgo band. GW190425 was detected by a search algorithm that assumes quasi-circular binary orbits. Its properties, presented in [33], were inferred by matched-filtering data against quasi-circular waveform models. Burst searches may flag eccentric signals, but cannot measure their eccentricity [e.g., 32]. Recently, Nitz, Lenon, and Brown [325]

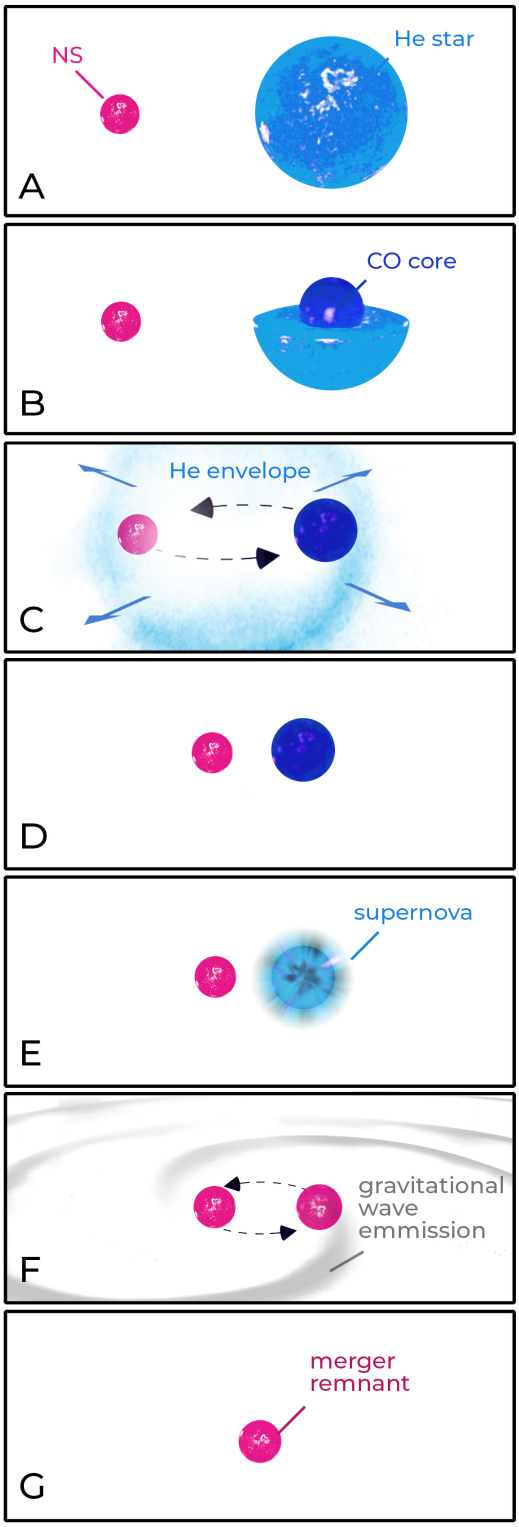

Figure 4.1: Illustration of unstable case BB mass transfer leading to a BNS merger. Credit: Carl Knox.

performed a matched-filtering search for eccentric BNS signals using inspiral-only eccentric waveform models. Computationally efficient, inspiral-merger-ringdown models of eccentric waveforms are not yet available, although development is ongoing [e.g., 232, 445]. Computationally inefficient models [e.g., 103] take too long to generate to be used for straightforward Bayesian inference, which relies on $\mathcal{O}(100)$ waveform computations per iteration of its sampling algorithm. We can, however, use such models to efficiently obtain eccentricity measurements by post-processing the posterior probabilities for quasi-circular waveform models, as demonstrated in Romero-Shaw, Lasky, and Thrane [376]; see also [291].

Here I refer to Chapter 3.

In this Letter, we take steps towards identifying the formation channel of GW190425 using orbital eccentricity measurements. We simulate BNS evolving through unstable case BB MT and compare the resulting eccentricity distribution to the posterior probability on eccentricity for GW190425. The remainder of this work is structured as follows. In Sec. 4.2, we describe unstable case BB MT and outline our method for simulating the expected eccentricity distribution at 10 Hz from this channel. We present upper limits on the orbital eccentricity of GW190425 when its gravitational radiation has a frequency of 10 Hz in Sec. 4.3, comparing the posterior probability distribution to the eccentricity distribution expected from supernova kicks. We discuss the implications of our results for the formation pathway of GW190425 in Sec. 4.4.

4.2 THE ISOLATED EVOLUTION OF GW190425

4.2.1 *Unstable mass transfer in the isolated binary evolution channel*

The immediate progenitor of an isolated BNS is a binary comprising a NS and a helium (He) star with orbital period $\sim 0.1 - 2$ days, which has evolved thus far via common-envelope (CE) evolution [74, 133, 238, 239, 489]. The He star then expands, filling its Roche lobe, and transferring mass onto the NS. If the mass transfer process is unstable, it can lead to a second CE (2CE) phase [132, 238]. The surviving post-2CE system consists of the carbon-oxygen (CO) core of the He star and the original NS. The latter has accreted only a small amount of mass ($\sim 0.05 - 0.1 M_\odot$) [293] during the 2CE phase. The binary can be tight enough that its orbital period is < 1 hr, making it likely to survive the subsequent supernova explosion of the CO core.

This asymmetric supernova explosion gives the compact object a kick. In population synthesis studies, kick velocities are often assumed to follow Maxwellian distributions. Core collapse supernovae are thought to produce large kicks, with one-dimensional standard deviation $\sigma \approx 265\,\mathrm{km\,s^{-1}}$ [225], while ultra-stripped supernovae and electron-capture supernovae are thought to produce small kicks, $\sigma \approx 30\,\mathrm{km\,s^{-1}}$ [197, 198, 462].

The relationship between the final He star mass (CO core mass) and the NS remnant mass is uncertain, but Müller et al. [318] predict that

a $\sim 4-5\,M_\odot$ He star (with a $\sim 3 M_\odot$ CO core) corresponds to a $\sim 2 M_\odot$ NS [see also 442]. It is assumed that there is an instantaneous mass loss of $\sim 1 M_\odot$ during supernova. If the pre-2CE binary consists of a $\sim 1.4 M_\odot$ NS and a $\sim 4-5 M_\odot$ He star, then the post-2CE, post-supernova binary is a $\sim (1.4+2.0) M_\odot$ BNS which merges in < 10 Myr. BNS with this lifespan are far less likely to be detected in radio pulsar surveys than their longer-lived counterparts, and BNS with orbital periods < 1 hr are effectively invisible in current pulsar searches. For example, the acceleration search of Cameron et al. [99], which found the most accelerated pulsar observed to date, was sensitive to binary pulsars with orbital periods down to 1.5 hr.

4.2.2 *Selection effects*

There are several selection effects that could cause discrepancy between the mass distribution of Galactic BNS observed in radio and that of extra-galactic BNS mergers detected in gravitational waves. First, more massive binary mergers are detectable at further distances with gravitational waves. Assuming a uniform-in-comoving-volume source distribution, the *observed* chirp mass distribution differs from the *true* distribution by a factor of $\mathcal{M}^{5/2}$ [495]. Second, more massive BNS merge faster, making them less likely to be discovered in pulsar surveys. However, the binary lifetime scales more strongly with its initial orbital period and eccentricity. As long as the binary chirp mass does not correlate *strongly* with initial orbital period or eccentricity[1], the mass distribution of BNS observed in radio is a good representation of the birth distribution. Third, the binary total masses (M) of Galactic BNS are known from measurements of the rate of advance of periastron, which is proportional to $M^{2/3}$. This leads to a slight preference within the observed Galactic BNS sample towards higher total masses as well as shorter orbital periods, which make periastron advance and orbital decay rates easier to measure. The fact that GW190425 is significantly more massive than all 17 known Galactic BNS may suggest an invisible Milky Way BNS population that is formed in ultra-tight, possibly highly eccentric orbits, as produced via unstable case BB MT.

4.2.3 *Eccentricity distribution*

Following Equations 2.1 to 2.8 from Brandt and Podsiadlowski [90], we calculate eccentricities introduced by supernova kicks in this formation scenario. We simulate binaries with first-born NS of mass $1.4\,M_\odot$ and CO core of mass $3.0\,M_\odot$, which lead to a second-born NS of mass $2.0\,M_\odot$, and draw orbital periods at time of supernova from a log-uniform distribution between 0.1 hr and 1 hr [see Fig. 8 from 462]. Supernova kick velocities are drawn from Maxwellian velocity distributions, with $\sigma = 265\,\mathrm{km\,s^{-1}}$ for large kicks and $\sigma = 30\,\mathrm{km\,s^{-1}}$

1 Noting the mild correlation between the mass of second-born NS and orbital eccentricity for Galactic BNS [e.g., Fig. 17 of 441].

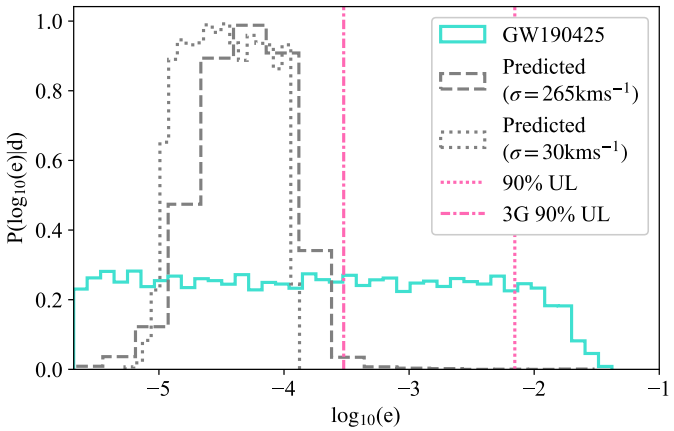

Figure 4.2: Posterior distribution on $\log_{10}(e)$ for GW190425, alongside eccentricities acquired during unstable case BB MT from kicks with velocities drawn from Maxwellian distributions. We indicate our measured 90% credible upper limit on the eccentricity of GW190425 at 10 Hz with a dotted bar at $e = 0.007$, and our estimate of the third-generation detector network upper limit with a dot-dashed bar at $e = 0.0003$. Space-based detector LISA will be able to resolve BNS eccentricities within the entire unstable case BB MT range; see Sec. 4.4, with reference to Lau et al. [276]. Our simulated eccentricity distributions agree with the subpopulation of ultra-compact BNS studied by Kowalska et al. [262].

for small kicks. We simulate isotropically-distributed kicks, and discard NS that receive kicks sufficient to disrupt the binary. Each binary's eccentricity is evolved according to Peters [343] until its gravitational-wave frequency reaches $f_{\mathrm{gw}} = 10\,\mathrm{Hz}$.
We present the distributions of $\log_{10}$ eccentricities obtained in this scenario in Fig. 4.2. Higher-velocity kicks tend to cause slightly higher eccentricities. Measured at 10 Hz, supernovae with large kicks lead to a $\log_{10}(e)$ distribution with a mean of -4.30, while the $\log_{10}(e)$ distribution arising from smaller kicks has a mean of -4.46. The 90% credible interval on $\log_{10}(e)$ spans $-4.94 \leq \log_{10}(e) \leq -3.98$ for small kick velocities, and $-4.89 \leq \log_{10}(e) \leq -3.79$ for large kick velocities.

4.3 Eccentricity of GW190425

See Chapter 3, in which our eccentricity-reweighting method is first described.

To compare GW190425 to the model described in Sec. 4.2, we measure its eccentricity when it enters the frequency band of LIGO/Virgo. Romero-Shaw, Lasky, and Thrane [376] demonstrated the calculation of Bayesian posterior probability distributions for the eccentricity of binaries detected in gravitational waves; see [341] for detailed formulation of the reweighting procedure that underlies such post-processing techniques. Following the same method, we use circular waveform model IMRPhenomD [249] to compute "proposal" posterior probability distributions for the binary parameters, and

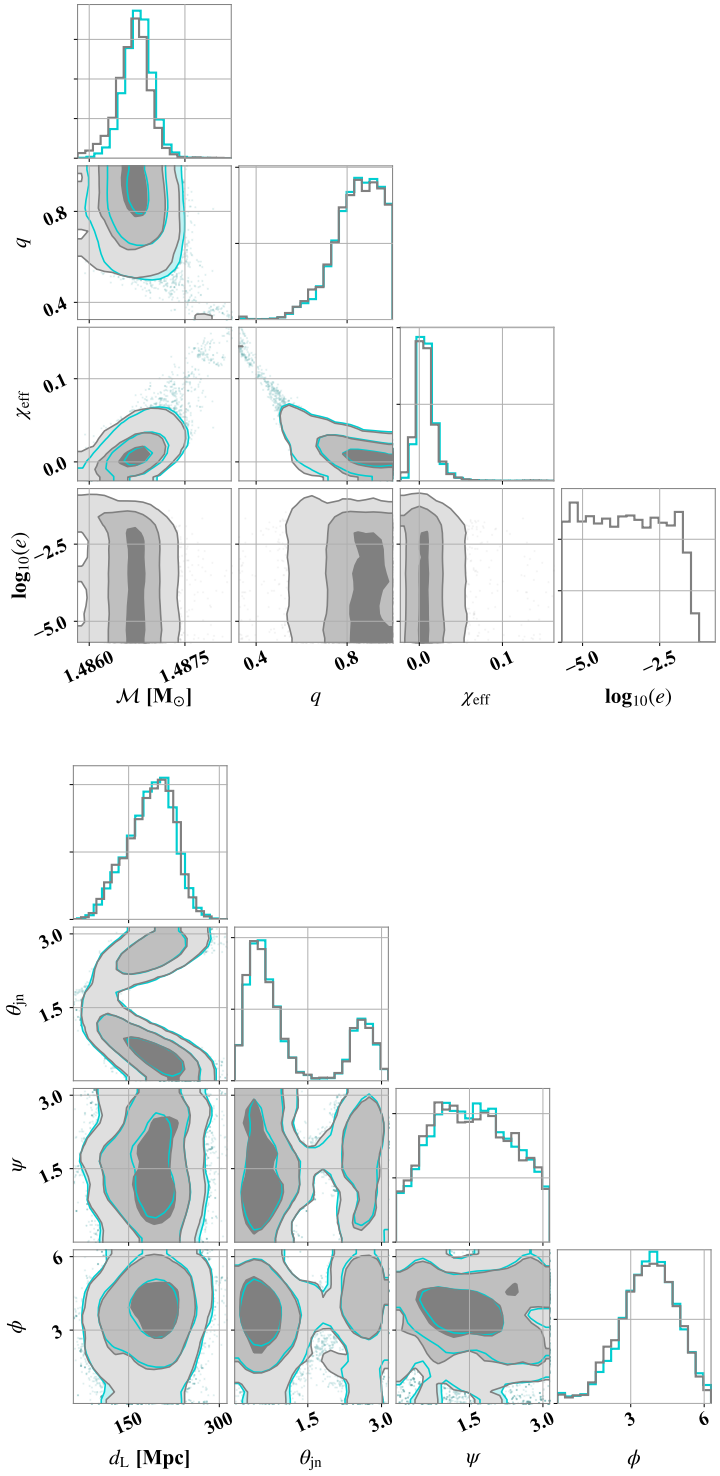

Figure 4.3: Recovered posterior probability distributions for GW190425. Intrinsic parameters chirp mass $\mathcal{M}$, mass ratio q, effective aligned spin χ_{eff}, and log eccentricity $\log_{10}(e)$ are displayed in the upper plot. Extrinsic parameters luminosity distance d_{L}, binary inclination angle θ_{jn}, polarisation angle ψ, and orbital phase ϕ are displayed on the lower plot. We plot the proposal posteriors in turquoise and the reweighted posteriors in gray.

eccentric waveform model SEOBNRE [103] to reweight to our "target" distribution.

We use the Bayesian inference library BILBY [54] to fit the data to the proposal model. Our prior on chirp mass $\mathcal{M}$ is uniform between 1.42 and 2.60 $M_\odot$, and our prior on mass ratio q is uniform between 0.125 and 1. Our prior on source luminosity distance d_L is uniform in co-moving volume between 1 and 500 Mpc. For dimensionless aligned component spins χ_1 and χ_2, we use priors that are uniform between -1 and 0.6 due to limitations of the SEOBNRE waveform model. For the remaining sampled parameters – right ascension, declination, source inclination angle, polarisation angle and reference phase – we use standard priors.

To reduce the time spent evaluating computationally-expensive SEOBNRE waveforms, we make initial measurements at a reference frequency of 20 Hz. To obtain orbital eccentricity measurements at 10 Hz, we follow Peters [343] to evolve the system backwards in time. We use a log-uniform prior on eccentricity, with a resolution of 30 bins per sample. At 20 Hz, our prior is in the range $-6 \leq \log_{10}(e) \leq -1$, translating to $-5.68 \leq \log_{10}(e) \leq -0.71$ at 10 Hz.

We constrain the eccentricity of GW190425 to be $e \leq 0.007$ at 10 Hz with 90% credibility. Our reweighting efficiency is 0.386, giving us 7718 effective samples; see [376] for a discussion of efficiency. We present the posterior probability distributions obtained for a selection of extrinsic and intrinsic parameters for GW190425 in Fig. 4.3; these are consistent with results from [33].

This discussion can be found in Chapter 3.

We compare the eccentricity posterior for GW190425 to the eccentricity distribution expected from supernova kicks during unstable case BB MT in Fig. 4.2. The posterior probability distribution for the eccentricity of GW190425 is consistent with our log-uniform prior for eccentricities $e \lesssim 7 \times 10^{-3}$ at 10 Hz, implying that we are unable to resolve differences between eccentricities lower than this with existing instruments. While the eccentricity of GW190425 is consistent with eccentricities induced during unstable case BB MT, we cannot distinguish this channel from other mechanisms using eccentricity measurements obtained with advanced LIGO/Virgo.

4.4 DISCUSSION

We constrain the eccentricity of GW190425 to $e \leq 0.007$ at 10 Hz. GW190425 may have formed through unstable case BB MT, but with present-day detectors, we are unable to distinguish the small residual eccentricity expected from this channel at 10 Hz. Proposed third-generation observatories such as Cosmic Explorer [CE; 28] and the Einstein Telescope [ET; 354] will detect GW190425-like binaries with higher signal-to-noise ratios, and at lower frequencies. Following the calculation outlined in Lower et al. [291], we find that a network of 2× CE can measure the eccentricity of a GW190425-like BNS if $e \geq 0.0003$ at 10 Hz, and will be able to observe the upper tail of the distribution expected from high-velocity kicks. The space-based

gravitational-wave detector LISA [44] will be sensitive down to 10^{-4} Hz, enabling sub-categories of both isolated and dynamical mergers to be distinguished [92, 124, 276, 323, 393]. From Lau et al. [276], the resolvable eccentricity of LISA at ~ 1 mHz is $e \gtrsim 0.001$, which translates to $e \gtrsim 10^{-7}$ at 10 Hz. Hence, the predicted eccentricity distribution from unstable case BB MT will be resolvable with LISA.

The inferred merger rate for GW190425-like systems is high compared to lighter BNS [33]. Since GW190425 is only the second BNS merger to be observed in gravitational waves, roughly half of all BNS mergers may form by the same means. This could imply that unstable case BB MT is a common pathway to BNS formation. Any proposed formation channel for this merger must also explain the relatively high formation rate of similar BNS.

Measurements of NS spins, which are imprinted on gravitational-wave signals through the effective spin parameter $\chi_{\rm eff}$, can provide additional clues to the formation channel of BNS. The $\chi_{\rm eff}$ of Galactic-field BNS, thought to have formed via standard isolated evolution, are predicted to range from 0.00 to 0.02 at merger [496]. Although we have not devoted much discussion to the dynamical formation hypothesis for GW190425 because it is theoretically disfavoured, it remains possible that GW190425-like BNS can form dynamically in, for example, globular clusters. Such BNS can have a wider range of spins than their isolated counterparts [see 140, and references therein]. A binary with measurably negative $\chi_{\rm eff}$ would be difficult to explain through anything other than dynamical formation. The $\chi_{\rm eff}$ of BNS formed through unstable case BB MT depends critically on the amount of angular momentum transferred onto the first-born NS during two CE stages, since the second-born NS is expected to spin down to effectively zero spin in a timescale comparable to the merger time ($\lesssim 10$ Myr). De et al. [129] suggest that black holes tend to preserve their natal masses and spins during CE evolution. If this holds up for BNS, it might imply that all BNS formed through unstable case BB MT are expected to have low dimensionless component spins of $\chi < 0.05$ at merger. While we are unable to measure NS spins in GW190425 (and in GW170817), it may be possible to do so for future discoveries, allowing stronger constraints to be placed on system origins.

We note that, in systems with misaligned component spins, the signature of spin-induced precession in the signal can mimic the signature of eccentricity, leading to non-negligible eccentricity measurements for precessing quasi-circular binaries (Romero-Shaw, Lasky & Thrane, in preparation). We see no evidence of significant eccentricity in the signal of GW190425, so any degeneracy between precession and eccentricity does not influence our conclusion. Regardless, the in-plane spin of BNS is believed to be small [e.g., 158], so this degeneracy is more important for binary black hole signals.

This is a forward reference to Chapter 5.

Note added.– While preparing this manuscript, we became aware of a pre-print claiming that the merger rate implied by GW190425 is inconsistent with population synthesis results for fast-merging BNS

[387]. Similar discrepancies have arisen for GW170817, but studies show that predicted merger rates are consistent with observations when various model uncertainties, e.g., NS natal kicks, CE evolution, metallicity-specific star formation rate [71, 114, 115, 196, 321, 439], are included. We therefore believe that we cannot rule out the formation of GW190425 through unstable case BB MT based solely on the inferred BNS merger rate.

5

GW190521A: ORBITAL ECCENTRICITY AND SIGNATURES OF DYNAMICAL FORMATION IN A BINARY BLACK HOLE MERGER SIGNAL

Note that the event referred to as 'GW190521A' in this chapter is the same as the event referred to as 'GW190521' in the original paper [377], and is renamed here for consistency with the subsequent chapter. Note also that the formatting of some tables has changed in order to fit all columns onto the page and some figures have been rearranged to increase the visibility of their legend labels.

ABSTRACT

Pair instability supernovae are thought to restrict the formation of black holes in the mass range $\sim 50 - 135\,M_\odot$. However, black holes with masses within this "high mass gap" are expected to form as the remnants of binary black hole mergers. These remnants can merge again dynamically in densely populated environments such as globular clusters. The hypothesis that the binary black hole merger GW190521A formed dynamically is supported by its high mass. Orbital eccentricity can also be a signature of dynamical formation, since a binary that merges quickly after becoming bound may not circularize before merger. In this work, we measure the orbital eccentricity of GW190521A. We find that the data prefer a signal with eccentricity $e \geq 0.1$ at 10 Hz to a non-precessing, quasi-circular signal, with a log Bayes factor $\ln \mathcal{B} = 5.0$. When compared to precessing, quasi-circular analyses, the data prefer a non-precessing, $e \geq 0.1$ signal, with log Bayes factors $\ln \mathcal{B} \approx 2$. Using injection studies, we find that a non-spinning, moderately eccentric ($e = 0.13$) GW190521A-like binary can be mistaken for a quasi-circular, precessing binary. Conversely, a quasi-circular binary with spin-induced precession may be mistaken for an eccentric binary. We therefore cannot confidently determine whether GW190521A was precessing or eccentric. Nevertheless, since both of these properties support the dynamical formation hypothesis, our findings support the hypothesis that GW190521A formed dynamically.

5.1 INTRODUCTION

The first and second observing runs of the Advanced LIGO [29] and Virgo [39] gravitational-wave observatories yielded ten observations of stellar-mass black-hole binaries [26, 27], reported in their first gravitational-wave transient catalogue [GWTC-1; 30]. The question of how these binaries came to merge within the age of the Universe remains unanswered. Proposed formation channels typically fall into

two categories: *isolated*, in which two stars evolve side-by-side until they form black holes and coalesce [see, e.g., 78, 239, 267, 290, 313, 498], and *dynamical*, in which two black holes become bound due to gravitationally-driven interactions inside dense star clusters [e.g., 89, 176, 178, 202, 316, 327, 349, 357, 358, 363, 364, 389, 391, 393, 395, 407] and/or active galactic nuclei disks [210, 308, 479]. Young star clusters may create something of a hybrid channel, with dynamical interactions perturbing the evolution of primordial stellar binaries, which evolve to make merging double compact objects [135, 360, 497].
The component masses and spins of a black-hole binary can illuminate its formation history, as can its orbital eccentricity (e.g., [155, 165, 370, 426, 436, 467]). Information about these parameters can be extracted from the gravitational-wave signal. Both isolated evolution and dynamical formation can produce black-hole binaries with properties like those presented in GWTC-1, with component masses $m_1, m_2 \lesssim 50\mathrm{M}_\odot$, dimensionless component spins a_1, a_2 consistent with 0, and eccentricities e consistent with 0 at 10 Hz [30, 376]. Dynamical formation is the preferred pathway for binaries with more extreme masses [89, 183, 184, 194, 369], isotropically distributed spin tilt angles [370, 436], and non-zero orbital eccentricities [203, 363, 393, 490, 492].

Here I refer to the eccentricity constraints presented in Chapter 3.

The mass distribution of black holes that form as the remnants of massive stars is thought to deplete between ~ 50 and $\sim 135\,\mathrm{M}_\odot$ due to pair-instability supernovae [PISN; 69, 165, 218, 300, 333, 476] unless exotic physics is invoked [388]. The precise lower limit of the PISN mass gap is an area of active reseach; see [72], and references therein. The remnants of binary black hole merger events can have masses within the PISN gap; see, e.g., [27, 106, 166, 252, 254].
Second-generation mergers—where at least one of the binary components is a remnant of a previous merger, potentially within the mass gap—can occur in the high-density environments conducive to dynamical mergers [89, 183, 194, 369]. Prior to the detection of GW190521A, no convincing evidence has emerged for hierarchical mergers [31, 106, 166, 252, 254].
Isolated binaries are thought to circularize efficiently, leading to negligible eccentricity close to merger [223, 343]. While it is possible that the late-inspiral eccentricity of field mergers can be increased by Kozai-Lidov resonance [263, 282] during three-body [51, 166, 182, 288, 365, 409] and four-body [181, 287] interactions in the field, the relative rate of such events is expected to be small, assuming moderate progenitor metallicities and black-hole natal kicks [51, 182, 288, 365, 409]. In contrast, some dynamically-formed binaries merge so rapidly after becoming bound that they retain non-negligible eccentricity in the LIGO–Virgo band [203, 364, 393, 489, 490]. Multiple authors [e.g., 363, 364, 389, 391, 397] show that we can expect $\mathcal{O}(5\%)$ of all dynamical mergers in globular clusters to have eccentricities $e > 0.1$ at a gravitational-wave frequency of 10 Hz.
The LIGO-Virgo Collaboration recently announced the detection of GW190521A, a gravitational-wave signal from the merger of a black hole binary with component masses $m_1 = 85^{+21}_{-14}\,\mathrm{M}_\odot$,

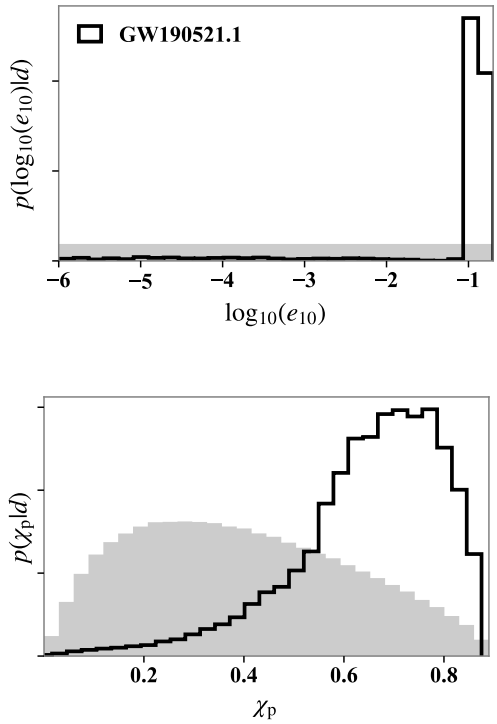

Figure 5.1: Results of analysis of GW190521A using SEOBNRE and IMRPhenomPv2. *Upper plot*: posterior probability density distribution for eccentricity at 10 Hz for GW190521A, recovered using SEOBNRE. At 90% credibility, $e_{10} \geq 0.11$. The posterior rails against the upper limit of the prior, $e_{10} = 0.2$, suggesting that the true value lies beyond this waveform-enforced constraint. *Lower plot*: posterior probability density distribution for the precession parameter χ_p for GW190521A, recovered using IMRPhenomPv2. The prior probability for each parameter is shown in gray.

$m_2 = 66^{+17}_{-18}\,\mathrm{M}_\odot$ [34, 35]. The median and 90% credible intervals quoted for these masses place at least one component within the PISN mass gap.[1] The data exhibit a modest preference (log Bayes factor $\ln \mathcal{B} \approx 2.4$) for spin-induced precession of the orbital plane, suggesting that the black-hole spin vectors may be significantly misaligned from the orbital angular momentum axis. If confirmed, the signature of precession would lend support for the dynamical hypothesis.

In this work, we show that GW190521A is consistent with an eccentric merger. For brevity, we hereafter refer to the eccentricity measured at a gravitational-wave frequency of 10 Hz as e_{10}. Our method allows us to study eccentricities up to $e_{10} = 0.2$, beyond which the waveform is not available.[2] Our analysis reveals overwhelming support for a spin-aligned eccentric signal with $e_{10} \geq 0.1$ over a spin-aligned quasi-circular signal. We use simulated events to demonstrate that

1 [167] find that m_1 is above the mass gap if $m_2 < 48\,\mathrm{M}_\odot$, below the mass gap.

2 As in our previous work, we are also unable to alter the initial argument of periapsis. While having a variable initial argument of periapsis might change the exact value of eccentricity recovered, it would not change our qualitative conclusions.

Table 5.1: Recovered GW190521A parameter values obtained using eccentric waveform model SEOBNRE, precessing waveform models IMRPhenomPv2 (IMRPv2) and NRSur7dq4 (NRSur), and NRSur7dq4 constrained to have aligned spins (NRSur||) . For the SEOBNRE analysis, we give the 90% credible lower limit on eccentricity at 10 Hz. For other parameters, the median of the posterior is given along with the 90% credible interval. In the final column, we state the values inferred from the LIGO–Virgo analysis, read from the public posterior samples obtained using NRSur7dq4 [2]. In the final row, we provide the log Bayes factor of each analysis against the signal-to-noise log Bayes factor obtained for $e_{10} \geq 0.1$ using SEOBNRE ($\ln \mathcal{B}_{S/N} = 85.7$).

Param.	SEOBNRE	IMRPv2	NRSur	NRSur||	NRSur LVC
m_1^{source}	92^{+26}_{-16}	126^{+61}_{-41}	86^{+18}_{-13}	85^{+22}_{-14}	85^{+21}_{-14}
m_2^{source}	69^{+18}_{-19}	59^{+32}_{-24}	69^{+18}_{-17}	61^{+15}_{-17}	66^{+17}_{-18}
$d_{\rm L}$	$4.1^{+1.8}_{-1.8}$	$2.4^{+2.3}_{-1.0}$	$4.7^{+2.2}_{-2.2}$	$4.7^{+1.6}_{-1.5}$	$5.3^{+2.4}_{-2.6}$
α	$3.6^{+2.7}_{-3.5}$	$4.3^{+1.9}_{-4.3}$	$3.4^{+2.9}_{-3.4}$	$3.7^{+2.6}_{-3.7}$	$3.5^{+2.8}_{-3.4}$
δ	$-0.7^{+1.4}_{-0.5}$	$-0.7^{+1.5}_{-0.4}$	$-0.8^{+1.5}_{-0.4}$	$-0.9^{+1.6}_{-0.3}$	$-0.8^{+1.5}_{-0.4}$
ϕ	$3.1^{+2.9}_{-2.7}$	$3.0^{+3.0}_{-2.7}$	$3.2^{+2.6}_{-2.6}$	$3.1^{+2.9}_{-2.8}$	$3.4^{+2.6}_{-3.2}$
ψ	$1.5^{+1.5}_{-1.4}$	$1.6^{+1.3}_{-1.5}$	$1.8^{+1.2}_{-1.5}$	$1.6^{+1.4}_{-1.4}$	$1.8^{+1.2}_{-1.6}$
$\theta_{\rm JN}$	$1.3^{+1.6}_{-1.0}$	$1.4^{+1.0}_{-0.7}$	$0.8^{+2.0}_{-0.6}$	$0.7^{+2.2}_{-0.5}$	$0.8^{+2.1}_{-0.6}$
$e_{10}^{\rm min}$	0.11	N/A	N/A	N/A	N/A
$\chi_{\rm eff}$	$0.0^{+0.2}_{-0.2}$	$0.1^{+0.4}_{-0.4}$	$0.0^{+0.3}_{-0.3}$	$0.0^{+0.2}_{-0.3}$	$0.1^{+0.3}_{-0.4}$
χ_p	N/A	$0.7^{+0.2}_{-0.3}$	$0.6^{+0.2}_{-0.3}$	N/A	$0.7^{+0.3}_{-0.4}$
$\ln \mathcal{B}_{X/E}$	0.0	-2.0	-1.8	-5.0	-1.2

Table 5.2: The 90% credible upper limit on eccentricity at 10 Hz, $e_{10}^{\max}$, and recovered spin-induced precession parameter χ_p for different injections with varying waveform model, e_{10} and χ_p settings. For the recovered χ_p we quote the posterior median and 90% credible interval.

Model	$e_{10,\text{inj.}}$	$\chi_{p,\text{inj.}}$	$e_{10,\text{rec.}}^{\max}$ (SEOBNRE)	$\chi_{p,\text{rec.}}$ (IMRPv2)
IMRPhenomD	0	0	0.025	$0.39^{+0.37}_{-0.29}$
NRSur7dq4	0	0	0.032	$0.33^{+0.40}_{-0.25}$
SEOBNRE	0	0	0.055	$0.42^{+0.36}_{-0.30}$
IMRPhenomPv2	0	0.63	0.077	$0.43^{+0.35}_{-0.32}$
NRSur7dq4	0	0.63	0.118	$0.53^{+0.29}_{-0.37}$
SEOBNRE	0.13	0	0.136	$0.57^{+0.26}_{-0.39}$

spin-induced precession and eccentricity cannot be distinguished for a GW190521A-like signal. We end with a discussion of the implications of our results on the potential formation mechanism of GW190521A.

5.2 Method

We construct eccentric posterior probability density distributions using the method developed in [376], which is built on those introduced by [341] and [291]. We use the Bayesian inference library Bilby [54, 378] to perform an analysis using our "proposal" model: the spin-aligned quasi-circular waveform model IMRPhenomD [249]. We reweight our IMRPhenomD posteriors to our "target" model: the spin-aligned eccentric waveform SEOBNRE [103, 289]. Our prior on eccentricity is log-uniform in the range $-6 \leq \log_{10}(e_{10}) \leq -0.7$. The upper limit arises from waveform limitations, although even a model allowing higher eccentricities would be restricted by the reweighting method. In order to reweight posterior samples efficiently, the samples obtained using the proposal model must cover the same region of the multidimensional parameter space as would be obtained by direct sampling with our target model. The overlap between eccentric and quasi-circular waveforms with otherwise-identical parameters falls drastically for higher eccentricities, so their posterior samples would not reside in the same region of the parameter space. We marginalise over the time and phase of coalescence as in [341] to account for differing definitions of these parameters between our proposal and target models.

Here I refer tothe method described in Chapter 3, and also to the Bilby paper provided in Chapter 2.

5.3 Analysis of GW190521A

We analyze publicly-available data and noise power spectral densities from [2, 34]. We reproduce the settings of the LVC analysis for our parameter estimation, with a data segment of 8 s, a frequency band 11–512 Hz, and sampling frequency 1024 Hz. In order to assess the role of waveform systematics, we perform four analyses using three

Table 5.3: Parameters shared by all injected waveforms.

Param.	Value
m_1^{source}	84
m_2^{source}	62
d_L	5.0
α	3.3
δ	0.5
ϕ	6.2
ψ	1.6
θ_{JN}	0.3
t_0	1242442967.46

different waveform models (one waveform is used twice with two different spin priors). The results of these analyses are summarized in Table 5.1.

First, we analyze the data using the aligned-spin eccentric waveform model SEOBNRE. We present the posterior distribution on the e_{10} of GW190521A in the left-hand panel of Fig. 5.1. The posterior drastically deviates from the log-uniform prior, strongly favouring eccentricities $e_{10} \geq 0.1$. There is little support for $e_{10} < 0.1$, with 90% of the posterior at $e_{10} \geq 0.11$. For other parameters, we obtain median posterior values similar to those given in Table 1 of [34], with a median source-frame total mass $M = 161^{+28}_{-20}\,M_\odot$, mass ratio $q = 0.7^{+0.2}_{-0.3}$, and $\chi_{\rm eff} = 0.0^{+0.2}_{-0.2}$. We obtain a luminosity distance, $d_L = 4.0^{+1.9}_{-1.7}\,$Gpc, which is slightly lower than (but consistent with) the value of $5.3^{+2.4}_{-2.6}\,$Gpc from the LIGO–Virgo analysis. Eccentricity causes a faster merger, reducing the signal power. Thus, in order to match the observed signal-to-noise ratio with an eccentric template, we may require a closer source. Additionally, models like SEOBNRE, IMRPhenomD and IMRPhenomPv2, which do not contain higher-order modes, cannot rule out edge-on binaries, which reduces the median distance estimate [35]. Posterior distribution plots for all other parameters are available online.[3]

Next, we perform an analysis using the precessing waveform IMRPhenomPv2 [402] with otherwise-identical settings. In Fig. 5.1, we show the posterior distribution for χ_p of GW190521A obtained with IMRPhenomPv2. This analysis recovers a smaller median d_L than the SEOBNRE analysis, with a more extreme mass ratio, $q \approx 0.5$. In order to carry out model selection comparing the IMRPhenomPv2 results to those obtained with SEOBNRE, we implement an astrophysically-motivated prior on eccentricity. Theoretical studies robustly predict that $\sim 5\%$ of binaries that form dynamically in globular clusters will have $e_{10} \geq 0.1$ [e.g., 264, 364, 389, 393]. To investigate this hypothesis, we assume a log-uniform distribution for $\log_{10} e_{10} \in (-1, -0.7)$. Using this astrophysically-motivated prior, the

3 git.ligo.org/isobel.romero-shaw/gw190521.1

eccentric model is mildly preferred to the precessing model by a factor of $\ln \mathcal{B}_{E/P} = 2.0$. If we repeat the same calculation using the (less well-motivated) prior range $\log_{10} e_{10} \in (-6, -0.7)$ as in Fig. 5.1, the eccentric (E) and precessing (P) waveform models are almost equally well-supported by the data, with a log Bayes factor $\ln \mathcal{B}_{E/P} = -0.35$.

Finally, we perform computationally-intensive analyses using the precessing, higher-order-model waveform NRSur7dq4, using parallel Bilby [417] to manage computational costs. We run two versions of the NRSur7dq4 analysis: one assuming aligned black-hole spins (no spin-induced precession) and one allowing arbitrary spin orientations (allowing spin-induced precession). Otherwise, the assumptions are identical to the IMRPhenomPv2 analysis above. While the two NRSur7dq4 analyses obtain near-identical results, the analysis that includes spin-induced precession (P) is preferred over the no-precession hypothesis with a moderate $\ln \mathcal{B}_{P/NP} = 3.2$. The eccentric SEOBNRE hypothesis (with $e_{10} > 0.1$) is preferred to the precessing and non-precessing NRSur7dq4 analyses by log Bayes factors of $\ln \mathcal{B}_{E/P} = 1.8$ and $\ln \mathcal{B}_{E/NP} = 5.0$, respectively.

We perform two additional analyses, identical in almost all aspects to the NRSur7dq4 studies described above, but without including higher-order modes. If we assume aligned spin, we obtain results similar to the SEOBNRE analysis. If we allow for spin-induced precession, we obtain results similar to the IMRPhenomPv2 results with luminosity distance $2.8^{+2.2}_{-1.5}$ Gpc (90% credibility) and $q \approx 0.5$.

5.4 Injection studies

Ideally, one would analyze gravitational-wave signals using models that include both spin-induced precession and eccentricity. This would allow simultaneous measurements of χ_p and e_{10}, as well as illuminating the full extent of the degeneracy between the two parameters and how that degeneracy changes with mass. Unfortunately, such models do not yet exist; see [217, 280] for a theoretical background of eccentric and precessing binary dynamics and waveforms. Thus, we use numerical tests to explore how our limited waveform models affect what we infer about eccentricity and spin-induced precession. We generate six GW190521A-like waveform templates using different waveform models, each with different values of e_{10} and χ_p; see Table 5.2. Other parameters are identical to those in Table 5.3. Using Bilby, we inject these waveforms into simulated detector networks consisting of LIGO Hanford, LIGO Livingston, and Virgo, with noise power spectral densities matching those used for analysis of GW190521A [34]. For each injection, we recover the signal using both the aligned-spin eccentric model SEOBNRE and the quasi-circular precessing model IMRPhenomPv2. In Fig. 5.2, we compare the posterior distributions for e_{10} (obtained using SEOBNRE) and χ_p (obtained using IMRPhenomPv2) for all injections. When circular, non-precessing waveforms are injected, the

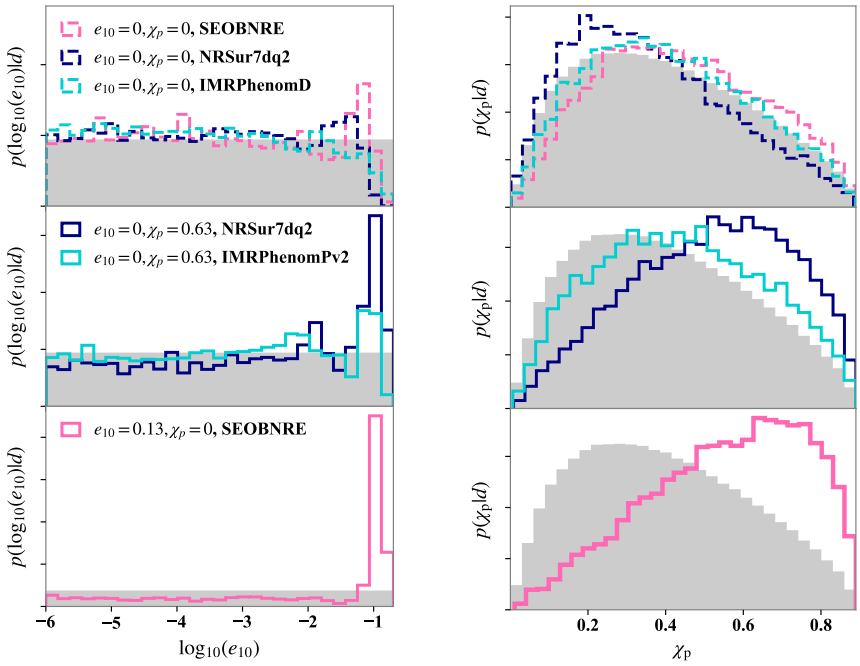

Figure 5.2: Results of SEOBNRE and IMRPhenomPv2 analysis of simulated data using GW190521A-like injections. *Left*: Posterior distributions for eccentricity at 10 Hz for GW190521A-like injection studies with varying e_{10} and χ_p, obtained using SEOBNRE. *Right*: Posterior distribution for spin-induced precession parameter χ_p for GW190521A-like injection studies with varying e_{10} and χ_p, recovered using IMRPhenomPv2. The prior distributions are shown in gray.

SEOBNRE analysis recovers posterior distributions for e_{10} consistent with the prior below the 90% credible upper limit, $e_{10}^{\max} \leq 0.025$ (0.032, 0.055) for injected IMRPhenomD (NRSur7dq4, SEOBNRE) waveforms. For these same waveforms, IMRPhenomPv2 analysis recovers posteriors consistent with the prior on χ_p. When we increase only χ_p, the posteriors on both χ_p and e_{10} skew away from their priors. This is most notable for the NRSur7dq4 injections, suggesting that higher-order modes (included in NRSur7dq4, but not in IMRPhenomPv2) may be important for distinguishing spin-induced precession and eccentricity. When we increase e_{10}, both posteriors deviate from their priors, more significantly than for the increased-precession case. These injection studies demonstrate that, for GW190521A-like binaries, spin-induced precession may be mistaken for eccentricity, and that the imprint of eccentricity may be mistaken for that of spin-induced precession. We provide the full posterior distributions for all parameters in these injection studies online.[4]

5.5 Discussion

Assuming the aligned-spin SEOBNRE waveform model, we infer an eccentricity $e_{10} \gtrsim 0.1$ for GW190521A. We find that the SEOBNRE waveform is slightly preferred over the circular-waveform models NRSur7dq4 and IMRPhenomPv2, both of which allow for spin-induced precession. While we lack a waveform model that can simultaneously account for spin-induced precession and eccentricity, GW190521A could be later verified as the first detection of a binary black hole with $e_{10} \geq 0.1$. The presence of either spin-induced precession or eccentricity adds weight to the hypothesis that the progenitor of GW190521A formed dynamically.

[389] predicts there are ~ 19 dynamical mergers with $e_{10} < 0.1$ for every merger with $e_{10} \geq 0.1$—a prediction thought to be robust to details about the globular cluster model; see also [364] and [305]. From the public alerts listed on GraceDB[5], there are $\mathcal{O}(30)$ binary black hole mergers from the first half of LIGO–Virgo's third observing run (O3a). Combining these with the results of [30] and [458, 459, 487], the total number of binary black holes observed in gravitational waves is $\mathcal{O}(50)$. If globular cluster mergers dominate LIGO and Virgo's observed black hole mergers, we expect $2.5^{+2.0}_{-2.5}$ mergers with $e_{10} \geq 0.1$ from the first 50 binary black hole observations. Thus, it would not be surprising if GW190521A is determined to be highly eccentric. Moreover, if GW190521A is eccentric, then O3a may provide us with another $1.5^{+2.0}_{-1.5}$ events with $e_{10} \geq 0.1$, assuming that O3a searches did not miss them; the signals of highly eccentric binaries may be missed by CBC and burst searches [139].

See [491] for a slight update to the number of expected mergers.

We note that while GW190521A may have formed within a globular cluster, this is not its only viable formation pathway. Dynamical

4 git.ligo.org/isobel.romero-shaw/gw190521.1/injection_studies
5 gracedb.ligo.org/superevents/public/O3/

formation may also occur in active galactic nuclei [e.g., 210, 259, 480], nuclear star clusters [e.g., 299], young open clusters [e.g., 136] and young massive clusters [60–63, 264]. Mergers in young star clusters are likely to take place after ejection, giving the binary ample time to circularise and making young star clusters a less promising explanation for eccentric binaries. Both active galactic nuclei and globular clusters may produce binary black holes with misaligned spin and/or eccentricity, and so it is not clear which dynamical formation pathway is favoured for GW190521A. Regardless, both spin-induced precession and eccentricity are signatures of dynamical formation; therefore, GW190521A is likely to have formed in a dense stellar environment conducive to dynamical interactions.
In dense environments like those mentioned above, binary black hole merger remnants may have masses within the mass gap. If these mergers are retained within the cluster, then they may merge again, producing intermediate-mass black holes. As an alternative to hierarchical black hole mergers, [382] argue that black holes may accrete enough gas in proto-clusters to enter into the mass gap. Another option is the direct collapse of stellar merger remnants to mass-gap black holes [e.g., 264, 421]. These black holes may undergo subsequent dynamical mergers if their environments are sufficiently densely populated. Although the high masses of GW190521A render it incompatible with current models of isolated binary evolution, these masses can be produced in models where various model assumptions are substantially relaxed [see, e.g., 150, 301, 425].
For GW190521A-like signals, we highlight the degeneracy between eccentricity and spin-induced precession[6]. This complements the results of [97], who found that for the gravitational-wave signal of a head-on black-hole collision ($e_{10} = 1$) with total mass in the range $M \in (130, 300)\,\mathrm{M}_\odot$ can be indistinguishable from the signal of a much more distant quasi-circular precessing binary. Recently, a candidate electromagnetic counterpart for GW190521A was observed at $\approx 2.8\,\mathrm{Gpc}$ and reported by [206], who propose that a binary black hole merger in an AGN disk might have such a counterpart. Extrapolating between the $e_{10} = 1$ results from [97] and the results shown here, the detected distance of GW190521A in gravitational waves is consistent with the electromagnetic counterpart if GW190521A had an eccentricity in the range $0.2 < e_{10} < 1.0$, a region of parameter space that cannot be fully explored with existing gravitational waveform models. However, new developments in eccentric waveforms [see, e.g., 110] may allow us to start probing previously unexplored parameter space in the near future. If the transient reported by [206] is truly an electromagnetic counterpart emanating from an AGN disk merger, it would be consistent with the hypothesis that GW190521A was an eccentric binary, since orbital eccentricity vastly increases the merger rate from such environments; see [210].

6 The degeneracy between eccentricity and spin-induced precession is less pronounced for less massive systems, which have longer signals in-band.

Note added.—During the final stages of preparation of this manuscript, we became aware of the work of [192], who compare numerical-relativity waveform simulations to GW190521A. Numerical relativity waveforms are too computationally expensive to be used for Bayesian parameter estimation. However, the fact that [192] find that eccentric numerical-relativity simulations are consistent with GW190521A supports the conclusions drawn in our work.

6

SIGNS OF ECCENTRICITY IN TWO GRAVITATIONAL-WAVE SIGNALS MAY INDICATE A SUB-POPULATION OF DYNAMICALLY ASSEMBLED BINARY BLACK HOLES

This Chapter was published as [379]. The original appendices appear as Sections in the same order as they appeared in the original text.

ABSTRACT

The orbital eccentricity of a merging binary black hole leaves an imprint on the associated gravitational-wave signal that can reveal whether the binary formed in isolation or in a dynamical environment, such as the core of a dense star cluster. We present measurements of the eccentricity of 26 binary black hole mergers in the second LIGO–Virgo gravitational-wave transient catalog, updating the total number of binary black holes analysed for orbital eccentricity to 36. Using the SEOBNRE waveform, we find the data for GW190620A is poorly explained by the zero-eccentricity hypothesis (frequentist p-value $\lesssim 0.1\%$). Using a log-uniform prior on eccentricity, the eccentricity at 10 Hz for GW190620A is constrained to $e_{10} \geq 0.05$ (0.1) at 74% (65%) credibility. With this log-uniform prior, we obtain a 90% credible lower eccentricity limit of 0.001, while assuming a uniform prior leads the data to prefer $e_{10} \geq 0.11$ at 90% credibility. This is the second measurement of a binary black hole system with statistical support for non-zero eccentricity; the intermediate-mass black hole merger GW190521 was the first. Interpretation of these two events is currently complicated by waveform systematics; we are unable to simultaneously model the effects of relativistic precession and eccentricity. However, if these two events are, in fact, eccentric mergers, then there are potentially many more dynamically assembled mergers in the LIGO–Virgo catalog without measurable eccentricity; $\gtrsim 27\%$ of the observed LIGO–Virgo binaries may have been assembled dynamically in dense stellar environments (95% credibility).

6.1 INTRODUCTION

The second gravitational-wave transient catalog [GWTC-2; 37] of the LIGO–Virgo collaboration [29, 39] confirmed the detection of 36 new binary black hole (BBH) mergers. Combined with the mergers presented in the first catalog [GWTC-1; 30], there are now 46 confirmed BBH merger detections.[1] This abundance of events poses

1 The exact number of "confirmed" mergers depends on the choice of detection threshold. Using a stricter threshold [38] counts 44 confirmed BBH mergers.

an intriguing question in gravitational-wave astronomy: how did these merging binaries form?

There are two primary channels that can produce binary compact object mergers that can merge in a Hubble time: isolated evolution and dynamical formation. An isolated binary contains two stars that are born together and evolve together, undergoing some mechanism that allows the two components to become close to merge within the age of the Universe, without merging before they become compact objects. A variety of mechanisms have been proposed, including common envelope evolution [e.g., 78, 239, 267, 290], chemically homogeneous evolution [e.g., 300, 313, 498], stable mass accretion onto a black hole from its stellar companion [66, 321, 499], or ambient gas-driven fallback [e.g., 432]. In contrast, a dynamically assembled binary does not become bound until the two components have already evolved into compact objects. This can occur in places like globular [e.g., 227, 370, 389] and nuclear [180, 185, 209, 224] star clusters. In these dense environments, mass segregation leads to a dark compact object core, where objects can undergo many frequent gravitational interactions [e.g., 47, 316, 363, 364, 393, 470, 474]. Subsequently, black holes can form binaries that are hardened through interactions with other compact objects, eventually merging.

There are three intrinsic properties of a binary that can distinguish its formation channel: its component masses, component spins, and orbital eccentricity. Multiple studies have shown that these properties can be used to identify the formation channel of a single binary and to constrain the relative fraction of mergers contributed by that channel to the overall merger rate [e.g., 155, 436, 467, 488, 491]. The formation channels of populations of mergers can also be distinguished using the redshift evolution of the merger rate [e.g., 322, 367]; however, it will take upwards of ~ 100 detections for this to become possible [168].

Identifying mergers with component masses between ~ 60–$130\ \mathrm{M}_\odot$ may indicate the presence of hierarchical mergers (from repeated dynamical mergers) [e.g., 166, 253, 254]. As pair-instability and pulsational pair-instability supernovae enforce an upper limit on the mass of a black hole that can form through stellar collapse [69, 166, 218, 300, 333, 433, 476], there is thought to be a dearth of black holes in this range, although these boundaries are sensitive to assumptions about the underlying physics [see, e.g., 72, 149, 151, 388, and references within]. In dynamical environments, on the other hand, merger remnants may go on to merge again if their formation kick does not eject them from the cluster, leading to black holes within this mass gap [89, 183, 194, 254, 264, 369, 394]. The intermediate-mass black hole binary GW190521 [34] has been interpreted as such a hierarchical merger [e.g., 45, 184, 253]. For an alternative interpretation, see [324, 330], which argue that GW190521 may be an intermediate-mass ratio inspiral with $q \equiv m_2/m_1 \approx 0.09$. In this work we assume the currently conventional interpretation, that $q \approx 0.8$.

Observing a population of BBH events in which some fraction of binaries have black-hole spins anti-aligned with the orbital angular

momentum would also hint that dynamical formation is at play [38, 423, 436]. Binary stars evolving together in the field tidally interact, leading them to have preferentially aligned spins [e.g., 100, 195, 242]. While the supernovae of one object can lead to a slight change in the spin orientation of the other, this change is believed to be minor [see, e.g., 195, 328, and references therein]. In contrast, objects that become bound during a gravitational interaction in the core of a dense star cluster may have any spin orientation relative to each other, and so we expect a population of binaries formed in clusters to have an isotropic spin distribution [370].

The LIGO–Virgo analysis of GWTC-2 found evidence for anti-aligned spin in the detected BBH population, and inferred from this that $\approx 25-93\%$ of the observed BBH had formed dynamically, at 90% credibility [38]. However, Roulet et al. [380] dispute this, finding that the signature from [38] is a model-dependent artefact. In either case, the dynamical formation scenario is unlikely to produce the entirety of mergers observed by LIGO and Virgo. The presence of ≈ 10 BBH signals with black-hole spins preferentially aligned with the orbital angular momentum suggests $\gtrsim 23\%$ of BBH events are associated with field mergers.

The third intrinsic property of a binary that can act as a signature of dynamical formation is its orbital eccentricity close to merger. Gravitational-wave emission efficiently circularises binaries on a shorter timescale than they tighten [223, 343]. We thus expect negligible eccentricity in the orbits of field binaries at detection—excepting field triples, a topic we return to below. In a dynamical environments such as dense star clusters, however, binaries can be driven to merge rapidly. They do not always have time to radiate away their eccentricity before they merge, and so they may retain detectable eccentricity when their gravitational radiation enters the LIGO–Virgo band at gravitational-wave frequencies $\gtrsim 10\,\mathrm{Hz}$ [203, 316, 363, 364, 389, 492].[2]

Dense star clusters are arguably the most well-studied dynamical formation environment [see, e.g., 89, 176, 178, 202, 316, 327, 349, 357, 358, 363, 364, 389, 391, 393, 395, 407]. Simulations of compact binary formation in such environments lead us to expect that $\sim 5\%$ ($\sim 7\%$) of their binary black holes retain eccentricities $e_{10} \geq 0.1(0.05)$ when their gravitational radiation frequency reaches $10\,\mathrm{Hz}$; see Kremer et al. [265], Rodriguez et al. [363, 364], Samsing [389], Samsing et al. [393], Samsing, MacLeod, and Ramirez-Ruiz [395], and Zevin et al. [491] and references within. Observing eccentricity in the gravitational waveform of a BBH coalescence therefore indicates that the system was formed dynamically. Young open clusters have also been proposed as a competitive channel [e.g., 177], which may produce mergers with traits associated with either dynamical or isolated formation.

Further alternatives to dynamical formation in dense star clusters include dynamical formation in active galactic nuclei discs [210, 281,

2 Throughout, we use the word "frequency" to refer to gravitational-wave frequency as opposed to orbital frequency.

308, 479], which may be efficient factories for eccentric binary black holes [390, 430]. However, the distribution of mass, spin, and eccentricity for binary black holes in active galactic nuclei discs are comparatively poorly understood owing to the complicated environment.
Additional classes of formation mechanism include field triples [51, 166, 182, 288, 365, 409] and quadruples [181, 287], which can cause the spins and eccentricities of isolated binary mergers to somewhat resemble those of dynamical mergers. Field triple mergers can have high eccentricities, as the third component can drive up the eccentricity of the inner binary in a process known as Kozai-Lidov resonance [263, 282]. The rate of mergers driven by Kozai-Lidov resonance in the field is thought to be low, unless black hole natal kicks are small and the formation metallicities of the systems are low [51, 182, 288, 365, 409].
It has also been suggested that the observed population of mergers may contain primordial black holes, which can have lower and/or higher masses than those formed through stellar collapse [e.g., 41, 80, 109, 128, 186, 401]. However, there is at present no evidence for the existence of primordial black holes [104], and if they do exist, it is not clear that they form merging binaries; [see, e.g., 261].
In [376], we presented measurements of orbital eccentricity for BBH events in GWTC-1, constraining the eccentricity of these ten mergers to less than 0.1 at 10 Hz. This result was in agreement with that of Abbott et al. [31], which found no eccentric signals within the data from LIGO and Virgo's first and second observing runs. In Romero-Shaw et al. [377], we presented tentative evidence that the highest-mass binary so far detected in gravitational waves, GW190521A [34, 35][3], had non-zero eccentricity, although the purported signal could also be the result of general relativistic precession induced by black-hole spin. This conclusion was supported by Gayathri et al. [192]. GW190521A may therefore be the first observation of an eccentric binary in the population of LIGO-Virgo detected events.

Here I reference Chapter 3, in which all binary black holes in GWTC-1 are shown to have negligible eccentricities at detection, and Chapter 5, in which the first potential detection of non-zero eccentricity is contained.

In this work, we present measurements of eccentricity for 36 of the 46 BBHs in GWTC-2.[4] We highlight GW190620A, an event for which the $e_{10} \geq 0.1$ hypothesis is preferred to the $e_{10} < 0.1$ case by a Bayes factor of $\mathcal{B} = 18.6$. We detail our analysis method in Section 6.2, where we provide updates to the analysis methods used in Romero-Shaw et al. [374], Romero-Shaw, Lasky, and Thrane [376], and Romero-Shaw et al. [377]. Our results are presented in Section 6.3,

Here I refer to all previous Chapters containing eccentricity measurements: Chapters 3, 4 and 5.

3 In this paper, we use the short event name, appending an A (B) if the event is the first (second) on that date.

4 The events in the GWTC-2 catalogue were detected using quasi-circular waveform templates. Some events were also detected with "burst" pipelines using excess power techniques [e.g., 119, 122, 138]. As eccentricity grows, signals increasingly deviate from quasi-circular signal templates, so can appear with low significance in circular searches [e.g., 93]. Unmodeled analyses can be particularly powerful in this case [e.g., 125], and eccentric signals may be recovered with a higher signal-to-noise ratio in a burst search than a circular search. All GWTC-2 candidates were detected with at least one circular search pipeline.

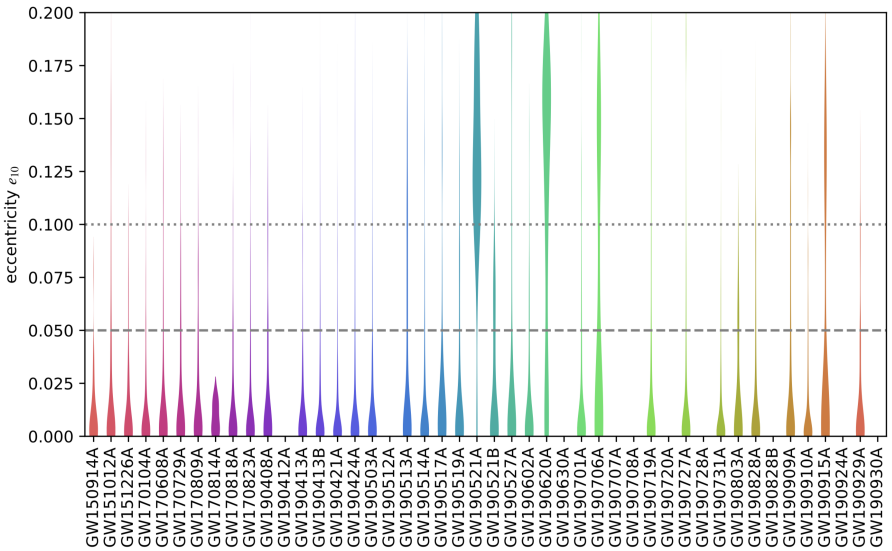

Figure 6.1: Marginal posterior distributions on eccentricity at 10 Hz, e_{10}, for 36 binary black hole merger events in GWTC-2 [37]. We assume a log-uniform eccentricity prior, which is suitable when we do not know the order of magnitude for e_{10}. The ten low-mass events that require further analysis due to under-sampling are left blank. For each event, the width of the violin at each value of eccentricity is proportional to the posterior distribution at that value. Eccentricity posteriors for events in GWTC-1 and for GW190521A were originally presented in Romero-Shaw, Lasky, and Thrane [376] and Romero-Shaw et al. [377], respectively. These previously-reported results have here been reweighted from their original prior on eccentricity, which was log-uniform between 10^{-6} and 0.2, to the prior used for analysing the new GWTC-2 events, which is log-uniform between 10^{-4} and 0.2.

where we investigate events that have significant posterior support for $e_{10} \geq 0.05$. We discuss the broader astrophysical interpretation of our results in Section 6.4.

6.2 METHOD

Original posteriors for previously-analysed binary black hole mergers can be found in Chapters 3 and 5.

We use the likelihood reweighting (importance sampling) method described in Romero-Shaw, Lasky, and Thrane [376], inspired by the importance sampling method used in Payne, Talbot, and Thrane [341], to efficiently estimate sets of posterior distributions for eccentricity. This method has been tested using injection studies [376, 377] to correctly recover the injected eccentricity of injected aligned-spin signals. We obtain initial samples using a quasi-circular waveform model IMRPhenomD [249] for our proposal likelihood. These samples are then reweighted using eccentric waveform model SEOBNRE [103, 289] to obtain samples from our target distribution. We perform Bayesian inference using `bilby` and the `bilby_pipe` pipeline [54, 378], running five parallel analyses with unique seeds for each event. We analyse publicly-available data from GWTC-2 [3], using a combination of the LIGO Livingston, LIGO Hanford and

These injection studies can be found in Chapters 3 and 5.

Virgo detectors that is consistent with the LIGO-Virgo analysis for each event.

We use power spectral densities generated using BayesWave [286]. We do not factor calibration uncertainty into our analysis; errors on our results caused by neglecting calibration uncertainty are expected to be negligible [e.g., 340, 466]. Similarly, we do not marginalise over the uncertainty in the noise power spectral density, but marginalising over this uncertainty is expected to yield modest changes in the posterior widths of $\lesssim 5\%$ [81].

Our sampling and reference frequencies are 4096 Hz and 10 Hz, respectively. We use 20 Hz as the default minimum frequency of analysis in all detectors for all newly-analysed events, except for GW190727A, which has a minimum frequency of 50 Hz in the LIGO Livingston detector in the LIGO-Virgo analysis [37].[5] We use the `dynesty` [420] sampler with 1000 live points, 100 walks and 10 auto-correlation times. To avoid spectral leakage, we soften the abrupt start of the time-domain inspiral using a half-Tukey window that turns on over 0.5 s.

We use standard priors for extrinsic angle parameters. We use a prior on luminosity distance d_{L} that is uniform in the source-frame. Our prior on mass ratio q is uniform between 0.125 and 1, where the lower bound is restricted by the choice of waveform approximants. The prior on the $\hat{z}$ component of the black hole spin vectors χ_i^z is created by combining a uniform prior on the component spin magnitudes, χ_i, with an isotropic prior for the spin orientation. Each χ_i is capped at 0.6, as SEOBNRE cannot tolerate spins of greater magnitude than this. This creates a prior with limits at $\chi_i = \pm 0.6$ and a peak at $\chi_i = 0$. We adopt a uniform prior on chirp mass $\mathcal{M}$.

The reweighting procedure is near-identical to that used in Romero-Shaw et al. [377], which built on that described in Romero-Shaw, Lasky, and Thrane [376], except that we increase the lower bound on our prior for e_{10} to $e_{10} = 10^{-4}$ since we cannot resolve the eccentricity for signals below this point. We employ a log-uniform prior for eccentricity, which is suitable given that we are unsure about the order of magnitude for e_{10}. For completeness, we also provide results obtained under a uniform eccentricity prior over the same range. The probability distributions over eccentricity (obtained by dividing out the log-uniform prior in post-processing) are presented in Figure 6.7 in Appendix 6.6.

Here is a reference to the Bilby paper in Chapter 2.

5 SEOBNRE is defined such that the minimum frequency requested in the waveform is also the reference frequency for the eccentricity. We therefore generate waveforms from 10 Hz, but only use the frequency content from 20 Hz and above in our analyses.

Table 6.1: A summary of the eccentricity signature for the 12 events with the most support for $e_{10} \geq 0.05$. The second and third columns provide the percentage of posterior support for $e_{10} > 0.1$ and $e > 0.05$ respectively. These two values are typical used as thresholds for 'detectable' binary eccentricity at 10 Hz using operational gravitational-wave detectors [e.g., 291, 363, 364, 389, 392, 491, 492], although the true threshold for eccentricity sensitivity is unique to each signal. The next two columns provide the natural log Bayes factors $\ln \mathcal{B}$ for the hypotheses that $e_{10} \geq 0.1$ (0.05) against the hypothesis that $e_{10} < 0.1$ (0.05). The two most compelling candidates for eccentric mergers are highlighted in bold. These same parameters for other events in GWTC-2 are provided in Appendix 6.5.

Event name	percentage $e_{10} \geq 0.1$	percentage $e_{10} \geq 0.05$	$\ln \mathcal{B}(e_{10} \geq 0.1)$	$\ln \mathcal{B}(e_{10} \geq 0.05)$	reweighting efficiency (%)
GW190424A	8.12	17.09	−0.11	−0.08	85
GW190513A	13.28	27.33	0.45	0.53	49
GW190521A	**92.25**	**93.42**	**4.65**	**3.90**	**2**
GW190521B	2.43	23.21	−0.17	0.55	6
GW190527A	8.64	17.72	−0.07	−0.06	15
GW190620A	**65.72**	**74.27**	**2.90**	**2.48**	**10**
GW190706A	28.27	38.02	1.36	1.01	42
GW190719A	9.29	19.01	0.04	0.07	70
GW190727A	8.27	17.07	−0.14	−0.09	87
GW190828A	7.30	19.37	−0.18	0.10	48
GW190909A	15.61	25.91	0.60	0.44	86
GW190915A	21.60	33.35	0.99	0.77	9

Like other eccentric waveform models [e.g., 110, 233], SEOBNRE does not include a variable initial argument of periapsis. The phase modulations caused by a varying initial argument of periapsis cannot be fully accounted for by reference phase- and time-marginalisation, which can lead to mismatches of up to 0.1 in otherwise-identical waveforms [237] assuming a white noise power spectral density. It is not clear how the mismatch changes for realistic detector noise. Our inferences of the eccentricities of our sources may be biased by neglecting this parameter, though, it is difficult to ascertain how this systematic error compares to other imperfections in the waveform model. Investigations into the extent of this bias are ongoing. However, the waveform amplitude modulations caused by orbital eccentricity appear to be qualitatively different than the changes induced by the initial argument of periapsis. Hence, we suspect that our conclusions are relatively insensitive to this parameter.

An additional parameter that is fixed within SEOBNRE is the value of the spin-induced precession parameter, $\chi_{\rm p}$ [214, 403]. While we can sample over the component aligned spins χ_1 and χ_2, we cannot probe misaligned spins with SEOBNRE, enforcing an assumption that $\chi_{\rm p} = 0$. Precession has been shown to mimic the effects of eccentricity in gravitational waveforms for high-mass systems like GW190521A [97, 377]. Efficient waveform models than include the effects of both spin-induced precession and eccentricity are not yet available, so we are not currently able to measure both parameters simultaneously.

I refer here to Chapter 5.

Reweighting is increasingly inefficient for low-mass events, i.e., those that require data segments with durations $D > 4\,\mathrm{s}$. With more cycles contained in longer-duration waveforms, systematic discrepancies between our proposal (quasi-circular) model IMRPhenomD and our target (eccentric) model SEOBNRE build up, manifesting in larger differences between the proposal and target likelihoods; see Figure 6.8 in Appendix 6.7 for a demonstration of the overlap between the two waveforms decreasing as source mass decreases, increasing the number of cycles in-band. There are two neutron star-black hole (NSBH) merger candidates in GWTC-2, with $D = 16\,\mathrm{s}$ (GW190814A) and $D = 64\,\mathrm{s}$ (GW190426A). There are three other events with $D = 16\,\mathrm{s}$ (GW190527A, GW190728A and GW190924A) and nine events with $D = 8\,\mathrm{s}$ (GW190412A, GW190512A, GW190630A, GWS190707A, GW190708A, GW190720A, GW190803A, GW190828A and GW190930A).[6] Reweighting samples for most of these long-duration events is currently computationally impractical. Low-mass black holes are less likely to merge via the gravitational-wave capture events that lead to eccentricities

6 We analyse segment durations that match those used in GWTC-2 [37]. An eccentric binary inspirals more rapidly than a non-eccentric binary with the same parameters. For a given orbital period, an eccentric binary is closer at periapsis than it would be in a circular orbit, increasing the energy that is therefore lost to gravitational radiation. Proposed eccentric waveforms are thus shorter than quasi-circular waveforms with otherwise identical parameters, so all waveforms that can be drawn from the eccentricity prior are therefore within the segment duration deemed adequate for quasi-circular parameter estimation.

approaching unity in dense cluster environments [see, e.g., 200]. Higher-mass binaries with masses close to the pair-instability mass gap are also more likely to contain components that have formed hierarchically in a dynamical environment. We therefore exclude ten low-mass BBH events and two NSBH candidates from this work. We anticipate that it will be possible to analyse these events with new eccentric waveforms that are efficient enough to use for direct parameter estimation, so defer this analysis to future work.

6.3 RESULTS

In Figure 6.1, we display the posterior probability distributions for eccentricity at 10 Hz, e_{10}, for all of the binary black hole systems so far analysed for eccentricity with SEOBNRE. Corner plots containing fully- and partially-marginalised single- and double-dimensional posterior probability distributions for all other waveform parameters are available online for all events.[7] Consistent with Payne, Talbot, and Thrane [341], we consider sampling efficiency $> 1\%$ to be adequate. The number of effective samples in the eccentric posterior after reweighting is > 500 for all events presented here, with an average of $17,477$, a maximum of $54,395$ (GW190413B) and a minimum of 541 (GW190521A). The average reweighting efficiency is 45%, with a maximum of 90% (GW190731A) and a minimum of 2% (GW190521A and GW190803A). The reweighting efficiency is particularly low for GW190521A because we also reweight from the old eccentricity prior to the new eccentricity prior; before doing this, the number of samples is 726. There are 12 events with marginalised eccentricity posteriors that show support for eccentricity $e_{10} \geq 0.05$. We display these posteriors in Figure 6.2. The eccentricity posteriors for all other events are provided in Appendix 6.5.

6.3.1 *Events with* $e_{10} \geq 0.05$

There are two events that have more than 50% of their posterior probability distribution above $e_{10} \geq 0.05$: GW190521A and GW190620A. There are also ten events that have support for $e_{10} \geq 0.05$ while remaining consistent with having negligible eccentricity. Of these ten events, three have eccentricity posteriors peaking in the range $0.1 \leq e_{10}$ and three have eccentricity posteriors peaking in the range $0.05 \leq e_{10} \leq 0.1$. We provide the percentages of the eccentricity posterior above 0.1 and 0.05 for the 12 events of interest in Table 6.1, in addition to the natural-log Bayes factors $\ln \mathcal{B}$ for the hypotheses that $e_{10} \geq 0.1$ (0.05) against the hypothesis that $e_{10} < 0.1$ (0.05). We display the posterior probability distribution for the eccentricity of these 12 events in Figure 6.2.
In a sufficiently large population of entirely circular binaries, some events will appear to have non-zero eccentricity due to random fluctuations. In order to provide a different perspective on the

7 github.com/IsobelMarguarethe/eccentric-GWTC-2/seobnre

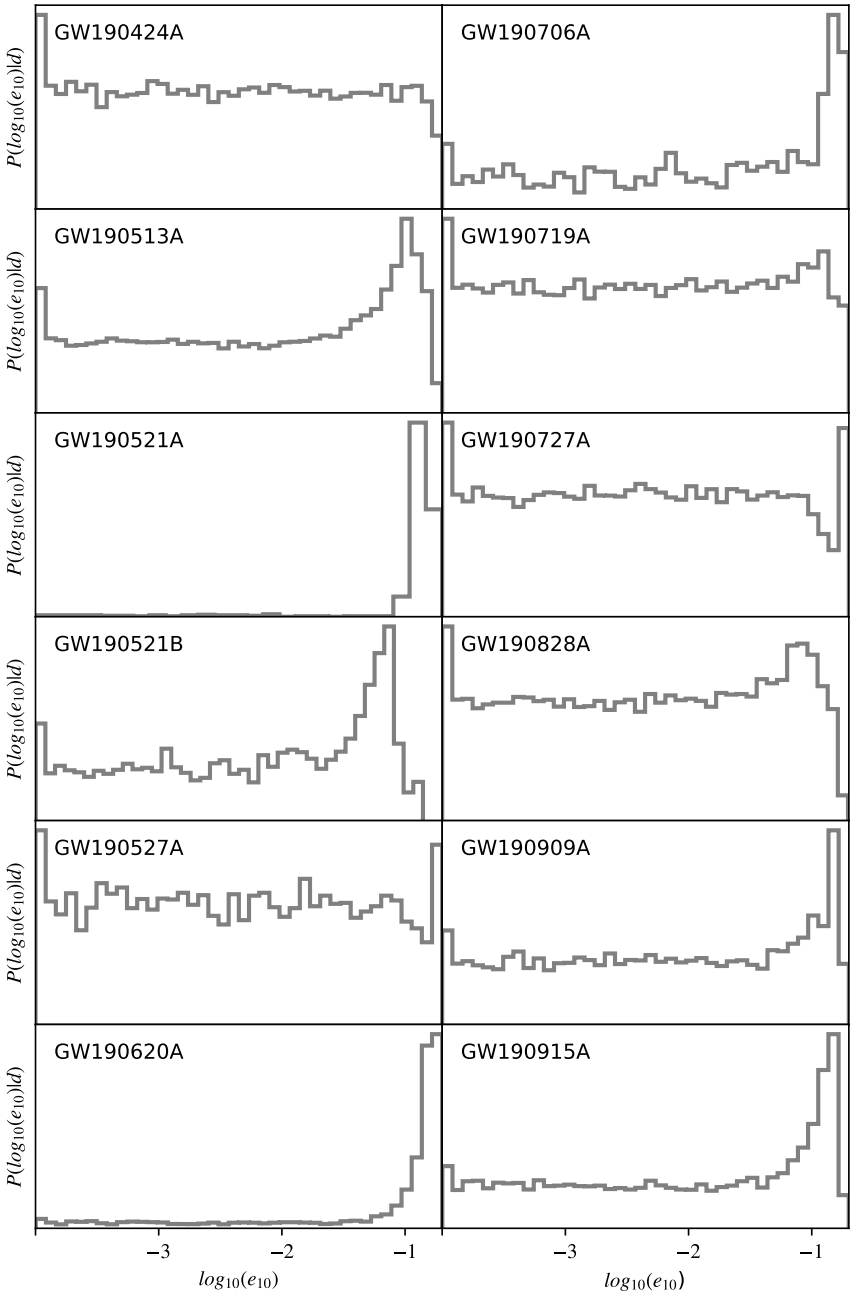

Figure 6.2: Posterior probability distributions on e_{10} for the 12 events in GWTC-2 with eccentricity posteriors that have the most support for eccentricity $e_{10} \geq 0.05$.

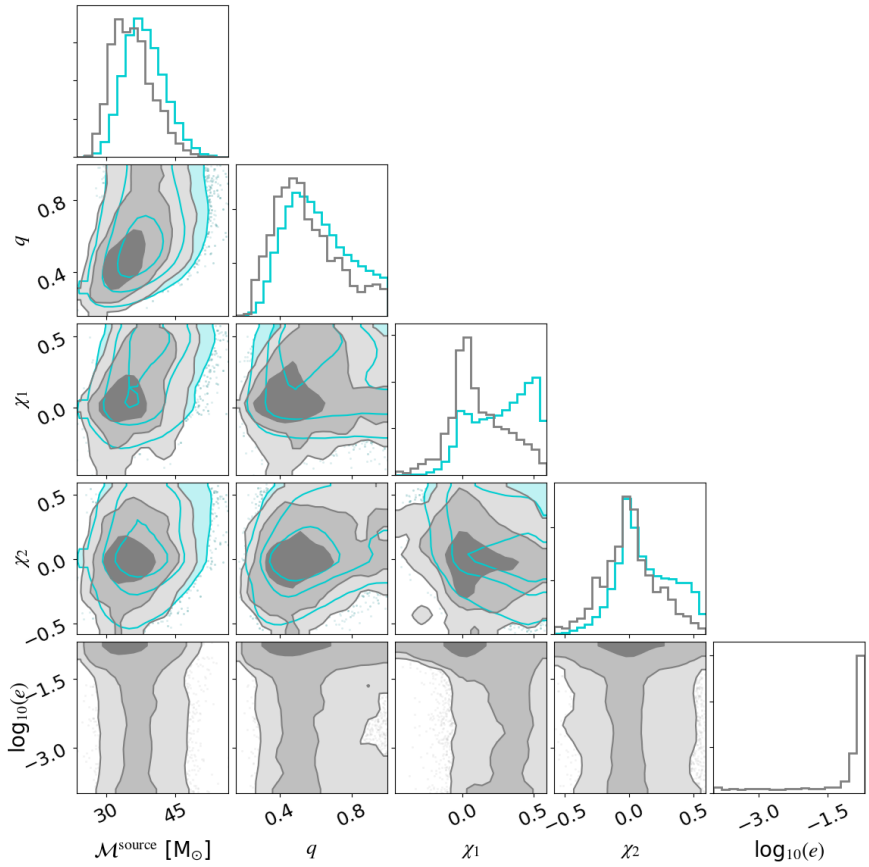

Figure 6.3: Posterior probability distributions on intrinsic parameters for GW190620A, with proposal (circular) parameter estimation results shown in teal and reweighted eccentric posteriors shown in grey. There is a slight visible correlation between source-frame chirp mass and eccentricity, as well as mass ratio and eccentricity. There is a clearer correlation between the aligned spin of the primary, χ_1, and eccentricity.

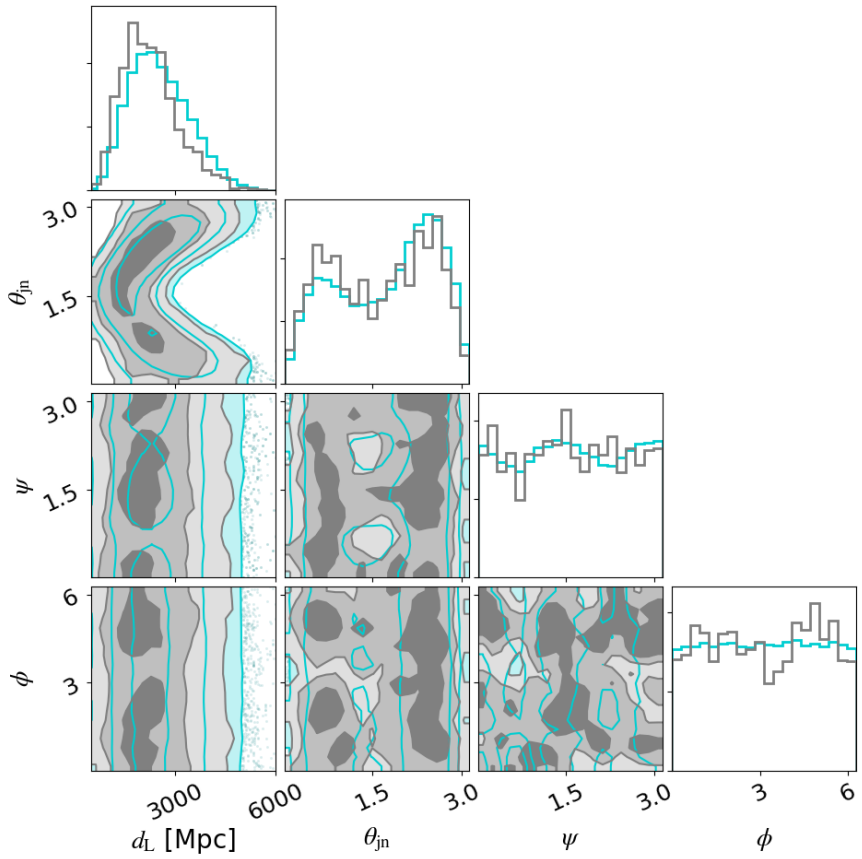

Figure 6.4: Posterior probability distributions on extrinsic parameters for GW190620A. The eccentric posterior causes a slight shift in the posterior to lower luminosity distances.

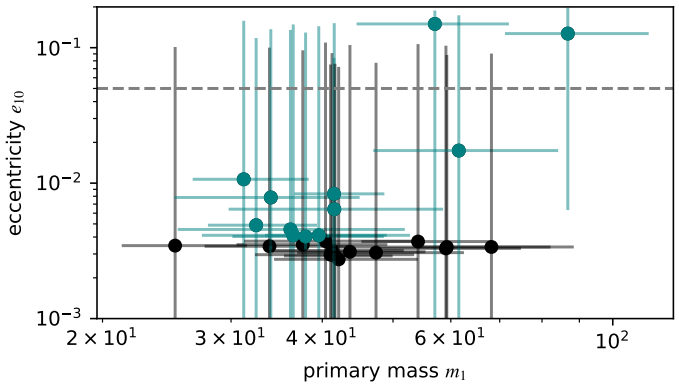

Figure 6.5: Scatter plot of source-frame primary mass m_1 against e_{10} for the 26 BBH newly analysed in this paper, with error bars showing the 90% credible range of the posterior across both axes and a dashed grey line at $e_{10} = 0.05$. Events with points above the grey dashed line are GW190620A and GW190521A, which are two of the highest-mass events in GWTC-2. Events highlighted in teal are those plotted in Figure 6.2 and tabulated in Table 6.1.

statistical significance for eccentricity in GW190521A and GW190620A, we also calculate a frequentist p-value testing the hypothesis that the data are described by the SEOBNRE waveform with an eccentricity value of $e_{10} = 0$. We find that the frequentist confidence intervals for e_{10} exclude $e_{10} = 0$ with $\gtrsim 99.9\%$ confidence (see Figure 6.7 in Appendix 6.6). This high statistical confidence illustrates that the eccentricity we observe is not due to random fluctuations amplified by trial factors. Of course, this test does not tell us if the observed eccentricity is actually due to covariance with spin-induced precession or other systematic error in the SEOBNRE waveform, a topic we return to below.

To do this calculation, we divide out the prior, then calculate the probability of drawing $e_{10} = 0$ from the resulting probability distribution.

6.3.1.1 *GW190620A*

The eccentricity posterior for GW190620A has $e_{10} \geq 0.05$ at 74% credibility, and contains 1269 samples after reweighting with an efficiency of 10%. The hypothesis that GW190620A has $e_{10} \geq 0.05$ is preferred to the hypothesis that $e_{10} < 0.05$ with $\ln \mathcal{B} = 2.48$. GW190620A is a moderately high-mass binary with a total mass $\approx 92\ M_\odot$ in the source-frame.
While GW190521A was found by the LIGO-Virgo analysis to have strong support for in-plane spin [34], the LIGO-Virgo posterior distribution for the GW190620A value of χ_p was uninformative, with little significant deviation from the prior. However, the posterior probability for effective aligned spin χ_{eff} is found to peak at ~ 0.3, consistent with the IMRPhenomD posterior, as shown in Figure 6.3. In contrast to the quasi-circular IMRPhenomD analysis, the eccentric SEOBNRE posterior probability distributions for component spins χ_1 and χ_2 more closely resemble the prior, with both distributions unimodally peaked at 0 and showing lower support for moderate positive spin. The eccentric posterior also has a slight preference for lower masses and a more extreme mass ratio, as shown in Figure 6.3, and a slightly lower distance, as shown in Figure 6.4.

6.3.1.2 *GW190521A*

We also provide updated statistics for GW190521A using the revised prior for e_{10}. These results are qualitatively similar to previously published analyses. The eccentricity posterior for GW190521A has $e_{10} \geq 0.1$ at greater than 92% credibility, and $e_{10} \geq 0.05$ at greater than 93% credibility. The hypothesis that GW190521A has $e_{10} \geq 0.05$ is preferred to the hypothesis that $e_{10} < 0.05$ with a natural-log Bayes factor $\ln \mathcal{B} = 3.90$. Since the eccentric posterior for GW190521A contains the fewest samples of all events, we confirm our eccentricity measurement by performing massively parallel inference with PARALLEL_BILBY [417], splitting our analysis with SEOBNRE over 800 CPUs. We restrict the chirp mass, component mass and spin priors to reduce the time required for such a computationally demanding endeavour. The posterior probability distribution obtained with direct sampling is consistent with that obtained with reweighting, and can

To read in more detail about PARALLEL_BILBY, *check Section 2.3.3.2 in Chapter 2.*

be found in Appendix 6.8, along with further details about that analysis.

6.3.2 *A correlation between primary mass and eccentricity?*

We speculate that eccentricity might be observed preferentially in high-mass systems. In Figure 6.5, we plot the median source-frame primary mass and median eccentricity of each event, with bars extending over the 90% credible range of each parameter.
Source-frame masses are obtained assuming a flat ΛCDM universe with cosmological parameters $H_0 = 67.7\,\mathrm{km s^{-1} Mpc^{-1}}$ and $\Omega_0 = 0.307$ as defined in Planck Collaboration et al. [345]. The two BBH events with signatures of eccentricity are both associated with large primary mass. If this correlation is real, it might provide clues as to the origin of eccentric mergers. Of course, the correlation could also be indicative of systematic error: gravitational waveform analysis is more sensitive to merger physics when the signal is short, as it is for high-mass BBH, and imperfections in the waveform are likely to be most pronounced in this regime.

6.3.3 *Correlation between spin / precession and eccentricity*

Here I refer to the original results for GW190521, presented in Chapter 5.

GW190521A has previously been shown to be consistent with both an eccentric and a spin-precessing system [34, 35, 192, 377]. GW190620A does not have strong evidence for precession [37], but is found by our quasi-circular analysis to support a non-zero value of the effective inspiral spin parameter, $\chi_{eff} \sim 0.3$ [250]. However, when we reweight to our target (eccentric) posterior, higher values of χ_1 and χ_2 are weighted lowly, giving us $\chi_{eff} = 0.06^{+0.2}_{-0.2}$ after reweighting. There is a clear correlation between χ_1 and eccentricity in the central-lower panel of Figure 6.3; this agrees with the correlation between effective spin and eccentricity noted by [329]. Our findings for GW190620A support the argument that eccentric systems may be mistaken by quasi-circular parameter estimation efforts as systems with non-zero aligned spin.

6.4 DISCUSSION

Since the fraction of binary black holes merging with detectable eccentricity in dense star clusters is thought to be robust to changes in simulation parameters, observations of orbital eccentricity can be used to constrain the fraction of LIGO–Virgo binaries being produced in these environments. In Zevin et al. [491], the lower limit on this branching fraction, β_c, is shown to be 0.14 (0.27) at 95% credibility for a number of observations with $e_{10} \geq 0.05$, $N_{ecc} = 1$ (2), when the total number of observed BBHs is $N_{obs} = 46$.
In this work, we present GW190620A, a source with 74% of its eccentricity posterior above $e_{10} = 0.05$. Combining this event with GW190521, there are now two gravitational-wave events with

signatures of non-zero eccentricity. We include measurements for 36 BBH in this work, but use $N_{obs} = 46$ to calculate conservative lower limits on the cluster branching fraction. With $N_{ecc} = 2$, the cluster branching fraction $\beta_c \geq 0.27$. If GW190521A is actually a quasi-circular precessing system and GW190620A is truly eccentric, then $\beta_c \geq 0.14$

While we highlight the two events with the majority of their posterior support at $e_{10} \geq 0.05$, there are an additional ten events that show support for eccentricity, remaining consistent with or peaking at $e_{10} \gtrsim \mathcal{O}(0.01)$. Although these events have less statistically significant support for eccentricity, with no more than 38% of their posterior probability in the region of $e_{10} \geq 0.05$, their support relative to other GWTC-2 events (see Table 6.2) introduces the possibility that we may have ≥ 4 eccentric events in GWTC-2. If these events truly are eccentric—not just statistical fluctuations, or capturing the effects of spin-induced precession—then dense star clusters alone cannot account for the abundance of eccentric binaries [491]. This would mean that other channels capable of producing eccentric compact binaries must be contributing significant quantities of mergers to our catalogues. Recent work has shown that in environments like active galactic nuclei discs, up to $\sim 70\%$ of binary black hole mergers retain detectable eccentricity within the LIGO–Virgo band [390, 430], depending on the freedoms of motion available to binaries within the disc. While we do not yet well-understand active galactic nuclei as dynamical formation environments, a spurious overabundance of eccentric mergers may, in fact, indicate that alternative dynamical environments, such as active galactic nuclei discs, play a significant role in producing mergers detected by LIGO and Virgo.

Eccentric waveform model development is ongoing, and recent models are becoming efficient enough to perform parameter estimation directly [e.g., 110, 237, 404, 483]. Additionally, model-independent analyses such as that simulated in Dálya, Raffai, and Bécsy [125] may be useful for future discovery of high-eccentricity sources, which can be missed by searches that assume quasi-circular signals [e.g., 93]. It is not computationally feasible to analyse tens of long-duration events with SEOBNRE, but we anticipate that it will soon be possible to compute eccentric analysis of catalogues using new, inexpensive waveform models. Different waveform model families are based on different physical approximations, and different eccentric waveform models may use different definitions of eccentricity; any future studies comparing analyses with multiple models must quantify the effects of these differences. Additionally, while there are no waveform models currently available that contain a variable initial argument of periapsis, the effects of eccentricity and the effects of spin-induced precession, we hope that waveform development in this direction [e.g., 258] will enable us to disentangle the effects of these three parameters in future work.

6.5 APPENDIX A: EVENTS CONSISTENT WITH QUASI-CIRCULARITY

We provide the percentages of the posterior above $e_{10} = 0.05$ and 0.1 in Table 6.2 for events that do not have significant posterior support for $e_{10} \geq 0.05$. All of these events have less than 16% of their posterior support above $e_{10} = 0.05$, so are consistent with quasi-circularity within our sensitivity limits to eccentricity. We also provide here the natural-log Bayes factors for the hypotheses that $e_{10} \geq 0.05$ and 0.1. All of these events have $ln\mathcal{B} \leq -0.2$ for the hypothesis that $e_{10} \geq 0.05$ relative to the hypothesis that $e_{10} \leq 0.05$, implying that the data does not favour the eccentric hypothesis over the quasi-circular hypothesis. We show the posterior probability distributions for the eccentricity of these events in Figure 6.6.

Table 6.2: Percentages of the eccentricity posterior probability distribution above 0.1 and 0.05 for the 14 events analysed in this paper that have low support for $e_{10} \geq 0.05$. We also provide the natural log Bayes factors $\ln \mathcal{B}$ for the hypotheses that $e_{10} \geq 0.1$ (0.05) against the hypothesis that $e_{10} \leq 0.1$ (0.05). These events all have less than 16% of their posterior above $e_{10} = 0.05$, and have $\ln \mathcal{B}(e_{10} \geq 0.05) \leq -0.2$.

Event name	percentage $e_{10} \geq 0.1$	percentage $e_{10} \geq 0.05$	$\ln \mathcal{B}(e_{10} \geq 0.1)$	$\ln \mathcal{B}(e_{10} \geq 0.05)$	reweighting efficiency (%)
GW190408A	4.86	13.79	-0.69	-0.35	48
GW190413A	2.17	9.84	-1.24	-0.65	70
GW190413B	4.73	13.49	-0.68	-0.35	88
GW190421A	1.58	9.58	-1.81	-0.75	79
GW190503A	3.67	11.78	-0.98	-0.51	61
GW190514A	5.83	14.81	-0.45	-0.24	85
GW190517A	5.38	13.04	-0.52	-0.34	4
GW190519A	5.08	14.95	-0.59	-0.20	27
GW190602A	3.85	12.27	-0.84	-0.43	54
GW190701A	5.64	15.30	-0.50	-0.20	84
GW190731A	2.21	9.71	-1.10	-0.55	90
GW190803A	4.08	11.65	-0.99	-0.58	2
GW190910A	1.32	10.04	-1.20	-0.47	63
GW190929A	3.28	12.91	-0.76	-0.30	48

6.6 Appendix B: Eccentric likelihood / eccentric posterior with uniform prior

We plot the eccentric model likelihood for all 36 BBH so far analysed for eccentricity in GWTC-2 in Figure 6.7. The eccentric likelihood is obtained by dividing out the log-uniform prior on eccentricity from the eccentric posterior distribution. The resulting likelihood is equivalent to the posterior that would be obtained if we used a uniform sampling prior on e_{10}. While the log-uniform prior represents our prior expectations of the eccentricity of our sources, dividing this out better illustrates which events are not well-supported by the negligible eccentricity hypothesis. GW190521A and GW190620A are the only two events with negligible likelihood amplitude at $e_{10} = 10^{-4}$.

6.7 Appendix C: Overlap between SEOBNRE and IMRPhenomD, and the mass dependence of the upper eccentricity constraint

We observe that higher-mass systems have higher credible limits on their minimum eccentricity at 10 Hz than lower-mass systems. It is easier to constrain the eccentricity of lower-mass systems because they have more cycles in-band than higher-mass systems, so more of the eccentricity-imprinted inspiral is observed. In Figure 6.8, we plot the overlap between SEOBNRE and IMRPhenomD as the eccentricity encoded in the SEOBNRE waveform is increased.[8] Where the overlap is roughly constant (with oscillations due to the hard-coded initial argument of periapsis of the eccentric waveform, which we cannot change), the eccentric and quasi-circular waveform are indistinguishable at current detector sensitivity. Above some value of eccentricity, the overlap between SEOBNRE and IMRPhenomD rapidly decreases. The value of eccentricity at which this happens is the lower limit of eccentricity sensitivity for that particular waveform. This means that, for lower-mass systems, it should be possible to measure smaller eccentricities than for higher-mass systems.

6.8 Appendix D: Massively parallel analysis to confirm eccentric posteriors with direct sampling

To confirm that our reweighted eccentricity posteriors are consistent with those obtained with direct sampling, we use parallel_bilby [417] to directly sample the posterior of GW190521A with eccentric waveform model SEOBNRE using 800 parallel cores. Even with a large number of cores, the full analysis is computationally prohibitive, so we restrict our priors to a region in the vicinity of the posterior maximum: detector-frame chirp masses between 90 and 140 $M_\odot$, individual component masses between 40

8 See Lower et al. [291] for details of the overlap calculation. For this demonstration we use just one detector with LIGO Livingston-like sensitivity.

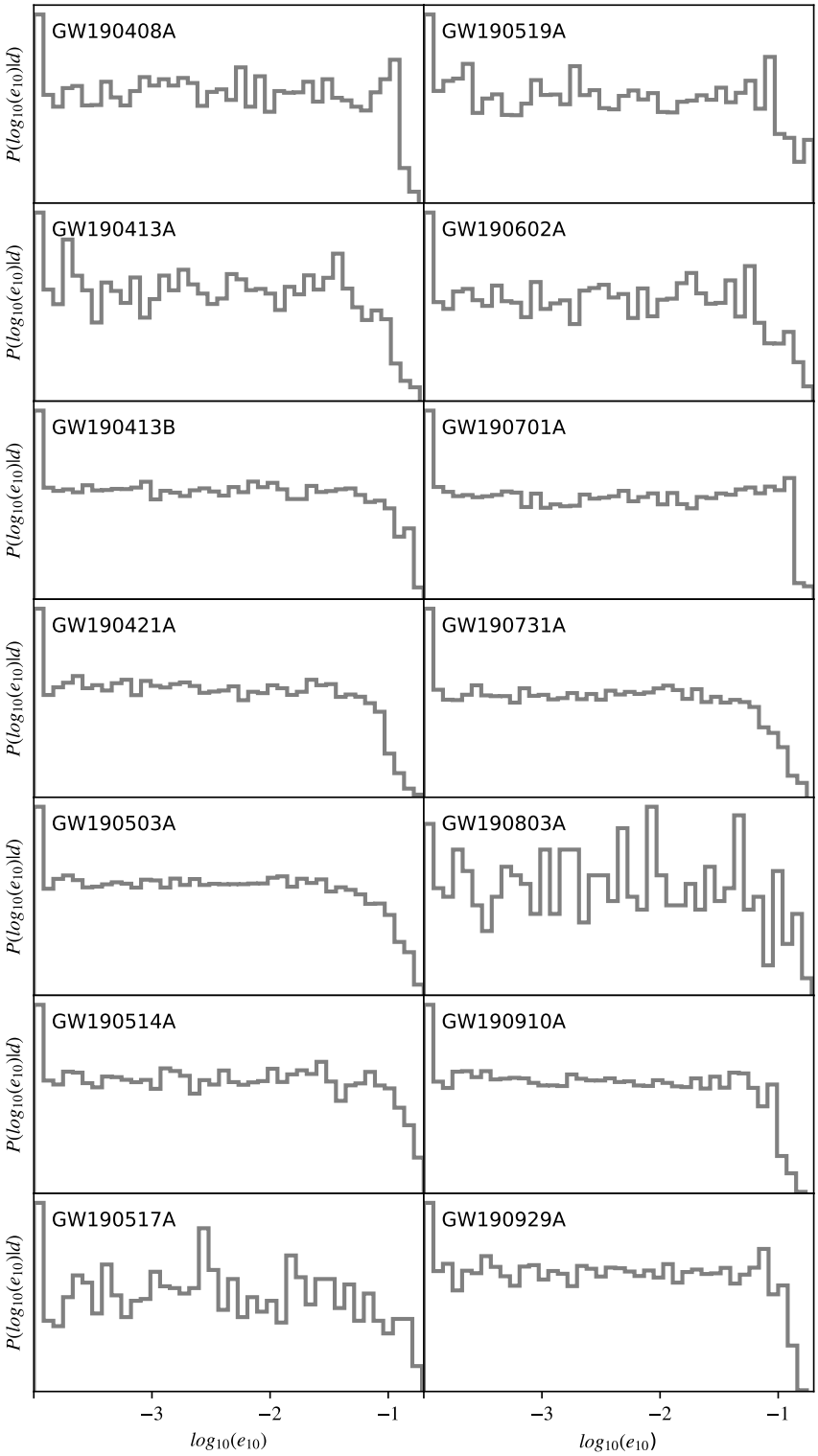

Figure 6.6: Posterior probability distributions on e_{10} for 14 events in GWTC-2 with eccentricity posteriors that have little support for $e_{10} \geq 0.05$.

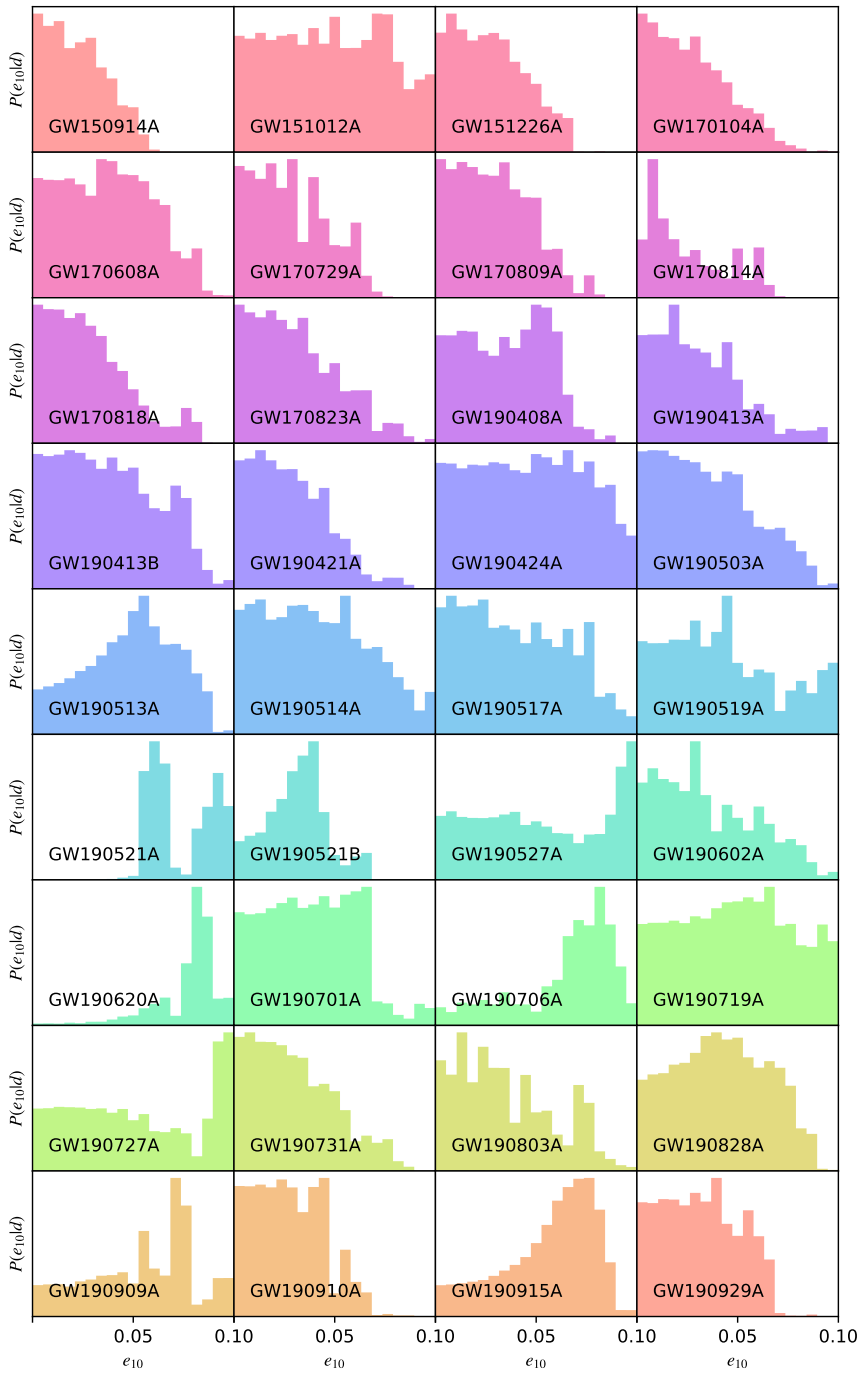

Figure 6.7: The posterior probability distributions under a uniform eccentricity prior for all 36 BBH events so far analysed for eccentricity using SEOBNRE. This is equivalent to the likelihood distribution used in our primary analysis using a log-uniform prior on eccentricity.

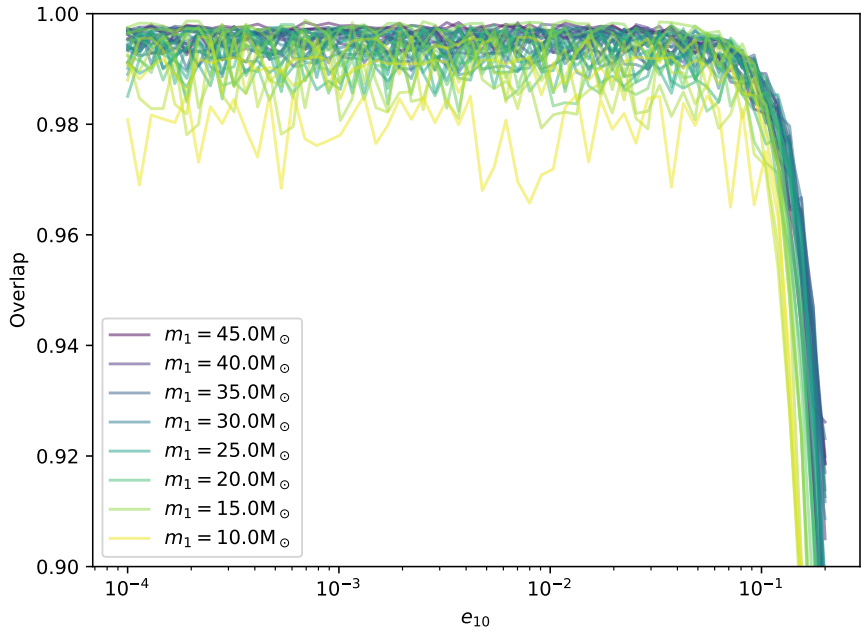

Figure 6.8: The overlap between SEOBNRE and IMRPhenomD with identical parameters but with eccentricity in the SEOBNRE waveform. We plot the overlap curves for systems with $q = 0.8$ and detector-frame m_1 from $10\,\mathrm{M}_\odot$ to $45\,\mathrm{M}_\odot$ at intervals of $1\,\mathrm{M}_\odot$, with legend labels at every $5\,\mathrm{M}_\odot$ interval. We use a duration of $4\,\mathrm{s}$ and sampling frequency of $4096\,\mathrm{Hz}$. Because the mismatch between two waveforms tends to worsen as the number of cycles in-band increases, the maximum overlap gets lower as the mass of the system decreases, leading to lower reweighting efficiency for lower-mass systems. However, lower-mass systems also deviate from semi-constant overlap at lower eccentricities, so we are able to constrain their eccentricity to lower values.

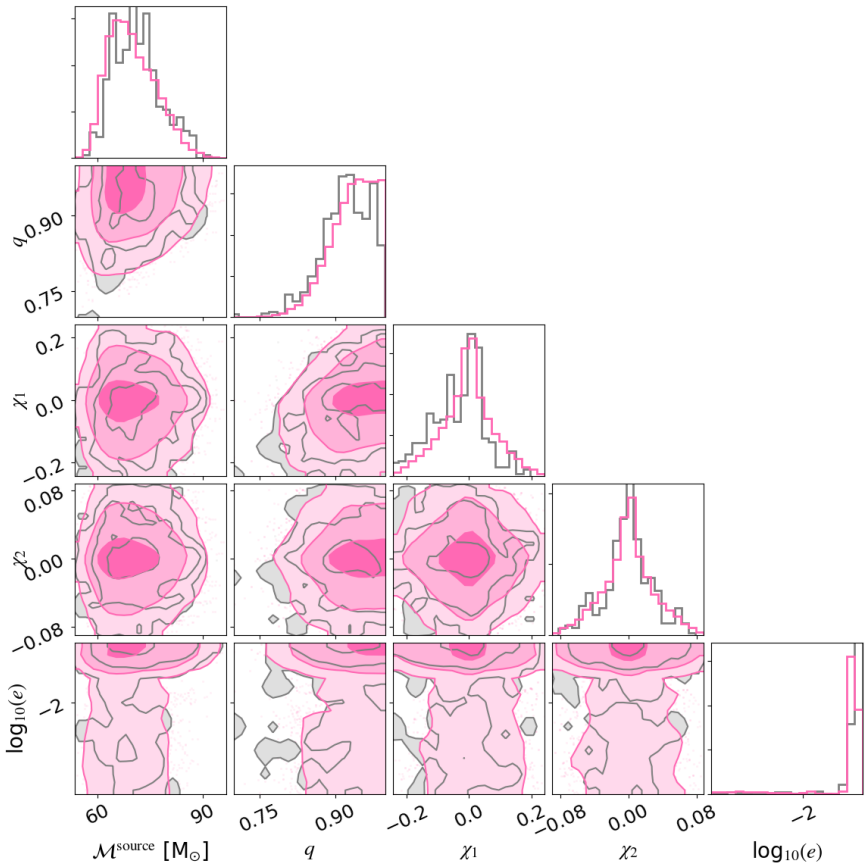

Figure 6.9: Posterior probability distributions on intrinsic parameters for GW190521A, with reweighted results shown in grey and directly sampled results shown in pink.

and 140 $M_\odot$, and $|\chi_1| < 0.5$ and $|\chi_2| < 0.3$.[9] The posterior obtained with direct sampling (pink) is compared to that obtained with reweighting under the same prior restrictions (grey) in Fig. 6.9. The two posteriors display the same strong posterior support for eccentricity above $e_{10} = 0.1$ while producing qualitatively similar posterior distributions for the other parameters. This check gives us confidence that the reweighting method is reliable. While direct sampling is possible for GW190521A—a single, short-duration event, with restricted priors—this is not practical for other events.

9 The restricted prior run required $\sim$ 35 hr of wall time with 800 cores.

Part IV

ECCENTRIC MERGERS AS SNAPSHOTS OF GLOBULAR CLUSTER FORMATION OVER COSMIC TIME

7

GRAVITATIONAL WAVES AS A PROBE OF GLOBULAR CLUSTER FORMATION AND EVOLUTION

This Chapter almost identically replicated the paper published as [375], with some changes to the layout of figures to increase readability. The original appendices appear as Sections in the same order as they appeared in the original text.

ABSTRACT

Globular clusters are considered to be likely breeding grounds for compact binary mergers. In this paper, we demonstrate how the gravitational-wave signals produced by compact object mergers can act as tracers of globular cluster formation and evolution. Globular cluster formation is a long-standing mystery in astrophysics, with multiple competing theories describing when and how globular clusters formed. The limited sensitivity of electromagnetic telescopes inhibits our ability to directly observe globular cluster formation. However, with future audio-band detectors sensitive out to redshifts of $z \approx 50$ for GW150914-like signals, gravitational-wave astronomy will enable us to probe the Universe when the first globular clusters formed. We simulate a population of binary black hole mergers from theoretically-motivated globular cluster formation models, and construct redshift measurements consistent with the predicted accuracy of third-generation detectors. We show that we can locate the peak time of a cluster formation epoch during reionisation to within 0.05 Gyr after one year of observations. The peak of a formation epoch that coincides with the Universal star formation rate can be measured to within 0.4 Gyr—10.5 Gyr after one year of observations, depending on the relative weighting of the model components.

7.1 INTRODUCTION

The first detections of gravitational waves, made over the last five years [30, 37], provide a new lens through which to observe the Universe. Advanced LIGO [29] and Virgo [39] have confirmed the existence of multiple phenomena that, prior to the era of gravitational-wave astronomy, had only been theoretically proposed; stellar-mass binary black holes (BBH) [26], merging neutron stars [12, 14], and intermediate-mass black holes [34] have all been directly observed with gravitational waves.

We are accruing gravitational-wave observations of merging black holes at an accelerating rate [26, 30, 37, 38]. This abundance of BBH

merger detections presents a variety of puzzles across theoretical astrophysics. One such question is how BBH systems that merge within the age of the Universe are assembled. If the binary evolves in isolation, this outcome may be achieved via the common envelope process [see, e.g., 78, 239, 267, 290], stable mass transfer of a stellar secondary onto the primary black hole [66, 321, 499], chemically homogeneous evolution [313, 498] and/or ambient gas-driven fallback [432]. Alternatively, the compact object binary may form dynamically. In this case, the two components evolve separately, only encountering one another once they are already black holes. For this encounter to take place, the components must reside in an environment facilitating dynamical interactions. Such environments include active galactic nuclei [e.g., 210], nuclear star clusters [e.g., 176, 224], young massive clusters [136] and globular clusters [e.g., 227, 368]. In globular clusters, mass segregation leads to the formation of a dark compact-object core [see, e.g., 265, 316, 470], where black holes may interact and merge dynamically. Evidence from LIGO–Virgo's third observing run suggests that a substantial fraction ($\approx 25-93\%$ with 90% credibility) of merging BBH form dynamically [38]; see also [34, 35, 377, 488].

Here I refer to the GW190521 paper, which can be found in Chapter 5.

The gravitational-wave signal from a binary compact object merger carries information about the source's component masses, component spins, and orbital eccentricity. These parameters can be used to distinguish which formation channel the binary evolved through. When a BBH system evolves in isolation, it is expected to have component masses $m \lesssim 65\,\mathrm{M}_\odot$ due to the effects of pair-instability supernovae (e.g., [165, 218, 433]; see [72] for a review of recent updates to this limit for various stellar populations). The co-evolution of the binary is thought to lead to component spins that are preferentially aligned with the orbital angular momentum [100, 242, 423, 436], and since compact binary orbits circularise through gravitational radiation at a faster rate than their separation reduces, any orbital eccentricity induced by the supernovae of the components becomes negligible by the time the gravitational-wave signal enters the observing band [223, 343].[1] When a BBH system forms and merges dynamically, its properties can be detectably different from those of isolated mergers. In the dense environments that support dynamical formation, repeated BH or stellar mergers can give rise to binaries in which one or both components have masses within the pulsational pair-instability mass gap [e.g., 194, 255, 264, 394]. Because the components do not co-evolve, their spins may have any orientation relative to each other [370], and few-body interactions and/or gravitational-wave captures can give rise to mergers with non-negligible eccentricity close to merger [see, e.g., 203, 265, 363, 393, 396, 492]. In globular clusters, $\sim 5\%$ of all BBH mergers are expected to have significant eccentricity close to merger ($e \geq 0.1$ at 10 Hz) [363, 364, 389, 391].

1 While Kozai-Lidov resonance [263, 282] is predicted to lead to eccentric mergers and mis-aligned spins, the Kozai-Lidov field merger rate is thought to be small [e.g., 51, 166, 182, 365, 409].

Globular clusters are observed in great quantities, both inside our Galaxy and beyond; there are ≈ 160 known globular clusters in the Milky Way [385], ≈ 500 in the neighbouring Andromeda Galaxy [342], and ~ 12000 in supergiant elliptical galaxies like M87 [438]. Despite their prolific nature, it is not known how globular clusters form. Globular clusters contain stars that are thought to be among some of the most ancient in their host galaxy [for example, the globular cluster Hpl contains some of the most ancient stars ($\gtrsim 12\,\mathrm{Gyr}$) in the Milky Way; 248], making their formation difficult to observe with electromagnetic telescopes. To date, the primary method to constrain cluster ages is main-sequence fitting of colour-magnitude diagrams [e.g., 207, 399, 452] with a small subset of cluster ages also determined from the white dwarf cooling sequence [e.g., 191, 215]. Typical globular cluster age measurements have uncertainties of order $\mathcal{O}(1\,\mathrm{Gyr})$; see [171, 173] and references therein. It is hoped that the James Webb Space Telescope (JWST)—due to be launched in October, 2021 [319]—will be able to constrain cluster ages to within 1 Gyr [e.g., 121].

Measurements of globular cluster ages and metallicities suggest two different globular cluster sub-populations: very old globular clusters, which are observed to have a wide range of ages and metallicities; and younger globular clusters, which have metallicities that anti-correlate with their ages [172, 173, 215, 278, 452]. Current theories of globular cluster formation fall into two main categories: (i) clusters formed as a byproduct of active star formation in galaxy discs [e.g., 144, 269, 405] and (ii) clusters formed due to the collapse of dark matter halos during or before the epoch of reionisation [e.g., 147, 245, 256, 292, 355, 447]. In category (i), the formation probability follows the observed star formation rate [SFR; 295], peaking at $z \approx 2.5$ [171, 173], while in category (ii) the formation probability peaks at $6 \lesssim z \lesssim 12$ [173, 447]. Constraining the primary formation epoch of globular clusters will answer long-established questions in astrophysics. If globular clusters predominantly form before $z \approx 6$, they may play a leading role in the reionisation of the Universe [e.g., 292]. On the other hand, if the globular cluster formation probability curve follows the SFR, and the majority of star formation takes place in such environments [e.g., 274], then detailed understanding of cluster formation histories may place critical constraints upon the overall SFR. If we know the formation epoch of clusters, then we can adjust N-body simulations to more correctly reproduce clusters observed at $z = 0$, thereby enhancing our physical descriptions of cluster initial conditions. Our understanding of the role that globular clusters play in the evolution of galaxies—for example, whether globular clusters are early galaxies [145], failed galaxies [147], or galaxy remnants [297]—can also be improved by observing globular clusters as they form and evolve.

As detectors improve, gravitational waves will allow us to trace compact binary mergers throughout cosmic time [see, e.g., 386, 465]. In turn, this will allow us to use gravitational waves as probes of cluster formation and evolution. The current generation of detectors can observe events out to redshifts $z \lesssim 1.5$—not far enough for

globular cluster formation to be traced through our observations. In order to examine globular cluster formation, we must wait for third-generation gravitational-wave observatories such as the Einstein Telescope [354] and Cosmic Explorer [28]. These observatories, proposed to begin taking data ca. 2035, will be able to detect BBH mergers with total mass of order $\mathcal{O}(100)\,\mathrm{M}_\odot$ out to redshifts $z \approx 30$, and GW150914-like mergers out to $z \approx 50$ [211].
In this paper, we demonstrate the power of gravitational-wave observations as probes of globular cluster formation and evolution. In Section 7.2.1, we motivate a Gaussian mixture model describing the globular cluster formation probability over cosmic time. We explain the metallicity-dependent merger time distribution used to convert this underlying globular cluster formation probability to the BBH merger probability in Section 7.2.2. In Section 7.3, we outline our population inference method. We test our ability to recover the underlying globular cluster formation probability in Section 7.4, obtaining population inference results using simulated third-generation gravitational-wave observatory data with realistic uncertainties. For these simulations, we use only mergers that are massive and rapid-merging—signatures of dynamical formation—as "snapshots" of the clusters at creation. We find that we can measure the formation epochs of globular clusters to 0.02—0.6 Gyr precision at 99% credibility after one year of third-generation gravitational-wave observations—comparable to the forecasted accuracy of JWST [e.g., 121]—unless cluster formation primarily occurs during reionisation, in which case the precision with which we can locate a secondary lower-redshift formation epoch is reduced to $\mathcal{O}(10)$ Gyr. If we use all cluster mergers instead of just the small fraction that we consider to be identifiable as such, our constraints on cluster formation epochs tighten by up to an order of magnitude. In Section 7.5, we state the assumptions and caveats underlying our model. We conclude in Section 7.6.

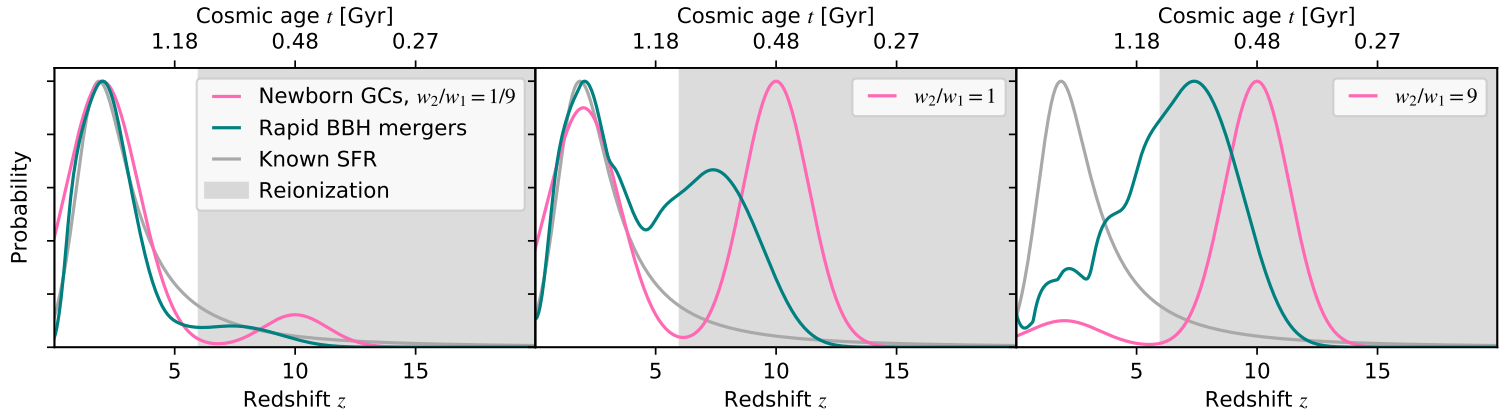

Figure 7.1: The three cases we consider in this work are illustrated from left to right: $w_2/w_1 = 1/9$, where SFR-driven globular cluster formation dominates clusters formed by $z = 0$; $w_2/w_1 = 1$, where there is equal contribution to clusters formed by $z = 0$ from both formation channels; and $w_2/w_1 = 9$, where reionisation-driven globular cluster formation dominates clusters formed by $z = 0$. The probability distributions of rapid-merging first-generation massive BBH mergers (where both components have $30M_\odot \leq m \leq 40M_\odot$) are plotted in teal, while the formation probability distributions of GCs in each model are plotted in pink.

7.2 MODEL

In the following section, we describe our model, which combines theoretically-motivated globular cluster formation probability distributions (described in Section 7.2.1) with simulated BBH merger distributions (described in Sections 7.2.2 and 7.2.3). We assume a flat ΛCDM Universe with $H_0 = 67.7\,\mathrm{km s^{-1} Mpc^{-1}}$ and $\Omega_0 = 0.307$ [345].

7.2.1 *Globular Cluster Formation Probability Distribution*

Our globular cluster formation probability is modelled by a two-component Gaussian mixture model in redshift. The first component represents SFR-driven globular cluster formation, with mean μ_1, standard deviation σ_1 and weight w_1; the other represents reionisation-driven globular cluster formation, with mean μ_2, standard deviation σ_2 and weight w_2.
We simulate a fiducial globular cluster formation probability using specific parameter values shown in Table 7.1. For the injection sets, we set the mean and standard deviation of the SFR-driven peak in order to best represent the true shape of the SFR [295]. The mean of the reionisation-driven peak is motivated by the results of [447]; see also [355].
To investigate our ability to distinguish the preferred channel of globular cluster formation, we vary the weight ratio w_2/w_1. We consider three cases: (i) that globular clusters are formed primarily as a byproduct of the SFR, and there is a small contribution formed during reionisation ($w_2/w_1 = 1/9$); (ii) that globular clusters are formed with equal probability during reionisation and through star formation ($w_2/w_1 = 1$); and (iii) that globular clusters are formed primarily during reionisation, with a small contribution forming in accordance with the SFR ($w_2/w_1 = 9$). All three cases lead to a similar merger probability at $z = 0$, so the scenarios cannot be distinguished by existing detectors. However, third-generation detectors will be able to constrain w_2/w_1. Our three globular cluster formation probability functions are plotted in pink in the three panels of Figure 7.1.

7.2.2 *Binary Black Hole Merger Probability Distribution*

In order to translate globular cluster formation probability into gravitational-wave observables, we calculate the distribution of BBH mergers in globular clusters. To simulate globular cluster evolution, we use the CMC Cluster Catalog [265]. These simulations were computed using CMC [241, 339], a Hénon-type Monte Carlo code which includes various physical processes relevant to the dynamical formation of BH binaries including two-body relaxation, stellar and binary evolution [computed using updated versions of SSE and BSE; 234, 235], and direct integration of small-N resonate encounters [187] including post-Newtonian effects [363]. A number of parameters relevant to the long-term cluster evolution are varied within this set

	Value	
Parameter	z	t [Gyr]
μ_1	2.00	3.30
σ_1	1.50	2.32
μ_2	10.00	0.48
σ_2	1.35	0.09
w_2/w_1	$1/9$, 1, 9	

Table 7.1: Parameter values chosen for our fiducial globular cluster formation probability models, used in the injection studies described in Section 7.4. Each of the two Gaussian peaks in our model has mean μ_j and standard deviation σ_j, where $j = 1$ refers to the SFR-driven peak and $j = 2$ refers to the reionisation-driven peak. The ratio w_2/w_1 determines the relative weight of the reionisation-driven peak against the SFR-driven peak. We vary w_2/w_1 to test our ability to recover the underlying globular cluster formation probability in three different scenarios, between which the dominant formation mechanism of clusters varies.

of simulations (namely the total cluster mass, initial virial radius, metallicity, and radial position within the Galactic potential), with values chosen to reflect the observed properties of the Milky Way globular clusters. Altogether, this catalogue nearly completely covers the full parameter space of the Milky Way globular clusters and captures the formation of a variety of astrophysical objects such as gravitational-wave sources as well as X-ray binaries, pulsars, and blue stragglers. By implementing a cluster age distribution model from El-Badry et al. [142], Kremer et al. [265] estimated a BBH merger rate of roughly $20\,\mathrm{Gpc}^{-3}\,\mathrm{yr}^{-1}$ in the local Universe, consistent with previous theoretical work on the subject [e.g., 49, 55, 366, 367] as well as with the observational rate inferred from the second LIGO/Virgo catalogue [37].

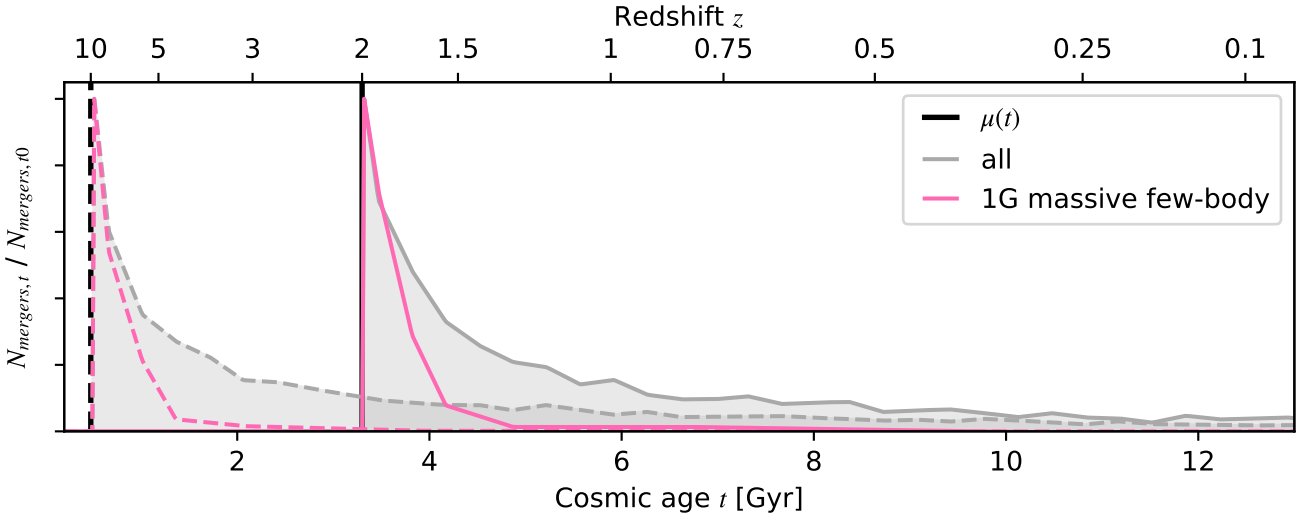

Figure 7.2: Merger time distributions for BBH mergers from two clusters formed at μ_1 ($z = 2$; during the peak of the SFR) and μ_2 ($z = 10$; during reionisation), with distributions shown with solid and dashed curves respectively. The distributions of all mergers from each cluster after its formation are shown in grey. The distributions of just the massive first-generation ($35\,M_\odot \leq m \leq 40.5\,M_\odot$; 1G) mergers formed through gravitational-wave capture during few-body interactions are shown in pink.

Each newborn globular cluster in our model has a metallicity-dependent merger time distribution. The clusters in the CMC Cluster Catalog have one of three absolute metallicities: 0.0002, 0.002, and 0.02. We combine mergers from clusters with the same metallicity, then sort the mergers into 100 time bins. We use a univariate spline to smoothly interpolate between the bin heights. We then perform a two-dimensional linear interpolation between these smoothed merger distributions of both cluster age and metallicity. To calculate the merger distribution for a cluster born at a certain redshift, we assume for simplicity that metallicity increases linearly with the age of the Universe. We assume a metallicity of $Z = 0.0002$ at a redshift of 24 and a metallicity of $Z = 0.02$ at the present day [see, e.g., Figure 6 of 283, for observationally-driven proposals for metallicity evolution over cosmic time].
We convert the sum of merger time distributions from all clusters into a probability distribution in redshift, from which we draw our source population. In Figure 7.1, the merger probability distributions from each of the three globular cluster formation probability models are plotted with teal curves. In Figure 7.2, we illustrate in grey the merger time distributions for two clusters: one formed at $z = 2$ and one formed at $z = 10$.

7.2.3 *Rapid mergers as cluster formation snapshots*

The merger time for a BBH formed dynamically in a stellar cluster is determined by three timescales: (i) the cluster formation time, (ii) the time required for BBH formation through dynamical encounters, and (iii) the gravitational-wave inspiral time from the time of last dynamical encounter to merger. The latter two timescales are sensitive to a variety of host cluster properties including total cluster mass, half-mass radius, and BH mass distribution [e.g., 55, 265, 370]. As a consequence, disentangling the cluster formation time distribution from the merger time distribution for a given list of dynamical BBH mergers may pose a challenge. This challenge may be circumvented by looking at specific classes of mergers known to have prompt merger times, $t_{merge} \lesssim \mathcal{O}(100\,\mathrm{Myr})$ since cluster formation. For these rapid mergers, the observed merger time distribution much more closely traces the underlying cluster formation time distribution. Rapid mergers in globular clusters are expected to have two primary characteristics: high eccentricities and high masses. During small-N ('few-body') resonant encounters, pairs of BHs can form that merge rapidly, making them more likely to retain orbital eccentricity at detection. As discussed in Samsing [389] and Kremer et al. [265], roughly $5-10\%$ of cluster mergers are expected to retain high eccentricity ($e \geq 0.1$) close to merger ($f_{\mathrm{GW}} = 10\,\mathrm{Hz}$). These binaries can have gravitational-wave inspiral times as short as days [e.g., 492]; this makes them ideal tracers of cluster formation, as they merge relatively quickly after the cluster forms and are more likely to retain the dynamically-induced eccentricity that can reveal their formation

As we found in [491], the detectable percentage after accounting for selection effects is more like 4%.

channel. As a natural consequence of dynamical friction, the most massive BHs in a cluster are expected, on average, to be the first to form BBHs and the first to merge [e.g., 316]. Thus, BHs with masses near the assumed upper limit of the BH mass distribution ($40.5M_\odot$ in the CMC Cluster Catalog) that merge through gravitational-wave capture encounters are ideal rapid merger candidates. For the anaysis presented in Section 7.4, we consider only globular cluster binaries that merge through resonant few-body encounters.
There is an inherent additional delay associated with second-generation BHs formed through previous BH mergers that remain bound to their host cluster. Although these will preferentially merge again quickly (within a few 10 Myr of the previous merger) due to their relatively high mass, we do not include second-generation mergers in this analysis. Here, we consider only those massive few-body mergers that are first-generation (1G), having both component masses above $35M_\odot$ and below $40.5M_\odot$. We plot this distribution of mergers in pink in Figure 7.2. Over the redshift range that we study, the fraction of 1G massive few-body mergers varies between 3% and 6% of all cluster mergers. We construct the merger time distribution using only 1G massive few-body mergers, and draw only 5% of the number of detections expected from the observing durations.

7.3 METHOD

We simulate redshift posterior probability distributions for a population of BBH mergers, and use the population inference framework to discern the injected distribution of the population. The likelihood for the data $\mathbf{d}$ is

$$\mathcal{L}_{tot}(\mathbf{d}|\mathbf{\Lambda}) = \prod_i^N \frac{\mathcal{Z}_\varnothing(d_i)}{n_i} \sum_k^{n_i} \frac{\pi(\theta_i^k|\mathbf{\Lambda})}{\pi(\theta_i^k|\varnothing)}. \tag{7.1}$$

In this equation, $\mathbf{\Lambda}$ is the set of parameters describing the population distribution, while θ_i^k are the parameters describing the kth posterior sample of event i (in our case, θ_i is only one parameter – redshift). Each event i has n_i posterior samples; there are a total of N events. The sampling prior used for inference on data d_i for event i is $\pi(\theta_i|\varnothing)$, which is reweighted to obtain results for a population-based prior $\pi(\theta_i|\mathbf{\Lambda})$. The evidence obtained with the original sampling is $\mathcal{Z}_\varnothing(d_i)$. In our case, the population prior $\pi(\theta_i|\mathbf{\Lambda})$ is the distribution described in Section 7.2.
Distance measurement uncertainties are likely to be $\mathcal{O}(10\%)$ for most binaries observed with third-generation detectors [464, 493] . To model uncertainty of approximately this magnitude, we assume Gaussian likelihoods of width $\sigma_{z_i} = 0.1z_i$. These likelihoods each have a mean $\mu_{z_i} = z_i + r_i$, where r_i is a random offset drawn from a Gaussian of mean $\mu_{r_i} = 0$ and $\sigma_{r_i} = \sigma_{z_i}$. We produce a posterior curve by multiplying the likelihood by a uniform sampling prior. (This prior is divided out in the calculation of Eq. 7.1.) From this posterior curve, we draw 50 simulated posterior samples for each event.

To execute our population analysis, we use the Bayesian inference library BILBY [54, 378]. We use uniform priors over all parameters. The prior covers the range $10^{-5} \leq z \leq 6$ for μ_1, $0.5 \leq z \leq 6$ for both σ values, and $6 \leq z \leq 20$ for μ_2. The prior on w_2/w_1 ranges from 10^{-2} to 10.

Here I refer to the BILBY *paper, which is provided in Chapter 2.*

The formation channel of a binary may be identified using a method such as that developed in [254], in which a BBH merger's mass and spin measurements are used to calculate its probability of being a hierarchical merger in a globular cluster. Similar methods may be extended to incorporate eccentricity measurements, which will be illuminating for globular clusters as we expect $\sim 5\%$ of globular cluster mergers to have eccentricity $e \geq 0.1$ at 10 Hz [see, e.g., 389]. While precession is considered a hallmark of dynamical mergers, there have been relatively few events that have clear precession measurements [30, 37]; however, both precession and anti-aligned spins can be measured at a population level, as demonstrated in [38]. With third-generation detectors, component spins and precession will be well measured [e.g., 468]. Using such measurements at both an individual and population level, it may be possible to estimate the sub-population of globular cluster mergers within a set of BBH mergers from a variety of formation channels.

In this paper, we assume that mergers identified as cluster mergers have 0% probability of having formed via a different channel. Such definitive statements are unlikely to be made based on the parameters of detected binaries for the vast majority of sources even if we allow for future improvements to our mechanisms for performing such identifications. In the future, binaries that form in globular clusters but are kicked out before merging may still be indistinguishable from isolated mergers, and those that do merge inside the cluster are likely to have properties similar to those in other dynamical environments (e.g., AGN discs and galactic nuclei) or field triples undergoing Kozai-Lidov resonance. More complex future analyses should weight the samples from each event by the probability that each binary formed inside a globular cluster. This is an additional complication that can be built upon the method presented here, and is left for future work.

7.4 INJECTION STUDIES

The Universal merger rate implied by current BBH merger observations is $\sim 0.2\,\mathrm{min}^{-1}$ [4]. For an all-seeing detector, this translates to a BBH signal detection count of $\mathcal{O}(500)$ per day [296]. Third-generation detectors like CE and ET will be close to all-seeing, detecting GW150914-like events out to redshifts $z \approx 50$, and GW190521-like out to $z \approx 30$ [211]. We use 500, 10000 and 100000 as order-of-magnitude estimates for the total number of GC mergers in one day, one month and one year, respectively. This is a reasonable approximation if GC mergers make up $\geq 10\%$ of all mergers in the Universe. We assume, based on the fraction of massive and

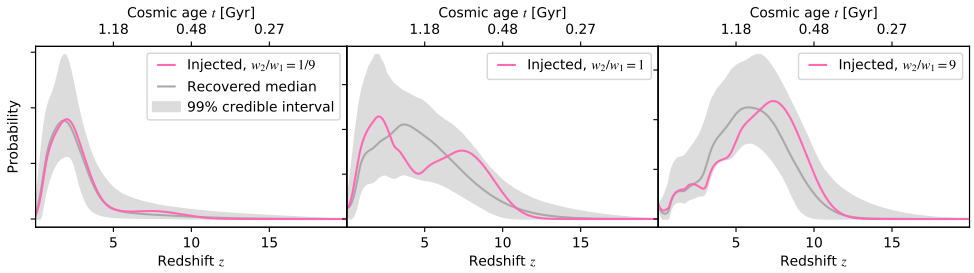

Figure 7.3

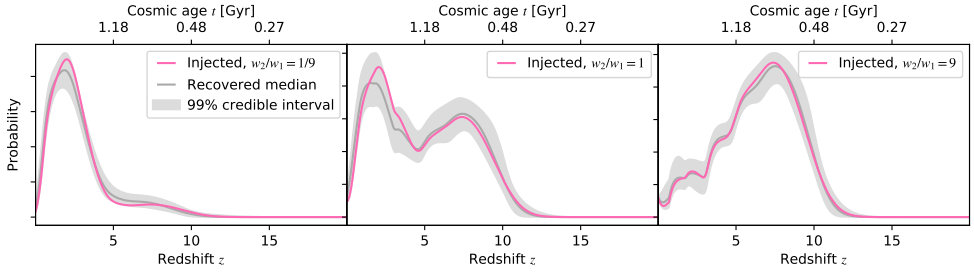

Figure 7.4

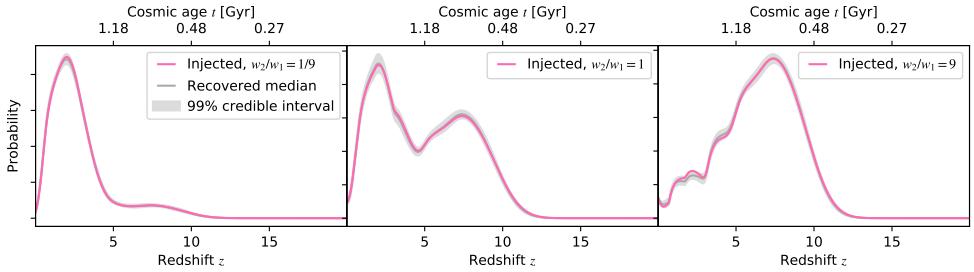

Figure 7.5

Figure 7.6: Globular cluster formation rates inferred from simulated third-generation detector observations of first-generation massive few-body mergers after (a) one day (using 25 1G massive few-body mergers from the total population of 500), (b) one month (using 500 of 10000) and (c) one year of detections (using 5000 of 100000). Each panel represents an underlying model with a different weighting of the two components of the Gaussian mixture model that represents the globular cluster formation rate. *Left*: SFR-driven peak dominates formation rate; *Middle*: Each peak contributes equally to formation rate; *Right*: Reionisation-driven peak dominates formation rate.

μ_1	99% CI width (Gyr)		
	w_2/w_1	Day	Month	Year
	9	11.92	12.01	10.49
	1	11.99	9.87	0.53
	$1/9$	10.44	4.32	0.39
μ_2				
	9	0.48	0.06	0.02
	1	0.74	0.08	0.02
	$1/9$	0.74	0.42	0.05

Table 7.2: Width of 99% credible intervals (CIs) around μ_1 (top) and μ_2 (bottom) for each injection study described in Section 7.4. For these injection studies we use only first-generation massive few-body mergers, and include a 10% uncertainty on source redshift. When the 10% uncertainty is removed, the width of these uncertainty intervals does not meaningfully change.

quick-merging binaries observed in the cluster simulations described in Section 7.2, that only $\sim 5\%$ of these observations can be confidently identified as cluster mergers. To simulate a month's worth of confidently-identified cluster mergers, for example, we use 500 events. We simulate data after one day, one month, and one year of observing, for three different models of the underlying globular cluster formation probability. The first case we consider is one where globular clusters do not form efficiently during reionisation. In this case, the globular cluster formation probability curve closely follows the observed SFR. We set the weight ratio $w_2/w_1 = 1/9$, such that 90% of all clusters form within the SFR peak. In the second case, we set the weight ratio $w_2/w_1 = 1$, which leads to a 50–50 split between clusters contributed from each peak. The final case we consider is one where globular clusters primarily form during reionisation, such that 90% of clusters are formed within the reionisation peak. We set $w_2/w_1 = 9$. For all three injected data sets, the remaining four parameters $(\mu_1, \mu_2, \sigma_1, \sigma_2)$ are fixed to the values provided in Table 7.1. We show the globular cluster formation probability curve and resulting probability distribution of observable BBH mergers for all three cases in Figure 7.1.

In Figure 7.6, we plot the injected underlying globular cluster formation probability curve in pink, and compare it to the recovered median and 99% credible intervals in grey. For all three observing periods, the injected distribution is within the 99% credible interval. Probability distributions on the five populations parameters μ_1, μ_2, σ_1, σ_2 and w_2/w_1 are provided as corner plots in Appendix 7.7. We state the widths of the 99% credible intervals around μ_1 and μ_2 for each study in Table 7.2.

We repeat the above injection studies for two additional scenarios. In the first, we neglect any measurement uncertainty and assume that each source is represented by a delta function at its true value of z. In

this case, we see negligible change in the widths of the 99% credible intervals around μ_1 and μ_2. In the second, we include redshift measurement uncertainty, but optimistically assume that all cluster mergers can be confidently identified, thereby allowing us to use 100% of the mergers from the CMC Cluster Catalog to construct our model. This leads to a reduction of up to an order of magnitude in the width of the 99% credible interval around μ_1 and μ_2; for one day of observing all cluster mergers, the credible intervals are nearly identical to those seen for a month of observing only 1G massive few-body mergers. These measurements are more precise—despite the longer average merger timescale—because we are able to use 20 times as many events to probe the cluster formation rate. The precision with which we can measure globular cluster formation epochs with third-generation observations, therefore, sensitively depends on the number of events that are confidently identified as globular cluster mergers.

7.5 Systematic error analysis and caveats

We make a number of simplifying assumptions and approximations in our analysis, allowing us to demonstrate a generic way to probe globular cluster formation using gravitational-wave detections. These are listed in this section, with the aim to reduce the number of assumptions we make in future work that builds upon this paper.
We approximate both epochs of globular cluster formation as simple Gaussians in redshift. However, the true SFR determining the shape of the cluster formation probability does not follow a Gaussian, and the shape of the reionisation-driven cluster formation probability is not known. More complex future extensions of this work may allow the shape of the Gaussians to vary, with the skewness of the Gaussian a model variable. We assume that the redshift posterior distributions are also Gaussian, but the true shape of the uncertainty distribution would vary depending on the noise in the data containing each signal.
We set our injection studies in an optimistic future where merger channels can be perfectly distinguished. While we analyse the merger distribution of only those globular cluster BBH that are high-mass, rapid-merging and highly likely to be detectably eccentric (signatures of dynamical origin) for our primary results, we still ignore any possibility of contamination from other dynamical formation channels that produce mergers with similar properties, such as mergers in AGN or Kozai-Lidov [263, 282] triples in the field.
We also do not account for any sources redshifting out-of-band due to high masses or high eccentricities at high redshift. We do not account for the disruption/creation of globular clusters during galaxy mergers; while the increased star formation of merging galaxies should be absorbed into the SFR peak of our models, the shape of the merger time distribution at a given epoch will differ if clusters are disrupted/created at that time due to galaxy mergers, even if the overall number of globular clusters remains the same.

We assume that metallicity increases linearly with the age of the Universe to obtain different merger time distributions for clusters born at different times, but do not consider a time-evolving initial mass/density function. Metallicity, mass and density may become globular cluster variables in future iterations of our model, allowing us to consider whether the physical properties of clusters can be inferred from observations of gravitational waves.

7.6 CONCLUSIONS

In this work, we show that observations from third-generation gravitational-wave detectors will allow us to measure the formation epochs of the population of globular clusters. Our primary results are obtained assuming that only first-generation massive few-body mergers can be confidently identified as globular cluster mergers. If up to 50% of clusters are born following the SFR, a cluster formation epoch at $z = 2$ can be resolved to within less than 1 Gyr precision after one year of observing; however, if the majority of clusters are born during reionisation, the time of this epoch will have an uncertainty $\mathcal{O}(10)$ Gyr. For all scenarios, a cluster formation epoch at $z = 10$ can be resolved to within less than 1 Gyr precision after just one day of observing, and to within 0.05 Gyr after a full year. If we are able to confidently identify all globular cluster mergers as such, these uncertainty bands can decrease by up to an order of magnitude. With third-generation detectors Cosmic Explorer and Einstein Telescope due to commence observing in the 2030s [296, 361], the question of how globular clusters formed may be answered with gravitational-wave observations within the next twenty years. These results will be complementary to measurements from electromagnetic telescopes, such as JWST, which will be able to constrain the ages of individual clusters to within $\mathcal{O}(1)$ Gyr [e.g., 121].
Our method can be extended for use in multiple future projects. For example, we could assign a population of mergers from multiple formation channels with a certain probability of being globular cluster mergers, and weight their contribution to the total merger distribution accordingly. We could also use intrinsic binary parameters, e.g. mass and eccentricity, to infer properties of their host clusters, like their densities at formation. The simple procedure outlined in this paper must be refined before application to real data. In particular, future work should address the fact that many signals from the more massive and highly-eccentric sources may be redshifted out-of-band. We leave potential extensions and improvements for future work.

7.7 APPENDIX: POSTERIOR PROBABILITY DISTRIBUTIONS FOR POPULATION PARAMETERS

In this section, we present posterior probability distributions for our five population parameters in cosmic time, recovered using the merger-time distributions of 1G massive few-body mergers. Posterior

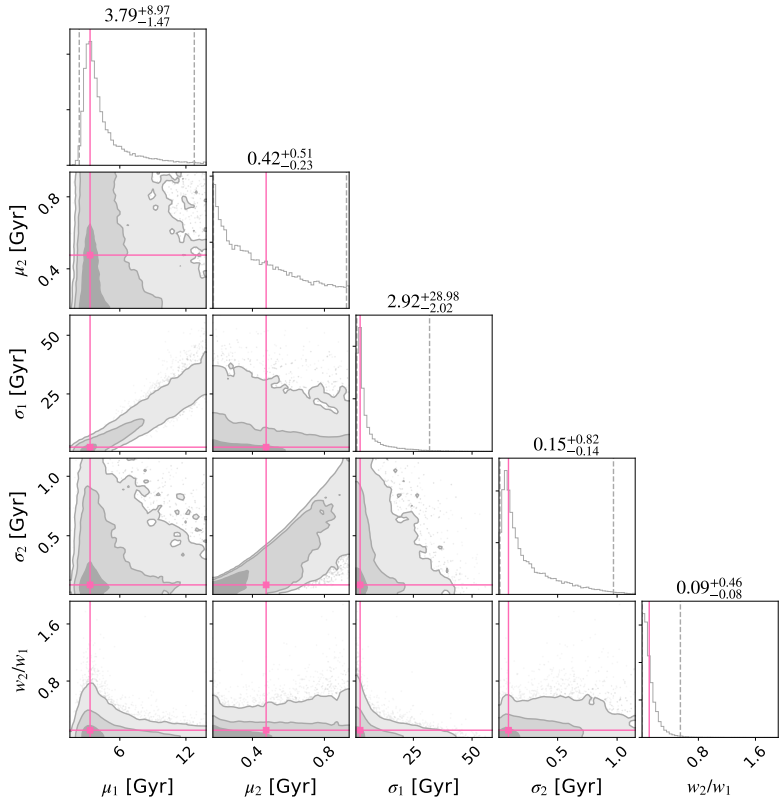

Figure 7.7: See the caption of Fig. 7.9.

distributions are plotted in grey, with the injected values indicated with pink lines, and the shading gradients on the two-dimensional posteriors indicate levels of 1σ, 2σ and 3σ credibility, while the dashed grey error bars around the median recovered values show 99% credible intervals.

7.7.1 *Results after one day of observing*

In Figures 7.7, 7.8 and 7.9 we present the one- and two-dimensional posterior probability distributions over each population parameter resolved after one day of observations with third-generation detectors.

7.7.2 *Results after one month of observing*

In Figures 7.10, 7.11 and 7.12 we present the one- and two-dimensional posterior probability distributions over each population parameter resolved after one month of observations with third-generation detectors.

7.7.3 *Results after one year of observing*

In Figures 7.13, 7.14 and 7.15 we present the one- and two-dimensional posterior probability distributions over each population parameter resolved after one year of observations with third-generation detectors.

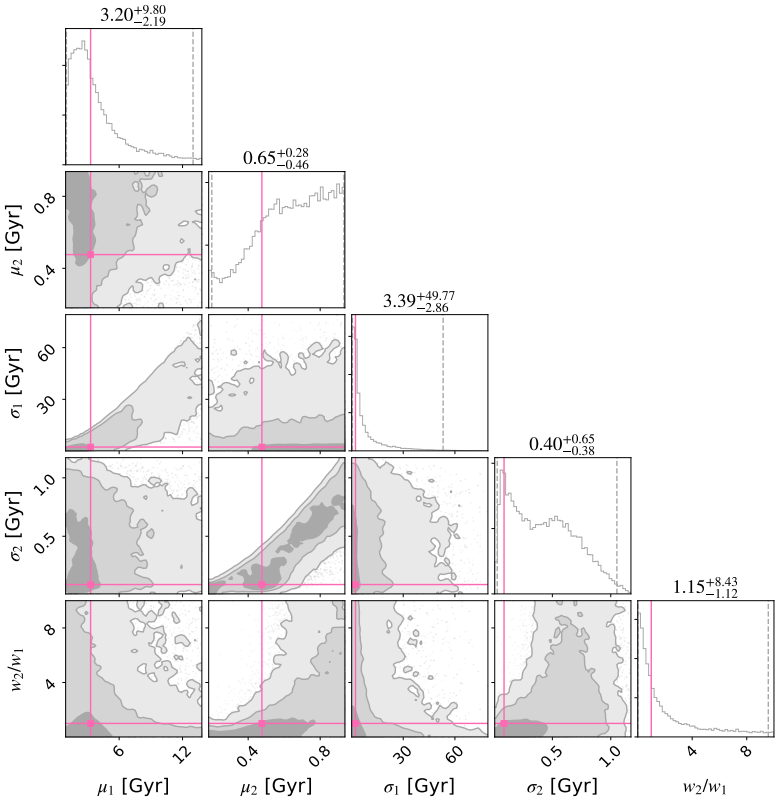

Figure 7.8: See the caption of Fig. 7.9.

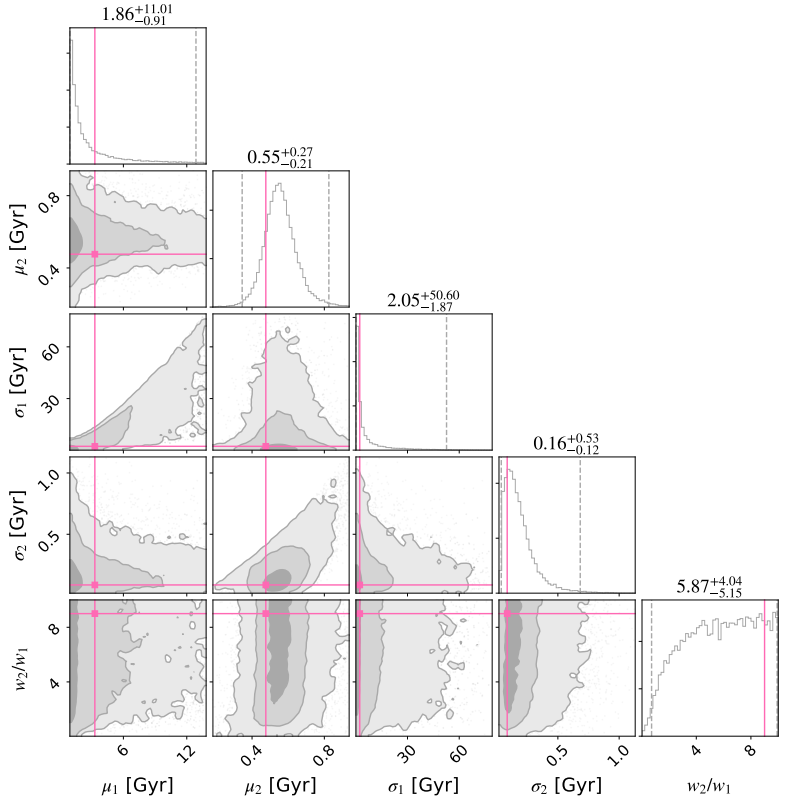

Figure 7.9: Posterior probability distributions on our five population parameters after one day of simulated third-generation detector observations of massive few-body mergers from globular clusters (25 events). Results are shown for three variations on our two-component Gaussian mixture model: (a) $w_2/w_1 = 1/9$, (b) $w_2/w_1 = 1$, and (c) $w_2/w_1 = 9$

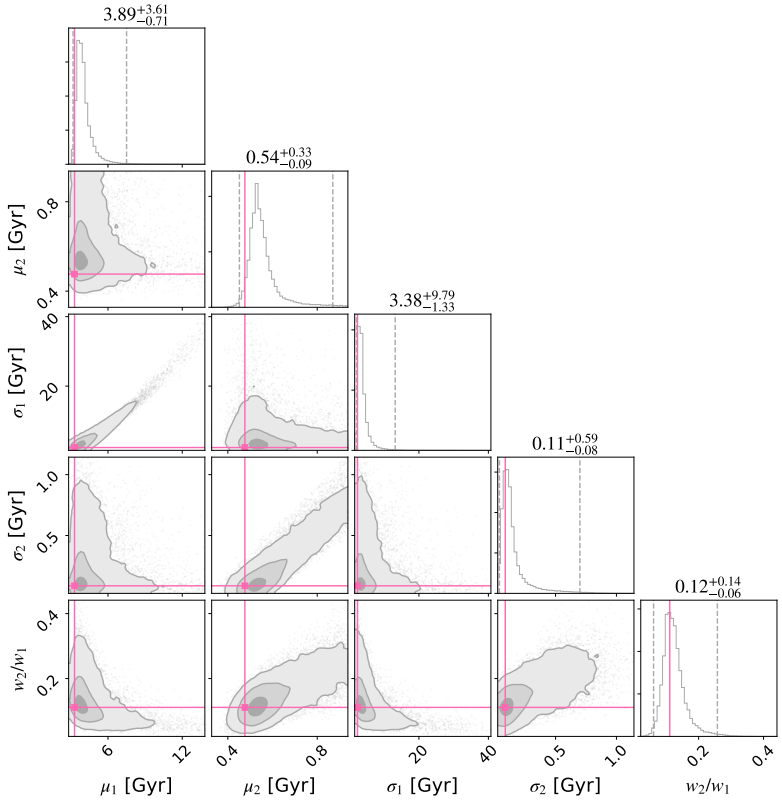

Figure 7.10: See the caption of Fig. 7.12.

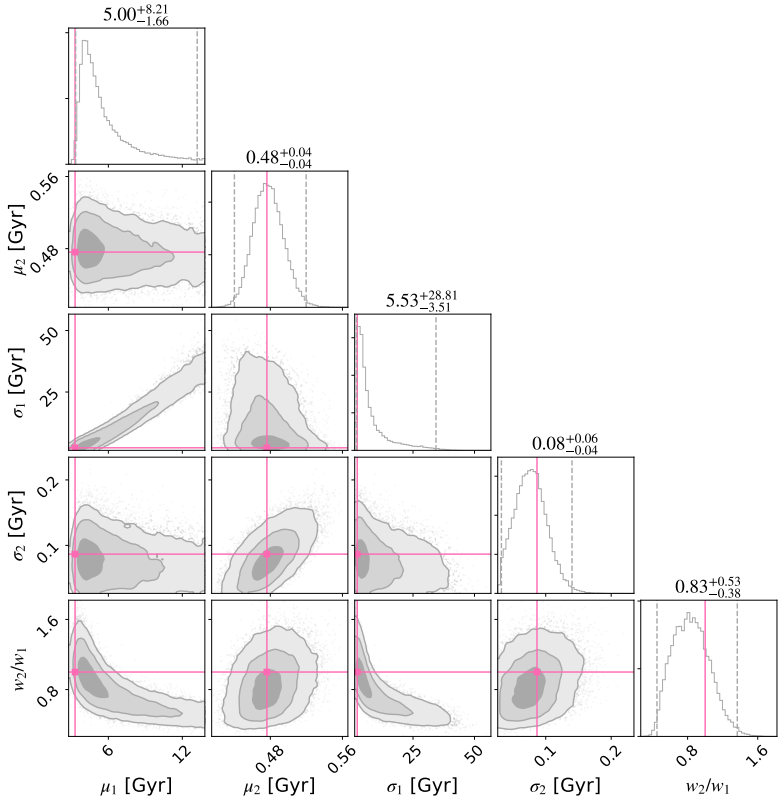

Figure 7.11: See the caption of Fig. 7.12.

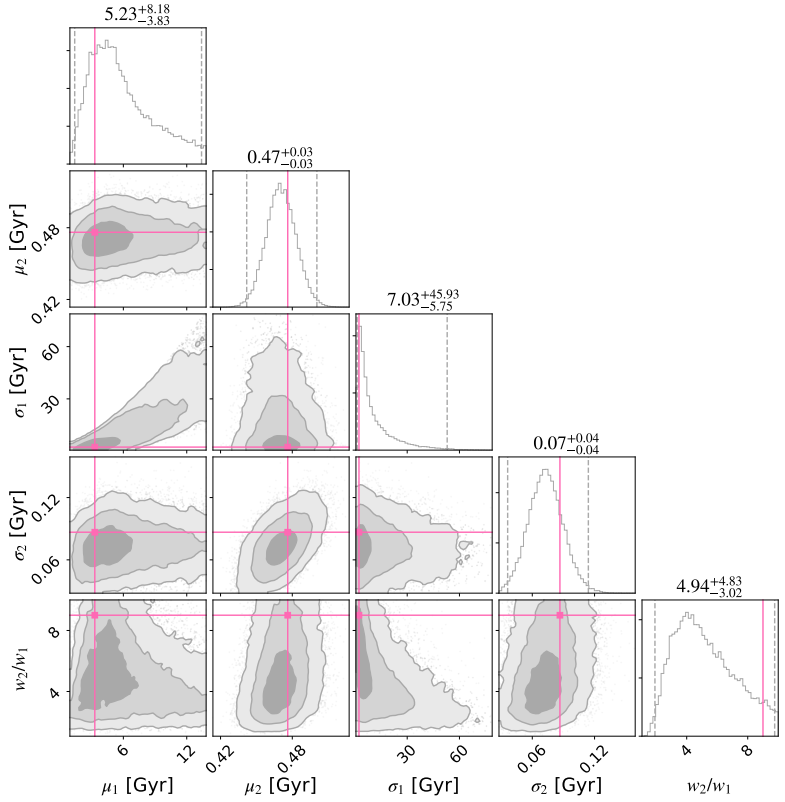

Figure 7.12: Posterior probability distributions on our five population parameters after one month of simulated third-generation detector observations of massive few-body mergers from globular clusters (500 events). Results are shown for three variations on our two-component Gaussian mixture model: (a) $w_2/w_1 = 1/9$, (b) $w_2/w_1 = 1$, and (c) $w_2/w_1 = 9$.

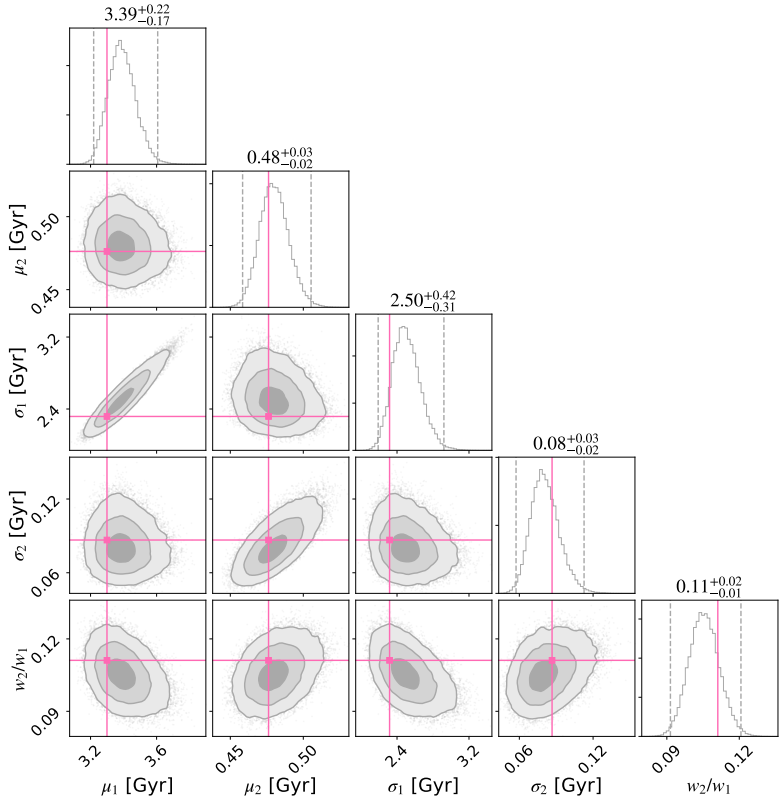

Figure 7.13: See the caption of Fig. 7.15.

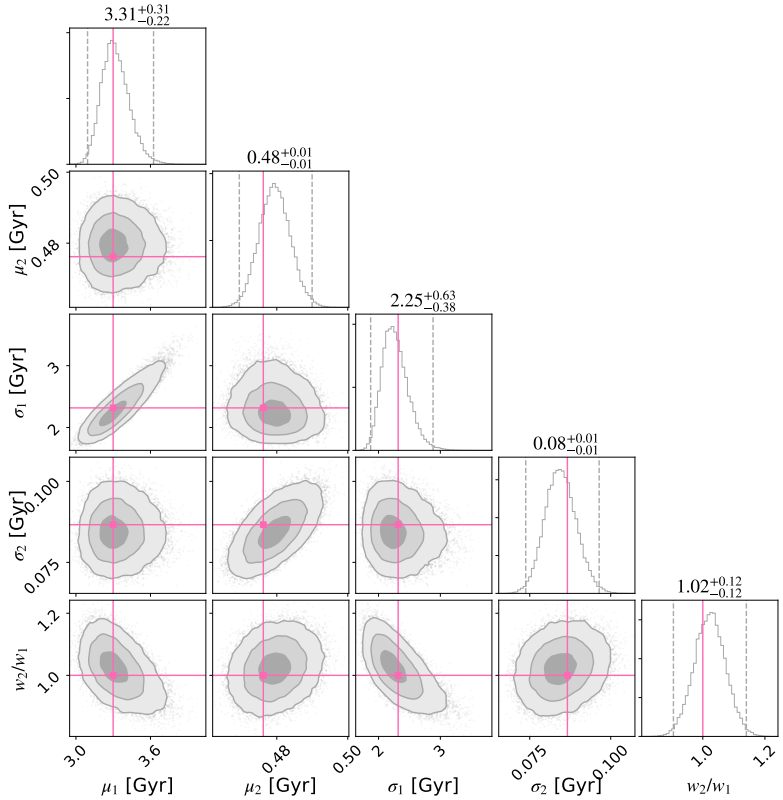

Figure 7.14: See the caption of Fig. 7.15.

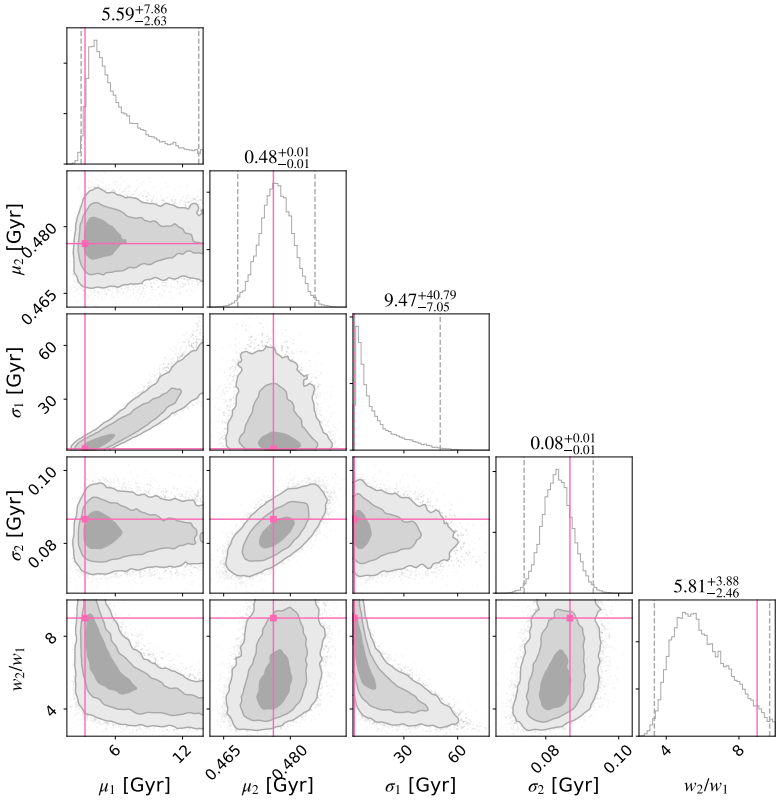

Figure 7.15: Posterior probability distributions on our five population parameters after one year of simulated third-generation detector observations of massive few-body mergers from globular clusters (5000 events). Results are shown for three variations on our two-component Gaussian mixture model: (a) $w_2/w_1 = 1/9$, (b) $w_2/w_1 = 1$, and (c) $w_2/w_1 = 9$.

Part V

CONCLUSION

8

SUMMARY AND CONCLUSION

In this thesis, I have made the first measurements of eccentricity in binary compact object orbits detected with gravitational waves. I first provided a thorough overview of computational Bayesian analysis for gravitational-wave inference, introducing the software libraries underlying the bulk of the analysis in this thesis. I then demonstrated the eccentricity-reconstruction technique on injections, as well as real data—gravitational-wave signals from the first and second gravitational-wave transient catalogues of Advanced LIGO and Virgo. The results from analyses on real events include those for the first event with support for non-zero eccentricity at detection: intermediate-mass black hole binary GW190521. They also include one other event with strong support for non-zero eccentricity, GW190620, and several others with moderate (but inconclusive) eccentricity support.
These measurements are caveated by two facts: that the eccentricity reconstruction technique cannot account for binary components with misaligned component spins, and that the initial argument of periapsis is fixed by the starting frequency of the eccentric waveform model. However, they do represent the first potential evidence for compact binary orbits that deviate from quasi-circular close to merger.
In the last chapter of this thesis, I have illustrated a proof-of-concept design for the kind of science that may be facilitated by gravitational waves in the future, when conclusive measurements of mass, spin, and eccentricity will identify the globular-cluster mergers in the population, and third-generation detectors will observe mergers occurring in the turbulent cores of newborn globular clusters.
In the remainder of this thesis, I conclude with some thoughts about how this work should be improved and extended in the coming years. The novel computational technique used to extend existing posterior probability distributions to include the extra parameter of orbital eccentricity is provided in the Appendix.

8.1 MEASURING THE COMPLETE PARAMETER PROFILE OF COMPACT BINARIES

As established in Chapter 5 and Chapter 6, our inability to measure eccentricity and precession simultaneously restricts the inferences that we can make, not just in terms of the nature of individual events, but also in terms of constraining the contributions from different formation channels to our compact merger catalogues. It is therefore of paramount importance that future analysis efforts work towards *complete* descriptions of merging compact binaries.
The most reliable way to make waveform approximants containing the influences of both non-zero eccentricity *and* non-zero precession

would be to obtain a selection of eccentric and precessing numerical relativity waveforms and make a surrogate model [e.g., 85, 237]. However, this may not be feasible for several years. Existing numerical relativity waveforms are rarely both eccentric and precessing, and the simulations that produce them are extremely time- and energy-consuming. Additionally, adding even one extra dimension vastly increases the size of the parameter space that needs to be explored, and hence drastically increases the number of numerical relativity waveforms that need to be generated. While we are waiting for sufficient numerical relativity simulations to become available, the number of compact binary coalescence detections will increase even more. Continuing to make eccentricity measurements of these binaries with non-precessing waveform models will motivate the development of waveform models that can contain both eccentricity and precession. Before the required waveform approximants exist, we may think about ways in which we can start to send feelers into this unexplored region of parameter space, which may involve extensions to the eccentricity-reweighting technique introduced in this work. Going forward, I will be looking out for ways to gain insights into the relationships between eccentricity and precession: how they can be confused by parameter estimation, how these two astrophysical effects feed into each other, and whether measurements made using an eccentric model can provide constraints on the binary's effective precession (and vice versa).
Waveform models containing eccentricity and tidal effects already exist [110], but in order to begin using additional eccentric waveform models, we must first understand how to compare their results (see further discussion below in 8.1.1). The final parameter to complete the set will be the argument of periapsis, which is tuneable through the starting frequency of the waveform simulation, and may therefore be added to inference goals in the near future.

8.1.1 *Defining eccentricity*

The eccentricity of an inspiralling orbit is hard to define, since the shape of the orbit is constantly in flux. There are three eccentricities that may be used in the quasi-Keplerian regime: the *radial*, *temporal* or *azimuthal* eccentricity may be referred to [126, 127]. Different simulations define eccentricity in different ways, and different waveforms employ different treatments of orbital dynamics [e.g., 103, 110]. Exacerbating the fact that eccentricity has no uniform definition between simulations is the fact that the calculation of the frequency at which this eccentricity is defined can vary. Some simulations use the *peak* gravitational-wave frequency (as defined, for example, in Equation 37 of [473]), while others use the *periastron*, *apastron* or *average* orbital frequency. At an average (secular) frequency of 10 Hz, the corresponding peak frequency for a moderate-eccentricity ($e_{10} \lesssim 0.2$) system differs by a small amount ($\lesssim 3$ Hz), but this difference worsens at higher frequencies and higher eccentricities.

Work is ongoing to establish conversion functions between the eccentricities defined by different waveforms, and increasing priority should be placed on obtaining a common definition of eccentricity converted from the outputs of various codes.

8.2 Using gravitational waves to probe the properties of compact binary formation environments

In Chapter 7, I demonstrated how third-generation gravitational wave detectors may be able to constrain the formation epochs of globular clusters by tracing the redshift evolution of globular cluster mergers. The natural next step for this project is to extend this method such that the initial properties of the globular clusters are also allowed to vary. Many properties of a globular cluster influence its expected merger rate: these include its initial mass/density profile and metallicity [48], primordial binary fraction [228], and existence of a central intermediate-mass black hole [179, 446]. By incorporating variations in these parameters into the existing framework for simulating third-generation detector observing runs, it will be possible to begin to predict the constraints that gravitational-wave observations will place on cluster formation *properties* as well as formation epochs (and correlations between these two things). Additional complexities that can be added to the model include realistic selection effects (such as the influence of sources redshifting out-of-band; [211]) and the weighting of observed events by the probability that they were formed in a globular cluster, along the lines of the astrophysical-probability weighting applied in [190]. The latter of these suggestions requires a prescription for assigning a formation channel probability to individual mergers based on its properties, for which we need robust predictions of the properties expected from different merger environments. Similarly, the properties of AGN may be revealed via the mergers that they produce; see, e.g., [175, 451, 478] for recent work in this field.

8.2.1 *Identifying formation channels and sub-channels*

In this thesis, I have primarily concentrated on globular clusters as the main example of a dynamical formation environment due to the robust prediction of the fraction of eccentric mergers formed within them. However, globular clusters are by no means the only environment that can dynamically assemble compact binary mergers. (If Kozai-Lidov triples [263, 282] are efficient at producing mergers, then dynamical assembly is not even the only way to produce eccentric binaries.)
To distinguish the fractional contribution from various channels (e.g., isolated, dynamical, or primordial) and their constituent sub-channels (e.g., mergers in globular clusters, active galactic nuclei, dense young clusters for the dynamical channel) to the population at large, we need to improve the stringency and the robustness of predictions from

alternative environments. This can be tricky for dynamical formation environments as these environments are highly complex and hard to model. This is particularly evident in the case of active galactic nuclei. Predictions from active galactic nuclei sensitively depend on model assumptions such as migration efficiency, the existence of migration traps, accretion disk thickness, whether merger remnants can merge with each other, and the black hole mass function [e.g., 174, 306, 309, 335, 390, 428–432, 481]. Narrowing these predictions requires more detailed observations and numerical models. As both telescopes and computational models increase even more in complexity and sophistication, active galactic nuclei may become another dynamical formation environment with robust predictions of its produced population's parameters. Moreover, if we continue to observe predominantly aligned spins and mass-gap mergers in the population, and are able to make confident detections of eccentricity, then active galactic nuclei will become a more probable dynamical formation channel for the observed mergers than globular clusters [174, 189, 381, 390, 428, 430, 431].

8.3 Giving the universe our full attention: watching *and* listening to compact objects in the future-detector era

Binary neutron star merger GW170817 [12] was the first astrophysical phenomenon to have been observed in both electromagnetic and gravitational radiation [14]. While electromagnetic counterparts to gravitational-wave detections of merging black holes have been proposed [e.g., 206], these are speculative. However, as both electromagnetic and gravitational-wave observatory powers increase, the number of multimessenger observations will increase. They may also come in a wide variety of flavours, with electromagnetic observations allowing us to predict forthcoming merger events. For example, sufficiently massive black holes in active galactic nuclei disks may open gaps in the disk that are observable in the disk iron line profile [307], which could enable forewarning of low-frequency gravitational wave signals that may be detected with space-based detectors like LISA [44] or DECIGO [246]. Furthermore, it has been proposed that recently-discovered quasi-periodic explosions [312] may be a result of highly-eccentric extreme-mass-ratio binaries in which the primary is a supermassive black hole at the centre of an active galactic nucleus [52]. This may be confirmed if the gravitational radiation from such systems is observed in future space-based detectors [57]. As we extend observing capabilities below the current limits on low-frequency gravitational-wave detection, we will be able to observe more massive black holes, which may have enduring electromagnetic counterparts that pinpoint their location. This will enable further constraints to be placed on compact binary formation environments.

BIBLIOGRAPHY

[1] J. Aasi, J. Abadie, B. P. Abbott, et al. "Parameter estimation for compact binary coalescence signals with the first generation gravitational-wave detector network." In: *Phys. Rev. D* 88.6, 062001 (Sept. 2013), p. 062001. DOI: 10.1103/PhysRevD.88.062001. arXiv: 1304.1775 [gr-qc].

[2] Abbott et al. *Gravitational Wave Open Science Center Strain Data Release for GW190521, LIGO Open Science Center*. 2020. URL: www.gw-openscience.org/eventapi/html/O3_Discovery_Papers/GW190521/v2/.

[3] Abbott et al. *Gravitational Wave Open Science Center Strain Data Release for GWTC-2, LIGO Open Science Center*. 2020. DOI: https://doi.org/10.7935/99gf-ax93. URL: https://doi.org/10.7935/99gf-ax93.

[4] B. P. Abbott, R. Abbott, T. D. Abbott, F. Acernese, et al. "GW170817: Implications for the Stochastic Gravitational-Wave Background from Compact Binary Coalescences." In: *Phys. Rev. Lett.* 120.9, 091101 (Mar. 2018), p. 091101. DOI: 10.1103/PhysRevLett.120.091101. arXiv: 1710.05837 [gr-qc].

[5] B. P. Abbott, R. Abbott, T. D. Abbott, et al. "Astrophysical Implications of the Binary Black-hole Merger GW150914." In: *Astrophys. J. Lett.* 818.2, L22 (Feb. 2016), p. L22. DOI: 10.3847/2041-8205/818/2/L22. arXiv: 1602.03846 [astro-ph.HE].

[6] B. P. Abbott, R. Abbott, T. D. Abbott, et al. "Properties of the Binary Black Hole Merger GW150914." In: *Phys. Rev. Lett.* 116.24 (June 2016), p. 241102. DOI: 10.1103/PhysRevLett.116.241102.

[7] B. P. Abbott, R. Abbott, T. D. Abbott, et al. "Tests of General Relativity with GW150914." In: *Phys. Rev. Lett.* 116.22, 221101 (2016), p. 221101. DOI: 10.1103/PhysRevLett.116.221101.

[8] B. P. Abbott, R. Abbott, T. D. Abbott, et al. "A gravitational-wave standard siren measurement of the Hubble constant." In: *Nature* 551 (2017), pp. 85–88. DOI: 10.1038/nature24471.

[9] B. P. Abbott, R. Abbott, T. D. Abbott, et al. "Effects of waveform model systematics on the interpretation of GW150914." In: *Classical and Quantum Gravity* 34.10, 104002 (May 2017), p. 104002. DOI: 10.1088/1361-6382/aa6854. arXiv: 1611.07531 [gr-qc].

[10] B. P. Abbott, R. Abbott, T. D. Abbott, et al. "Estimating the Contribution of Dynamical Ejecta in the Kilonova Associated with GW170817." In: *Astrophys. J. Lett.* 850.2, L39 (Dec. 2017), p. L39. DOI: 10.3847/2041-8213/aa9478. arXiv: 1710.05836 [astro-ph.HE].

[11] B. P. Abbott, R. Abbott, T. D. Abbott, et al. "GW170104: Observation of a 50-Solar-Mass Binary Black Hole Coalescence at Redshift 0.2." In: *Phys. Rev. Lett.* 118, 221101 (2017), p. 221101. DOI: 10.1103/PhysRevLett.118.221101.

[12] B. P. Abbott, R. Abbott, T. D. Abbott, et al. "GW170817: Observation of Gravitational Waves from a Binary Neutron Star Inspiral." In: *Phys. Rev. Lett.* 119.16, 161101 (2017), p. 161101. DOI: 10.1103/PhysRevLett.119.161101.

[13] B. P. Abbott, R. Abbott, T. D. Abbott, et al. "Gravitational Waves and Gamma-Rays from a Binary Neutron Star Merger: GW170817 and GRB 170817A." In: *Astrophys. J.* 848, L13 (Oct. 2017), p. L13. DOI: 10.3847/2041-8213/aa920c.

[14] B. P. Abbott, R. Abbott, T. D. Abbott, et al. "Multi-messenger Observations of a Binary Neutron Star Merger." In: *Astrophys. J.* 848, L12 (Oct. 2017), p. L12. DOI: 10.3847/2041-8213/aa91c9.

[15] B. P. Abbott, R. Abbott, T. D. Abbott, et al. "On the Progenitor of Binary Neutron Star Merger GW170817." In: *Astrophys. J. Lett.* 850.2, L40 (Dec. 2017), p. L40. DOI: 10.3847/2041-8213/aa93fc. arXiv: 1710.05838 [astro-ph.HE].

[16] B. P. Abbott, R. Abbott, T. D. Abbott, et al. https://dcc.ligo.org/LIGO-P1800370/public. https://dcc.ligo.org/LIGO-P1800370/public. 2018.

[17] B. P. Abbott, R. Abbott, T. D. Abbott, et al. "GW170817: Measurements of Neutron Star Radii and Equation of State." In: *Phys. Rev. Lett.* 121.16, 161101 (Oct. 2018), p. 161101. DOI: 10.1103/PhysRevLett.121.161101. arXiv: 1805.11581 [gr-qc].

[18] B. P. Abbott, R. Abbott, T. D. Abbott, et al. https://dcc.ligo.org/LIGO-P1900011/public. https://dcc.ligo.org/LIGO-P1900011/public. 2019.

[19] B. P. Abbott, R. Abbott, T. D. Abbott, et al. https://dcc.ligo.org/LIGO-P1900040/public. https://dcc.ligo.org/LIGO-P1900040/public. 2019.

[20] B. P. Abbott, R. Abbott, T. D. Abbott, et al. "A gravitational-wave measurement of the Hubble constant following the second observing run of Advanced LIGO and Virgo." In: *arXiv e-prints*, arXiv:1908.06060 (Aug. 2019), arXiv:1908.06060. arXiv: 1908.06060 [astro-ph.CO].

[21] B. P. Abbott, R. Abbott, T. D. Abbott, et al. "A guide to LIGO-Virgo detector noise and extraction of transient gravitational-wave signals." In: *arXiv preprint arXiv:1908.11170* (2019).

[22] B. P. Abbott, R. Abbott, T. D. Abbott, et al. "Properties of the Binary Neutron Star Merger GW170817." In: *Phys. Rev. X* 9.1, 011001 (Jan. 2019), p. 011001. DOI: 10.1103/PhysRevX.9.011001. arXiv: 1805.11579 [gr-qc].

[23] B. P. Abbott, R. Abbott, T. D. Abbott, et al. "Tests of general relativity with the binary black hole signals from the LIGO-Virgo catalog GWTC-1." In: *Phys. Rev. D* 100.10, 104036 (Nov. 2019), p. 104036. DOI: 10.1103/PhysRevD.100.104036.

[24] B. P. Abbott, R. Abbott, T. D. Abbott, et al. "GW190412: Observation of a Binary-Black-Hole Coalescence with Asymmetric Masses." In: *arXiv e-prints*, arXiv:2004.08342 (Apr. 2020), arXiv:2004.08342. arXiv: 2004.08342 [astro-ph.HE].

[25] B. P. Abbott, R. Abbott, T. D. Abbott, et al. "Model comparison from LIGO–Virgo data on GW170817's binary components and consequences for the merger remnant." In: *Classical and Quantum Gravity* 37.4, 045006 (Feb. 2020), p. 045006. DOI: 10.1088/1361-6382/ab5f7c. arXiv: 1908.01012 [gr-qc].

[26] B. P. Abbott et al. "Binary Black Hole Mergers in the First Advanced LIGO Observing Run." In: *Phys. Rev. X* 6, 041015 (Oct. 2016), p. 041015. DOI: 10.1103/PhysRevX.6.041015.

[27] B. P. Abbott et al. "Observation of Gravitational Waves from a Binary Black Hole Merger." In: *Phys. Rev. Lett.* 116.6 (Feb. 2016), p. 061102. DOI: 10.1103/PhysRevLett.116.061102.

[28] B P Abbott et al. "Exploring the sensitivity of next generation gravitational wave detectors." In: *Class. Quant. Grav.* 34.4, 044001 (Feb. 2017), p. 044001. DOI: 10.1088/1361-6382/aa51f4. arXiv: 1607.08697 [astro-ph.IM].

[29] B. P. Abbott et al. "Prospects for Observing and Localizing Gravitational-Wave Transients with Advanced LIGO, Advanced Virgo and KAGRA." In: *Living Rev. Rel.* 21.1 (2018), p. 3. DOI: 10.1007/s41114-018-0012-9,10.1007/lrr-2016-1. arXiv: 1304.0670 [gr-qc].

[30] B. P. Abbott et al. "GWTC-1: A Gravitational-Wave Transient Catalog of Compact Binary Mergers Observed by LIGO and Virgo during the First and Second Observing Runs." In: *Phys. Rev. X* 9 (3 Sept. 2019), p. 031040. DOI: 10.1103/PhysRevX.9.031040. URL: https://link.aps.org/doi/10.1103/PhysRevX.9.031040.

[31] B. P. Abbott et al. "Search for intermediate mass black hole binaries in the first and second observing runs of the Advanced LIGO and Virgo network." In: *Phys. Rev. D* 100.6, 064064 (Sept. 2019), p. 064064. DOI:

10.1103/PhysRevD.100.064064. arXiv: 1907.09384 [astro-ph.HE].

[32] B. P. Abbott et al. "Search for intermediate mass black hole binaries in the first and second observing runs of the Advanced LIGO and Virgo network." In: *Phys. Rev. D* 100.6, 064064 (Sept. 2019), p. 064064. DOI: 10.1103/PhysRevD.100.064064. arXiv: 1907.09384 [astro-ph.HE].

[33] B. P. Abbott et al. "GW190425: Observation of a Compact Binary Coalescence with Total Mass $\sim 3.4\ M_{\odot}$." In: *Astrophys. J. Lett.* 892.1, L3 (Mar. 2020), p. L3. DOI: 10.3847/2041-8213/ab75f5. arXiv: 2001.01761 [astro-ph.HE].

[34] R. Abbott, T. D. Abbott, S. Abraham, F. Acernese, K. Ackley, et al. "GW190521: A Binary Black Hole Merger with a Total Mass of 150 $M_{\odot}$." In: *Phys. Rev. Lett.* 125 (10 Sept. 2020), p. 101102. DOI: 10.1103/PhysRevLett.125.101102. URL: https://link.aps.org/doi/10.1103/PhysRevLett.125.101102.

[35] R. Abbott, T. D. Abbott, S. Abraham, F. Acernese, K. Ackley, et al. "GW190521.1: Physical Properties and Astrophysical Implications of an Intermediate Mass Binary Black Hole Merger." In: *Astrophys. J.* (Sept. 2020). DOI: 10.3847/2041-8213/aba493. URL: https://doi.org/10.3847/2041-8213/aba493.

[36] R. Abbott, T. D. Abbott, S. Abraham, et al. "Open data from the first and second observing runs of Advanced LIGO and Advanced Virgo." In: *arXiv e-prints*, arXiv:1912.11716 (Dec. 2019), arXiv:1912.11716. arXiv: 1912.11716 [gr-qc].

[37] R. Abbott et al. "GWTC-2: Compact Binary Coalescences Observed by LIGO and Virgo During the First Half of the Third Observing Run." In: *Phys. Rev. X* 11 (2021), p. 021053. DOI: 10.1103/PhysRevX.11.021053. arXiv: 2010.14527 [gr-qc].

[38] R. Abbott et al. "Population Properties of Compact Objects from the Second LIGO-Virgo Gravitational-Wave Transient Catalog." In: *Astrophys. J. Lett.* 913.1, L7 (May 2021), p. L7. DOI: 10.3847/2041-8213/abe949. arXiv: 2010.14533 [astro-ph.HE].

[39] F. Acernese et al. "Advanced Virgo: a second-generation interferometric gravitational wave detector." In: *Class. Quant. Grav.* 32.2 (2015), p. 024001. DOI: 10.1088/0264-9381/32/2/024001. arXiv: 1408.3978 [gr-qc].

[40] P. Ajith et al. "Inspiral-Merger-Ringdown Waveforms for Black-Hole Binaries with Nonprecessing Spins." In: *Phys. Rev. Lett.* 106.24, 241101 (June 2011), p. 241101. DOI: 10.1103/PhysRevLett.106.241101. arXiv: 0909.2867 [gr-qc].

[41] Yacine Ali-Haïmoud, Ely D. Kovetz, and Marc Kamionkowski. "Merger rate of primordial black-hole binaries." In: *Phys. Rev. D.* 96.12, 123523 (Dec. 2017), p. 123523. DOI: 10.1103/PhysRevD.96.123523. arXiv: 1709.06576 [astro-ph.CO].

[42] Bruce Allen, Warren G. Anderson, Patrick R. Brady, Duncan A. Brown, and Jolien D. E. Creighton. "FINDCHIRP: An algorithm for detection of gravitational waves from inspiraling compact binaries." In: *Phys. Rev. D* 85.12, 122006 (June 2012), p. 122006. DOI: 10.1103/PhysRevD.85.122006. arXiv: gr-qc/0509116 [gr-qc].

[43] J. Alsing, H. O. Silva, and E. Berti. "Evidence for a maximum mass cut-off in the neutron star mass distribution and constraints on the equation of state." In: *Mon. Not. Roy. Astron. Soc.* 478 (July 2018), pp. 1377–1391. DOI: 10.1093/mnras/sty1065. arXiv: 1709.07889 [astro-ph.HE].

[44] Pau Amaro-Seoane et al. "Laser Interferometer Space Antenna." In: *arXiv e-prints*, arXiv:1702.00786 (Feb. 2017), arXiv:1702.00786. arXiv: 1702.00786 [astro-ph.IM].

[45] Oliver Anagnostou, Michele Trenti, and Andrew Melatos. "Hierarchical Formation Of An Intermediate Mass Black Hole Via Seven Mergers: Implications For GW190521." In: *arXiv e-prints*, arXiv:2010.06161 (Oct. 2020), arXiv:2010.06161. arXiv: 2010.06161 [astro-ph.HE].

[46] Jeff J. Andrews and Ilya Mandel. "Double Neutron Star Populations and Formation Channels." In: *Astrophys. J. Lett.* 880.1, L8 (July 2019), p. L8. DOI: 10.3847/2041-8213/ab2ed1. arXiv: 1904.12745 [astro-ph.HE].

[47] Fabio Antonini, Sourav Chatterjee, Carl L. Rodriguez, Meagan Morscher, Bharath Pattabiraman, Vicky Kalogera, and Frederic A. Rasio. "Black hole mergers and blue stragglers from hierarchical triples formed in globular clusters." In: *Astrophys. J.* 816.2 (2016), p. 65. DOI: 10.3847/0004-637X/816/2/65. arXiv: 1509.05080 [astro-ph.GA].

[48] Fabio Antonini and Mark Gieles. "Merger rate of black hole binaries from globular clusters: Theoretical error bars and comparison to gravitational wave data from GWTC-2." In: *Phys. Rev. D.* 102.12, 123016 (Dec. 2020), p. 123016. DOI: 10.1103/PhysRevD.102.123016. arXiv: 2009.01861 [astro-ph.HE].

[49] Fabio Antonini and Mark Gieles. "Merger rate of black hole binaries from globular clusters: theoretical error bars and comparison to gravitational wave data." In: *arXiv e-prints*, arXiv:2009.01861 (Sept. 2020), arXiv:2009.01861. arXiv: 2009.01861 [astro-ph.HE].

[50] Fabio Antonini and Hagai B. Perets. "Secular Evolution of Compact Binaries near Massive Black Holes: Gravitational Wave Sources and Other Exotica." In: *Astrophys. J.* 757.1, 27 (Sept. 2012), p. 27. DOI: 10.1088/0004-637X/757/1/27. arXiv: 1203.2938 [astro-ph.GA].

[51] Fabio Antonini, Silvia Toonen, and Adrian S. Hamers. "Binary black hole mergers from field triples: properties, rates and the impact of stellar evolution." In: *Astrophys. J.* 841.2 (2017), p. 77. DOI: 10.3847/1538-4357/aa6f5e. arXiv: 1703.06614.

[52] R. Arcodia et al. "X-ray quasi-periodic eruptions from two previously quiescent galaxies." In: *Nature* 592.7856 (Apr. 2021), pp. 704–707. DOI: 10.1038/s41586-021-03394-6. arXiv: 2104.13388 [astro-ph.HE].

[53] Gregory Ashton and Sebastian Khan. "Multiwaveform inference of gravitational waves." In: *Phys. Rev. D* 101.6, 064037 (Mar. 2020), p. 064037. DOI: 10.1103/PhysRevD.101.064037. arXiv: 1910.09138 [gr-qc].

[54] Gregory Ashton et al. "Bilby: A user-friendly Bayesian inference library for gravitational-wave astronomy." In: *Astrophys. J. Suppl.* 241.2 (2019), p. 27. DOI: 10.3847/1538-4365/ab06fc. arXiv: 1811.02042 [astro-ph.IM].

[55] A. Askar, M. Szkudlarek, D. Gondek-Rosińska, M. Giersz, and T. Bulik. "MOCCA-SURVEY Database - I. Coalescing binary black holes originating from globular clusters." In: *Mon. Not. R. Ast. Soc.* 464 (Jan. 2017), pp. L36–L40. DOI: 10.1093/mnrasl/slw177. arXiv: 1608.02520 [astro-ph.HE].

[56] Stanislav Babak, John G. Baker, Matthew J. Benacquista, Neil J. Cornish, Shane L. Larson, Ilya Mandel, Sean T. McWilliams, Antoine Petiteau, Edward K. Porter, and the Challenge 3 others. "The Mock LISA Data Challenges: from challenge 3 to challenge 4." In: *Classical and Quantum Gravity* 27.8, 084009 (Apr. 2010), p. 084009. DOI: 10.1088/0264-9381/27/8/084009. arXiv: 0912.0548 [gr-qc].

[57] Stanislav Babak, Jonathan Gair, Alberto Sesana, Enrico Barausse, Carlos F. Sopuerta, Christopher P. L. Berry, Emanuele Berti, Pau Amaro-Seoane, Antoine Petiteau, and Antoine Klein. "Science with the space-based interferometer LISA. V. Extreme mass-ratio inspirals." In: *Phys. Rev. D* 95.10, 103012 (May 2017), p. 103012. DOI: 10.1103/PhysRevD.95.103012. arXiv: 1703.09722 [gr-qc].

[58] Stanislav Babak et al. "The Mock LISA Data Challenges: from Challenge 1B to Challenge 3." In: *Classical and Quantum Gravity* 25.18, 184026 (Sept. 2008), p. 184026. DOI: 10.1088/0264-9381/25/18/184026. arXiv: 0806.2110 [gr-qc].

[59] Yeong-Bok Bae, Chunglee Kim, and Hyung Mok Lee. "Compact binaries ejected from globular clusters as gravitational wave sources." In: *Mon. Not. Roy. Astron. Soc.* 440.3 (May 2014), pp. 2714–2725. DOI: 10.1093/mnras/stu381. arXiv: 1308.1641 [astro-ph.HE].

[60] Sambaran Banerjee. "Stellar-mass black holes in young massive and open stellar clusters and their role in gravitational-wave generation." In: *Mon. Not. R. Ast. Soc.* 467.1 (May 2017), pp. 524–539. DOI: 10.1093/mnras/stw3392. arXiv: 1611.09357 [astro-ph.HE].

[61] Sambaran Banerjee. "Stellar-mass black holes in young massive and open stellar clusters and their role in gravitational-wave generation - II." In: *Mon. Not. R. Ast. Soc.* 473.1 (Jan. 2018), pp. 909–926. DOI: 10.1093/mnras/stx2347. arXiv: 1707.00922 [astro-ph.HE].

[62] Sambaran Banerjee. "Stellar-mass black holes in young massive and open stellar clusters and their role in gravitational-wave generation III: dissecting black hole dynamics." In: *Mon. Not. R. Ast. Soc.* 481.4 (Dec. 2018), pp. 5123–5145. DOI: 10.1093/mnras/sty2608. arXiv: 1805.06466 [astro-ph.HE].

[63] Sambaran Banerjee. "Stellar-mass black holes in young massive and open stellar clusters IV: updated stellar-evolutionary and black hole spin models and comparisons with the LIGO-Virgo O1/O2 merger-event data." In: *Mon. Not. R. Ast. Soc.* (Sept. 2020). DOI: 10.1093/mnras/staa2392. arXiv: 2004.07382 [astro-ph.HE].

[64] Jim W Barrett, Sebastian M Gaebel, Coenraad J Neijssel, Alejandro Vigna-Gómez, Simon Stevenson, Christopher P L Berry, Will M Farr, and Ilya Mandel. "Accuracy of inference on the physics of binary evolution from gravitational-wave observations." In: *Mon. Not. Roy. Astron. Soc.* 477.4 (Nov. 2018), pp. 4685–4695. ISSN: 0035-8711. DOI: 10.1093/mnras/sty908. URL: https://academic.oup.com/mnras/article/477/4/4685/4969691.

[65] Simone S. Bavera, Tassos Fragos, Ying Qin, Emmanouil Zapartas, Coenraad J. Neijssel, Ilya Mandel, Aldo Batta, Sebastian M. Gaebel, Chase Kimball, and Simon Stevenson. "The origin of spin in binary black holes. Predicting the distributions of the main observables of Advanced LIGO." In: *Astron. Astrophys.* 635, A97 (Mar. 2020), A97. DOI: 10.1051/0004-6361/201936204. arXiv: 1906.12257 [astro-ph.HE].

[66] Simone S. Bavera et al. "The impact of mass-transfer physics on the observable properties of field binary black hole populations." In: *Astron. Astrophys.* 647, A153 (Mar. 2021), A153. DOI: 10.1051/0004-6361/202039804. arXiv: 2010.16333 [astro-ph.HE].

[67] Thomas Bayes. "An essay towards solving a problem in the doctrine of chances." In: *Philosophical Transactions of The Royal Society* (Jan. 1763). DOI: 10.1098/rstl.1763.0053. URL: https://doi.org/10.1098/rstl.1763.0053.

[68] Amanda Baylor, Rory Smith, and Eve Chase. *IMRPhenomPv2_NRTidal_GW190425_narrow_Mc*. Oct. 2019. DOI: 10.5281/zenodo.3478659. URL: https://doi.org/10.5281/zenodo.3478659.

[69] K. Belczynski et al. "The effect of pair-instability mass loss on black-hole mergers." In: *Astron. Astrophys.* 594, A97 (Oct. 2016), A97. DOI: 10.1051/0004-6361/201628980. arXiv: 1607.03116 [astro-ph.HE].

[70] K. Belczynski et al. "Binary neutron star formation and the origin of GW170817." In: *arXiv e-prints*, arXiv:1812.10065 (Dec. 2018), arXiv:1812.10065. arXiv: 1812.10065 [astro-ph.HE].

[71] K. Belczynski et al. "The origin of the first neutron star - neutron star merger." In: *Astron. Astrophys.* 615, A91 (July 2018), A91. DOI: 10.1051/0004-6361/201732428. arXiv: 1712.00632 [astro-ph.HE].

[72] Krzysztof Belczynski. "The Most Ordinary Formation of the Most Unusual Double Black Hole Merger." In: *Astrophys. J. Lett.* 905.2, L15 (Dec. 2020), p. L15. DOI: 10.3847/2041-8213/abcbf1. arXiv: 2009.13526 [astro-ph.HE].

[73] Krzysztof Belczynski, Tomasz Bulik, and Vassiliki Kalogera. "Merger Sites of Double Neutron Stars and Their Host Galaxies." In: *Astrophys. J. Lett.* 571.2 (June 2002), pp. L147–L150. DOI: 10.1086/341365. arXiv: astro-ph/0204416 [astro-ph].

[74] Krzysztof Belczynski, Vassiliki Kalogera, and Tomasz Bulik. "A Comprehensive Study of Binary Compact Objects as Gravitational Wave Sources: Evolutionary Channels, Rates, and Physical Properties." In: *Astrophys. J.* 572.1 (June 2002), pp. 407–431. DOI: 10.1086/340304. arXiv: astro-ph/0111452 [astro-ph].

[75] Matthew J. Benacquista and Jonathan M. B. Downing. "Relativistic Binaries in Globular Clusters." In: *Living Rev. Rel.* 16 (2013), p. 4. DOI: 10.12942/lrr-2013-4. arXiv: 1110.4423 [astro-ph.SR].

[76] Paz Beniamini and Tsvi Piran. "Formation of Double Neutron Star systems as implied by observations." In: *Mon. Not. Roy. Astron. Soc.* 456.4 (2016), pp. 4089–4099. DOI: 10.1093/mnras/stv2903. arXiv: 1510.03111 [astro-ph.HE].

[77] Christopher P. L. Berry, Ilya Mandel, Hannah Middleton, Leo P. Singer, et al. "Parameter Estimation for Binary Neutron-star Coalescences with Realistic Noise during the Advanced LIGO Era." In: *Astrophys. J.* 804.2, 114 (May 2015), p. 114. DOI: 10.1088/0004-637X/804/2/114. arXiv: 1411.6934 [astro-ph.HE].

[78] Hans A. Bethe and G. E. Brown. "Evolution of binary compact objects which merge." In: *Astrophys. J.* 506 (1998), pp. 780–789. DOI: 10.1086/306265. arXiv: astro-ph/9802084 [astro-ph].

[79] Eugenio Bianchi, Anuradha Gupta, Hal M. Haggard, and B. S. Sathyaprakash. "Quantum gravity and black hole spin in gravitational wave observations: a test of the Bekenstein-Hawking entropy." In: *arXiv e-prints*, arXiv:1812.05127 (2018), arXiv:1812.05127. arXiv: 1812.05127 [gr-qc].

[80] Simeon Bird, Ilias Cholis, Julian B. Muñoz, Yacine Ali-Haïmoud, Marc Kamionkowski, Ely D. Kovetz, Alvise Raccanelli, and Adam G. Riess. "Did LIGO Detect Dark Matter?" In: *Phys. Rev. L.* 116.20, 201301 (May 2016), p. 201301. DOI: 10.1103/PhysRevLett.116.201301. arXiv: 1603.00464 [astro-ph.CO].

[81] Sylvia Biscoveanu, Carl-Johan Haster, Salvatore Vitale, and Jonathan Davies. "Quantifying the effect of power spectral density uncertainty on gravitational-wave parameter estimation for compact binary sources." In: *Phys. Rev. D* 102.2, 023008 (July 2020), p. 023008. DOI: 10.1103/PhysRevD.102.023008. arXiv: 2004.05149 [astro-ph.HE].

[82] Sylvia Biscoveanu, Eric Thrane, and Salvatore Vitale. "Constraining Short Gamma-Ray Burst Jet Properties with Gravitational Waves and Gamma-Rays." In: *Astrophys. J.* 893.1, 38 (Apr. 2020), p. 38. DOI: 10.3847/1538-4357/ab7eaf. arXiv: 1911.01379 [astro-ph.HE].

[83] Sylvia Biscoveanu, Salvatore Vitale, and Carl-Johan Haster. "The Reliability of the Low-latency Estimation of Binary Neutron Star Chirp Mass." In: *Astrophys. J. Lett.* 884.2, L32 (Oct. 2019), p. L32. DOI: 10.3847/2041-8213/ab479e. arXiv: 1908.03592 [astro-ph.HE].

[84] C. M. Biwer, Collin D. Capano, Soumi De, Miriam Cabero, Duncan A. Brown, Alexander H. Nitz, and V. Raymond. "PyCBC Inference: A Python-based Parameter Estimation Toolkit for Compact Binary Coalescence Signal." In: *Pub. ASP* 131.996 (Feb. 2019), p. 024503. DOI: 10.1088/1538-3873/aaef0b. arXiv: 1807.10312 [astro-ph.IM].

[85] Jonathan Blackman, Scott E. Field, Mark A. Scheel, et al. "Numerical relativity waveform surrogate model for generically precessing binary black hole mergers." In: *Phys. Rev. D* 96 (2 July 2017), p. 024058. DOI: 10.1103/PhysRevD.96.024058. URL: https://link.aps.org/doi/10.1103/PhysRevD.96.024058.

[86] Luc Blanchet, Thibault Damour, Bala R. Iyer, Clifford M. Will, and Alan G. Wiseman. "Gravitational-Radiation Damping of Compact Binary Systems to Second Post-Newtonian Order." In: *Phys. Rev. Lett.* 74.18 (May 1995), pp. 3515–3518. DOI: 10.1103/PhysRevLett.74.3515. arXiv: gr-qc/9501027 [gr-qc].

[87] Alejandro Bohé, Mark Hannam, Sascha Husa, Frank Ohme, Michael Puerrer, and Patricia Schmidt. *PhenomPv2 - Technical Notes for LAL Implementation*. Tech. rep. LIGO-T1500602. LIGO Project, 2016. URL: https://dcc.ligo.org/LIGO-T1500602.

[88] Alejandro Bohé, Lijing Shao, Andrea Taracchini, Alessandra Buonanno, et al. "Improved effective-one-body model of spinning, nonprecessing binary black holes for the era of gravitational-wave astrophysics with advanced detectors." In: *Phys. Rev. D* 95 (4 2017), p. 044028. DOI: 10.1103/PhysRevD.95.044028. URL: https://link.aps.org/doi/10.1103/PhysRevD.95.044028.

[89] Yann Bouffanais, Michela Mapelli, Davide Gerosa, Ugo N. Di Carlo, Nicola Giacobbo, Emanuele Berti, and Vishal Baibhav. "Constraining the Fraction of Binary Black Holes Formed in Isolation and Young Star Clusters with Gravitational-wave Data." In: *Astrophys. J.* 886.1, 25 (Nov. 2019), p. 25. DOI: 10.3847/1538-4357/ab4a79. arXiv: 1905.11054 [astro-ph.HE].

[90] Niel Brandt and Philipp Podsiadlowski. "The effects of high-velocity supernova kicks on the orbital properties and sky distributions of neutron-star binaries." In: *Mon. Not. R. Ast. Soc.* 274.2 (May 1995), pp. 461–484. ISSN: 0035-8711. DOI: 10.1093/mnras/274.2.461. URL: https://doi.org/10.1093/mnras/274.2.461.

[91] Philip G. Breen and Douglas C. Heggie. "On black hole subsystems in idealized nuclear star clusters." In: *Mon. Not. Roy. Astron. Soc.* 436.1 (Nov. 2013), pp. 584–589. DOI: 10.1093/mnras/stt1599. arXiv: 1308.4641 [astro-ph.GA].

[92] Katelyn Breivik, Carl L. Rodriguez, Shane L. Larson, Vassiliki Kalogera, and Frederic A. Rasio. "Distinguishing Between Formation Channels for Binary Black Holes with LISA." In: *Astrophys. J.* 830.1 (2016), p. L18. DOI: 10.3847/2041-8205/830/1/L18. arXiv: 1606.09558 [astro-ph.GA].

[93] Duncan A. Brown and Peter J. Zimmerman. "The Effect of Eccentricity on Searches for Gravitational-Waves from Coalescing Compact Binaries in Ground-based Detectors." In: *Phys. Rev. D* D81 (2010), p. 024007. DOI: 10.1103/PhysRevD.81.024007. arXiv: 0909.0066.

[94] J. Buchner et al. "X-ray spectral modelling of the AGN obscuring region in the CDFS: Bayesian model selection and catalogue." In: *Astron. Astrophys.* 564, A125 (2014), A125. DOI: 10.1051/0004-6361/201322971.

[95] Johannes Buchner. "A statistical test for Nested Sampling algorithms." In: *arXiv e-prints*, arXiv:1407.5459 (July 2014), arXiv:1407.5459. arXiv: 1407.5459 [stat.CO].

[96] Johannes Buchner. "Collaborative Nested Sampling: Big Data versus Complex Physical Models." In: *Publications of the Astronomical Society of the Pacific* 131.1004 (Aug. 2019), p. 108005. DOI: 10.1088/1538-3873/aae7fc.

[97] Juan Calderón Bustillo, Nicolas Sanchis-Gual, Alejandro Torres-Forné, and José A. Font. "Confusing Head-On Collisions with Precessing Intermediate-Mass Binary Black Hole Mergers." In: *Phys. Rev. Lett.* 126.20, 201101 (May 2021), p. 201101. DOI: 10.1103/PhysRevLett.126.201101. arXiv: 2009.01066 [gr-qc].

[98] Craig Cahillane et al. "Calibration uncertainty for Advanced LIGO's first and second observing runs." In: *Phys. Rev. D* 96.10, 102001 (Nov. 2017), p. 102001. DOI: 10.1103/PhysRevD.96.102001. arXiv: 1708.03023 [astro-ph.IM].

[99] A. D. Cameron et al. "The High Time Resolution Universe Pulsar Survey - XIII. PSR J1757-1854, the most accelerated binary pulsar." In: *Mon. Not. Roy. Astron. Soc.* 475 (Mar. 2018), pp. L57–L61. DOI: 10.1093/mnrasl/sly003. arXiv: 1711.07697 [astro-ph.HE].

[100] Manuela Campanelli, C. O. Lousto, and Yosef Zlochower. "Spin-orbit interactions in black-hole binaries." In: *Phys. Rev. D* D74 (2006), p. 084023. DOI: 10.1103/PhysRevD.74.084023. arXiv: astro-ph/0608275.

[101] Ramon Canal, Jordi Isern, and Javier Labay. "The Origin of Neutron Stars in Binary Systems." In: *Ann. Rev. Astron. Astrophys.* 28.1 (1990), pp. 183–214. DOI: 10.1146/annurev.aa.28.090190.001151. eprint: https://doi.org/10.1146/annurev.aa.28.090190.001151. URL: https://doi.org/10.1146/annurev.aa.28.090190.001151.

[102] Michele Cantiello, J. B. Jensen, J. P. Blakeslee, E. Berger, A. J. Levan, et al. "A Precise Distance to the Host Galaxy of the Binary Neutron Star Merger GW170817 Using Surface Brightness Fluctuations." In: *Astrophys. J. Lett.* 854.2, L31 (2018),

p. L31. DOI: 10.3847/2041-8213/aaad64. arXiv: 1801.06080 [astro-ph.GA].

[103] Zhoujian Cao and Wen-Biao Han. "Waveform model for an eccentric binary black hole based on the effective-one-body-numerical-relativity formalism." In: *Phys. Rev.* D96.4 (2017), p. 044028. DOI: 10.1103/PhysRevD.96.044028. arXiv: 1708.00166 [gr-qc].

[104] Bernard Carr, Kazunori Kohri, Yuuiti Sendouda, and Jun'ichi Yokoyama. "Constraints on Primordial Black Holes." In: *arXiv e-prints*, arXiv:2002.12778 (Feb. 2020), arXiv:2002.12778. arXiv: 2002.12778 [astro-ph.CO].

[105] Marco Celoria, Roberto Oliveri, Alberto Sesana, and Michela Mapelli. "Lecture notes on black hole binary astrophysics." In: 2018. arXiv: 1807.11489 [astro-ph.GA].

[106] K Chatziioannou et al. "On the properties of the massive binary black hole merger GW170729." In: *Phys. Rev. D* 100 (2019), p. 104015.

[107] Katerina Chatziioannou, Carl-Johan Haster, Tyson B. Littenberg, Will M. Farr, Sudarshan Ghonge, Margaret Millhouse, James A. Clark, and Neil Cornish. "Noise spectral estimation methods and their impact on gravitational wave measurement of compact binary mergers." In: *Phys. Rev. D* 100.10, 104004 (Nov. 2019), p. 104004. DOI: 10.1103/PhysRevD.100.104004.

[108] Hsin-Yu Chen, Maya Fishbach, and Daniel E. Holz. "A two per cent Hubble constant measurement from standard sirens within five years." In: *Nature* 562.7728 (Oct. 2018), pp. 545–547. DOI: 10.1038/s41586-018-0606-0. arXiv: 1712.06531 [astro-ph.CO].

[109] Zu-Cheng Chen, Chen Yuan, and Qing-Guo Huang. "Confronting the primordial black hole scenario with the gravitational-wave events detected by LIGO-Virgo." In: *arXiv e-prints*, arXiv:2108.11740 (Aug. 2021), arXiv:2108.11740. arXiv: 2108.11740 [astro-ph.CO].

[110] Danilo Chiaramello and Alessandro Nagar. "Faithful analytical effective-one-body waveform model for spin-aligned, moderately eccentric, coalescing black hole binaries." In: *Phys. Rev. D* 101.10, 101501 (May 2020), p. 101501. DOI: 10.1103/PhysRevD.101.101501. arXiv: 2001.11736 [gr-qc].

[111] R. Chornock, E. Berger, D. Kasen, P. S. Cowperthwaite, M. Nicholl, et al. "The Electromagnetic Counterpart of the Binary Neutron Star Merger LIGO/Virgo GW170817. IV. Detection of Near-infrared Signatures of r-process Nucleosynthesis with Gemini-South." In: *Astrophys. J. Lett.* 848.2, L19 (Oct. 2017), p. L19. DOI: 10.3847/2041-8213/aa905c. arXiv: 1710.05454 [astro-ph.HE].

[112] Nelson Christensen and Renate Meyer. "Markov chain Monte Carlo methods for Bayesian gravitational radiation data analysis." In: *Phys. Rev. D* 58.8, 082001 (Oct. 1998), p. 082001. DOI: 10.1103/PhysRevD.58.082001.

[113] Nelson Christensen and Renate Meyer. "Using Markov chain Monte Carlo methods for estimating parameters with gravitational radiation data." In: *Phys. Rev. D* 64.2, 022001 (July 2001), p. 022001. DOI: 10.1103/PhysRevD.64.022001. arXiv: gr-qc/0102018 [gr-qc].

[114] Martyna Chruslinska, Krzysztof Belczynski, Jakub Klencki, and Matthew Benacquista. "Double neutron stars: merger rates revisited." In: *Mon. Not. R. Ast. Soc.* 474.3 (2018), pp. 2937–2958. DOI: 10.1093/mnras/stx2923. arXiv: 1708.07885 [astro-ph.HE].

[115] Martyna Chruslinska, Gijs Nelemans, and Krzysztof Belczynski. "The influence of the distribution of cosmic star formation at different metallicities on the properties of merging double compact objects." In: *Mon. Not. Roy. Astron. Soc.* 482.4 (2019), pp. 5012–5017. DOI: 10.1093/mnras/sty3087. arXiv: 1811.03565 [astro-ph.HE].

[116] Samantha R. Cook, Andrew Gelman, and Donald B. Rubin. "Validation of Software for Bayesian Models Using Posterior Quantiles." In: *Journal of Computational and Graphical Statistics* 15.3 (2006), pp. 675–692. DOI: 10.1198/106186006X136976. eprint: https://doi.org/10.1198/106186006X136976. URL: https://doi.org/10.1198/106186006X136976.

[117] Neil J. Cornish. "Fast Fisher Matrices and Lazy Likelihoods." In: *arXiv e-prints*, arXiv:1007.4820 (July 2010), arXiv:1007.4820. arXiv: 1007.4820 [gr-qc].

[118] Neil J. Cornish and Tyson B. Littenberg. "BayesWave: Bayesian Inference for Gravitational Wave Bursts and Instrument Glitches." In: *Class. Quant. Grav.* 32.13 (2015), p. 135012. DOI: 10.1088/0264-9381/32/13/135012. arXiv: 1410.3835 [gr-qc].

[119] Neil J. Cornish and Tyson B. Littenberg. "BayesWave: Bayesian Inference for Gravitational Wave Bursts and Instrument Glitches." In: *Class. Quant. Grav.* 32.13 (2015), p. 135012. DOI: 10.1088/0264-9381/32/13/135012. arXiv: 1410.3835 [gr-qc].

[120] Neil J. Cornish and Kevin Shuman. "Black Hole Hunting with LISA." In: *arXiv e-prints*, arXiv:2005.03610 (May 2020), arXiv:2005.03610. arXiv: 2005.03610 [gr-qc].

[121] Matteo Correnti, Mario Gennaro, Jason S. Kalirai, Thomas M. Brown, and Annalisa Calamida. "Constraining Globular Cluster Age Uncertainties using the IR Color-Magnitude Diagram." In: *Astrophys. J.* 823.1, 18 (May 2016), p. 18. DOI: 10.3847/0004-637X/823/1/18. arXiv: 1603.05254 [astro-ph.SR].

[122] M. Coughlin, P. Meyers, E. Thrane, J. Luo, and N. Christensen. "Detectability of eccentric compact binary coalescences with advanced gravitational-wave detectors." In: *Phys. Rev. D.* 91.6, 063004 (Mar. 2015), p. 063004. DOI: 10.1103/PhysRevD.91.063004. arXiv: 1412.4665 [gr-qc].

[123] Michael W. Coughlin and Tim Dietrich. "Can a black hole-neutron star merger explain GW170817, AT2017gfo, and GRB170817A?" In: *Phys. Rev. D* 100.4, 043011 (Aug. 2019), p. 043011. DOI: 10.1103/PhysRevD.100.043011. arXiv: 1901.06052 [astro-ph.HE].

[124] Daniel J. D'Orazio and Johan Samsing. "Black Hole Mergers From Globular Clusters Observable by LISA II: Resolved Eccentric Sources and the Gravitational Wave Background." In: *Mon. Not. R. Ast. Soc.* 481.4 (2018), pp. 4775–4785. DOI: 10.1093/mnras/sty2568. arXiv: 1805.06194 [astro-ph.HE].

[125] Gergely Dálya, Peter Raffai, and Bence Bécsy. "Bayesian reconstruction of gravitational-wave signals from binary black holes with nonzero eccentricities." In: *Classical and Quantum Gravity* 38.6, 065002 (Mar. 2021), p. 065002. DOI: 10.1088/1361-6382/abd7bf. arXiv: 2006.06256 [astro-ph.HE].

[126] T. Damour and N Deruelle. "General relativistic celestial mechanics of binary systems. I. The post-Newtonian motion." In: *Ann. Inst. Henri Poincaré, Phys. Théor.* 43 (1985), pp. 107–132.

[127] T. Damour and N Deruelle. "General relativistic celestial mechanics of binary systems. II. The post-Newtonian timing formula." In: *Ann. Inst. Henri Poincaré, Phys. Théor.* 44 (1986), pp. 263–292.

[128] V. De Luca, G. Franciolini, P. Pani, and A. Riotto. "Bayesian evidence for both astrophysical and primordial black holes: mapping the GWTC-2 catalog to third-generation detectors." In: *J. Cosmo. Astropart. Phys.* 2021.5, 003 (May 2021), p. 003. DOI: 10.1088/1475-7516/2021/05/003. arXiv: 2102.03809 [astro-ph.CO].

[129] Soumi De, Morgan MacLeod, Rosa Wallace Everson, Andrea Antoni, Ilya Mandel, and Enrico Ramirez-Ruiz. "Common Envelope Wind Tunnel: The Effects of Binary Mass Ratio and Implications for the Accretion-Driven Growth of LIGO Binary Black Holes." In: *arXiv e-prints*, arXiv:1910.13333 (Oct. 2019), arXiv:1910.13333. arXiv: 1910.13333 [astro-ph.SR].

[130] W. Del Pozzo, C. P. L. Berry, A. Ghosh, T. S. F. Haines, L. P. Singer, and A. Vecchio. "Dirichlet process Gaussian-mixture model: An application to localizing coalescing binary neutron stars with gravitational-wave observations." In: *Mon. Not. Roy. Astron. Soc.* 479.1 (Sept. 2018), pp. 601–614. DOI: 10.1093/mnras/sty1485. arXiv: 1801.08009 [astro-ph.IM].

[131] A. J. Delgado and H. C. Thomas. "Mass transfer in a binary system - The evolution of the mass-giving helium star." In: *Astron. Astrophys.* 96.1-2 (Mar. 1981), pp. 142–145.

[132] J. D. M. Dewi and O. R. Pols. "The late stages of evolution of helium star-neutron star binaries and the formation of double neutron star systems." In: *Mon. Not. Roy. Astron. Soc.* 344.2 (Sept. 2003), pp. 629–643. DOI: 10.1046/j.1365-8711.2003.06844.x. arXiv: astro-ph/0306066 [astro-ph].

[133] J. D. M. Dewi, O. R. Pols, G. J. Savonije, and E. P. J. van den Heuvel. "The evolution of naked helium stars with a neutron-star companion in close binary systems." In: *Mon. Not. R. Ast. Soc.* 331 (2002), p. 1027. DOI: 10.1046/j.1365-8711.2002.05257.x. arXiv: astro-ph/0201239 [astro-ph].

[134] S. Dhawan, M. Bulla, A. Goobar, A. Sagués Carracedo, and C. N. Setzer. "Constraining the Observer Angle of the Kilonova AT2017gfo Associated with GW170817: Implications for the Hubble Constant." In: *Astrophys. J.* 888.2, 67 (Jan. 2020), p. 67. DOI: 10.3847/1538-4357/ab5799. arXiv: 1909.13810 [astro-ph.HE].

[135] Ugo N. Di Carlo, Nicola Giacobbo, Michela Mapelli, Mario Pasquato, Mario Spera, Long Wang, and Francesco Haardt. "Merging black holes in young star clusters." In: *Mon. Not. R. Ast. Soc.* 487.2 (Aug. 2019), pp. 2947–2960. DOI: 10.1093/mnras/stz1453. arXiv: 1901.00863 [astro-ph.HE].

[136] Ugo N. Di Carlo, Nicola Giacobbo, Michela Mapelli, Mario Pasquato, Mario Spera, Long Wang, and Francesco Haardt. "Merging black holes in young star clusters." In: *Mon. Not. R. Ast. Soc.* 487.2 (Aug. 2019), pp. 2947–2960. DOI: 10.1093/mnras/stz1453. arXiv: 1901.00863 [astro-ph.HE].

[137] Tim Dietrich, Anuradha Samajdar, Sebastian Khan, Nathan K. Johnson-McDaniel, Reetika Dudi, and Wolfgang Tichy. "Improving the NRTidal model for binary neutron star systems." In: *Phys. Rev. D* 100.4, 044003 (Aug. 2019), p. 044003. DOI: 10.1103/PhysRevD.100.044003. arXiv: 1905.06011 [gr-qc].

[138] M. Drago et al. "Coherent WaveBurst, a pipeline for unmodeled gravitational-wave data analysis." In: *arXiv e-prints*, arXiv:2006.12604 (June 2020), arXiv:2006.12604. arXiv: 2006.12604 [gr-qc].

[139] William E. East, Sean T. McWilliams, Janna Levin, and Frans Pretorius. "Observing complete gravitational wave signals from dynamical capture binaries." In: *Phys. Rev. D* 87.4, 043004 (Feb. 2013), p. 043004. DOI: 10.1103/PhysRevD.87.043004. arXiv: 1212.0837 [gr-qc].

[140] William E. East, Vasileios Paschalidis, and Frans Pretorius. "Eccentric mergers of black holes with spinning neutron stars." In: *Astrophys. J.* 807.1 (2015), p. L3. DOI: 10.1088/2041-8205/807/1/L3. arXiv: 1503.07171 [astro-ph.HE].

[141] William E. East and Frans Pretorius. "Dynamical Capture Binary Neutron Star Mergers." In: *Astrophys. J.* 760 (2012), p. L4. DOI: 10.1088/2041-8205/760/1/L4. arXiv: 1208.5279 [astro-ph.HE].

[142] Kareem El-Badry, Eliot Quataert, Daniel R. Weisz, Nick Choksi, and Michael Boylan-Kolchin. "The formation and hierarchical assembly of globular cluster populations." In: *Mon. Not. R. Ast. Soc.* 482.4 (Feb. 2019), pp. 4528–4552. DOI: 10.1093/mnras/sty3007. arXiv: 1805.03652 [astro-ph.GA].

[143] Justin Ellis and Rutger van Haasteren. *jellis18/PTMCMCSampler: Official Release*. Oct. 2017. DOI: 10.5281/zenodo.1037579. URL: https://doi.org/10.5281/zenodo.1037579.

[144] Bruce G. Elmegreen. "THE GLOBULAR CLUSTER MASS FUNCTION AS A REMNANT OF VIOLENT BIRTH." In: *The Astrophysical Journal* 712.2 (Mar. 2010), pp. L184–L188. DOI: 10.1088/2041-8205/712/2/l184. URL: https://doi.org/10.1088%2F2041-8205%2F712%2F2%2Fl184.

[145] Debra Meloy Elmegreen and Bruce G. Elmegreen. "Little Blue Dots in the Hubble Space Telescope Frontier Fields: Precursors to Globular Clusters?" In: *Astrophys. J. Lett.* 851.2, L44 (Dec. 2017), p. L44. DOI: 10.3847/2041-8213/aaa0ce. arXiv: 1712.02935 [astro-ph.GA].

[146] Reed Essick, Philippe Landry, and Daniel E. Holz. "Nonparametric inference of neutron star composition, equation of state, and maximum mass with GW170817." In: *Phys. Rev. D* 101.6, 063007 (Mar. 2020), p. 063007. DOI: 10.1103/PhysRevD.101.063007. arXiv: 1910.09740 [astro-ph.HE].

[147] S. M. Fall and M. J. Rees. "A theory for the origin of globular clusters." In: *Astrophys. J.* 298 (Nov. 1985), pp. 18–26. DOI: 10.1086/163585.

[148] W. Farah, C. Flynn, M. Bailes, A. Jameson, T. Bateman, et al. "Five new real-time detections of fast radio bursts with UTMOST." In: *Mon. Not. Roy. Astron. Soc.* 488.3 (Sept. 2019), pp. 2989–3002. DOI: 10.1093/mnras/stz1748. arXiv: 1905.02293 [astro-ph.HE].

[149] R. Farmer, M. Renzo, S. E. de Mink, P. Marchant, and S. Justham. "Mind the Gap: The Location of the Lower Edge of the Pair-instability Supernova Black Hole Mass Gap." In: *Astrophys. J. Lett.* 887 (2019), p. 53.

[150] R. Farmer, M. Renzo, S. E. de Mink, P. Marchant, and S. Justham. "Mind the Gap: The Location of the Lower Edge of the Pair-instability Supernova Black Hole Mass Gap." In: *Astrophys. J.* 887.1, 53 (Dec. 2019), p. 53. DOI: 10.3847/1538-4357/ab518b. arXiv: 1910.12874 [astro-ph.SR].

[151] R. Farmer, M. Renzo3, S. E. de Mink, M. Fishbach, and S. Justham. "Constraints from Gravitational-wave Detections of Binary Black Hole Mergers on the 12C(α, γ)16O Rate." In: *Astrophys. J. Lett.* 902 (2020), p. L36.

[152] B. Farr and W. M. Farr. *kombine: a kernel-density-based, embarrassingly parallel ensemble sampler*. in prep. 2015.

[153] W. M. Farr. *Marginalisation of the time and phase parameters in CBC parameter estimation*. Tech. rep. LIGO-T1400460. 2014. URL: https://dcc.ligo.org/LIGO-T1400460/public.

[154] W. M Farr, B. Farr, and T. Littenberg. *Modelling calibration errors in CBC waveforms*. Tech. rep. LIGO-T1400682. 2014. URL: https://dcc.ligo.org/LIGO-T1400682/public.

[155] W. M. Farr, S. Stevenson, M. C. Miller, I. Mandel, B. Farr, and A. Vecchio. "Distinguishing spin-aligned and isotropic black hole populations with gravitational waves." In: *nature* 548 (Aug. 2017), pp. 426–429. DOI: 10.1038/nature23453.

[156] Nicholas Farrow, Xing-Jiang Zhu, and Eric Thrane. "The Mass Distribution of Galactic Double Neutron Stars." In: *Astrophys. J.* 876.1, 18 (May 2019), p. 18. DOI: 10.3847/1538-4357/ab12e3. arXiv: 1902.03300 [astro-ph.HE].

[157] Marc Favata. "Systematic Parameter Errors in Inspiraling Neutron Star Binaries." In: *Phys. Rev. Lett.* 112.10, 101101 (Mar. 2014), p. 101101. DOI: 10.1103/PhysRevLett.112.101101. arXiv: 1310.8288 [gr-qc].

[158] R. D. Ferdman et al. "The Double Pulsar: Evidence for Neutron Star Formation without an Iron Core-collapse Supernova." In: *Astrophys. J.* 767.1, 85 (Apr. 2013), p. 85. DOI: 10.1088/0004-637X/767/1/85. arXiv: 1302.2914 [astro-ph.SR].

[159] Robert D Ferdman. "PSR J1913+ 1102: a pulsar in a highly asymmetric and relativistic double neutron star system." In: *Proceedings of the International Astronomical Union* 13.S337 (2017), pp. 146–149. DOI: 10.1017/S1743921317009139.

[160] F. Feroz and M. P. Hobson. "Multimodal nested sampling: an efficient and robust alternative to Markov Chain Monte Carlo methods for astronomical data analyses." In: *Mon. Not. Roy. Astron. Soc.* 384 (Feb. 2008), pp. 449–463. DOI: 10.1111/j.1365-2966.2007.12353.x.

[161] F. Feroz, M. P. Hobson, and M. Bridges. "MULTINEST: an efficient and robust Bayesian inference tool for cosmology and particle physics." In: *Mon. Not. Roy. Astron. Soc.* 398 (Oct. 2009), pp. 1601–1614. DOI: 10.1111/j.1365-2966.2009.14548.x.

[162] Farhan Feroz, Michael P. Hobson, Ewan Cameron, and Anthony N. Pettitt. "Importance Nested Sampling and the MultiNest Algorithm." In: *The Open Journal of Astrophysics* 2.1, 10 (Nov. 2019), p. 10. DOI: 10.21105/astro.1306.2144. arXiv: 1306.2144 [astro-ph.IM].

[163] Lee S. Finn. "Detection, measurement, and gravitational radiation." In: *Phys. Rev. D* 46 (12 Dec. 1992), pp. 5236–5249. DOI: 10.1103/PhysRevD.46.5236. URL: https://link.aps.org/doi/10.1103/PhysRevD.46.5236.

[164] Lee Samuel Finn and David F. Chernoff. "Observing binary inspiral in gravitational radiation: One interferometer." In: *Phys. Rev. D* 47.6 (Mar. 1993), pp. 2198–2219. DOI: 10.1103/PhysRevD.47.2198. arXiv: gr-qc/9301003 [gr-qc].

[165] M. Fishbach and D. E. Holz. "Where Are LIGO's Big Black Holes?" In: *Astrophys. J.* 851, L25 (Dec. 2017), p. L25. DOI: 10.3847/2041-8213/aa9bf6.

[166] M. Fishbach, D. E. Holz, and B. Farr. "Are LIGO's Black Holes Made from Smaller Black Holes?" In: *Astrophys. J.* 840, L24 (May 2017), p. L24. DOI: 10.3847/2041-8213/aa7045.

[167] Maya Fishbach and Daniel E. Holz. "Don't fall into the gap: GW190521 as a straddling binary." In: *arXiv e-prints*, arXiv:2009.05472 (Sept. 2020), arXiv:2009.05472. arXiv: 2009.05472 [astro-ph.HE].

[168] Maya Fishbach, Daniel E. Holz, and Will M. Farr. "Does the Black Hole Merger Rate Evolve with Redshift?" In: *Astrophys. J. Lett.* 863.2, L41 (Aug. 2018), p. L41. DOI: 10.3847/2041-8213/aad800. arXiv: 1805.10270 [astro-ph.HE].

[169] É. É. Flanagan and T. Hinderer. "Constraining neutron-star tidal Love numbers with gravitational-wave detectors." In: *Phys. Rev. D* 77.2, 021502 (Jan. 2008), p. 021502. DOI: 10.1103/PhysRevD.77.021502.

[170] W. Fong, P. K. Blanchard, et al. "The Optical Afterglow of GW170817: An Off-axis Structured Jet and Deep Constraints on a Globular Cluster Origin." In: *Astrophys. J. Lett.* 883.1, L1 (Sept. 2019), p. L1. DOI: 10.3847/2041-8213/ab3d9e. arXiv: 1908.08046 [astro-ph.HE].

[171] Duncan A. Forbes, Nate Bastian, Mark Gieles, Robert A. Crain, J. M. Diederik Kruijssen, et al. "Globular cluster formation and evolution in the context of cosmological galaxy assembly: open questions." In: *Proceedings of the Royal Society of London Series A* 474.2210, 20170616 (Feb. 2018), p. 20170616. DOI: 10.1098/rspa.2017.0616. arXiv: 1801.05818 [astro-ph.GA].

[172] Duncan A. Forbes and Terry Bridges. "Accreted versus in situ Milky Way globular clusters." In: *Mon. Not. Roy. Astron. Soc.* 404.3 (May 2010), pp. 1203–1214. DOI: 10.1111/j.1365-2966.2010.16373.x. arXiv: 1001.4289 [astro-ph.GA].

[173] Duncan A. Forbes, Nicola Pastorello, Aaron J. Romanowsky, Christopher Usher, Jean P. Brodie, and Jay Strader. "The SLUGGS survey: inferring the formation epochs of metal-poor and metal-rich globular clusters." In: *Mon. Not. R. Ast. Soc.* 452.1 (Sept. 2015), pp. 1045–1051. DOI: 10.1093/mnras/stv1312. arXiv: 1506.06820 [astro-ph.GA].

[174] K. E. Saavik Ford and Barry McKernan. "Binary Black Hole Merger Rates in AGN Disks versus Nuclear Star Clusters: Loud beats Quiet." In: *arXiv e-prints*, arXiv:2109.03212 (Sept. 2021), arXiv:2109.03212. arXiv: 2109.03212 [astro-ph.HE].

[175] K. E. Saavik Ford et al. "AGN (and other) astrophysics with Gravitational Wave Events." In: *Bulletin of the AAS* 51.3, 247 (May 2019), p. 247. arXiv: 1903.09529 [astro-ph.HE].

[176] G. Fragione and B. Kocsis. "Black hole mergers from an evolving population of globular clusters." In: *Phys. Rev. Lett.* 121 (2018). DOI: 10.1103/PhysRevLett.121.161103.

[177] Giacomo Fragione and Sambaran Banerjee. "Binary Black Hole Mergers from Young Massive and Open Clusters: Comparison to GWTC-2 Gravitational Wave Data." In: *Astrophys. J. Lett.* 913.2, L29 (June 2021), p. L29. DOI: 10.3847/2041-8213/ac00a7. arXiv: 2103.10447 [astro-ph.HE].

[178] Giacomo Fragione and Omer Bromberg. "Eccentric binary black hole mergers in globular clusters hosting intermediate-mass black holes." In: *Mon. Not. Roy. Astron. Soc.* 488.3 (Sept. 2019), pp. 4370–4377. DOI: 10.1093/mnras/stz2024. arXiv: 1903.09659 [astro-ph.GA].

[179] Giacomo Fragione, Idan Ginsburg, and Bence Kocsis. "Gravitational Waves and Intermediate-mass Black Hole Retention in Globular Clusters." In: *Astrophys. J.* 856.2, 92 (Apr. 2018), p. 92. DOI: 10.3847/1538-4357/aab368. arXiv: 1711.00483 [astro-ph.GA].

[180] Giacomo Fragione, Evgeni Grishin, Nathan W. C. Leigh, Hagai B. Perets, and Rosalba Perna. "Black hole and neutron star mergers in galactic nuclei." In: *Mon. Not. Roy. Astron. Soc.* 488.1 (Sept. 2019), pp. 47–63. DOI: 10.1093/mnras/stz1651. arXiv: 1811.10627 [astro-ph.GA].

[181] Giacomo Fragione and Bence Kocsis. "Black hole mergers from quadruples." In: *Mon. Not. Roy. Astron. Soc.* 486.4 (July 2019), pp. 4781–4789. DOI: 10.1093/mnras/stz1175. arXiv: 1903.03112 [astro-ph.GA].

[182] Giacomo Fragione and Bence Kocsis. "Effective spin distribution of black hole mergers in triples." In: *Mon. Not. Roy. Astron. Soc.* 493.3 (Apr. 2020), pp. 3920–3931. DOI: 10.1093/mnras/staa443. arXiv: 1910.00407 [astro-ph.GA].

[183] Giacomo Fragione, Abraham Loeb, and Frederic A. Rasio. "Merging Black Holes in the Low-mass and High-mass Gaps from 2 + 2 Quadruple Systems." In: *Astrophys. J. Lett.* 895.1, L15 (May 2020), p. L15. DOI: 10.3847/2041-8213/ab9093. arXiv: 2002.11278 [astro-ph.GA].

[184] Giacomo Fragione, Abraham Loeb, and Frederic A. Rasio. "On the Origin of GW190521-like Events from Repeated Black Hole Mergers in Star Clusters." In: *Astrophys. J. Lett.* 902.1, L26 (Oct. 2020), p. L26. DOI: 10.3847/2041-8213/abbc0a. arXiv: 2009.05065 [astro-ph.GA].

[185] Giacomo Fragione, Rosalba Perna, and Abraham Loeb. "Calibrating the binary black hole population in nuclear star clusters through tidal disruption events." In: *Mon. Not. Roy. Astron. Soc.* 500.4 (Jan. 2021), pp. 4307–4318. DOI: 10.1093/mnras/staa3493. arXiv: 2006.14632 [astro-ph.GA].

[186] Gabriele Franciolini, Vishal Baibhav, Valerio De Luca, Ken K. Y. Ng, Kaze W. K. Wong, Emanuele Berti, Paolo Pani, Antonio Riotto, and Salvatore Vitale. "Quantifying the evidence for primordial black holes in LIGO/Virgo gravitational-wave data." In: *arXiv e-prints*, arXiv:2105.03349 (May 2021), arXiv:2105.03349. arXiv: 2105.03349 [gr-qc].

[187] J. M. Fregeau and F. A. Rasio. "Monte Carlo Simulations of Globular Cluster Evolution. IV. Direct Integration of Strong Interactions." In: *Astrophys. J.* 658 (Apr. 2007), pp. 1047–1061. DOI: 10.1086/511809. eprint: astro-ph/0608261.

[188] Hunter Gabbard, Chris Messenger, Ik Siong Heng, Francesco Tonolini, and Roderick Murray-Smith. "Bayesian parameter estimation using conditional variational autoencoders for gravitational-wave astronomy." In: *arXiv e-prints*, arXiv:1909.06296 (Sept. 2019), arXiv:1909.06296. arXiv: 1909.06296 [astro-ph.IM].

[189] Shanika Galaudage, Colm Talbot, Tushar Nagar, Deepnika Jain, Eric Thrane, and Ilya Mandel. "Building better spin models for merging binary black holes: Evidence for non-spinning and rapidly spinning nearly aligned sub-populations." In: *arXiv e-prints*, arXiv:2109.02424 (Sept. 2021), arXiv:2109.02424. arXiv: 2109.02424 [gr-qc].

[190] Shanika Galaudage, Colm Talbot, and Eric Thrane. "Gravitational-wave inference in the catalog era: evolving priors and marginal events." In: *arXiv e-prints*, arXiv:1912.09708 (Dec. 2019), arXiv:1912.09708. arXiv: 1912.09708 [astro-ph.HE].

[191] Enrique García-Berro, Santiago Torres, Leand ro G. Althaus, and Marcelo M. Miller Bertolami. "The white dwarf cooling sequence of 47 Tucanae." In: *Astron. Astrophys.* 571, A56 (Nov. 2014), A56. DOI: 10.1051/0004-6361/201424652. arXiv: 1410.0536 [astro-ph.GA].

[192] V. Gayathri, J. Healy, J. Lange, B. O'Brien, M. Szczepanczyk, I. Bartos, M. Campanelli, S. Klimenko, C. Lousto, and R. O'Shaughnessy. "GW190521 as a Highly Eccentric Black Hole Merger." In: *arXiv e-prints*, arXiv:2009.05461 (Sept. 2020), arXiv:2009.05461. arXiv: 2009.05461 [astro-ph.HE].

[193] Daniel George and E. A. Huerta. "Deep Learning for real-time gravitational wave detection and parameter estimation: Results with Advanced LIGO data." In: *Physics Letters B* 778 (Mar. 2018), pp. 64–70. DOI: 10.1016/j.physletb.2017.12.053. arXiv: 1711.03121 [gr-qc].

[194] Davide Gerosa and Emanuele Berti. "Are merging black holes born from stellar collapse or previous mergers?" In: *Phys. Rev.* D95.12 (2017), p. 124046. DOI: 10.1103/PhysRevD.95.124046. arXiv: 1703.06223 [gr-qc].

[195] Davide Gerosa, Emanuele Berti, Richard O'Shaughnessy, Krzysztof Belczynski, Michael Kesden, Daniel Wysocki, and Wojciech Gladysz. "Spin orientations of merging black holes formed from the evolution of stellar binaries." In: *Phys. Rev. D* 98.8 (2018), p. 084036. DOI: 10.1103/PhysRevD.98.084036. arXiv: 1808.02491 [astro-ph.HE].

[196] Nicola Giacobbo and Michela Mapelli. "The progenitors of compact-object binaries: impact of metallicity, common envelope and natal kicks." In: *Mon. Not. R. Ast. Soc.* 480.2 (Oct. 2018), pp. 2011–2030. DOI: 10.1093/mnras/sty1999. arXiv: 1806.00001 [astro-ph.HE].

[197] Nicola Giacobbo and Michela Mapelli. "The impact of electron-capture supernovae on merging double neutron stars." In: *Mon. Not. R. Ast. Soc.* 482.2 (Jan. 2019), pp. 2234–2243. DOI: 10.1093/mnras/sty2848. arXiv: 1805.11100 [astro-ph.SR].

[198] Nicola Giacobbo and Michela Mapelli. "Revising Natal Kick Prescriptions in Population Synthesis Simulations." In: *Astrophys. J.* 891.2, 141 (Mar. 2020), p. 141. DOI: 10.3847/1538-4357/ab7335. arXiv: 1909.06385 [astro-ph.HE].

[199] Boris Goncharov, Xing-Jiang Zhu, and Eric Thrane. "Is there a spectral turnover in the spin noise of millisecond pulsars?" In: *arXiv e-prints*, arXiv:1910.05961 (Oct. 2019), arXiv:1910.05961. arXiv: 1910.05961 [astro-ph.HE].

[200] László Gondán and Bence Kocsis. "High eccentricities and high masses characterize Gravitational-wave captures in Galactic Nuclei as seen by Earth-based detectors." In: *Mon. Not. Roy. Astron. Soc.* (July 2021). DOI: 10.1093/mnras/stab1722. arXiv: 2011.02507 [astro-ph.HE].

[201] László Gondán, Bence Kocsis, Péter Raffai, and Zsolt Frei. "Accuracy of Estimating Highly Eccentric Binary Black Hole Parameters with Gravitational-Wave Detections." In: *Astrophys. J.* 855.1 (2018), p. 34. DOI: 10.3847/1538-4357/aaad0e. arXiv: 1705.10781 [astro-ph.HE].

[202] László Gondán, Bence Kocsis, Péter Raffai, and Zsolt Frei. "Eccentric Black Hole Gravitational-Wave Capture Sources in Galactic Nuclei: Distribution of Binary Parameters." In: *Astrophys. J.* 860.1 (2018), p. 5. DOI: 10.3847/1538-4357/aabfee. arXiv: 1711.09989.

[203] László Gondán and Bence Kocsis. "Measurement Accuracy of Inspiraling Eccentric Neutron Star and Black Hole Binaries Using Gravitational Waves." In: *Astrophys. J.* 871.2 (2019), p. 178. DOI: 10.3847/1538-4357/aaf893. arXiv: 1809.00672.

[204] K. M. Górski, E. Hivon, A. J. Banday, B. D. Wandelt, F. K. Hansen, M. Reinecke, and M. Bartelmann. "HEALPix: A Framework for High-Resolution Discretization and Fast Analysis of Data Distributed on the Sphere." In: *Astrophys. J. Lett.* 622 (2005), pp. 759–771. DOI: 10.1086/427976.

[205] K. M. Górski and et al. "Analysis issues for large CMB data sets." In: *Evolution of Large Scale Structure : From Recombination to Garching*. Ed. by A. J. Banday, R. K. Sheth, and L. N. da Costa. Jan. 1999, p. 37. arXiv: astro-ph/9812350 [astro-ph].

[206] M. J. Graham et al. "Candidate Electromagnetic Counterpart to the Binary Black Hole Merger Gravitational-Wave Event S190521g*." In: *Phys. Rev. Lett.* 124.25, 251102 (June 2020), p. 251102. DOI: 10.1103/PhysRevLett.124.251102. arXiv: 2006.14122 [astro-ph.HE].

[207] Raffaele G. Gratton, Flavio Fusi Pecci, Eugenio Carretta, Gisella Clementini, Carlo E. Corsi, and Mario Lattanzi. "Ages of Globular Clusters from HIPPARCOS Parallaxes of Local Subdwarfs." In: *Astrophys. J.* 491.2 (Dec. 1997), pp. 749–771. DOI: 10.1086/304987. arXiv: astro-ph/9704150 [astro-ph].

[208] Jonathan Grindlay, Simon Portegies Zwart, and Stephen McMillan. "Short gamma-ray bursts from binary neutron star mergers in globular clusters." In: *Nature Phys.* 2 (2006), p. 116. DOI: 10.1038/nphys214. arXiv: astro-ph/0512654 [astro-ph].

[209] Evgeni Grishin, Hagai B. Perets, and Giacomo Fragione. "Quasi-secular evolution of mildly hierarchical triple systems: analytics and applications for GW sources and hot Jupiters."

In: *Mon. Not. R. Ast. Soc.* 481.4 (Dec. 2018), pp. 4907–4923. DOI: 10.1093/mnras/sty2477. arXiv: 1808.02030 [astro-ph.EP].

[210] M. Gröbner, W. Ishibashi, S. Tiwari, M. Haney, and P. Jetzer. "Binary black hole mergers in AGN accretion discs: gravitational wave rate density estimates." In: *Astron. Astrophys.* 638, A119 (June 2020), A119. DOI: 10.1051/0004-6361/202037681. arXiv: 2005.03571 [astro-ph.GA].

[211] Evan D. Hall and Matthew Evans. "Metrics for next-generation gravitational-wave detectors." In: *Classical and Quantum Gravity* 36.22, 225002 (Nov. 2019), p. 225002. DOI: 10.1088/1361-6382/ab41d6. arXiv: 1902.09485 [astro-ph.IM].

[212] W. J. Handley, M. P. Hobson, and A. N. Lasenby. "polychord: nested sampling for cosmology." In: *Mon. Not. Roy. Astron. Soc. Lett.* 450.1 (Apr. 2015), pp. L61–L65. ISSN: 1745-3925. DOI: 10.1093/mnrasl/slv047. eprint: https://academic.oup.com/mnrasl/article-pdf/450/1/L61/3087909/slv047.pdf. URL: https://doi.org/10.1093/mnrasl/slv047.

[213] W. J. Handley, M. P. Hobson, and A. N. Lasenby. "polychord: next-generation nested sampling." In: *Mon. Not. Roy. Astron. Soc.* 453.4 (Sept. 2015), pp. 4384–4398. ISSN: 0035-8711. DOI: 10.1093/mnras/stv1911. eprint: https://academic.oup.com/mnras/article-pdf/453/4/4384/8034904/stv1911.pdf. URL: https://doi.org/10.1093/mnras/stv1911.

[214] Mark Hannam, Patricia Schmidt, Alejandro Bohé, Leïla Haegel, Sascha Husa, Frank Ohme, Geraint Pratten, and Michael Pürrer. "Simple Model of Complete Precessing Black-Hole-Binary Gravitational Waveforms." In: *Phys. Rev. Lett.* 113 (15 Oct. 2014), p. 151101. DOI: 10.1103/PhysRevLett.113.151101. URL: https://link.aps.org/doi/10.1103/PhysRevLett.113.151101.

[215] B. M. S. Hansen, J. S. Kalirai, J. Anderson, A. Dotter, H. B. Richer, et al. "An age difference of two billion years between a metal-rich and a metal-poor globular cluster." In: *nat* 500.7460 (Aug. 2013), pp. 51–53. DOI: 10.1038/nature12334. arXiv: 1308.0032 [astro-ph.SR].

[216] W Keith Hastings. "Monte Carlo sampling methods using Markov chains and their applications." In: *Biometrika* 57.1 (1970), pp. 97–109.

[217] James Healy, Janna Levin, and Deirdre Shoemaker. "Zoom-Whirl Orbits in Black Hole Binaries." In: *Phys. Rev. Lett.* 103.13, 131101 (Sept. 2009), p. 131101. DOI: 10.1103/PhysRevLett.103.131101. arXiv: 0907.0671 [gr-qc].

[218] A. Heger and S. E. Woosley. "The Nucleosynthetic Signature of Population III." In: *Astrophy. J.* 567 (Mar. 2002), pp. 532–543. DOI: 10.1086/338487. eprint: astro-ph/0107037.

[219] Martin Hendry. "An Introduction to General Relativity, Gravitational Waves and Detection Principles." In: 2007.

[220] Francisco Hernandez Vivanco, Rory Smith, Eric Thrane, and Paul D. Lasky. "Accelerated detection of the binary neutron star gravitational-wave background." In: *Phys. Rev. D* 100.4, 043023 (Aug. 2019), p. 043023. DOI: 10.1103/PhysRevD.100.043023. arXiv: 1903.05778 [gr-qc].

[221] Francisco Hernandez Vivanco, Rory Smith, Eric Thrane, Paul D. Lasky, Colm Talbot, and Vivien Raymond. "Measuring the neutron star equation of state with gravitational waves: The first forty binary neutron star merger observations." In: *Phys. Rev. D* 100.10, 103009 (Nov. 2019), p. 103009. DOI: 10.1103/PhysRevD.100.103009. arXiv: 1909.02698 [gr-qc].

[222] Ian Hinder, Birjoo Vaishnav, Frank Herrmann, Deirdre M. Shoemaker, and Pablo Laguna. "Circularization and final spin in eccentric binary-black-hole inspirals." In: *Phys. Rev. D* 77.8, 081502 (Apr. 2008), p. 081502. DOI: 10.1103/PhysRevD.77.081502. arXiv: 0710.5167 [gr-qc].

[223] Ian Hinder, Birjoo Vaishnav, Frank Herrmann, Deirdre Shoemaker, and Pablo Laguna. "Universality and final spin in eccentric binary black hole inspirals." In: *Phys. Rev. D* D77 (2008), p. 081502. DOI: 10.1103/PhysRevD.77.081502. arXiv: 0710.5167.

[224] Bao-Minh Hoang, Smadar Naoz, Bence Kocsis, Frederic A. Rasio, and Fani Dosopoulou. "Black Hole Mergers in Galactic Nuclei Induced by the Eccentric Kozai-Lidov Effect." In: *Astrophys. J.* 856.2, 140 (Apr. 2018), p. 140. DOI: 10.3847/1538-4357/aaafce. arXiv: 1706.09896 [astro-ph.HE].

[225] G. Hobbs, D. R. Lorimer, A. G. Lyne, and M. Kramer. "A statistical study of 233 pulsar proper motions." In: *Mon. Not. Roy. Astron. Soc.* 360.3 (July 2005), pp. 974–992. DOI: 10.1111/j.1365-2966.2005.09087.x. arXiv: astro-ph/0504584 [astro-ph].

[226] David W. Hogg and Daniel Foreman-Mackey. "Data Analysis Recipes: Using Markov Chain Monte Carlo." In: *The Astrophysical Journal Supplement Series* 236.1 (May 2018), p. 11. DOI: 10.3847/1538-4365/aab76e. URL: https://doi.org/10.3847\%2F1538-4365\%2Faab76e.

[227] Jongsuk Hong, Enrico Vesperini, Abbas Askar, Mirek Giersz, Magdalena Szkudlarek, and Tomasz Bulik. "Binary black hole mergers from globular clusters: the impact of globular cluster properties." In: *Mon. Not. R. Ast. Soc.* 480.4 (Nov. 2018),

pp. 5645–5656. DOI: 10.1093/mnras/sty2211. arXiv: 1808.04514 [astro-ph.HE].

[228] Jongsuk Hong, Enrico Vesperini, Abbas Askar, Mirek Giersz, Magdalena Szkudlarek, and Tomasz Bulik. "Binary black hole mergers from globular clusters: the impact of globular cluster properties." In: *Mon. Not. Roy. Astron. Soc.* 480.4 (Nov. 2018), pp. 5645–5656. DOI: 10.1093/mnras/sty2211. arXiv: 1808.04514 [astro-ph.HE].

[229] K. Hotokezaka, E. Nakar, O. Gottlieb, S. Nissanke, K. Masuda, G. Hallinan, K. P. Mooley, and A. T. Deller. "A Hubble constant measurement from superluminal motion of the jet in GW170817." In: *Nature Astron.* 3 (July 2019), pp. 940–944. DOI: 10.1038/s41550-019-0820-1. arXiv: 1806.10596 [astro-ph.CO].

[230] Charlie Hoy and Vivien Raymond. "PESummary: the code agnostic Parameter Estimation Summary page builder." In: *arXiv e-prints*, arXiv:2006.06639 (June 2020), arXiv:2006.06639. arXiv: 2006.06639 [astro-ph.IM].

[231] Moritz Hübner, Colm Talbot, Paul D. Lasky, and Eric Thrane. "Measuring gravitational-wave memory in the first LIGO/Virgo gravitational-wave transient catalog." In: *Phys. Rev. D* 101.2, 023011 (Jan. 2020), p. 023011. DOI: 10.1103/PhysRevD.101.023011. arXiv: 1911.12496 [astro-ph.HE].

[232] E. A. Huerta et al. "Eccentric, nonspinning, inspiral, Gaussian-process merger approximant for the detection and characterization of eccentric binary black hole mergers." In: *Phys. Rev. D* 97.2, 024031 (Jan. 2018), p. 024031. DOI: 10.1103/PhysRevD.97.024031. arXiv: 1711.06276 [gr-qc].

[233] E.A. Huerta et al. "Accurate and efficient waveforms for compact binaries on eccentric orbits." In: *Phys. Rev. D* 90 (2014). DOI: 10.1103/PhysRevD.90.084016.

[234] J. R. Hurley, O. R. Pols, and C. A. Tout. "Comprehensive analytic formulae for stellar evolution as a function of mass and metallicity." In: *Mon. Not. R. Ast. Soc.* 315 (July 2000), pp. 543–569. DOI: 10.1046/j.1365-8711.2000.03426.x. eprint: astro-ph/0001295.

[235] J. R. Hurley, C. A. Tout, and O. R. Pols. "Evolution of binary stars and the effect of tides on binary populations." In: *Mon. Not. R. Ast. Soc.* 329 (Feb. 2002), pp. 897–928. DOI: 10.1046/j.1365-8711.2002.05038.x. eprint: astro-ph/0201220.

[236] Maximiliano Isi, Matthew Giesler, Will M. Farr, Mark A. Scheel, and Saul A. Teukolsky. "Testing the No-Hair Theorem with GW150914." In: *Phys. Rev. L* 123.11, 111102 (Sept. 2019), p. 111102. DOI: 10.1103/PhysRevLett.123.111102. arXiv: 1905.00869 [gr-qc].

[237] Tousif Islam, Vijay Varma, Jackie Lodman, Scott E. Field, Gaurav Khanna, Mark A. Scheel, Harald P. Pfeiffer, Davide Gerosa, and Lawrence E. Kidder. "Eccentric binary black hole surrogate models for the gravitational waveform and remnant properties: Comparable mass, nonspinning case." In: *Phys. Rev. D* 103.6, 064022 (Mar. 2021), p. 064022. DOI: 10.1103/PhysRevD.103.064022. arXiv: 2101.11798 [gr-qc].

[238] N. Ivanova, K. Belczynski, V. Kalogera, F. A. Rasio, and R. E. Taam. "The Role of Helium Stars in the Formation of Double Neutron Stars." In: *Astrophys. J.* 592.1 (July 2003), pp. 475–485. DOI: 10.1086/375578. arXiv: astro-ph/0210267 [astro-ph].

[239] N. Ivanova et al. "Common envelope evolution: where we stand and how we can move forward." In: *Astron. Astrophys. Rev.* 21, 59 (Feb. 2013), p. 59. DOI: 10.1007/s00159-013-0059-2. arXiv: 1209.4302 [astro-ph.HE].

[240] Natalia Ivanova, Craig O. Heinke, and Frederic A. Rasio. "Neutron Stars in Globular Clusters." In: *IAU Symp.* 246 (2008), pp. 316–320. DOI: 10.1017/S1743921308015846. arXiv: 0711.3181 [astro-ph].

[241] Kriten J. Joshi, Frederic A. Rasio, S P Zwart, and Simon Portegies Zwart. "Monte Carlo Simulations of Globular Cluster Evolution. I. Method and Test Calculations." In: *The Astrophysical Journal* 540.2 (Sept. 2000), pp. 969–982. ISSN: 0004-637X. DOI: 10.1086/309350. URL: http://arxiv.org/abs/astro-ph/9909115http://stacks.iop.org/0004-637X/540/i=2/a=969http://iopscience.iop.org/0004-637X/540/2/969papers3://publication/uuid/333FB256-2459-42E3-B115-0A8D7D241C52.

[242] Vassiliki Kalogera. "Spin-Orbit Misalignment in Close Binaries with Two Compact Objects." In: *Astrophys. J.* 541.1 (Sept. 2000), pp. 319–328. DOI: 10.1086/309400. arXiv: astro-ph/9911417 [astro-ph].

[243] Vassiliki Kalogera, K. Belczynski, C. Kim, Richard W. O'Shaughnessy, and B. Willems. "Formation of Double Compact Objects." In: *Phys. Rept.* 442 (2007), pp. 75–108. DOI: 10.1016/j.physrep.2007.02.008. arXiv: astro-ph/0612144 [astro-ph].

[244] Mansi M. Kasliwal et al. "Spitzer Mid-Infrared Detections of Neutron Star Merger GW170817 Suggests Synthesis of the Heaviest Elements." In: *Mon. Not. Roy. Astron. Soc.* (Jan. 2019), p. L14. DOI: 10.1093/mnrasl/slz007. arXiv: 1812.08708 [astro-ph.HE].

[245] Harley Katz and Massimo Ricotti. "Clues on the missing sources of reionization from self-consistent modelling of Milky Way and dwarf galaxy globular clusters." In: *Monthly Notices of the Royal Astronomical Society* 444.3 (Sept. 2014), pp. 2377–2395.

ISSN: 0035-8711. DOI: 10.1093/mnras/stu1489. eprint: https://academic.oup.com/mnras/article-pdf/444/3/2377/18502495/stu1489.pdf. URL: https://doi.org/10.1093/mnras/stu1489.

[246] Seiji Kawamura et al. "Current status of space gravitational wave antenna DECIGO and B-DECIGO." In: *Progress of Theoretical and Experimental Physics* 2021.5, 05A105 (May 2021), 05A105. DOI: 10.1093/ptep/ptab019. arXiv: 2006.13545 [gr-qc].

[247] David Keitel. "Multiple-image Lensing Bayes Factor for a Set of Gravitational-wave Events." In: *Research Notes of the American Astronomical Society* 3.3, 46 (Mar. 2019), p. 46. DOI: 10.3847/2515-5172/ab0c0b.

[248] L. O. Kerber, M. Libralato, S. O. Souza, R. A. P. Oliveira, S. Ortolani, et al. "A deep view of a fossil relic in the Galactic bulge: the Globular Cluster HP 1." In: *Mon. Not. R. Ast. Soc.* 484.4 (Apr. 2019), pp. 5530–5550. DOI: 10.1093/mnras/stz003. arXiv: 1901.03721 [astro-ph.SR].

[249] Sebastian Khan, Sascha Husa, Mark Hannam, Frank Ohme, Michael Pürrer, et al. "Frequency-domain gravitational waves from nonprecessing black-hole binaries. II. A phenomenological model for the advanced detector era." In: *Phys. Rev. D* 93.4, 044007 (Feb. 2016), p. 044007. DOI: 10.1103/PhysRevD.93.044007. arXiv: 1508.07253 [gr-qc].

[250] L E Kidder. In: *Phys. Rev. D.* 52 (1995).

[251] Paul Kiel, John Fregeau, Stefan Umbreit, Sourav Chatterjee, and Fred Rasio. "Neutron Stars and Binary Pulsars in Globular Clusters." In: *AIP Conference Proceedings* 1314.1 (2010), pp. 367–368. DOI: 10.1063/1.3536402. eprint: https://aip.scitation.org/doi/pdf/10.1063/1.3536402. URL: https://aip.scitation.org/doi/abs/10.1063/1.3536402.

[252] Chase Kimball, Christopher Berry, and Vicky Kalogera. "What GW170729's Exceptional Mass and Spin Tells Us about Its Family Tree." In: *RNAAS* 4 (2019), p. 2.

[253] Chase Kimball, C. Talbot, Christopher P.L. Berry, Michael Zevin, Eric Thrane, et al. "Evidence for hierarchical black hole mergers in the second LIGO–Virgo gravitational-wave catalog." In: *Astrophys. J. Lett.* 915 (2021), p. L35.

[254] Chase Kimball, Colm Talbot, Christopher P. L. Berry, Matthew Carney, Michael Zevin, Eric Thrane, and Vicky Kalogera. "Black Hole Genealogy: Identifying Hierarchical Mergers with Gravitational Waves." In: *Astrophys. J. Lett.* 900.2, 177 (Sept. 2020), p. 177. DOI: 10.3847/1538-4357/aba518. arXiv: 2005.00023 [astro-ph.HE].

[255] Chase Kimball et al. "Evidence for hierarchical black hole mergers in the second LIGO–Virgo gravitational-wave catalog." In: *arXiv e-prints*, arXiv:2011.05332 (Nov. 2020), arXiv:2011.05332. arXiv: 2011.05332 [astro-ph.HE].

[256] Taysun Kimm, Renyue Cen, Joakim Rosdahl, and Sukyoung K. Yi. "Formation of Globular Clusters in Atomic-cooling Halos Via Rapid Gas Condensation and Fragmentation during the Epoch of Reionization." In: *Astrophys. J.* 823.1, 52 (May 2016), p. 52. DOI: 10.3847/0004-637X/823/1/52. arXiv: 1510.05671 [astro-ph.GA].

[257] Leslie Kish. *Survey Sampling*. 3rd ed. Wiley-Interscience, 1995.

[258] Antoine Klein. "EFPE: Efficient fully precessing eccentric gravitational waveforms for binaries with long inspirals." In: *arXiv e-prints*, arXiv:2106.10291 (June 2021), arXiv:2106.10291. arXiv: 2106.10291 [gr-qc].

[259] Bence Kocsis and Janna Levin. "Repeated bursts from relativistic scattering of compact objects in galactic nuclei." In: *Phys. Rev. D* 85.12, 123005 (June 2012), p. 123005. DOI: 10.1103/PhysRevD.85.123005. arXiv: 1109.4170 [astro-ph.CO].

[260] A. N. Kolmogorov. "Sulla deterinazione empirica di una legge di distribuzione." In: *G. Ist. Ital. Attuari.* 4 (1933), pp. 83–91.

[261] Valeriya Korol, Ilya Mandel, M. Coleman Miller, Ross P. Church, and Melvyn B. Davies. "Merger rates in primordial black hole clusters without initial binaries." In: *Mon. Not. Roy. Astron. Soc.* 496.1 (July 2020), pp. 994–1000. DOI: 10.1093/mnras/staa1644. arXiv: 1911.03483 [astro-ph.HE].

[262] I. Kowalska, T. Bulik, K. Belczynski, M. Dominik, and D. Gondek-Rosinska. "The eccentricity distribution of compact binaries." In: *Astron. Astrophys.* 527, A70 (Mar. 2011), A70. DOI: 10.1051/0004-6361/201015777. arXiv: 1010.0511 [astro-ph.CO].

[263] Y. Kozai. "Secular perturbations of asteroids with high inclination and eccentricity." In: *Astrophys. J.* 67 (Nov. 1962), p. 591. DOI: 10.1086/108790.

[264] Kyle Kremer, Mario Spera, Devin Becker, Sourav Chatterjee, Ugo N. Di Carlo, Giacomo Fragione, Carl L. Rodriguez, Claire S. Ye, and Frederic A. Rasio. "Populating the Upper Black Hole Mass Gap through Stellar Collisions in Young Star Clusters." In: *Astrophys. J.* 903.1, 45 (Nov. 2020), p. 45. DOI: 10.3847/1538-4357/abb945. arXiv: 2006.10771 [astro-ph.HE].

[265] Kyle Kremer, Claire S. Ye, Nicholas Z. Rui, Newlin C. Weatherford, Sourav Chatterjee, Giacomo Fragione, Carl L. Rodriguez, Mario Spera, and Frederic A. Rasio. "Modeling Dense Star Clusters in the Milky Way and Beyond with the CMC Cluster Catalog." In: *Astrophys. J. Supp.* 247.2, 48 (Apr. 2020), p. 48. DOI: 10.3847/1538-4365/ab7919. arXiv: 1911.00018 [astro-ph.HE].

[266] A. Krolak and Bernard F. Schutz. "Coalescing binaries—Probe of the universe." In: *General Relativity and Gravitation* 19.12 (Dec. 1987), pp. 1163–1171. DOI: 10.1007/BF00759095.

[267] M. U. Kruckow, T. M. Tauris, N. Langer, D. Szécsi, P. Marchant, and Ph. Podsiadlowski. "Common envelope ejection in massive binary stars - Implications for the progenitors of GW150914 and GW151226." In: *Astron. Astrophys.* 596 (2016), A58. DOI: 10.1051/0004-6361/201629420. arXiv: 1610.04417 [astro-ph.SR].

[268] Matthias U. Kruckow, Thomas M. Tauris, Norbert Langer, Michael Kramer, and Robert G. Izzard. "Progenitors of gravitational wave mergers: binary evolution with the stellar grid-based code COMBINE." In: *Mon. Not. Roy. Astron. Soc.* 481.2 (Dec. 2018), pp. 1908–1949. DOI: 10.1093/mnras/sty2190. arXiv: 1801.05433 [astro-ph.SR].

[269] J. M. Diederik Kruijssen. "Globular clusters as the relics of regular star formation in 'normal' high-redshift galaxies." In: *Monthly Notices of the Royal Astronomical Society* 454.2 (Oct. 2015), pp. 1658–1686. ISSN: 0035-8711. DOI: 10.1093/mnras/stv2026. eprint: https://academic.oup.com/mnras/article-pdf/454/2/1658/20688297/stv2026.pdf. URL: https://doi.org/10.1093/mnras/stv2026.

[270] S. Kullback and R. A. Leibler. "On Information and Sufficiency." In: *Ann. Math. Statist.* 22.1 (Mar. 1951), pp. 79–86. DOI: 10.1214/aoms/1177729694. URL: https://doi.org/10.1214/aoms/1177729694.

[271] A. G. Kuranov and K. A. Postnov. "Neutron stars in globular clusters: Formation and observational manifestations." In: *Astronomy Letters* 32.6 (June 2006), pp. 393–405. ISSN: 1562-6873. DOI: 10.1134/S106377370606003X. URL: https://doi.org/10.1134/S106377370606003X.

[272] LIGO Scientific Collaboration. *LIGO Algorithm Library - LALSuite*. free software (GPL). 2018. DOI: 10.7935/GT1W-FZ16.

[273] Benjamin D. Lackey, Michael Pürrer, Andrea Taracchini, and Sylvain Marsat. "Surrogate model for an aligned-spin effective-one-body waveform model of binary neutron star inspirals using Gaussian process regression." In: *Phys. Rev. D* 100.2, 024002 (July 2019), p. 024002. DOI: 10.1103/PhysRevD.100.024002. arXiv: 1812.08643 [gr-qc].

[274] Charles J. Lada and Elizabeth A. Lada. "Embedded Clusters in Molecular Clouds." In: *Ann. Rev. Astron. Astrophys.* 41 (Jan. 2003), pp. 57–115. DOI: 10.1146/annurev.astro.41.011802.094844. arXiv: astro-ph/0301540 [astro-ph].

[275] Jacob Lange, Richard O'Shaughnessy, and Monica Rizzo. "Rapid and accurate parameter inference for coalescing, precessing compact binaries." In: *arXiv:1805.10457* (2018).

[276] Mike Y. M. Lau, Ilya Mandel, Alejandro Vigna-Gómez, Coenraad J. Neijssel, Simon Stevenson, and Alberto Sesana. "Detecting double neutron stars with LISA." In: *Mon. Not. Roy. Astron. Soc.* 492.3 (Mar. 2020), pp. 3061–3072. DOI: 10.1093/mnras/staa002. arXiv: 1910.12422 [astro-ph.HE].

[277] P. Lazarus et al. "Einstein at Home discovery of a Double-Neutron Star Binary in the PALFA Survey." In: *Astrophys. J.* 831.2 (2016), p. 150. DOI: 10.3847/0004-637X/831/2/150. arXiv: 1608.08211 [astro-ph.HE].

[278] Ryan Leaman, Don A. VandenBerg, and J. Trevor Mendel. "The bifurcated age-metallicity relation of Milky Way globular clusters and its implications for the accretion history of the galaxy." In: *Mon. Not. R. Ast. Soc.* 436.1 (Nov. 2013), pp. 122–135. DOI: 10.1093/mnras/stt1540. arXiv: 1309.0822 [astro-ph.GA].

[279] L. Lentati, P. Alexander, M. P. Hobson, F. Feroz, R. van Haasteren, K. J. Lee, and R. M. Shannon. "TEMPONEST: a Bayesian approach to pulsar timing analysis." In: *Mon. Not. Roy. Astron. Soc.* 437.3 (Jan. 2014), pp. 3004–3023. DOI: 10.1093/mnras/stt2122. arXiv: 1310.2120 [astro-ph.IM].

[280] Janna Levin, Sean T. McWilliams, and Hugo Contreras. "Inspiral of generic black hole binaries: spin, precession and eccentricity." In: *Classical and Quantum Gravity* 28.17, 175001 (Sept. 2011), p. 175001. DOI: 10.1088/0264-9381/28/17/175001. arXiv: 1009.2533 [gr-qc].

[281] Ya-Ping Li, Adam M. Dempsey, Shengtai Li, Hui Li, and Jiaru Li. "Orbital Evolution of Binary Black Holes in Active Galactic Nucleus Disks: A Disk Channel for Binary Black Hole Mergers?" In: *Astrophys. J.* 911.2, 124 (Apr. 2021), p. 124. DOI: 10.3847/1538-4357/abed48. arXiv: 2101.09406 [astro-ph.HE].

[282] M. L. Lidov. "The evolution of orbits of artificial satellites of planets under the action of gravitational perturbations of external bodies." In: *Planetary and Space Science* 9 (Oct. 1962), pp. 719–759. DOI: 10.1016/0032-0633(62)90129-0.

[283] Simon J. Lilly, C. Marcella Carollo, and Alan N. Stockton. "The metallicity of star-forming gas over cosmic time." In: *arXiv e-prints*, astro-ph/0209243 (Sept. 2002), astro–ph/0209243. arXiv: astro-ph/0209243 [astro-ph].

[284] J. Lin. "Divergence measures based on the Shannon entropy." In: *IEEE Transactions on Information Theory* 37.1 (Jan. 1991), pp. 145–151. ISSN: 1557-9654. DOI: 10.1109/18.61115.

[285] Tyson B. Littenberg and Neil J. Cornish. "Bayesian inference for spectral estimation of gravitational wave detector noise." In: *Phys. Rev. D* 91 (8 Apr. 2015), p. 084034. DOI: 10.1103/PhysRevD.91.084034. URL: https://link.aps.org/doi/10.1103/PhysRevD.91.084034.

[286] Tyson B. Littenberg and Neil J. Cornish. "Bayesian inference for spectral estimation of gravitational wave detector noise." In: *Phys. Rev. D* 91.8 (2015), p. 084034. DOI: 10.1103/PhysRevD.91.084034. arXiv: 1410.3852 [gr-qc].

[287] Bin Liu and Dong Lai. "Enhanced black hole mergers in binary-binary interactions." In: *Mon. Not. Roy. Astron. Soc.* 483.3 (Mar. 2019), pp. 4060–4069. DOI: 10.1093/mnras/sty3432. arXiv: 1809.07767 [astro-ph.HE].

[288] Bin Liu, Dong Lai, and Yi-Han Wang. "Black Hole and Neutron Star Binary Mergers in Triple Systems. II. Merger Eccentricity and Spin-Orbit Misalignment." In: *Astrophys. J.* 881.1, 41 (Aug. 2019), p. 41. DOI: 10.3847/1538-4357/ab2dfb. arXiv: 1905.00427 [astro-ph.HE].

[289] Xiaolin Liu, Zhoujian Cao, and Lijing Shao. "Validating the effective-one-body numerical-relativity waveform models for spin-aligned binary black holes along eccentric orbits." In: *Phys. Rev. D.* 101.4, 044049 (Feb. 2020), p. 044049. DOI: 10.1103/PhysRevD.101.044049. arXiv: 1910.00784 [gr-qc].

[290] M. Livio and N. Soker. "The common envelope phase in the evolution of binary stars." In: *Astrophys. J.* 329 (June 1988), pp. 764–779. DOI: 10.1086/166419.

[291] M. Lower et al. "Measuring eccentricity in binary black hole inspirals with gravitational waves." In: *Phys. Rev. D* 98 (Oct. 2018). DOI: 10.1103/PhysRevD.98.083028.

[292] Xiangcheng Ma, Eliot Quataert, Andrew Wetzel, Claude-André Faucher-Giguère, and Michael Boylan-Kolchin. "The contribution of globular clusters to cosmic reionization." In: *arXiv e-prints*, arXiv:2006.10065 (June 2020), arXiv:2006.10065. arXiv: 2006.10065 [astro-ph.GA].

[293] Morgan MacLeod and Enrico Ramirez-Ruiz. "On the Accretion-Fed Growth of Neutron Stars During Common Envelope." In: *Astrophys. J.* 798.1 (2015), p. L19. DOI: 10.1088/2041-8205/798/1/L19. arXiv: 1410.5421 [astro-ph.SR].

[294] D. Macleod, S. Coughlin, A. L. Urban, T. Massinger, et al. *gwpy/gwpy: 0.12.0*. Aug. 2018. DOI: 10.5281/zenodo.1346349.

[295] Piero Madau and Mark Dickinson. "Cosmic Star-Formation History." In: *Ann. Rev. Astron. Astrophys.* 52 (Aug. 2014), pp. 415–486. DOI: 10.1146/annurev-astro-081811-125615. arXiv: 1403.0007 [astro-ph.CO].

[296] Michele Maggiore et al. "Science case for the Einstein telescope." In: *J. Cosmo. Astropart. Phys.* 2020.3, 050 (Mar. 2020), p. 050. DOI: 10.1088/1475-7516/2020/03/050. arXiv: 1912.02622 [astro-ph.CO].

[297] S. R. Majewski, R. J. Patterson, D. I. Dinescu, W. Y. Johnson, J. C. Ostheimer, W. E. Kunkel, and C. Palma. "ω Centauri : Nucleus of a milky way dwarf spheroidal ?" In: *Liege International Astrophysical Colloquia*. Ed. by A. Noels, P. Magain, D. Caro, E. Jehin, G. Parmentier, and A. A. Thoul. Vol. 35. Liege International Astrophysical Colloquia. Jan. 2000, p. 619. arXiv: astro-ph/9910278 [astro-ph].

[298] Michela Mapelli and Nicola Giacobbo. "The cosmic merger rate of neutron stars and black holes." In: *Mon. Not. R. Ast. Soc.* 479.4 (Oct. 2018), pp. 4391–4398. DOI: 10.1093/mnras/sty1613. arXiv: 1806.04866 [astro-ph.HE].

[299] Michela Mapelli, Filippo Santoliquido, Yann Bouffanais, Manuel Arca Sedda, Nicola Giacobbo, M. Celeste Artale, and Alessandro Ballone. "Hierarchical mergers in young, globular and nuclear star clusters: black hole masses and merger rates." In: *arXiv e-prints*, arXiv:2007.15022 (July 2020), arXiv:2007.15022. arXiv: 2007.15022 [astro-ph.HE].

[300] Pablo Marchant, Norbert Langer, Philipp Podsiadlowski, Thomas M. Tauris, and Takashi J. Moriya. "A new route towards merging massive black holes." In: *Astron. Astrophys.* 588, A50 (Apr. 2016), A50. DOI: 10.1051/0004-6361/201628133. arXiv: 1601.03718 [astro-ph.SR].

[301] Pablo Marchant and Takashi Moriya. "The impact of stellar rotation on the black hole mass-gap from pair-instability supernovae." In: *arXiv e-prints*, arXiv:2007.06220 (July 2020), arXiv:2007.06220. arXiv: 2007.06220 [astro-ph.HE].

[302] R. Margutti, K. D. Alexander, et al. "The Binary Neutron Star Event LIGO/Virgo GW170817 160 Days after Merger: Synchrotron Emission across the Electromagnetic Spectrum." In: *Astrophys. J. Lett.* 856.1, L18 (Mar. 2018), p. L18. DOI: 10.3847/2041-8213/aab2ad. arXiv: 1801.03531 [astro-ph.HE].

[303] Sylvain Marsat, John G. Baker, and Tito Dal Canton. "Exploring the Bayesian parameter estimation of binary black holes with LISA." In: *arXiv e-prints*, arXiv:2003.00357 (Feb. 2020), arXiv:2003.00357. arXiv: 2003.00357 [gr-qc].

[304] Karl Martel and Eric Poisson. "Gravitational waves from eccentric compact binaries: Reduction in signal-to-noise ratio due to nonoptimal signal processing." In: *Phys. Rev.* D60 (1999), p. 124008. DOI: 10.1103/PhysRevD.60.124008. arXiv: gr-qc/9907006 [gr-qc].

[305] Miguel A. S. Martinez et al. "Black Hole Mergers from Hierarchical Triples in Dense Star Clusters." In: *arXiv e-prints*, arXiv:2009.08468 (Sept. 2020), arXiv:2009.08468. arXiv: 2009.08468 [astro-ph.GA].

[306] B. McKernan, K. E. S. Ford, T. Callister, W. M. Farr, R. O'Shaughnessy, R. Smith, E. Thrane, and A. Vajpeyi. "LIGO–Virgo correlations between mass ratio and effective inspiral spin: testing the active galactic nuclei channel." In: *arXiv e-prints*, arXiv:2107.07551 (July 2021), arXiv:2107.07551. arXiv: 2107.07551 [astro-ph.HE].

[307] B. McKernan, K. E. S. Ford, B. Kocsis, and Z. Haiman. "Ripple effects and oscillations in the broad Fe Kα line as a probe of massive black hole mergers." In: *Mon. Not. Roy. Astron. Soc.* 432.2 (June 2013), pp. 1468–1482. DOI: 10.1093/mnras/stt567. arXiv: 1303.7206 [astro-ph.HE].

[308] B. McKernan, K. E. S. Ford, and R. O'Shaughnessy. "Black hole, neutron star, and white dwarf merger rates in AGN discs." In: *Mon. Not. R. Ast. Soc.* 498.3 (Nov. 2020), pp. 4088–4094. DOI: 10.1093/mnras/staa2681. arXiv: 2002.00046 [astro-ph.HE].

[309] B. McKernan, K. E. S. Ford, and R. O'Shaughnessy. "Black hole, neutron star, and white dwarf merger rates in AGN discs." In: *Mon. Not. Roy. Astron. Soc.* 498.3 (Nov. 2020), pp. 4088–4094. DOI: 10.1093/mnras/staa2681. arXiv: 2002.00046 [astro-ph.HE].

[310] Nicholas Metropolis, Arianna W Rosenbluth, Marshall N Rosenbluth, Augusta H Teller, and Edward Teller. "Equation of state calculations by fast computing machines." In: *The journal of chemical physics* 21.6 (1953), pp. 1087–1092.

[311] Erez Michaely, Dimitry Ginzburg, and Hagai B. Perets. "Neutron star natal kicks: Collisions, μTDEs, faint SNe, GRBs and GW sources with preceding electromagnetic counterparts." In: *arXiv e-prints*, arXiv:1610.00593 (Sept. 2016), arXiv:1610.00593. arXiv: 1610.00593 [astro-ph.HE].

[312] G. Miniutti et al. "Nine-hour X-ray quasi-periodic eruptions from a low-mass black hole galactic nucleus." In: *Nature* 573.7774 (Sept. 2019), pp. 381–384. DOI: 10.1038/s41586-019-1556-x. arXiv: 1909.04693 [astro-ph.HE].

[313] S. E. de Mink and I. Mandel. "The chemically homogeneous evolutionary channel for binary black hole mergers: rates and properties of gravitational-wave events detectable by advanced LIGO." In: *Mon. Not. Roy. Astron. Soc.* 460.4 (2016), pp. 3545–3553. DOI: 10.1093/mnras/stw1219. arXiv: 1603.02291.

[314] Mirriam-Webster. *Eccentric*. Merriam-Webster.com Dictionary. Accessed 31 Oct. 2021. URL: https://www.merriam-webster.com/dictionary/eccentric.

[315] K. P. Mooley, A. T. Deller, O. Gottlieb, E. Nakar, G. Hallinan, S. Bourke, D. A. Frail, A. Horesh, A. Corsi, and K. Hotokezaka. "Superluminal motion of a relativistic jet in the neutron-star merger GW170817." In: *Nature* 561.7723 (Sept. 2018), pp. 355–359. DOI: 10.1038/s41586-018-0486-3. arXiv: 1806.09693 [astro-ph.HE].

[316] Meagan Morscher, Bharath Pattabiraman, Carl Rodriguez, Frederic A. Rasio, and Stefan Umbreit. "The Dynamical Evolution of Stellar Black Holes in Globular Clusters." In: *Astrophys. J.* 800.1, 9 (Feb. 2015), p. 9. DOI: 10.1088/0004-637X/800/1/9. arXiv: 1409.0866 [astro-ph.GA].

[317] Elias R. Most, Lukas R. Weih, Luciano Rezzolla, and Jürgen Schaffner-Bielich. "New Constraints on Radii and Tidal Deformabilities of Neutron Stars from GW170817." In: *Phys. Rev. Lett.* 120.26, 261103 (June 2018), p. 261103. DOI: 10.1103/PhysRevLett.120.261103. arXiv: 1803.00549 [gr-qc].

[318] Bernhard Müller, Alexander Heger, David Liptai, and Joshua B. Cameron. "A simple approach to the supernova progenitor-explosion connection." In: *Mon. Not. R. Ast. Soc.* 460.1 (July 2016), pp. 742–764. DOI: 10.1093/mnras/stw1083. arXiv: 1602.05956 [astro-ph.SR].

[319] NASA. *NASA Announces New James Webb Space Telescope Target Launch Date*. NASA press release. 2020. URL: www.nasa.gov/press-release/nasa-announces-new-james-webb-space-telescope-target-launch-date.

[320] Alessandro Nagar, Sebastiano Bernuzzi, et al. "Time-domain effective-one-body gravitational waveforms for coalescing compact binaries with nonprecessing spins, tides, and self-spin effects." In: *Phys. Rev. D* 98.10, 104052 (Nov. 2018), p. 104052. DOI: 10.1103/PhysRevD.98.104052. arXiv: 1806.01772 [gr-qc].

[321] Coenraad J. Neijssel, Alejandro Vigna-Gómez, Simon Stevenson, Jim W. Barrett, Sebastian M. Gaebel, Floor S. Broekgaarden, Selma E. de Mink, Dorottya Szécsi, Serena Vinciguerra, and Ilya Mandel. "The effect of the metallicity-specific star formation history on double compact object mergers." In: *Mon. Not. Roy. Astron. Soc.* 490.3 (Dec.

2019), pp. 3740–3759. DOI: 10.1093/mnras/stz2840. arXiv: 1906.08136 [astro-ph.SR].

[322] Ken K. Y. Ng, Shiqi Chen, Boris Goncharov, Ulyana Dupletsa, Ssohrab Borhanian, Marica Branchesi, Jan Harms, Michele Maggiore, B. S. Sathyaprakash, and Salvatore Vitale. "On the single-event-based identification of primordial black hole mergers at cosmological distances." In: *arXiv e-prints*, arXiv:2108.07276 (Aug. 2021), arXiv:2108.07276. arXiv: 2108.07276 [astro-ph.CO].

[323] Atsushi Nishizawa, Alberto Sesana, Emanuele Berti, and Antoine Klein. "Constraining stellar binary black hole formation scenarios with eLISA eccentricity measurements." In: *Mon. Not. R. Ast. Soc.* 465.4 (Mar. 2017), pp. 4375–4380. DOI: 10.1093/mnras/stw2993. arXiv: 1606.09295 [astro-ph.HE].

[324] Alexander H. Nitz and Collin D. Capano. "GW190521 May Be an Intermediate-mass Ratio Inspiral." In: *Astrophys. J. Lett.* 907 (2020), p. L9.

[325] Alexander H. Nitz, Amber Lenon, and Duncan A. Brown. "Search for Eccentric Binary Neutron Star Mergers in the First and Second Observing Runs of Advanced LIGO." In: *Astrophys. J.* 890.1, 1 (Feb. 2020), p. 1. DOI: 10.3847/1538-4357/ab6611. arXiv: 1912.05464 [astro-ph.HE].

[326] Ryan M. O'Leary, Bence Kocsis, and Abraham Loeb. "Gravitational waves from scattering of stellar-mass black holes in galactic nuclei." In: *Mon. Not. Roy. Astron. Soc.* 395.4 (June 2009), pp. 2127–2146. DOI: 10.1111/j.1365-2966.2009.14653.x. arXiv: 0807.2638 [astro-ph].

[327] Ryan M. O'Leary, Frederic A. Rasio, John M. Fregeau, Natalia Ivanova, and Richard W. O'Shaughnessy. "Binary mergers and growth of black holes in dense star clusters." In: *Astrophys. J.* 637 (2006), pp. 937–951. DOI: 10.1086/498446. arXiv: astro-ph/0508224 [astro-ph].

[328] Richard O'Shaughnessy, Davide Gerosa, and Daniel Wysocki. "Inferences about Supernova Physics from Gravitational-Wave Measurements: GW151226 Spin Misalignment as an Indicator of Strong Black-Hole Natal Kicks." In: *Phys. Rev. L.* 119.1, 011101 (July 2017), p. 011101. DOI: 10.1103/PhysRevLett.119.011101. arXiv: 1704.03879 [astro-ph.HE].

[329] Eamonn O'Shea and Prayush Kumar. "Correlations in parameter estimation of low-mass eccentric binaries: GW151226 & GW170608." In: *arXiv e-prints*, arXiv:2107.07981 (July 2021), arXiv:2107.07981. arXiv: 2107.07981 [astro-ph.HE].

[330] Seth Olsen, Javier Roulet, Horng Sheng Chia, Liang Dai, Tejaswi Venumadhav, Barak Zackay, and Matias Zaldarriaga. "Mapping the Likelihood of GW190521 with Diverse Mass and Spin Priors." In: *arXiv e-prints*, arXiv:2106.13821 (June 2021), arXiv:2106.13821. arXiv: 2106.13821 [astro-ph.HE].

[331] Serguei Ossokine, Alessandra Buonanno, Sylvain Marsat, et al. "Multipolar Effective-One-Body Waveforms for Precessing Binary Black Holes: Construction and Validation." In: *arXiv e-prints*, arXiv:2004.09442 (Apr. 2020), arXiv:2004.09442. arXiv: 2004.09442 [gr-qc].

[332] Feryal Özel and Paulo Freire. "Masses, Radii, and the Equation of State of Neutron Stars." In: *Ann. Rev. Astron. Ast.* 54 (Sept. 2016), pp. 401–440. DOI: 10.1146/annurev-astro-081915-023322. arXiv: 1603.02698 [astro-ph.HE].

[333] Feryal Özel, Dimitrios Psaltis, Ramesh Narayan, and Jeffrey E. McClintock. "The Black Hole Mass Distribution in the Galaxy." In: *Astrophys. J.* 725.2 (Dec. 2010), pp. 1918–1927. DOI: 10.1088/0004-637X/725/2/1918. arXiv: 1006.2834 [astro-ph.GA].

[334] A. Palmese et al. "Evidence for Dynamically Driven Formation of the GW170817 Neutron Star Binary in NGC 4993." In: *Astrophys. J.* 849.2 (2017), p. L34. DOI: 10.3847/2041-8213/aa9660. arXiv: 1710.06748 [astro-ph.HE].

[335] Zhen Pan and Huan Yang. "Formation rate of extreme mass ratio inspirals in active galactic nuclei." In: *Phys. Rev. D.* 103.10, 103018 (May 2021), p. 103018. DOI: 10.1103/PhysRevD.103.103018. arXiv: 2101.09146 [astro-ph.HE].

[336] C. Pankow, P. Brady, E. Ochsner, and R. O'Shaughnessy. "Novel scheme for rapid parallel parameter estimation of gravitational waves from compact binary coalescences." In: *Phys. Rev. D* 92.2, 023002 (July 2015), p. 023002. DOI: 10.1103/PhysRevD.92.023002. arXiv: 1502.04370 [gr-qc].

[337] Chris Pankow et al. "Mitigation of the instrumental noise transient in gravitational-wave data surrounding GW170817." In: *Phys. Rev. D* 98.8, 084016 (Oct. 2018), p. 084016. DOI: 10.1103/PhysRevD.98.084016. arXiv: 1808.03619 [gr-qc].

[338] L. Jens Papenfort, Roman Gold, and Luciano Rezzolla. "Dynamical ejecta and nucleosynthetic yields from eccentric binary neutron-star mergers." In: *Phys. Rev. D* 98.10, 104028 (Nov. 2018), p. 104028. DOI: 10.1103/PhysRevD.98.104028. arXiv: 1807.03795 [gr-qc].

[339] Bharath Pattabiraman, Stefan Umbreit, Wei-keng Liao, Alok Choudhary, Vassiliki Kalogera, Gokhan Memik, and Frederic A. Rasio. "A PARALLEL MONTE CARLO CODE FOR SIMULATING COLLISIONAL N -BODY SYSTEMS." en. In: *The Astrophysical Journal Supplement Series* 204.2 (Feb. 2013), p. 15. ISSN: 0067-0049. DOI: 10.1088/0067-0049/204/2/15. URL: http://labs.adsabs.harvard.edu/ui/abs/2013ApJS..204...15P.

[340] Ethan Payne, Colm Talbot, Paul D. Lasky, Eric Thrane, and Jeffrey S. Kissel. "Gravitational-wave astronomy with a physical calibration model." In: *Phys. Rev. D.* 102.12, 122004 (Dec. 2020), p. 122004. DOI: 10.1103/PhysRevD.102.122004. arXiv: 2009.10193 [astro-ph.IM].

[341] Ethan Payne, Colm Talbot, and Eric Thrane. "Higher order gravitational-wave modes with likelihood reweighting." In: *Phys. Rev. D* 100.12 (2019), p. 123017. DOI: 10.1103/PhysRevD.100.123017. arXiv: 1905.05477 [astro-ph.IM].

[342] Mark B. Peacock, Thomas J. Maccarone, Christian Knigge, Arunav Kundu, Christopher Z. Waters, Stephen E. Zepf, and David R. Zurek. "The M31 globular cluster system: ugriz and K-band photometry and structural parameters." In: *Mon. Not. Roy. Astron. Soc.* 402 (2010), p. 803. DOI: 10.1111/j.1365-2966.2009.15952.x. arXiv: 0910.5475 [astro-ph.CO].

[343] P. C. Peters. "Gravitational Radiation and the Motion of Two Point Masses." In: *Phys. Rev.* 136 (4B Nov. 1964), B1224–B1232. DOI: 10.1103/PhysRev.136.B1224.

[344] E. S. Phinney and S. Sigurdsson. "Ejection of pulsars and binaries to the outskirts of globular clusters." In: *Nature* 349 (Jan. 1991), pp. 220–223. DOI: 10.1038/349220a0.

[345] Planck Collaboration, P. A. R. Ade, N. Aghanim, M. Arnaud, M. Ashdown, J. Aumont, C. Baccigalupi, et al. "Planck 2015 results. XIII. Cosmological parameters." In: *Astron. Astrophys.* 594, A13 (Sept. 2016), A13. DOI: 10.1051/0004-6361/201525830. arXiv: 1502.01589 [astro-ph.CO].

[346] Eric Poisson and Clifford M. Will. "Gravitational waves from inspiraling compact binaries: Parameter estimation using second-post-Newtonian waveforms." In: *Phys. Rev. D* 52.2 (July 1995), pp. 848–855. DOI: 10.1103/PhysRevD.52.848. arXiv: gr-qc/9502040 [gr-qc].

[347] S. F. Portegies Zwart and F. Verbunt. "Population synthesis of high-mass binaries." In: *Astron. Astrophys.* 309 (May 1996), pp. 179–196.

[348] S. F. Portegies Zwart and L. R. Yungelson. "Formation and evolution of binary neutron stars." In: *Astron. Astrophys.* 332 (Apr. 1998), pp. 173–188. arXiv: astro-ph/9710347 [astro-ph].

[349] Simon F. Portegies Zwart and Stephen McMillan. "Black hole mergers in the universe." In: *Astrophys. J.* 528 (2000), p. L17. DOI: 10.1086/312422. arXiv: astro-ph/9910061 [astro-ph].

[350] Konstantin A. Postnov and Lev R. Yungelson. "The Evolution of Compact Binary Star Systems." In: *Living Rev. Rel.* 17 (2014), p. 3. DOI: 10.12942/lrr-2014-3. arXiv: 1403.4754 [astro-ph.HE].

[351] J. Powell. "Parameter estimation and model selection of gravitational wave signals contaminated by transient detector noise glitches." In: *Class. Quant. Grav.* 35.15, 155017 (2018), p. 155017. DOI: 10.1088/1361-6382/aacf18.

[352] Jade Powell and Bernhard Müller. "Gravitational wave emission from 3D explosion models of core-collapse supernovae with low and normal explosion energies." In: *Mon. Not. Roy. Astron. Soc.* 487.1 (July 2019), pp. 1178–1190. DOI: 10.1093/mnras/stz1304. arXiv: 1812.05738 [astro-ph.HE].

[353] A. M. Price-Whelan et al. "The Astropy Project: Building an Open-science Project and Status of the v2.0 Core Package." In: *Astron. J.* 156, 123 (Sept. 2018), p. 123. DOI: 10.3847/1538-3881/aabc4f.

[354] M. Punturo et al. "The Einstein Telescope: a third-generation gravitational wave observatory." In: *Class. Quant. Grav.* 27.19, 194002 (Oct. 2010), p. 194002. DOI: 10.1088/0264-9381/27/19/194002.

[355] Enrico Ramirez-Ruiz, Michele Trenti, Morgan MacLeod, Luke F. Roberts, William H. Lee, et al. "Compact Stellar Binary Assembly in the First Nuclear Star Clusters and r-process Synthesis in the Early Universe." In: *Astrophys. J. Lett.* 802.2, L22 (Apr. 2015), p. L22. DOI: 10.1088/2041-8205/802/2/L22. arXiv: 1410.3467 [astro-ph.GA].

[356] Antoni Ramos-Buades, Sascha Husa, Geraint Pratten, Héctor Estellés, Cecilio García-Quirós, Maite Mateu-Lucena, Marta Colleoni, and Rafel Jaume. "First survey of spinning eccentric black hole mergers: Numerical relativity simulations, hybrid waveforms, and parameter estimation." In: *Phys. Rev. D* 101.8, 083015 (Apr. 2020), p. 083015. DOI: 10.1103/PhysRevD.101.083015. arXiv: 1909.11011 [gr-qc].

[357] L. Randall and Z-Z. Xianyu. "Induced Ellipticity for Inspiraling Binary Systems." In: *Astrophys. J.* 853 (2018). DOI: 10.3847/1538-4357/aaa1a2.

[358] Lisa Randall and Zhong-Zhi Xianyu. "An Analytical Portrait of Binary Mergers in Hierarchical Triple Systems." In: *Astrophys. J.* 864.2 (2018), p. 134. DOI: 10.3847/1538-4357/aad7fe. arXiv: 1802.05718.

[359] Lisa Randall and Zhong-Zhi Xianyu. "Eccentricity Without Measuring Eccentricity: Discriminating Among Stellar Mass Black Hole Binary Formation Channels." In: *arXiv e-prints*, arXiv:1907.02283 (July 2019), arXiv:1907.02283. arXiv: 1907.02283 [astro-ph.HE].

[360] Sara Rastello, Michela Mapelli, Ugo N. Di Carlo, Nicola Giacobbo, Filippo Santoliquido, Mario Spera, Alessandro Ballone, and Giuliano Iorio. "Dynamics of black hole - neutron star binaries in young star clusters." In: *Mon. Not. R. Ast. Soc.* (July 2020). DOI: 10.1093/mnras/staa2018. arXiv: 2003.02277 [astro-ph.HE].

[361] David Reitze et al. "Cosmic Explorer: The U.S. Contribution to Gravitational-Wave Astronomy beyond LIGO." In: *Bulletin of the American Astronomical Society*. Vol. 51. Sept. 2019, p. 35. arXiv: 1907.04833 [astro-ph.IM].

[362] T. P. Robitaille et al. "Astropy: A community Python package for astronomy." In: *Astron. Astrophys.* 558, A33 (Oct. 2013), A33. DOI: 10.1051/0004-6361/201322068. arXiv: 1307.6212 [astro-ph.IM].

[363] Carl L. Rodriguez, Pau Amaro-Seoane, Sourav Chatterjee, Kyle Kremer, Frederic A. Rasio, Johan Samsing, Claire S. Ye, and Michael Zevin. "Post-Newtonian Dynamics in Dense Star Clusters: Formation, Masses, and Merger Rates of Highly-Eccentric Black Hole Binaries." In: *Phys. Rev.* D98.12 (2018), p. 123005. DOI: 10.1103/PhysRevD.98.123005. arXiv: 1811.04926 [astro-ph.HE].

[364] Carl L. Rodriguez, Pau Amaro-Seoane, Sourav Chatterjee, and Frederic A. Rasio. "Post-Newtonian Dynamics in Dense Star Clusters: Highly-Eccentric, Highly-Spinning, and Repeated Binary Black Hole Mergers." In: *Phys. Rev. Lett.* 120.15 (2018), p. 151101. DOI: 10.1103/PhysRevLett.120.151101. arXiv: 1712.04937.

[365] Carl L. Rodriguez and Fabio Antonini. "A Triple Origin for the Heavy and Low-Spin Binary Black Holes Detected by LIGO/Virgo." In: *Astrophys. J.* 863.1 (2018), p. 7. DOI: 10.3847/1538-4357/aacea4. arXiv: 1805.08212 [astro-ph.HE].

[366] Carl L. Rodriguez, Sourav Chatterjee, and Frederic A. Rasio. "Binary black hole mergers from globular clusters: Masses, merger rates, and the impact of stellar evolution." In: *Physical Review D* 93.8 (Apr. 2016), p. 084029. ISSN: 2470-0010. DOI: 10.1103/PhysRevD.93.084029. URL: http://arxiv.org/abs/1602.02444http:

//dx.doi.org/10.1103/PhysRevD.93.084029http://link.aps.org/doi/10.1103/PhysRevD.93.084029.

[367] Carl L. Rodriguez and Abraham Loeb. "Redshift Evolution of the Black Hole Merger Rate from Globular Clusters." In: *Astrophys. J. Lett.* 866.1, L5 (Oct. 2018), p. L5. DOI: 10.3847/2041-8213/aae377. arXiv: 1809.01152 [astro-ph.HE].

[368] Carl L Rodriguez, Meagan Morscher, Bharath Pattabiraman, Sourav Chatterjee, Carl-Johan Haster, and Frederic A Rasio. "Binary Black Hole Mergers from Globular Clusters: Implications for Advanced LIGO." In: *Physical review letters* 115.5 (July 2015), p. 051101. ISSN: 0031-9007. DOI: 10.1103/physrevlett.115.051101. URL: https://doi.org/10.1103/PhysRevLett.115.051101.

[369] Carl L. Rodriguez, Michael Zevin, Pau Amaro-Seoane, Sourav Chatterjee, Kyle Kremer, Frederic A. Rasio, and Claire S. Ye. "Black holes: The next generation—repeated mergers in dense star clusters and their gravitational-wave properties." In: *Phys. Rev. D* 100.4, 043027 (Aug. 2019), p. 043027. DOI: 10.1103/PhysRevD.100.043027. arXiv: 1906.10260 [astro-ph.HE].

[370] Carl L. Rodriguez, Michael Zevin, Chris Pankow, Vasilliki Kalogera, and Frederic A. Rasio. "Illuminating Black Hole Binary Formation Channels with Spins in Advanced LIGO." In: *Astrophys. J.* 832.1 (2016), p. L2. DOI: 10.3847/2041-8205/832/1/L2. arXiv: 1609.05916 [astro-ph.HE].

[371] Joseph D. Romano and Neil. J. Cornish. "Detection methods for stochastic gravitational-wave backgrounds: a unified treatment." In: *Living Reviews in Relativity* 20.1 (Apr. 2017), p. 2. ISSN: 1433-8351. DOI: 10.1007/s41114-017-0004-1. URL: https://doi.org/10.1007/s41114-017-0004-1.

[372] I. Romero-Shaw et al. https://doi.org/10.5281/zenodo.4017046. https://doi.org/10.5281/zenodo.4017046. 2020. DOI: 10.5281/zenodo.4017046.

[373] I. Romero-Shaw et al. https://dcc.ligo.org/LIGO-P2000193/public. https://dcc.ligo.org/LIGO-P2000193/public. 2020.

[374] Isobel M. Romero-Shaw, Nicholas Farrow, Simon Stevenson, Eric Thrane, and Xing-Jiang Zhu. "On the origin of GW190425." In: *Mon. Not. Roy. Astron. Soc.* 496.1 (2020), pp. L64–L69. DOI: 10.1093/mnrasl/slaa084. arXiv: 2001.06492 [astro-ph.HE].

[375] Isobel M. Romero-Shaw, Kyle Kremer, Paul D. Lasky, Eric Thrane, and Johan Samsing. "Gravitational waves as a probe of globular cluster formation and evolution." In: *Mon. Not. Roy. Astron. Soc.* 506.2 (Sept. 2021), pp. 2362–2372. DOI: 10.1093/mnras/stab1815. arXiv: 2011.14541 [astro-ph.HE].

[376] Isobel M. Romero-Shaw, Paul D. Lasky, and Eric Thrane. "Searching for Eccentricity: Signatures of Dynamical Formation in the First Gravitational-Wave Transient Catalogue of LIGO and Virgo." In: *Mon. Not. Roy. Astron. Soc.* 490.4 (2019), pp. 5210–5216. DOI: 10.1093/mnras/stz2996. arXiv: 1909.05466 [astro-ph.HE].

[377] Isobel M. Romero-Shaw, Paul D. Lasky, Eric Thrane, and Juan Calderon Bustillo. "GW190521: orbital eccentricity and signatures of dynamical formation in a binary black hole merger signal." In: *Astrophys. J. Lett.* 903.1 (2020), p. L5. DOI: 10.3847/2041-8213/abbe26. arXiv: 2009.04771 [astro-ph.HE].

[378] Isobel M. Romero-Shaw et al. "Bayesian inference for compact binary coalescences with bilby: validation and application to the first LIGO–Virgo gravitational-wave transient catalogue." In: *Mon. Not. Roy. Astron. Soc.* 499.3 (2020), pp. 3295–3319. DOI: 10.1093/mnras/staa2850. arXiv: 2006.00714 [astro-ph.IM].

[379] Isobel Romero-Shaw, Paul D. Lasky, and Eric Thrane. "Signs of Eccentricity in Two Gravitational-wave Signals May Indicate a Subpopulation of Dynamically Assembled Binary Black Holes." In: 921.2 (2021), p. L31. DOI: 10.3847/2041-8213/ac3138. URL: https://doi.org/10.3847/2041-8213/ac3138.

[380] Javier Roulet, Horng Sheng Chia, Seth Olsen, Liang Dai, Tejaswi Venumadhav, Barak Zackay, and Matias Zaldarriaga. "Distribution of effective spins and masses of binary black holes from the LIGO and Virgo O1-O3a observing runs." In: *Phys. Rev. D.* 104.8, 083010 (Oct. 2021), p. 083010. DOI: 10.1103/PhysRevD.104.083010. arXiv: 2105.10580 [astro-ph.HE].

[381] Javier Roulet, Horng Sheng Chia, Seth Olsen, Liang Dai, Tejaswi Venumadhav, Barak Zackay, and Matias Zaldarriaga. "Distribution of effective spins and masses of binary black holes from the LIGO and Virgo O1-O3a observing runs." In: *Physical Review D* 104.8, 083010 (Oct. 2021), p. 083010. DOI: 10.1103/PhysRevD.104.083010. arXiv: 2105.10580 [astro-ph.HE].

[382] Zacharias Roupas and Demosthenes Kazanas. "Generation of massive stellar black holes by rapid gas accretion in primordial dense clusters." In: *Astron. Astrophys.* 632, L8 (Dec. 2019), p. L8. DOI: 10.1051/0004-6361/201937002. arXiv: 1911.03915 [astro-ph.GA].

[383] Christian Röver, Renate Meyer, and Nelson Christensen. "Bayesian inference on compact binary inspiral gravitational radiation signals in interferometric data." In: *Class. Quant. Grav.* 23.15 (Aug. 2006), pp. 4895–4906. DOI: 10.1088/0264-9381/23/15/009. arXiv: gr-qc/0602067 [gr-qc].

[384] Christian Röver, Renate Meyer, and Nelson Christensen. "Coherent Bayesian inference on compact binary inspirals using a network of interferometric gravitational wave detectors." In: *Phys. Rev. D* 75.6, 062004 (Mar. 2007), p. 062004. DOI: 10.1103/PhysRevD.75.062004. arXiv: gr-qc/0609131 [gr-qc].

[385] SEDS Messier Database. *Milky Way Globular Clusters*. https://www.messier.seds.org/xtra/supp/mw_gc.html. 2020.

[386] Mohammadtaher Safarzadeh, Edo Berger, Ken K. Y. Ng, Hsin-Yu Chen, Salvatore Vitale, Chris Whittle, and Evan Scannapieco. "Measuring the Delay Time Distribution of Binary Neutron Stars. II. Using the Redshift Distribution from Third-generation Gravitational-wave Detectors Network." In: *Astrophys. J. Lett.* 878.1, L13 (June 2019), p. L13. DOI: 10.3847/2041-8213/ab22be. arXiv: 1904.10976 [astro-ph.HE].

[387] Mohammadtaher Safarzadeh, Enrico Ramirez-Ruiz, and Edo Berger. "GW190425 is inconsistent with being a binary neutron star born from a fast merging channel." In: *arXiv e-prints*, arXiv:2001.04502 (Jan. 2020), arXiv:2001.04502. arXiv: 2001.04502 [astro-ph.HE].

[388] Jeremy Sakstein, Djuna Croon, Samuel D. McDermott, Maria C. Straight, and Eric J. Baxter. "Beyond the Standard Model Explanations of GW190521." In: *Phys. Rev. Lett.* 125.26, 261105 (Dec. 2020), p. 261105. DOI: 10.1103/PhysRevLett.125.261105. arXiv: 2009.01213 [gr-qc].

[389] J. Samsing. "Eccentric Black Hole Mergers Forming in Globular Clusters." In: *Phys. Rev. D* D97.10 (2018), p. 103014. DOI: 10.1103/PhysRevD.97.103014. arXiv: 1711.07452.

[390] J. Samsing, I. Bartos, D. J. D'Orazio, Z. Haiman, B. Kocsis, N. W. C. Leigh, B. Liu, M. E. Pessah, and H. Tagawa. "Active Galactic Nuclei as Factories for Eccentric Black Hole Mergers." In: *arXiv e-prints*, arXiv:2010.09765 (Oct. 2020), arXiv:2010.09765. arXiv: 2010.09765 [astro-ph.HE].

[391] J. Samsing and D. J. D'Orazio. "Black Hole Mergers From Globular Clusters Observable by LISA I: Eccentric Sources Originating From Relativistic N-body Dynamics." In: *Mon. Not. Roy. Astron. Soc.* 481 (2018). DOI: 10.1093/mnras/sty2334.

[392] Johan Samsing, Abbas Askar, and Mirek Giersz. "MOCCA-SURVEY Database. I. Eccentric Black Hole Mergers during Binary-Single Interactions in Globular Clusters." In: *Astrophys. J.* 855.2, 124 (Mar. 2018), p. 124. DOI: 10.3847/1538-4357/aaab52. arXiv: 1712.06186 [astro-ph.HE].

[393] Johan Samsing, Daniel J. D'Orazio, Abbas Askar, and Mirek Giersz. "Black Hole Mergers from Globular Clusters Observable by LISA and LIGO: Results from post-Newtonian Binary-Single Scatterings." In: *arXiv e-prints*, arXiv:1802.08654 (2018), arXiv:1802.08654. arXiv: 1802.08654 [astro-ph.HE].

[394] Johan Samsing and Kenta Hotokezaka. "Populating the Black Hole Mass Gaps In Stellar Clusters: General Relations and Upper Limits." In: *arXiv e-prints*, arXiv:2006.09744 (June 2020), arXiv:2006.09744. arXiv: 2006.09744 [astro-ph.HE].

[395] Johan Samsing, Morgan MacLeod, and Enrico Ramirez-Ruiz. "The Formation of Eccentric Compact Binary Inspirals and the Role of Gravitational Wave Emission in Binary-Single Stellar Encounters." In: *Astrophys. J.* 784 (2014), p. 71. DOI: 10.1088/0004-637X/784/1/71. arXiv: 1308.2964.

[396] Johan Samsing, Morgan MacLeod, and Enrico Ramirez-Ruiz. "The Formation of Eccentric Compact Binary Inspirals and the Role of Gravitational Wave Emission in Binary-Single Stellar Encounters." In: *Astrophys. J.* 784.1, 71 (Mar. 2014), p. 71. DOI: 10.1088/0004-637X/784/1/71. arXiv: 1308.2964 [astro-ph.HE].

[397] Johan Samsing and Enrico Ramirez-Ruiz. "On the Assembly Rate of Highly Eccentric Binary Black Hole Mergers." In: *Astrophys. J.* 840.2 (2017), p. L14. DOI: 10.3847/2041-8213/aa6f0b. arXiv: 1703.09703 [astro-ph.HE].

[398] L. Santamaría et al. "Matching post-Newtonian and numerical relativity waveforms: Systematic errors and a new phenomenological model for nonprecessing black hole binaries." In: *Phys. REv. D* 82.6, 064016 (Sept. 2010), p. 064016. DOI: 10.1103/PhysRevD.82.064016. arXiv: 1005.3306 [gr-qc].

[399] Ata Sarajedini et al. "The ACS Survey of Galactic Globular Clusters. I. Overview and Clusters without Previous Hubble Space Telescope Photometry." In: *aj* 133.4 (Apr. 2007), pp. 1658–1672. DOI: 10.1086/511979. arXiv: astro-ph/0612598 [astro-ph].

[400] Nikhil Sarin, Paul D. Lasky, and Gregory Ashton. "Gravitational waves or deconfined quarks: What causes the premature collapse of neutron stars born in short gamma-ray bursts?" In: *Phys. Rev. D* 101.6, 063021 (Mar. 2020), p. 063021. DOI: 10.1103/PhysRevD.101.063021. arXiv: 2001.06102 [astro-ph.HE].

[401] Misao Sasaki, Teruaki Suyama, Takahiro Tanaka, and Shuichiro Yokoyama. "Primordial Black Hole Scenario for the Gravitational-Wave Event GW150914." In: *Phys. Rev. L.* 117.6, 061101 (Aug. 2016), p. 061101. DOI: 10.1103/PhysRevLett.117.061101. arXiv: 1603.08338 [astro-ph.CO].

[402] P. Schmidt et al. "Towards models of gravitational waveforms from generic binaries: A simple approximate mapping between precessing and nonprecessing inspiral signals." In: *Phys. Rev. D* 86.10, 104063 (2012), p. 104063.

[403] Patricia Schmidt, Frank Ohme, and Mark Hannam. "Towards models of gravitational waveforms from generic binaries: II. Modelling precession effects with a single effective precession parameter." In: *Phys. Rev. D* 91 (2 Jan. 2015), p. 024043. DOI: 10.1103/PhysRevD.91.024043. URL: https://link.aps.org/doi/10.1103/PhysRevD.91.024043.

[404] Yoshinta Setyawati and Frank Ohme. "Adding eccentricity to quasicircular binary-black-hole waveform models." In: *Phys. Rev. D* 103.12, 124011 (June 2021), p. 124011. DOI: 10.1103/PhysRevD.103.124011. arXiv: 2101.11033 [gr-qc].

[405] Kristen L. Shapiro, Reinhard Genzel, and Natascha M. Förster Schreiber. "Star-forming galaxies at z 2 and the formation of the metal-rich globular cluster population." In: *Monthly Notices of the Royal Astronomical Society: Letters* 403.1 (Mar. 2010), pp. L36–L40. ISSN: 1745-3925. DOI: 10.1111/j.1745-3933.2010.00810.x. eprint: https://academic.oup.com/mnrasl/article-pdf/403/1/L36/4010728/403-1-L36.pdf. URL: https://doi.org/10.1111/j.1745-3933.2010.00810.x.

[406] T. Sidery, B. Aylott, N. Christensen, B. Farr, et al. "Reconstructing the sky location of gravitational-wave detected compact binary systems: Methodology for testing and comparison." In: *Phys. Rev. D* 89.8, 084060 (Apr. 2014), p. 084060. DOI: 10.1103/PhysRevD.89.084060. arXiv: 1312.6013 [astro-ph.IM].

[407] Steinn Sigurdsson and Lars Hernquist. "Primordial black holes in globular clusters." In: *Nature* 364 (1993), pp. 423–425. DOI: 10.1038/364423a0.

[408] Steinn Sigurdsson and E. S. Phinney. "Dynamics and Interactions of Binaries and Neutron Stars in Globular Clusters." In: *Astrophys. J. Supp.* 99 (Aug. 1995), p. 609. DOI: 10.1086/192199. arXiv: astro-ph/9412078 [astro-ph].

[409] Kedron Silsbee and Scott Tremaine. "Lidov-Kozai Cycles with Gravitational Radiation: Merging Black Holes in Isolated Triple Systems." In: *Astrophys. J.* 836.1 (2017), p. 39. DOI: 10.3847/1538-4357/aa5729. arXiv: 1608.07642 [astro-ph.HE].

[410] L. P. Singer and L. R. Price. "Rapid Bayesian position reconstruction for gravitational-wave transients." In: *Phys. Rev. D* 93.2, 024013 (Jan. 2016), p. 024013. DOI: 10.1103/PhysRevD.93.024013.

[411] L. P. Singer et al. "Going the Distance: Mapping Host Galaxies of LIGO and Virgo Sources in Three Dimensions Using Local Cosmography and Targeted Follow-up." In: *Astrophys. J.* 829, L15 (2016), p. L15. DOI: 10.3847/2041-8205/829/1/L15.

[412] L. P. Singer et al. *GWCelery*. https://git.ligo.org/emfollow/gwcelery. 2020.

[413] Leo P. Singer et al. "The First Two Years of Electromagnetic Follow-Up with Advanced LIGO and Virgo." In: *Astrophys. J.* 795.2 (2014), p. 105. DOI: 10.1088/0004-637X/795/2/105. arXiv: 1404.5623 [astro-ph.HE].

[414] John Skilling. "Skilling, J.: Nested sampling for general Bayesian computation. Bayesian Anal. 1(4), 833-860." In: *Bayesian Analysis* 1 (Dec. 2006), pp. 833–860. DOI: 10.1214/06-BA127.

[415] L. L. Smarr and R. Blandford. "The binary pulsar - Physical processes, possible companions, and evolutionary histories." In: *Astrophys. J.* 207 (July 1976), pp. 574–588. DOI: 10.1086/154524.

[416] N. Smirnov. "Table for Estimating the Goodness of Fit of Empirical Distributions." In: *Ann. Math. Statist.* 19.2 (1948), pp. 279–281. DOI: 10.1214/aoms/1177730256. URL: https://doi.org/10.1214/aoms/1177730256.

[417] Rory Smith, Gregory Ashton, Avi Vajpeyi, and Colm Talbot. "Massively parallel Bayesian inference for transient gravitational-wave astronomy." In: *Mon. Not. Roy. Astron. Soc.* 498.3 (Nov. 2020), pp. 4492–4502. DOI: 10.1093/mnras/staa2483. arXiv: 1909.11873 [gr-qc].

[418] Rory Smith, Scott E Field, Kent Blackburn, Carl-Johan Haster, Michael Pürrer, Vivien Raymond, and Patricia Schmidt. "Fast and accurate inference on gravitational waves from precessing compact binaries." In: *Phys. Rev. D* 94 (Aug. 2016). DOI: 10.1103/PhysRevD.94.044031. URL: https://link.aps.org/doi/10.1103/PhysRevD.94.044031.

[419] Alan D. Sokal. "Monte Carlo Methods for the Self-Avoiding Walk." In: *arXiv e-prints*, hep-lat/9405016 (May 1994), hep–lat/9405016. arXiv: hep-lat/9405016 [hep-lat].

[420] Joshua S. Speagle. "DYNESTY: a dynamic nested sampling package for estimating Bayesian posteriors and evidences." In: *Mon. Not. Roy. Astron. Soc.* 493.3 (Apr. 2020), pp. 3132–3158. DOI: 10.1093/mnras/staa278. arXiv: 1904.02180 [astro-ph.IM].

[421] Mario Spera, Michela Mapelli, Nicola Giacobbo, Alessandro A. Trani, Alessandro Bressan, and Guglielmo Costa. "Merging black hole binaries with the SEVN code." In: *Mon. Not. R. Ast. Soc.* 485.1 (May 2019), pp. 889–907. DOI: 10.1093/mnras/stz359. arXiv: 1809.04605 [astro-ph.HE].

[422] G. Srinivasan. "Pulsars - Their origin and evolution." In: *Astronomy and Astrophyics Review* 1 (Nov. 1989), pp. 209–260. DOI: 10.1007/BF00873079.

[423] Simon Stevenson, Christopher P. L. Berry, and Ilya Mandel. "Hierarchical analysis of gravitational-wave measurements of binary black hole spin–orbit misalignments." In: *Mon. Not. Roy. Astron. Soc.* 471.3 (2017), pp. 2801–2811. DOI: 10.1093/mnras/stx1764. arXiv: 1703.06873 [astro-ph.HE].

[424] Simon Stevenson, Frank Ohme, and Stephen Fairhurst. "Distinguishing Compact Binary Population Synthesis Models Using Gravitational Wave Observations of Coalescing Binary Black Holes." In: *Astrophys. J.* 810.1, 58 (Sept. 2015), p. 58. DOI: 10.1088/0004-637X/810/1/58. arXiv: 1504.07802 [astro-ph.HE].

[425] Simon Stevenson, Matthew Sampson, Jade Powell, Alejandro Vigna-Gómez, Coenraad J. Neijssel, Dorottya Szécsi, and Ilya Mandel. "The Impact of Pair-instability Mass Loss on the Binary Black Hole Mass Distribution." In: *Astrophys. J.* 882.2, 121 (Sept. 2019), p. 121. DOI: 10.3847/1538-4357/ab3981. arXiv: 1904.02821 [astro-ph.HE].

[426] Simon Stevenson et al. "Distinguishing compact binary population synthesis models using gravitational-wave observations of coalescing binary black holes." In: *Astrophys. J.* 810.1 (2015), p. 58. DOI: 10.1088/0004-637X/810/1/58. arXiv: 1504.07802 [astro-ph.HE].

[427] Hidemaro Suwa and Synge Todo. "Markov Chain Monte Carlo Method without Detailed Balance." In: *Phys. Rev. Lett.* 105 (12 Sept. 2010), p. 120603. DOI: 10.1103/PhysRevLett.105.120603. URL: https://link.aps.org/doi/10.1103/PhysRevLett.105.120603.

[428] Hiromichi Tagawa, Zoltán Haiman, Imre Bartos, and Bence Kocsis. "Spin Evolution of Stellar-mass Black Hole Binaries in Active Galactic Nuclei." In: *Astrophys. J.* 899.1, 26 (Aug. 2020), p. 26. DOI: 10.3847/1538-4357/aba2cc. arXiv: 2004.11914 [astro-ph.HE].

[429] Hiromichi Tagawa, Zoltán Haiman, and Bence Kocsis. "Formation and Evolution of Compact-object Binaries in AGN Disks." In: *Astrophys. J.* 898.1, 25 (July 2020), p. 25. DOI: 10.3847/1538-4357/ab9b8c. arXiv: 1912.08218 [astro-ph.GA].

[430] Hiromichi Tagawa, Bence Kocsis, Zoltán Haiman, Imre Bartos, Kazuyuki Omukai, and Johan Samsing. "Eccentric Black Hole Mergers in Active Galactic Nuclei." In: *Astrophys. J. Lett.* 907.1, L20 (Jan. 2021), p. L20. DOI: 10.3847/2041-8213/abd4d3. arXiv: 2010.10526 [astro-ph.HE].

[431] Hiromichi Tagawa, Bence Kocsis, Zoltán Haiman, Imre Bartos, Kazuyuki Omukai, and Johan Samsing. "Mass-gap Mergers in Active Galactic Nuclei." In: *Astrophys. J.* 908.2, 194 (Feb. 2021), p. 194. DOI: 10.3847/1538-4357/abd555. arXiv: 2012.00011 [astro-ph.HE].

[432] Hiromichi Tagawa, Bence Kocsis, and Takayuki R. Saitoh. "Compact object mergers driven by gas fallback." In: *Phys. Rev. Lett.* 120.26 (2018), p. 261101. DOI: 10.1103/PhysRevLett.120.261101. arXiv: 1802.00441 [astro-ph.HE].

[433] C. Talbot and E Thrane. "Measuring the binary black hole mass spectrum with an astrophysically motivated parameterization." In: *Astrophys. J.* 856 (2018), p. 173.

[434] Colm Talbot. "Astrophysics of Binary Black Holes at the Dawn of Gravitational-Wave Astronomy." PhD thesis. Monash University, Mar. 2020. DOI: 10.26180/5e61a9fc39b73. URL: https://bridges.monash.edu/articles/Astrophysics_of_Binary_Black_Holes_at_the_Dawn_of_Gravitational-Wave_Astronomy/11944914/1.

[435] Colm Talbot, Rory Smith, Eric Thrane, and Gregory B. Poole. "Parallelized inference for gravitational-wave astronomy." In: *Phys. Rev. D* 100.4, 043030 (Aug. 2019), p. 043030. DOI: 10.1103/PhysRevD.100.043030. arXiv: 1904.02863 [astro-ph.IM].

[436] Colm Talbot and Eric Thrane. "Determining the population properties of spinning black holes." In: *Phys. Rev. D* 96.2, 023012 (July 2017), p. 023012. DOI: 10.1103/PhysRevD.96.023012. arXiv: 1704.08370 [astro-ph.HE].

[437] Sean Talts, Michael Betancourt, Daniel Simpson, Aki Vehtari, and Andrew Gelman. "Validating Bayesian Inference Algorithms with Simulation-Based Calibration." In: *arXiv e-prints*, arXiv:1804.06788 (Apr. 2018), arXiv:1804.06788. arXiv: 1804.06788 [stat.ME].

[438] Naoyuki Tamura, Ray M. Sharples, Nobuo Arimoto, Masato Onodera, Kouji Ohta, and Yoshihiko Yamada. "A Subaru/Suprime-Cam wide-field survey of globular cluster populations around M87 - I. Observation, data analysis and luminosity function." In: *Mon. Not. R. Ast. Soc.* 373.2 (Dec. 2006), pp. 588–600. DOI: 10.1111/j.1365-2966.2006.11067.x. arXiv: astro-ph/0609067 [astro-ph].

[439] Petra N Tang, J J Eldridge, Elizabeth R Stanway, and J C Bray. "Dependence of gravitational wave transient rates on cosmic star formation and metallicity evolution history." In: *Mon. Not. Roy. Astron. Soc.* 493.1 (Jan. 2020), pp. L6–L10. ISSN: 1745-3933. DOI: 10.1093/mnrasl/slz183. URL: http://dx.doi.org/10.1093/mnrasl/slz183.

[440] N. R. Tanvir, A. J. Levan, C. González-Fernández, et al. "The Emergence of a Lanthanide-rich Kilonova Following the Merger of Two Neutron Stars." In: *Astrophys. J. Lett.* 848.2, L27 (Oct. 2017), p. L27. DOI: 10.3847/2041-8213/aa90b6. arXiv: 1710.05455 [astro-ph.HE].

[441] T. M. Tauris et al. "Formation of Double Neutron Star Systems." In: *Astrophys. J.* 846.2 (2017), p. 170. DOI: 10.3847/1538-4357/aa7e89. arXiv: 1706.09438 [astro-ph.HE].

[442] Thomas M. Tauris, Norbert Langer, and Philipp Podsiadlowski. "Ultra-stripped supernovae: progenitors and fate." In: *Mon. Not. Roy. Astron. Soc.* 451.2 (Aug. 2015), pp. 2123–2144. DOI: 10.1093/mnras/stv990. arXiv: 1505.00270 [astro-ph.SR].

[443] The LIGO Scientific Collaboration, the Virgo Collaboration, the KAGRA Collaboration, R. Abbott, T. D. Abbott, F. Acernese, K. Ackley, C. Adams, N. Adhikari, et al. *GWTC-3: Compact Binary Coalescences Observed by LIGO and Virgo During the Second Part of the Third Observing Run*. Nov. 2021. arXiv: 2111.03606 [gr-qc].

[444] Eric Thrane and Colm Talbot. "An introduction to Bayesian inference in gravitational-wave astronomy: parameter estimation, model selection, and hierarchical models." In: *arXiv e-prints*, arXiv:1809.02293 (Sept. 2018), arXiv:1809.02293. arXiv: 1809.02293 [astro-ph.IM].

[445] Srishti Tiwari, Gopakumar Achamveedu, Maria Haney, and Phurailatapam Hemantakumar. "Ready-to-use Fourier domain templates for compact binaries inspiralling along moderately eccentric orbits." In: *Phys. Rev.* D99.12 (2019), p. 124008. DOI: 10.1103/PhysRevD.99.124008. arXiv: 1905.07956 [gr-qc].

[446] M. Trenti, E. Ardi, S. Mineshige, and P. Hut. "Primordial binaries and intermediate mass black holes in globular clusters." In: *arXiv e-prints*, astro-ph/0508517 (Aug. 2005), astro–ph/0508517. arXiv: astro-ph/0508517 [astro-ph].

[447] Michele Trenti, Paolo Padoan, and Raul Jimenez. "The Relative and Absolute Ages of Old Globular Clusters in the LCDM Framework." In: *Astrophys. J. Lett.* 808.2, L35 (Aug. 2015), p. L35. DOI: 10.1088/2041-8205/808/2/L35. arXiv: 1502.02670 [astro-ph.GA].

[448] David Tsang. "Shattering Flares during Close Encounters of Neutron Stars." In: *Astrophys. J.* 777.2, 103 (Nov. 2013), p. 103. DOI: 10.1088/0004-637X/777/2/103. arXiv: 1307.3554 [astro-ph.HE].

[449] A. V. Tutukov and L. R. Yungelson. "Formation of neutron stars in binary systems." In: *Astronomy Reports* 37.4 (July 1993), pp. 411–431.

[450] A. V. Tutukov and L. R. Yungelson. "The merger rate of neutron star and black hole binaries." In: *Mon. Not. Roy. Astron. Soc.* 260 (Feb. 1993), pp. 675–678. DOI: 10.1093/mnras/260.3.675.

[451] Avi Vajpeyi, Eric Thrane, Rory Smith, Barry McKernan, and K. E. Saavik Ford. "Measuring the properties of active galactic nuclei disks with gravitational waves." In: *arXiv e-prints*, arXiv:2111.03992 (Nov. 2021), arXiv:2111.03992. arXiv: 2111.03992 [gr-qc].

[452] Don A. VandenBerg, K. Brogaard, R. Leaman, and L. Casagrand e. "The Ages of 55 Globular Clusters as Determined Using an Improved delta V$\hat{H}$B_TO Method along with Color-Magnitude Diagram Constraints, and Their Implications for Broader Issues." In: *Astrophys. J.* 775.2, 134 (Oct. 2013), p. 134. DOI: 10.1088/0004-637X/775/2/134. arXiv: 1308.2257 [astro-ph.GA].

[453] J. Veitch and W. Del Pozzo. *Analytic Marginalisation of Phase Parameter*. Tech. rep. LIGO-T1300326. 2013. URL: https://dcc.ligo.org/LIGO-T1300326/public.

[454] J. Veitch and A. Vecchio. "Bayesian approach to the follow-up of candidate gravitational wave signals." In: *Phys. Rev. D* 78.2, 022001 (2008), p. 022001. DOI: 10.1103/PhysRevD.78.022001.

[455] J. Veitch and A. Vecchio. "Bayesian coherent analysis of in-spiral gravitational wave signals with a detector network." In: *Phys. Rev. D* 81.6, 062003 (2010), p. 062003. DOI: 10.1103/PhysRevD.81.062003.

[456] J. Veitch et al. "Parameter estimation for compact binaries with ground-based gravitational-wave observations using the LALInference software library." In: *Phys. Rev. D* 91.4, 042003 (2015), p. 042003. DOI: 10.1103/PhysRevD.91.042003.

[457] John Veitch, Walter Del Pozzo, Cody, Matt Pitkin, and ed1d1a8d. *johnveitch/cpnest: Minor optimisation*. Version 0.1.4. July 2017. DOI: 10.5281/zenodo.835874. URL: https://doi.org/10.5281/zenodo.835874.

[458] Tejaswi Venumadhav, Barak Zackay, Javier Roulet, Liang Dai, and Matias Zaldarriaga. "New binary black hole mergers in the second observing run of Advanced LIGO and Advanced Virgo." In: *Phys. Rev. D* 101.8, 083030 (Apr. 2020), p. 083030. DOI: 10.1103/PhysRevD.101.083030. arXiv: 1904.07214 [astro-ph.HE].

[459] Tejaswi Venumadhav et al. "New search pipeline for compact binary mergers: Results for binary black holes in the first observing run of Advanced LIGO." In: *Phys. Rev. D* 100.2, 023011 (July 2019), p. 023011. DOI: 10.1103/PhysRevD.100.023011. arXiv: 1902.10341 [astro-ph.IM].

[460] A. D. Viets, M. Wade, A. L. Urban, S. Kandhasamy, et al. "Reconstructing the calibrated strain signal in the Advanced LIGO detectors." In: *Class. Quant. Grav.* 35.9, 095015 (May 2018), p. 095015. DOI: 10.1088/1361-6382/aab658. arXiv: 1710.09973 [astro-ph.IM].

[461] Sarah J. Vigeland and Michele Vallisneri. "Bayesian inference for pulsar-timing models." In: *Mon. Not. Roy. Astron. Soc.* 440.2 (May 2014), pp. 1446–1457. DOI: 10.1093/mnras/stu312. arXiv: 1310.2606 [astro-ph.IM].

[462] Alejandro Vigna-Gómez et al. "On the formation history of Galactic double neutron stars." In: *Mon. Not. Roy. Astron. Soc.* 481.3 (Dec. 2018), pp. 4009–4029. DOI: 10.1093/mnras/sty2463. arXiv: 1805.07974 [astro-ph.SR].

[463] Salvatore Vitale, Walter Del Pozzo, Tjonnie G. F. Li, Chris Van Den Broeck, Ilya Mandel, Ben Aylott, and John Veitch. "Effect of calibration errors on Bayesian parameter estimation for gravitational wave signals from inspiral binary systems in the advanced detectors era." In: *Phys. Rev. D* 85 (6 Mar. 2012), p. 064034. DOI: 10.1103/PhysRevD.85.064034. URL: https://link.aps.org/doi/10.1103/PhysRevD.85.064034.

[464] Salvatore Vitale and Matthew Evans. "Parameter estimation for binary black holes with networks of third-generation gravitational-wave detectors." In: *Phys. Rev. D* 95.6, 064052 (Mar. 2017), p. 064052. DOI: 10.1103/PhysRevD.95.064052. arXiv: 1610.06917 [gr-qc].

[465] Salvatore Vitale, Will M. Farr, Ken K. Y. Ng, and Carl L. Rodriguez. "Measuring the Star Formation Rate with Gravitational Waves from Binary Black Holes." In: *Astrophys. J. Lett.* 886.1, L1 (Nov. 2019), p. L1. DOI: 10.3847/2041-8213/ab50c0. arXiv: 1808.00901 [astro-ph.HE].

[466] Salvatore Vitale, Carl-Johan Haster, Ling Sun, Ben Farr, Evan Goetz, Jeff Kissel, and Craig Cahillane. "Physical approach to the marginalization of LIGO calibration uncertainties." In: *Phys. Rev. D.* 103.6, 063016 (Mar. 2021), p. 063016. DOI: 10.1103/PhysRevD.103.063016. arXiv: 2009.10192 [gr-qc].

[467] Salvatore Vitale, Ryan Lynch, Riccardo Sturani, and Philip Graff. "Use of gravitational waves to probe the formation channels of compact binaries." In: *Class. Quant. Grav.* 34.3 (2017), 03LT01. DOI: 10.1088/1361-6382/aa552e. arXiv: 1503.04307 [gr-qc].

[468] Salvatore Vitale and Chris Whittle. "Characterization of binary black holes by heterogeneous gravitational-wave networks." In: *Phys. Rev. D* 98.2, 024029 (July 2018), p. 024029. DOI: 10.1103/PhysRevD.98.024029. arXiv: 1804.07866 [gr-qc].

[469] Leslie Wade, Jolien D. E. Creighton, Evan Ochsner, Benjamin D. Lackey, Benjamin F. Farr, Tyson B. Littenberg, and Vivien Raymond. "Systematic and statistical errors in a Bayesian approach to the estimation of the neutron-star equation of state using advanced gravitational wave detectors." In: *Phys. Rev. D* 89.10, 103012 (May 2014), p. 103012. DOI: 10.1103/PhysRevD.89.103012. arXiv: 1402.5156 [gr-qc].

[470] Long Wang, Rainer Spurzem, Sverre Aarseth, Mirek Giersz, Abbas Askar, Peter Berczik, Thorsten Naab, Riko Schadow, and M. B. N. Kouwenhoven. "The DRAGON simulations: globular cluster evolution with a million stars." In: *Mon. Not. R. Ast. Soc.* 458.2 (May 2016), pp. 1450–1465. DOI: 10.1093/mnras/stw274. arXiv: 1602.00759 [astro-ph.SR].

[471] Sai Wang and Zhi-Chao Zhao. "Observational verification of CPT invariance with binary black hole gravitational waves in the LIGO-Virgo catalog GWTC-1." In: *arXiv e-prints*, arXiv:2002.00396 (Feb. 2020), arXiv:2002.00396. arXiv: 2002.00396 [gr-qc].

[472] Darach Watson et al. "Identification of strontium in the merger of two neutron stars." In: *nature* 574.7779 (Oct. 2019), pp. 497–500. DOI: 10.1038/s41586-019-1676-3. arXiv: 1910.10510 [astro-ph.HE].

[473] Linqing Wen. "On the Eccentricity Distribution of Coalescing Black Hole Binaries Driven by the Kozai Mechanism in Globular Clusters." In: *Astrophys. J.* 598.1 (Nov. 2003), pp. 419–430. DOI: 10.1086/378794. arXiv: astro-ph/0211492 [astro-ph].

[474] Linqing Wen. "On the eccentricity distribution of coalescing black hole binaries driven by the Kozai mechanism in globular clusters." In: *Astrophys. J.* 598 (2003), pp. 419–430. DOI: 10.1086/378794. arXiv: astro-ph/0211492 [astro-ph].

[475] Peter Whittle. *Peter. Hypothesis Testing in Time Series Analysis*. Uppsala: Almquist and Wiksells, 1951.

[476] S. E. Woosley. "Pulsational Pair-instability Supernovae." In: *Astrophys. J.* 836.2, 244 (Feb. 2017), p. 244. DOI: 10.3847/1538-4357/836/2/244. arXiv: 1608.08939 [astro-ph.HE].

[477] Daniel Wysocki, Jacob Lange, and Richard O. 'shaughnessy. "Reconstructing phenomenological distributions of compact binaries via gravitational wave observations." In: (2018). arXiv: 1805.06442 [gr-qc].

[478] Y. Yang, I. Bartos, Z. Haiman, B. Kocsis, S. Márka, and H. Tagawa. "Cosmic Evolution of Stellar-mass Black Hole Merger Rate in Active Galactic Nuclei." In: *Astrophys. J* 896.2 (2020), p. 138. DOI: 10.3847/1538-4357/ab91b4. URL: https://doi.org/10.3847/1538-4357/ab91b4.

[479] Y. Yang, I. Bartos, Z. Haiman, B. Kocsis, Z. Márka, N. C. Stone, and S. Márka. "AGN Disks Harden the Mass Distribution of Stellar-mass Binary Black Hole Mergers." In: *Astrophys. J.* 876.2, 122 (May 2019), p. 122. DOI: 10.3847/1538-4357/ab16e3. arXiv: 1903.01405 [astro-ph.HE].

[480] Y. Yang et al. "Hierarchical Black Hole Mergers in Active Galactic Nuclei." In: *Phys. Rev. Lett.* 123 (18 Nov. 2019), p. 181101. DOI: 10.1103/PhysRevLett.123.181101. URL: https://link.aps.org/doi/10.1103/PhysRevLett.123.181101.

[481] Y. Yang et al. "Hierarchical Black Hole Mergers in Active Galactic Nuclei." In: *Phys. Rev. Lett.* 123.18, 181101 (Nov. 2019), p. 181101. DOI: 10.1103/PhysRevLett.123.181101. arXiv: 1906.09281 [astro-ph.HE].

[482] Claire S. Ye, Wen-fai Fong, Kyle Kremer, Carl L. Rodriguez, Sourav Chatterjee, Giacomo Fragione, and Frederic A. Rasio. "On the Rate of Neutron Star Binary Mergers from Globular Clusters." In: *Astrophys. J. Lett.* 888.1, L10 (Jan. 2020), p. L10. DOI: 10.3847/2041-8213/ab5dc5. arXiv: 1910.10740 [astro-ph.HE].

[483] Qianyun Yun, Wen-Biao Han, Xingyu Zhong, and Carlos A. Benavides-Gallego. "Surrogate model for gravitational waveforms of spin-aligned binary black holes with eccentricities." In: *Phys. Rev. D.* 103.12, 124053 (June 2021), p. 124053. DOI: 10.1103/PhysRevD.103.124053. arXiv: 2104.03789 [gr-qc].

[484] Nicolás Yunes and Xavier Siemens. "Gravitational-Wave Tests of General Relativity with Ground-Based Detectors and Pulsar-Timing Arrays." In: *Living Reviews in Relativity* 16.1, 9 (Nov. 2013), p. 9. DOI: 10.12942/lrr-2013-9. arXiv: 1304.3473 [gr-qc].

[485] Nicolás Yunes, Kent Yagi, and Frans Pretorius. "Theoretical physics implications of the binary black-hole mergers GW150914 and GW151226." In: *Phys. Rev. D* 94.8, 084002 (Oct. 2016), p. 084002. DOI: 10.1103/PhysRevD.94.084002. arXiv: 1603.08955 [gr-qc].

[486] Barak Zackay, Liang Dai, and Tejaswi Venumadhav. "Relative Binning and Fast Likelihood Evaluation for Gravitational Wave Parameter Estimation." In: *arXiv e-prints*, arXiv:1806.08792 (June 2018), arXiv:1806.08792. arXiv: 1806.08792 [astro-ph.IM].

[487] Barak Zackay, Liang Dai, Tejaswi Venumadhav, Javier Roulet, and Matias Zaldarriaga. "Detecting Gravitational Waves With Disparate Detector Responses: Two New Binary Black Hole Mergers." In: *arXiv e-prints*, arXiv:1910.09528 (Oct. 2019). arXiv: 1910.09528 [astro-ph.HE].

[488] Michael Zevin, Simone S. Bavera, Christopher P. L. Berry, Vicky Kalogera, Tassos Fragos, Pablo Marchant, Carl L. Rodriguez, Fabio Antonini, Daniel E. Holz, and Chris Pankow. "One Channel to Rule Them All? Constraining the Origins of Binary Black Holes Using Multiple Formation Pathways." In: *apj* 910.2, 152 (Apr. 2021), p. 152. DOI: 10.3847/1538-4357/abe40e. arXiv: 2011.10057 [astro-ph.HE].

[489] Michael Zevin, Kyle Kremer, Daniel M. Siegel, Scott Coughlin, Benny T. H. Tsan, Christopher P. L. Berry, and Vicky Kalogera. "Can Neutron-Star Mergers Explain the r-process Enrichment in Globular Clusters?" In: (2019). arXiv: 1906.11299 [astro-ph.HE].

[490] Michael Zevin, Chris Pankow, Carl L. Rodriguez, Laura Sampson, Eve Chase, Vassiliki Kalogera, and Frederic A. Rasio. "Constraining Formation Models of Binary Black Holes with Gravitational-Wave Observations." In: *Astrophys. J.* 846.1 (2017), p. 82. DOI: 10.3847/1538-4357/aa8408. arXiv: 1704.07379.

[491] Michael Zevin, Isobel M. Romero-Shaw, Kyle Kremer, Eric Thrane, and Paul D. Lasky. "Implications of Eccentric Observations on Binary Black Hole Formation Channels." In: *arXiv e-prints*, arXiv:2106.09042 (June 2021), arXiv:2106.09042. arXiv: 2106.09042 [astro-ph.HE].

[492] Michael Zevin, Johan Samsing, Carl Rodriguez, Carl-Johan Haster, and Enrico Ramirez-Ruiz. "Eccentric Black Hole Mergers in Dense Star Clusters: The Role of Binary–Binary Encounters." In: *Astrophys. J.* 871.1 (2019), p. 91. DOI: 10.3847/1538-4357/aaf6ec. arXiv: 1810.00901 [astro-ph.HE].

[493] Wen Zhao and Linqing Wen. "Localization accuracy of compact binary coalescences detected by the third-generation gravitational-wave detectors and implication for cosmology." In: *Phys. Rev. D* 97.6, 064031 (Mar. 2018), p. 064031. DOI: 10.1103/PhysRevD.97.064031. arXiv: 1710.05325 [astro-ph.CO].

[494] Zhi-Chao Zhao, Hai-Nan Lin, and Zhe Chang. "The prospects of using gravitational waves for constraining the anisotropy of the Universe." In: *Chinese Physics C* 43.7, 075102 (July 2019), p. 075102. DOI: 10.1088/1674-1137/43/7/075102. arXiv: 1904.03460 [gr-qc].

[495] Xing-Jiang Zhu, E. Howell, T. Regimbau, D. Blair, and Zong-Hong Zhu. "Stochastic Gravitational Wave Background from Coalescing Binary Black Holes." In: *Astrophys. J* 739.2, 86 (Oct. 2011), p. 86. DOI: 10.1088/0004-637X/739/2/86. arXiv: 1104.3565 [gr-qc].

[496] Xingjiang Zhu, Eric Thrane, Stefan Osłowski, Yuri Levin, and Paul D. Lasky. "Inferring the population properties of binary neutron stars with gravitational-wave measurements of spin." In: *Phys. Rev. D* 98.4, 043002 (Aug. 2018), p. 043002. DOI: 10.1103/PhysRevD.98.043002. arXiv: 1711.09226 [astro-ph.HE].

[497] B. M. Ziosi, M. Mapelli, M. Branchesi, and G. Tormen. "Dynamics of stellar black holes in young star clusters with different metallicities – II. Black hole–black hole binaries." In: *Monthly Notices of the Royal Astronomical Society* 441.4 (2014), pp. 3703–3717. URL: https://doi.org/10.1093/mnras/stu824.

[498] S. E. de Mink, M. Cantiello, N. Langer, and O. R. Pols. "Chemically Homogeneous Evolution in Massive Binaries." In: *American Institute of Physics Conference Series*. Ed. by Vicky Kalogera and Marc van der Sluys. Vol. 1314. American Institute of Physics Conference Series. Dec. 2010, pp. 291–296. DOI: 10.1063/1.3536387. arXiv: 1010.2177 [astro-ph.SR].

[499] E. P. J. van den Heuvel, S. F. Portegies Zwart, and S. E. de Mink. "Forming short-period Wolf-Rayet X-ray binaries and double black holes through stable mass transfer." In: *Mon. Not. R. Ast. Soc.* 471.4 (Nov. 2017), pp. 4256–4264. DOI: 10.1093/mnras/stx1430. arXiv: 1701.02355 [astro-ph.SR].

[500] M. V. van der Sluys, C. Röver, A. Stroeer, V. Raymond, I. Mandel, N. Christensen, V. Kalogera, R. Meyer, and A. Vecchio. "Gravitational-Wave Astronomy with Inspiral Signals of Spinning Compact-Object Binaries." In: *Astrophys. J. Lett.* 688 (Dec. 2008), p. L61. DOI: 10.1086/595279. arXiv: 0710.1897.

[501] Marc van der Sluys, Vivien Raymond, Ilya Mandel, Christian Röver, Nelson Christensen, Vicky Kalogera, Renate Meyer, and Alberto Vecchio. "Parameter estimation of spinning binary inspirals using Markov chain Monte Carlo." In: *Classical and Quantum Gravity* 25.18, 184011 (Sept. 2008), p. 184011. DOI: 10.1088/0264-9381/25/18/184011. arXiv: 0805.1689 [gr-qc].

A

CONSTRUCTING AN ECCENTRICITY MEASUREMENT

I describe here in detail the process by which an eccentricity posterior probability distribution is constructed. I start with a set of posterior samples for the 11-dimensional proposal model, $p_{\text{ø}}(\theta|d)$, and transform them into posterior samples for the 12-dimensional target model, $p(\theta, e_{10}|d)$, using the following procedure.

A.1 LIKELIHOOD REWEIGHTING

The set of proposal posterior samples, $p_{\text{ø}}(\theta|d)$, is computed using non-eccentric waveform model $\mu_{\text{ø}}(\theta)$. This posterior is evaluated using the non-eccentric likelihood $\mathcal{L}_{\text{ø}}(d|\theta)$. My task is now to transform to the target posterior distribution, $p(\theta, e_{10}|d)$, which uses eccentric waveform model $\mu(\theta, e_{10})$, eccentric likelihood $\mathcal{L}(d|\theta, e_{10})$, and a prior with an extra dimension, $\pi(\theta, e_{10}) = \pi(\theta)\pi(e_{10})$.
I start by reweighting to the marginal eccentric posterior $p(\theta|d)_{e_{10}}$, which has been marginalised over eccentricity. To do this, I first evaluate the eccentric likelihood for each set of parameters θ_i, $\mathcal{L}(d|\theta_i, e_{10})$, over the log-uniformly distributed prior on eccentricity, $\pi(e_{10})$, and integrate over eccentricity(see Equation 9 of [444]):

$$\mathcal{L}(d|\theta)_{e_{10}} = \int \mathcal{L}(d|\theta, e_{10})\pi(e_{10})de_{10}. \tag{A.1}$$

The relationship between $p(\theta|d)_{e_{10}}$ and $p(\theta|d)_{\text{ø}}$ is then obtained by multiplying Bayes' theorem (Equation 1.3) by unity:

$$\begin{aligned} p(\theta|d)_{e_{10}} &= \frac{\mathcal{L}(d|\theta)_{e_{10}}\pi(\theta)}{\mathcal{Z}(d)} \times \frac{\mathcal{L}_{\text{ø}}(d|\theta)}{\mathcal{L}_{\text{ø}}(d|\theta)} \frac{\mathcal{Z}_{\text{ø}}(d)}{\mathcal{Z}_{\text{ø}}(d)} \\ &= \frac{\mathcal{L}_{\text{ø}}(d|\theta)\pi(\theta)}{\mathcal{Z}_{\text{ø}}(d)} \times \frac{\mathcal{L}(d|\theta)_{e_{10}}}{\mathcal{L}_{\text{ø}}(d|\theta)} \times \frac{\mathcal{Z}_{\text{ø}}(d)}{\mathcal{Z}(d)} \\ &= p_{\text{ø}}(\theta|d) \times w(\theta) \times \frac{\mathcal{Z}_{\text{ø}}(d)}{\mathcal{Z}(d)}. \end{aligned} \tag{A.2}$$

In the last step of Equation A.2, I have written the ratio between $\mathcal{L}(d|\theta)_{e_{10}}$ and $\mathcal{L}_{\text{ø}}(d|\theta)$ as weight $w(\theta)$. The ratio between $\mathcal{Z}_{\text{ø}}(d)$ and $\mathcal{Z}(d)$ can be ignored when comparing two normalised distribution, but its value is useful for telling us which model is preferred by the data.
When we compute the likelihoods $\mathcal{L}_{\text{ø}}$ and $\mathcal{L}$, we must take into account the fact that different waveform models may have different definitions of the reference phase ϕ and geocent time t. There are two methods of solving this problem. The simplest is to *maximise* over phase and time by taking the values of these parameters that lead to the largest overlap between the target and proposal waveforms,

$$\mathcal{O} \equiv \max_{t,\phi} \frac{\langle h^{+}_{\emptyset}, h^{+} \rangle + \langle h^{\times}_{\emptyset}, h^{\times} \rangle}{\sqrt{\left(\langle h^{+}_{\emptyset}, h^{+}_{\emptyset} \rangle + \langle h^{\times}_{\emptyset}, h^{\times}_{\emptyset} \rangle\right)\left(\langle h^{+}, h^{+} \rangle + \langle h^{\times}, h^{\times} \rangle\right)}}, \quad \text{(A.3)}$$

where the angled brackets represent noise-weighted inner products and $h^{+,\times}_{\emptyset}$ ($h^{+,x}$) are the plus and cross modes of the proposal (target) waveform. The alternative is to *marginalise* over phase and time. This produces similar posterior probability distributions, but is better-motivated from a statistical perspective and leads to higher reweighting efficiency. In papers [374, 376] (Chapters 3 and 4), we maximise over phase and time, while in [377, 379] (Chapters 5 and 6) we marginalise over these parameters.

A.1.1 *Effective sample size*

The act of reweighting changes the effective number of samples in the posterior distribution. The ratio of the effective number of samples, n_{eff}, to the total number of samples, N, is known as the *efficiency*. The effective number of samples is computed as

$$n_{\text{eff}} = \frac{\left(\sum_{i=1}^{N} w(\theta_i)\right)^2}{\sum_{i=1}^{N} w(\theta_i)^2}. \quad \text{(A.4)}$$

A.2 RECONSTRUCTING THE ECCENTRIC POSTERIOR

In the analyses presented in Chapters 3–6, I assume a log-uniform prior on e_{10}. I enforce this prior, $\pi(e_{10})$, by constructing a log-uniformly spaced grid of n eccentricity bins. For each non-eccentric proposal posterior sample, $p_{\emptyset}(\theta_i|d)$, there is an associated vector of parameters, θ_i. Keeping these parameters fixed, the eccentric likelihood, $\mathcal{L}(d|\theta_i, e_{10,j})$, is evaluated at each eccentricity $e_{10,j}$ in the log-uniformly distributed grid of the prior. I then convert the likelihood distribution into a normalised cumulative likelihood function, $CLF(e_{10})$. I generate a random value, V, between 0 and 1, and find the eccentricity bin $e_{10,j}$ in our grid for which $CLF(e_{10,j}) \geq V$. I select an eccentricity at random from this bin and assign that eccentricity, $e_{10,i}$, to sample i. Appendix C.6 of [444] describes the same procedure, which is used to reconstruct marginalised posterior distributions within Bilby.

A.3 BAYES FACTORS

The Bayes factor, $\mathcal{B}$, is the ratio of the model evidences. It tells us which model is preferred by the data, and by how much. The Bayes factor between the target and proposal models is given as

$$\mathcal{B} = \frac{\mathcal{Z}(d)}{\mathcal{Z}_{\emptyset}(d)}. \quad \text{(A.5)}$$

This ratio can be expressed in terms of the model weights, $w(e_{10})$, by first multiplying the target evidence by unity,

$$\begin{aligned}\mathcal{Z}(d) &= \int\int \mathcal{L}(d|\theta, e_{10})\pi(\theta, e_{10})d\theta de_{10} \\ &= \int \mathcal{L}(d|\theta)_{e_{10}}\pi(\theta)d\theta \times \frac{\mathcal{L}_{\varnothing}(d|\theta)}{\mathcal{L}_{\varnothing}(d|\theta)} \\ &= \int \mathcal{L}_{\varnothing}(d|\theta)\pi(\theta)w(\theta)d\theta \\ &= \mathcal{Z}_{\varnothing}(d)\int w(\theta)d\theta \\ &= \frac{\mathcal{Z}_{\varnothing}(d)}{N}\sum_{i=0}^{N} w(\theta_i),\end{aligned} \tag{A.6}$$

where in the last step I have replaced the integral with a mean average over N posterior samples. The Bayes factor can then be expressed in terms of the weights,

$$\mathcal{B} = \frac{\mathcal{Z}(d)}{\mathcal{Z}_{\varnothing}(d)} = \frac{1}{N}\sum_{i}^{N} w(\theta_i). \tag{A.7}$$

In some of the papers in this thesis, we compare different hypotheses about the eccentricity distribution, e.g., that the majority of the support lies above some value $e_{10}^{\rm lim}$. In this case, we compute the following:

$$\mathcal{B}_{e_{10}^{\rm lim}<e_{10}} = \frac{\mathcal{Z}(d, e_{10}^{\rm lim} < e_{10})}{\mathcal{Z}(d, e_{10} \leq e_{10}^{\rm lim})}. \tag{A.8}$$